DEVELOPMENT OF ROLL WAVES IN OPEN CHANNELS

by

Richard R. Brock

Project Supervisor:
Vito A. Vanoni
Professor of Hydraulics

Supported by the
Los Angeles County Flood Control District
and the
Alfred P. Sloan Foundation

W. M. Keck Laboratory of Hydraulics and Water Resources
Division of Engineering and Applied Science
California Institute of Technology
Pasadena, California

Report No. KH-R-16 July 1967

102.923

DEVELOPMENT OF ROLL WAVES IN OPEN CHANNELS

by

Richard R. Brock

Project Supervisor:

Vito A. Vanoni
Professor of Hydraulics

Supported by the
Los Angeles County Flood Control District
and the
Alfred P. Sloan Foundation

W. M. Keck Laboratory of Hydraulics and Water Resources
Division of Engineering and Applied Science
California Institute of Technology
Pasadena, California

Report No. KH-R-16

July 1967

ACKNOWLEDGMENTS

To Dr. Vito A. Vanoni, the writer expresses his deepest appreciation for the advice and encouragement offered throughout the investigation. For their advice on various phases of the investigation the writer wishes to thank Dr. Norman H. Brooks and Dr. Fredric Raichlen.

The writer is indebted to Mr. Elton Daly for the construction of the channel used in this study. The writer also wishes to extend his gratitude to the following persons for their contributions to the project: Mr. Robert L. Greenway for assisting with the construction of the channel; Mr. Robert Dickenson and Mr. Edward Thompson for analyzing data and preparing drawings; Mr. Jiin-jen Lee for analyzing data; Mr. Leonard Fisher for assisting with the preliminary experiments; Mr. Carl Green for preparing drawings; Mr. Carl Eastvedt for all the photographic work; Mrs. Patricia A. Rankin for typing the manuscript; Miss Sophia Yen for preparing tables; and Mrs. Patricia A. Brock for typing much of the first draft.

Financial assistance was received by the writer in the form of a United States Public Health Service Training Grant (1963-64), Graduate Research Assistantship (1964-65) from the California Institute of Technology, fellowship provided by the George H. Mayr Educational Foundation (1964-65), and National Science Foundation Graduate Traineeship (1965-66 and 1966-67). This assistance is gratefully acknowledged.

The investigation was supported by the Los Angeles County Flood Control District from August 1964 to September 1966. Support for the last year was from the Alfred P. Sloan Foundation. The research was performed in the W. M. Keck Laboratory of Hydraulics and Water Resources at the California Institute of Technology.

This report was submitted by the writer, in June 1967, as a thesis with the same title to the California Institute of Technology in partial fulfillment of the requirements for the degree of Doctor of Philosophy in Civil Engineering.

ABSTRACT

This study is concerned with some of the properties of roll waves that develop naturally from a turbulent uniform flow in a wide rectangular channel on a constant steep slope. The wave properties considered were depth at the wave crest, depth at the wave trough, wave period, and wave velocity. The primary focus was on the mean values and standard deviations of the crest depths and wave periods at a given station and how these quantities varied with distance along the channel.

The wave properties were measured in a laboratory channel in which roll waves developed naturally from a uniform flow. The Froude number F ($F = u_n/\sqrt{gh_n}$, u_n = normal velocity, h_n = normal depth, g = acceleration of gravity) ranged from 3.4 to 6.0 for channel slopes S_o of .05 and .12 respectively. In the initial phase of their development the roll waves appeared as small amplitude waves with a continuous water surface profile. These small amplitude waves subsequently developed into large amplitude shock waves. Shock waves were found to overtake and combine with other shock waves with the result that the crest depth of the combined wave was larger than the crest depths before the overtake. Once roll waves began to develop, the mean value of the crest depths h_{max} increased with distance. Once the shock waves began to overtake, the mean wave period T_{av} increased approximately linearly with distance.

For a given Froude number and channel slope the observed quantities $\overline{h}_{max}/h_n$, T' ($T' = S_o T_{av} \sqrt{g/h_n}$), and the standard deviations of

$\bar{h}_{max}/h_n$ and T', could be expressed as unique functions of ℓ/h_n (ℓ = distance from beginning of channel) for the two-fold change in h_n occurring in the observed flows. A given value of $\bar{h}_{max}/h_n$ occurred at smaller values of ℓ/h_n as the Froude number was increased. For a given value of $\bar{h}_{max}/h_n$ the growth rate $\partial\bar{h}_{max}/\partial\ell$ of the shock waves increased as the Froude number was increased.

A laboratory channel was also used to measure the wave properties of periodic permanent roll waves. For a given Froude number and channel slope the h_{max}/h_n vs. T' relation did not agree with a theory in which the weight of the shock front was neglected. After the theory was modified to include this weight, the observed values of h_{max}/h_n were within an average of 6.5 percent of the predicted values, and the maximum discrepancy was 13.5 percent.

For $\bar{h}_{max}/h_n$ sufficiently large ($\bar{h}_{max}/h_n$ > approximately 1.5) it was found that the $\bar{h}_{max}/h_n$ vs. T' relation for natural roll waves was practically identical to the h_{max}/h_n vs. T' relation for periodic permanent roll waves at the same Froude number and slope. As a result of this correspondence between periodic and natural roll waves, the growth rate $\partial\bar{h}_{max}/\partial\ell$ of shock waves was predicted to depend on the channel slope, and this slope dependence was observed in the experiments.

TABLE OF CONTENTS

Chapter		Page
I.	INTRODUCTION	2
II.	PREVIOUS STUDIES	5
	A. Basic Equations	5
	B. Criteria for Unstable Flow	7
	C. Large Amplitude Wave Studies	9
	D. Friction Factors in Unstable Flows	11
	E. Summary	11
III.	ANALYTICAL INVESTIGATION	12
	A. Small Amplitude Theory	13
	1. Statement and Solution of Problem	13
	2. Discussion of Solution	18
	B. Large Amplitude Periodic Permanent Roll Wave Theory	23
	1. Statement and Solution of Problem	23
	2. Discussion of Solution	35
IV.	LABORATORY EXPERIMENTS - APPARATUS AND PROCEDURE	37
	A. Introduction and Objective	37
	B. Preliminary Experiments	37
	C. Apparatus	39
	1. Steep Channel	39
	2. Measuring and Recording Equipment	48

TABLE OF CONTENTS (Cont'd)

Chapter		Page
	D. Experimental Procedure	56
	1. Design of Experiments	56
	2. Normal Depth	58
	3. Wave Properties Measured	60
	4. General Procedure for Natural and Periodic Roll Wave Runs	63
V.	PRESENTATION OF EXPERIMENTAL RESULTS	65
	A. Inlet Condition	65
	1. Smooth and Rough Inlet	65
	2. Drawdown Curves Near Inlet	73
	B. Hydraulic Characteristics of Laboratory Channel	75
	C. Natural Roll Waves	79
	1. General Description	79
	2. Tabulated Basic Data	81
	3. Dimensionless Development Relations	81
	4. Frequency Distributions and Wave Shape	97
	D. Periodic Permanent Roll Waves	107
	1. 130-ft Channel	107
	2. Steep Channel	107
	E. Observations on Individual Waves	111
	F. Additional Data - Laboratory and Field	116
	1. Ghambarian Laboratory Data	116
	2. Field Data	122

TABLE OF CONTENTS (Cont'd)

Chapter		Page
VI.	DISCUSSION OF RESULTS	130
	A. Development of Natural Roll Waves in Terms of Distance Along Channel	130
	1. Average Maximum Depth and Average Period	130
	2. Small Amplitude Roll Waves and the Linear Theory	134
	3. Effect of Channel Slope on Small Amplitude Natural Roll Waves	139
	4. Frequency Distributions	142
	B. Development of Natural Roll Waves in Terms of Wave Period	144
	C. Effect of Inlet on Development of Natural Roll Waves	150
	D. Motion of Individual Natural Roll Waves	153
	E. Ghambarian and LACFCD Data	156
	1. Ghambarian Laboratory Data	156
	2. LACFCD Field Data	157
VII.	MODIFIED PERIODIC PERMANENT ROLL WAVE THEORY	159
	A. Assumptions in Periodic Permanent Roll Wave Theory	159
	B. Effect of Side-Walls and Variable Friction Factor	162
	1. Problem and Method of Solution	162
	2. Discussion of Results	167

TABLE OF CONTENTS (Cont'd)

Chapter		Page
	C. Modified Shock Condition	170
	1. General Shock Condition	170
	2. Theory Based on Modified Shock Condition	176
	3. Discussion of Modified Theory	181
	D. Re-Evaluation of Laboratory Results with Consideration to Effect of Channel Slope	188
	1. Periodic Permanent Waves	188
	2. Natural Roll Waves	190
VIII.	PREDICTION OF MAXIMUM DEPTHS IN LARGE CHANNELS	194
	A. Channel Slope Effect	195
	B. Prediction of Maximum Depths in Wide Rectangular Channels with a Constant Slope	196
	C. Prediction of Maximum Depths in Wide Rectangular Channels with a Changing Slope	199
	D. Influence of Side-Walls	205
IX.	RESULTS AND CONCLUSIONS	207
LIST OF SYMBOLS		212
BIBLIOGRAPHY		215
APPENDIX I		219

LIST OF FIGURES

Figure No.	Title	Page No.
1	View of roll waves in Santa Anita Wash, Arcadia, California, about one mile downstream of inlet, discharge about 195 cfs	2
2	Graph of dimensionless amplification factor $2\pi C_i/C_r Y$, against $S_o\lambda/F^2 h_n$ from small amplitude theory	19
3	Graph of dimensionless wave velocity, C_r, against $S_o\lambda/F^2 h_n$ from small amplitude theory	20
4	Definition sketch for periodic permanent roll waves	25
5	Periodic permanent roll wave water-surface profile with point of inflection	25
6	Graphs of solutions for h_{max}, h_{min}, and c as functions of Froude number, F, and $S_o\lambda/h_n$ from periodic permanent roll wave theory	33
7	General view of channel, $S_o = .08429$, $\ell = 128$ ft, no flow	40
8	View of typical joint for channel	40
9	View of channel showing support bracket and pressure measuring station	41
10	Drawing of cross section of channel at a station with a supporting bracket	42
11	Drawing of inlet box for channel	43

LIST OF FIGURES (Cont'd)

Figure No.	Title	Page No.
12	View of inlet box and channel near inlet with flow	45
13	Closeup view of rough channel	45
14	Typical pressure and wire gage record for shock-type roll waves, $S_o = .1192$, $h_n = .210$ in., station 36, smooth inlet	49
15	View of wire gage and pressure transducer with waves approaching	50
16	View of 4-channel oscillograph recorder with wire gage and pressure transducer	53
17	Typical calibration of the pressure measuring system	55
18	Typical wire gage record used to measure normal depths	59
19	Graph of typical water-surface profiles near a smooth inlet for a normal depth of .2 in.	68
20	Typical smooth-inlet and rough-inlet development curves for average maximum depth, $\bar{h}_{max}$, at normal depth of .2 in.	72
21	Graphs of water-surface profiles near inlet of channel	74
22	Graph of the rough channel relation $\sqrt{1/f} - 2.03 \log_{10}(r/k)$ as a function of k/δ, using measured friction factors, f, in rough channel	77
23	Graph of friction factors, f, measured in smooth channel as a function of Reynolds number, R	77

LIST OF FIGURES (Cont'd)

Figure No.	Title	Page No.
24	General view of channel with natural roll waves, $S_o = .1192$, $h_n = .210$ in.	80
25	Side view of roll wave, $S_o = .08429$, $h_n = .208$ in., station 94-98	80
26	Development curve for average maximum depth, $\bar{h}_{max}$, in channel with slope of .05011	92
27	Development curve for average maximum depth, $\bar{h}_{max}$, in channel with slope of .08429	93
28	Development curve for average maximum depth, $\bar{h}_{max}$, in channel with slope of .1192	94
29	Development curve for average maximum depth, $\bar{h}_{max}$, in rough channel with slope of .1192	94
30	Development curve for average wave period, T_{av}, in channel with slope of .05011	95
31	Development curve for average period, T_{av}, in channel with slope of .08429	96
32	Development curve for average period, T_{av}, in channel with slope of .1192	96
33	Development curves for average minimum depth, $\bar{h}_{min}$, for channel slopes of .05011, .08429, .1192	98
34	Development curves for average wave velocity, c_{av}, for channel slopes of .05011, .08429, .1192	99

LIST OF FIGURES (Cont'd)

Figure No.	Title	Page No.
35	Development curves for the standard deviation of the maximum depth $\sigma_{h_{max}}$, for channel slopes of .05011, .08429, .1192	100
36	Development curves for the standard deviation of the wave period, σ_T, for channel slopes of .05011, .08429, .1192	101
37	Typical cumulative frequency distributions of maximum depth, h_{max}	102
38	Typical cumulative frequency distributions of wave period, T	103
39	Typical cumulative frequency distributions of minimum depth, h_{min}	104
40	Typical cumulative frequency distributions of wave velocity, c	105
41	Typical pressure and wire gage record for small amplitude roll waves, S_o = .05011, h_n = .314 in., station 36, smooth inlet	106
42	Definition sketch for coordinates of water-surface profiles for periodic permanent roll waves	108
43	Graph of measured and theoretical water-surface profile for periodic permanent roll waves in 130 ft channel, F = 2.65, T' = 1.30, S_o = .0194	108
44	Graph of experimental and theoretical solutions for h_{max}, h_{min}, and c as functions of dimensionless wave period T' and Froude number F, for periodic permanent roll waves	110

LIST OF FIGURES (Cont'd)

Figure No.	Title	Page No.
45	Graphs of measured water-surface profiles for periodic permanent roll waves	115
46	Pressure records for a train of 12 shock-type roll waves at stations 42, 54, 66, 78, for h_n = .210 in., S_o = .1192, rough inlet	117
47	Pressure records for shock-type roll waves at stations 60, 66, 72, 78, for h_n = .210 in., S_o = .1192, smooth inlet, showing 3 overtakes: waves 1 and 2 in fig. 47a; waves 3 and 4 in fig. 47b; and waves 5 and 6 in fig. 47c	119
48	Graph of Ghambarian's results for average maximum depth $\overline{h}_{max}$ as a function of distance from beginning of channel ℓ, for channel slope = .10	123
49	View of inlet to Santa Anita Wash, Arcadia, California, discharge about 210 cfs	124
50	Graph of average maximum depth $\overline{h}_{max}$ as a function of distance from beginning of channel ℓ for Santa Anita Wash	129
51	Graph of average maximum depth $\overline{h}_{max}$ as a function of dimensionless wave period T', for Santa Anita Wash	129
52	Development curves for average maximum depth $\overline{h}_{max}$ for channel slopes of .05011, .08429, and .1192	131
53	Development curves for small values of average maximum depth $\overline{h}_{max}$ for channel slopes of .05011, .08429, and .1192	136

LIST OF FIGURES (Cont'd)

Figure No.	Title	Page No.
54	Graph of relations between average maximum depth $\overline{h}_{max}$ and dimensionless wave period T' for: periodic permanent wave theory with Froude number of 3.5, periodic permanent wave experiments in channel with slope of .05011, and natural wave experiments in channel with slope of .05011	145
55	Graph of relations between average maximum depth $\overline{h}_{max}$ and dimensionless wave period T' for: periodic permanent wave theory with Froude number of 4.6, periodic permanent wave experiments in channel with slope of .08429, and natural wave experiments in channel with slope of .08429	146
56	Graph of relations between average maximum depth $\overline{h}_{max}$ and dimensionless wave period T' for: periodic permanent wave theory with Froude number of 5.6, periodic permanent wave experiments in channel with slope of .1192, and natural wave experiments in channel with slope of .1192	147
57	Graph of relations between average maximum depth $\overline{h}_{max}$ and dimensionless wave period T' for: periodic permanent wave theory with Froude number of 3.7, periodic permanent wave experiments in rough channel with slope of .1192, and natural wave experiments in rough channel with slope of .1192	148
58	Graph of theoretical period permanent water-surface profiles including effects of variable friction factor f and side-walls, Froude number = 5.6, dimensionless wave length $S_o\lambda/h_n = 27.3$	169
59	Drawing of typical shape of shock front, based on periodic permanent wave run with F = 5.60, $S_o = .1192$, T' = 4.25	172

LIST OF FIGURES (Cont'd)

Figure No.	Title	Page No.
60	Graph of measured geometric properties for shock front: average depth of shock front h_e, length of shock front L_j, and volume of shock front per unit width $h_e L_j$, all expressed as a function of ratio between depth at crest and depth at trough h_{max}/h_{min}	179
61	Graph of experimental values and theoretical solutions (from modified and unmodified theory) for h_{max}, h_{min}, and c as functions of dimensionless wave period T' for periodic permanent waves: Froude number = 3.5, channel slope = .05011	182
62	Graph of experimental values and theoretical solutions (from modified and unmodified theory) for h_{max}, h_{min}, and c as functions of dimensionless wave period T' for periodic permanent waves: Froude number = 4.6, channel slope = .08429	183
63	Graph of experimental values and theoretical solutions (from modified and unmodified theory) for h_{max}, h_{min}, and c as functions of dimensionless wave period T' for periodic permanent waves: Froude number = 5.6, channel slope = .1192	184
64	Graph of experimental values and theoretical solutions (from modified and unmodified theory) for h_{max}, h_{min}, and c as functions of dimensionless wave period T' for periodic permanent waves: Froude number = 3.7, rough channel, channel slope = .1192	185
65	Graph of the length of hydraulic jumps L_j in sloping channels as a function of the Froude number at the minimum depth F_{min} (from Chow (29))	187

LIST OF TABLES

Table No.	Title	Page No.
1	Sieve Analysis of Sand in Rough Channel	47
2	Types of Measurements Obtained for Each Slope and Discharge	57
3	Correction Lengths Added to Smooth-Inlet Development Relations	73
4	Hydraulic Characteristics of Laboratory Channel	76
5	Basic Data for Natural Roll Waves	82
6	Basic Data for Periodic Permanent Roll Waves	109
7	Observed Wave Shape for Periodic Permanent Roll Waves	112
8	Values of h_{max}/h_n for Twelve Consecutive Natural Waves	118
9	Wave Velocities during Overtaking	120
10	Maximum Average Wave Depths After Ghambarian	121
11	Summary of Santa Anita Data	125
12	Slopes and Widths for Santa Anita Channel	127
13	Observed Dimensionless Wave Lengths of Small Amplitude Natural Roll Waves	137
14	Sample Calculations of Maximum Depth for Channel with a Break in Slope	202

CHAPTER I

INTRODUCTION

When water flows down a long and sufficiently steep open channel, it is found that the depth of flow is not uniform as it would be if the same channel had a very small slope. The flow is characterized by a series of hydraulic bores that extend across the width of the channel and propagate downstream. Across these bores or shocks the depth of flow varies abruptly. Between successive bores the depth of flow varies gradually. Waves of this kind are termed roll waves and flows with such waves are called slug flows by some workers. Figure 1 shows a typical roll wave train.

In 1904 Cornish (1)* observed and elegantly described roll waves in prismatic or artificial channels which is the type of channel in which they are usually observed. However they have also been observed in a superglacial stream (2) which indicates that roll waves are not restricted to artificial channels.

The maximum depth of flow in a roll wave train must necessarily be greater than the normal or undisturbed depth. Thus a prismatic channel designed to convey a discharge at normal depth, may not be capable of conveying this same discharge with roll waves present without some of the water leaving the confines of the channel. A dramatic example of this was observed by Holmes (3) in a channel

*Numbers in parentheses refer to publications listed in the Bibliography.

Negative No. 7804

Fig. 1. View of roll waves in Santa Anita Wash, Arcadia, California, about one mile downstream of inlet, discharge about 195 cfs

that had water overtopping the 8 ft side walls when the discharge was estimated to be less than 25 per cent of the design discharge. Thus the practical need for understanding the mechanics of roll waves is clear.

In general one would like to be able to predict whether a channel will exhibit roll waves for any particular discharge. Furthermore, if roll waves are to be present, it is desirable to know where they will start, and how high they will be at any section of the channel. From the present knowledge (1967) of roll waves, one can determine the necessary conditions for roll waves to exist. However the sufficient conditions (the length of channel), and the dimensions of a developing roll wave train have not been defined.

The purpose of this investigation is to describe the geometric properties of roll wave trains that develop naturally from a turbulent flow at normal depth in a wide rectangular channel on a constant slope. This was done by means of experiments in a steep laboratory channel where roll waves formed naturally. Some analytical work also aided in the understanding of the basic phenomenon.

In Chapter II the previous work on roll waves is summarized. In Chapter III theories for small amplitude perturbations on a uniform flow, and large amplitude periodic permanent roll wave trains are presented. Chapter IV describes the laboratory experiments performed, the results of which are in Chapter V. In Chapter VI these results are discussed and compared with theory where possible.

The large amplitude theory is examined closely in Chapter VII and modified to substantially improve the agreement between theory and experiment. In Chapter VIII methods for utilizing the results of this study to determine maximum depths for roll wave trains are presented. In Chapter IX the primary results and conclusions are stated.

CHAPTER II

PREVIOUS STUDIES

This chapter summarizes the significant analytical and experimental work that has been done on roll waves. First, the basic differential equations that are used in all of the analytical studies to be discussed will be considered.

II-A BASIC EQUATIONS

The continuity equation for a flow of an incompressible fluid in an open channel is,

$$A_t + (uA)_x = 0 \tag{2.1}$$

where $A = A(x,t)$ is the cross-sectional area of the fluid, $u = u(x,t)$ is the average velocity (Q/A, where $Q = Q(x,t)$ is the discharge in volume of fluid per unit of time) over A, x is the coordinate along the channel, t is time, and the subscripts x and t denote partial derivatives with respect to these variables.

Flows with roll waves are characterized by typical horizontal dimensions (wave lengths) that are large compared to typical vertical dimensions (water depths), so that the well-known shallow-water equations are valid. For a turbulent flow in an inclined channel, the integrated (over the cross-section A) form of the momentum equation is,

$$u_t + \alpha u\, u_x + (1-\alpha)\frac{u}{A} A_t + g\, h_x = g\, S_o - \frac{1}{\rho}\frac{\tau_o}{r}\,. \tag{2.2}$$

In this equation:

$S_o = \sin\theta$, θ = angle of inclination of channel;

$h = h(x,t)$ = depth of flow in cross section;

g = gravitational constant (32.16 ft/sec^2);

$$\alpha = \frac{1}{Au^2}\int_A u_p^2\, dA = \text{velocity distribution coefficient;} \qquad (2.3)$$

$u_p = u_p(x,y,z,t)$ = fluid velocity at the point (y,z) in the cross section A;

ρ = mass density of fluid;

$\tau_o = \tau_o(x,t)$ = shear stress in the x-direction averaged over the channel walls and bottom; and

$r = r(x,t)$ = A/(wetted perimeter of channel) = hydraulic radius.

Equation 2.2 can be derived from the Navier-Stokes equations by assuming that the predominate motion is in the x-direction, and thus for example the term v_t is small compared to u_t. Equation 2.2 implies that the pressure distribution in a cross section is hydrostatic. A particularly lucid derivation of this equation has been given by Keulegan and Patterson (4).

In all of the studies concerning roll waves, τ_o has been evaluated by using a relation derived from uniform flow considerations. A uniform flow is one in which all partial derivatives in the x-direction are zero, $\partial/\partial x \equiv 0$, and by definition the depth of flow for a uniform flow is the normal depth, h_n. For example, from the Chezy equation there results,

$$\tau_o = \rho f u_n^2/8 \qquad (2.4)$$

where u_n is the average velocity (Q/A) for uniform flow, and f is the Darcy-Weisbach friction factor. It has been assumed that this same relation is valid for unsteady, gradually varied flow, where u_n is replaced by u. For uniform flows f varies with the Reynolds number and/or the relative roughness. In some roll wave studies it has been assumed that f does not vary in the x-direction and is equal to its value for uniform flow. However in cases where f has not been held fixed, its variation in the x-direction has been assumed to have the same dependence on the Reynolds number (smooth channel) or relative roughness (rough channel) as it does for uniform flows.

II-B CRITERIA FOR UNSTABLE FLOW

The majority of the literature on roll waves is concerned with the determination of the necessary conditions under which roll waves can exist. The approach has been to investigate the stability of a uniform flow on a constant slope by imposing small free-surface perturbations on it. If these perturbations increase in amplitude as time increases, the flow is said to be unstable. Presumably these small amplifying perturbations would eventually result in the clearly visible large amplitude roll waves. (Figure 1)

Jeffreys (5) considered a wide rectangular channel, uniform velocity distribution ($\alpha = 1$), and an unvarying friction factor (f). For this case, the condition for an unstable flow was that the Froude number F, ($F = u_n / \sqrt{gh_n}$, h_n = normal depth) be greater than 2.

Since Jeffreys, many others (6, 7, 8, 9) have derived criteria of varying degrees of generality. Dressler and Pohle (7) considered a wide rectangular channel, $\alpha = 1$, and a general power law resistance relation (τ_o = const. u^n/h^m). Craya (6) considered a channel of arbitrary shape, $\alpha = 1$, and a power law resistance. Iwasa (8) developed a general expression for the critical Froude number (F_{cr}) applicable for arbitrary channel shape, friction law, and value of α. Using Iwasa's result for a rectangular channel of any width, Koloseus (9) has evaluated values of F_{cr} by using the logarithmic resistance law for both a smooth and a rough boundary.

From all of these studies there results F_{cr} values which in general depend on the channel shape, frictional resistance law, and the value of α. The value of F_{cr} is 2.0 for a wide rectangular channel with an unvarying f. If f is evaluated from the logarithmic resistance law, F_{cr} for a wide rectangular channel (rough or smooth) depends slightly on f, but is about 1.6 for f = .02. F_{cr} is increased as α is increased, and also increases as the rectangular channel becomes narrower. In general, channels of other shapes, such as circular or triangular, have a higher F_{cr} than a rectangular channel.

A flow with a value of F considerably higher than F_{cr} may not exhibit visible roll waves. This fact was noted by Montouri (10) in his investigation of field data collected in Europe and Russia. This led him to develop a criterion for predicting formation of roll waves (but not their dimensions), involving not only the value of F_{cr}, but also the length of the channel. From this criterion, one finds that

as the discharge and hence normal depth increases, the length required for visible roll waves to develop also increases. This basic observation is most important in studying the development of roll waves.

II-C LARGE AMPLITUDE WAVE STUDIES

Prior to 1940 Thomas conducted experiments on artificially produced periodic permanent roll waves (to be considered in Chapter III) in a laboratory channel. This study is referred to in a paper by Thomas (11) but personal communication with him revealed that his results were never published and have since been lost. However, he did state that his experiments gave a satisfactory check on the theoretical analysis of periodic permanent waves.

In 1954 laboratory work on roll waves was done at Kyoto University in a smooth channel 36 feet long. This work was referred to in a later paper by Ishihara et al. (12). By contacting personnel at Kyoto, it was found that the data taken were not sufficient to describe the growth of roll waves as a function of the distance along the channel. In fact for many runs depths were not measured.

In a recent paper (1965), Ghambarian (13) discusses some laboratory work that has been done in the Armenian Soviet Socialist Republic. The channel slope varied from $S_o = .10$ to $.86$, and the length from 10 m to 60 m. Roll waves developed naturally and measurements of maximum depth, wave length, wave velocity, and wave period were taken at various stations along the channel. Frequency distributions of these quantities were measured as a function of distance along the channel.

Unfortunately the results of maximum depth vs. distance for all slopes are compressed into one small graph and only the experimental relations are shown without the numerical data that were used to derive these relations. However in the paper for $S_o = .10$ by Ghambarian and Mayilian (14) the experimental points were taken from a graph. These data, along with some extracted from the 1965 paper will be presented in Chapter V. More information concerning these experiments will be presented also.

In 1965 the Los Angeles County Flood Control District conducted a field study in Santa Anita Wash located in Arcadia, California. Data on the roll waves that developed were taken and will be presented in Chapter V along with a description of the experiments.

The first attempt to describe large amplitude roll waves analytically was by Thomas (11). He considered a periodic train of waves of constant shape and velocity (permanent). By piecing together two gradually varied water-surface profiles for unsteady flow, he managed to construct a wave profile similar to observed roll waves. Dressler (15), using Thomas's basic ideas, was able to find closed form solutions for a wide rectangular channel with an unvarying friction factor. In Chapter III the procedure for constructing these periodic permanent solutions will be given.

II-D FRICTION FACTORS IN UNSTABLE FLOWS

When the Froude number for a flow is greater than F_{cr}, the flow is said to be unstable. Some investigators have found that in unstable flows the friction factor measured in a reach of uniform flow is a function of the Froude number as well as the relative roughness (rough boundary) or Reynolds number (smooth boundary). Koloseus (16) found this Froude number effect in a rough channel, and Rouse (17) found it in a smooth channel.

In the course of the present investigation friction factors were measured in two smooth channels: a 130 ft tiltable channel, and a steep aluminum channel. The Froude number effect noted above was not detected in either of these channels. These results for the 130 ft channel are included in a published discussion of Rouse's paper (17), which is in Appendix I. The hydraulic characteristics of the steep aluminum channel are given in Chapter V.

II-E SUMMARY

After presenting the basic equations used for roll wave investigations, the significant studies that have been done on roll waves were discussed. The criterion for unstable flow can be expressed by a critical Froude number which in general depends on the channel shape, frictional resistance law, and the velocity distribution in a cross section. Some analytical work on non-linear waves has been done for a periodic permanent wave train. The only available laboratory data on roll wave development were discussed briefly and will be presented in Chapter V, along with some available field data.

CHAPTER III

ANALYTICAL INVESTIGATION

The laboratory results to be presented in Chapter V show that the geometric properties of roll waves (i.e. maximum and minimum depth, wave length, etc.) are not only functions of distance along the channel, but vary from one wave to another at a fixed station. This was observed both for the small amplitude waves with a continuous water surface (which occurred downstream of the uniform flow and upstream of the shock waves), and the large amplitude shock waves. Thus a complete theory for describing natural roll waves must be able to predict the frequency distributions of the geometric properties as a function of distance. Needless to say, no such theory exists.

In this chapter two theories are presented for periodic wave trains; one for small amplitude sinusoidal waves, and the other for large amplitude permanent waves with shocks. Because of the periodicity assumption, it is clear from the above description that these theories do not directly relate to natural roll waves. However it will be shown in Chapter VII that the large amplitude theory is at least indirectly related to natural roll waves in terms of average values of the geometric properties. Periodic permanent waves were produced in the laboratory channel and in Chapter VI their characteristics will be compared with the theory. Also in Chapter VI it will be shown that some trends derived from the small amplitude theory agree with the observations on the small amplitude natural waves.

III-A SMALL AMPLITUDE THEORY

1. Statement and Solution of Problem

Jeffreys (5) imposed a small sinusoidal perturbation on a uniform flow in a wide rectangular channel with an unvarying friction factor. The result was that for a value of F of two the disturbance was neutrally stable, or its amplitude neither increased or decreased with time. In fact all of the work on stability criteria discussed in Chapter II was concerned with finding this neutrally stable condition.

The object of this investigation, as stated above, is to study the development of natural roll wave trains from a uniform flow. This development only occurs if the uniform flow is unstable and therefore the growth rates of small perturbations for Froude numbers above 2.0 are of interest.

For a wide rectangular channel ($r = h$), $\alpha = 1$, and the simplifying assumptions outlined in Chapter II, equations 2.1 and 2.2 become,

$$h_t + (uh)_x = 0 \tag{3.1}$$

$$u_t + uu_x + gh_x = gS_o\,(1 - u^2/F^2\,gh), \tag{3.2}$$

after using the relation,

$$f = 8S_o/F^2 \tag{3.3}$$

which results from assuming that f does not vary from its value at uniform flow. To render these equations dimensionless the following dimensionless quantities are introduced:

$$x' = x/\lambda, \quad \lambda = \text{wave length;} \tag{3.4}$$

$$t' = u_n t/\lambda, \; u_n = \text{normal velocity } (q/h_n); \tag{3.5}$$

$$H = h/h_n, \quad h_n = \text{normal depth; and} \tag{3.6}$$

$$U = u/u_n. \tag{3.7}$$

Equations 3.1 and 3.2 can now be written as,

$$H_{t'} + (UH)_{x'} = 0 \tag{3.8}$$

$$U_{t'} + UU_{x'} + H_{x'}/F^2 = (S_o/F^2)\,(\lambda/h_n)(1 - U^2/H) \tag{3.9}$$

where F is the Froude number for uniform flow ($F = u_n/\sqrt{gh_n}$).

Equations 3.8 and 3.9 are now linearized by assuming that the deviations from the undisturbed or uniform flow condition are small. This assumption is expressed as,

$$U = 1 + U' \tag{3.10}$$

$$H = 1 + \eta \tag{3.11}$$

where U' and η are the perturbation quantities which are small compared to unity. It is further assumed that the derivatives of U' and η are also small compared to unity. Substituting equations 3.10 and 3.11 into 3.8 and 3.9, and neglecting products of any two small terms (i.e. $U'U'_{x'}$, $U'\eta_{x'}$, $\eta U'_{x'}$, etc.), yields two linear equations,

$$\eta_{t'} + \eta_{x'} + U'_{x'} = 0 \tag{3.12}$$

$$U'_{t'} + U'_{x'} + \eta_{x'}/F^2 = (S_o/F^2)\,(\lambda/h_n)\,(\eta - 2U') \tag{3.13}$$

The quantity U' is then eliminated from equations 3.12 and 3.13 to give a second order linear partial differential equation for η,

$$(1 - 1/F^2)\,\eta_{x'x'} + 2\eta_{x't'} + \eta_{t't'} + (S_o/F^2)(\lambda/h_n)(3\eta_{x'} + 2\eta_{t'}) = 0 \qquad (3.14)$$

A sinusoidal perturbation can be expressed as the real part of,

$$\eta = \eta_o \exp\left[i\, 2\pi\, (x' - Ct')\right] \qquad (3.15)$$

which is equivalent to,

$$\eta = \eta_o e^{2\pi C_i t'} \exp\left[i\, 2\pi\, (x' - C_r t')\right] \qquad (3.16)$$

where:

η_o = the amplitude at $t' = 0$;

$C = C_r + iC_i$ dimensionless complex velocity;

C_r = dimensionless phase velocity of the perturbation η; and

C_i = dimensionless number pertaining to the growth rate.

To convert the amplitude of the perturbation $(\eta_o e^{2\pi C_i t'})$ from a function of time to a function of distance, the expression,

$$\ell = ct \qquad (3.17)$$

is used, where ℓ is the dimensional distance over which the wave train travels in the time t, and c is the dimensional phase velocity. Using the expression,

$$C_r = c/u_n \qquad (3.18)$$

and equations 3.5 and 3.17, an expression for t' can be written as,

$$t' = (h_n / C_r \lambda)(\ell / h_n) \tag{3.19}$$

Then equation 3.16 can be expressed as,

$$\eta = \eta_o e^{(2\pi C_i / C_r Y)(S_o / F^2)(\ell / h_n)} \exp\left[i2\pi (x' - C_r t')\right] \tag{3.20}$$

where Y is defined by,

$$Y \equiv (S_o / F^2)(\lambda / h_n). \tag{3.21}$$

Y is a dimensionless wave length, and the term $(2\pi C_i / C_r Y)$ will be referred to as the amplification factor.

The problem is reduced to finding a solution for the amplification factor and C_r. When these two quantities are known, equation 3.20 shows that the behavior of η will be known. To obtain the expressions involving C_i and C_r, equation 3.15 is substituted into equation 3.14 which results in,

$$2\pi \left[2C - C^2 - (1 - 1/F^2)\right] + iY(3-2C) = 0 \tag{3.22}$$

Separating real and imaginary parts of this equation leads to,

$$\pi \left[2 C_r + C_i^2 - C_r^2 - (1 - 1/F^2)\right] + C_i Y = 0 \tag{3.23}$$

$$4\pi C_i (1 - C_r) + Y (3 - 2C_r) = 0. \tag{3.24}$$

These two equations give,

$$C_r = (3Y + 4\pi C_i)/(2Y + 4\pi C_i) \tag{3.25}$$

$$F = 1/\sqrt{1 - (2C_r + C_i^2 + C_r^2 + C_i Y/\pi)} \tag{3.26}$$

These expressions show that the quantities C_r and C_i are functions of Y and F, and thus the amplification factor can also be expressed in terms of Y and F. The functional relationships for the amplification factor and the phase velocity were determined numerically for values of F of 2.5, 3.5, and 5.0, and are shown in figures 2 and 3.

The neutrally stable solution occurs when the amplitude does not change with time which requires the value of C_i to vanish. Then from equations 3.25 and 3.26 there results,

$$C_r = 3/2 \tag{3.27}$$

$$F = 2 \tag{3.28}$$

which was the solution obtained by Jeffreys (5).

For small values of Y ($Y << 1$) equations 3.23 and 3.24 become,

$$2C_r + C_i^2 - C_r^2 - (1 - 1/F^2) = 0 \tag{3.29}$$

$$C_i (1 - C_r) = 0 \tag{3.30}$$

Equation 3.30 requires that C_r equal unity, or that C_i is of the same order of magnitude as Y. If C_r is unity, equation 3.29 shows that C_i must be imaginary which it is not. Therefore C_i is also small, and equation 3.29 is further simplified to,

$$C_r^2 - 2C_r + (1 - 1/F^2) = 0 \tag{3.31}$$

from which there results,

$$C_r = 1 + 1/F \tag{3.32}$$

Then equation 3.24 yields,

$$2\pi C_i / C_r Y = F(1/2F - 1)/(1 + F) \tag{3.33}$$

This asymptotic solution for the amplification factor is shown on figure 2.

For large values of Y (Y>> 1) equations 3.23 and 3.24 become,

$$\pi\left[2C_r - C_r^2 - (1 - 1/F^2)\right] + C_i Y = 0 \tag{3.34}$$

and

$$Y\,(3 - 2C_r) = 0 \tag{3.35}$$

from which results,

$$C_r = 3/2 \tag{3.36}$$

and

$$2\pi\, C_i / C_r Y = (1/4 - 1/F^2)\, 4\pi^2/3Y^2 \tag{3.37}$$

This asymptotic solution is shown on figure 2.

2. Discussion of Solution

The solution for η is given by equation 3.20 where the amplification factor and phase velocity are shown in figures 2 and 3, respectively. At a fixed time $t \geq 0$, the solution describes a train of sinusoidally shaped waves, each wave having the same amplitude, phase velocity, and wave length. Furthermore this train of waves extends indefinitely along the channel because x was not restricted in

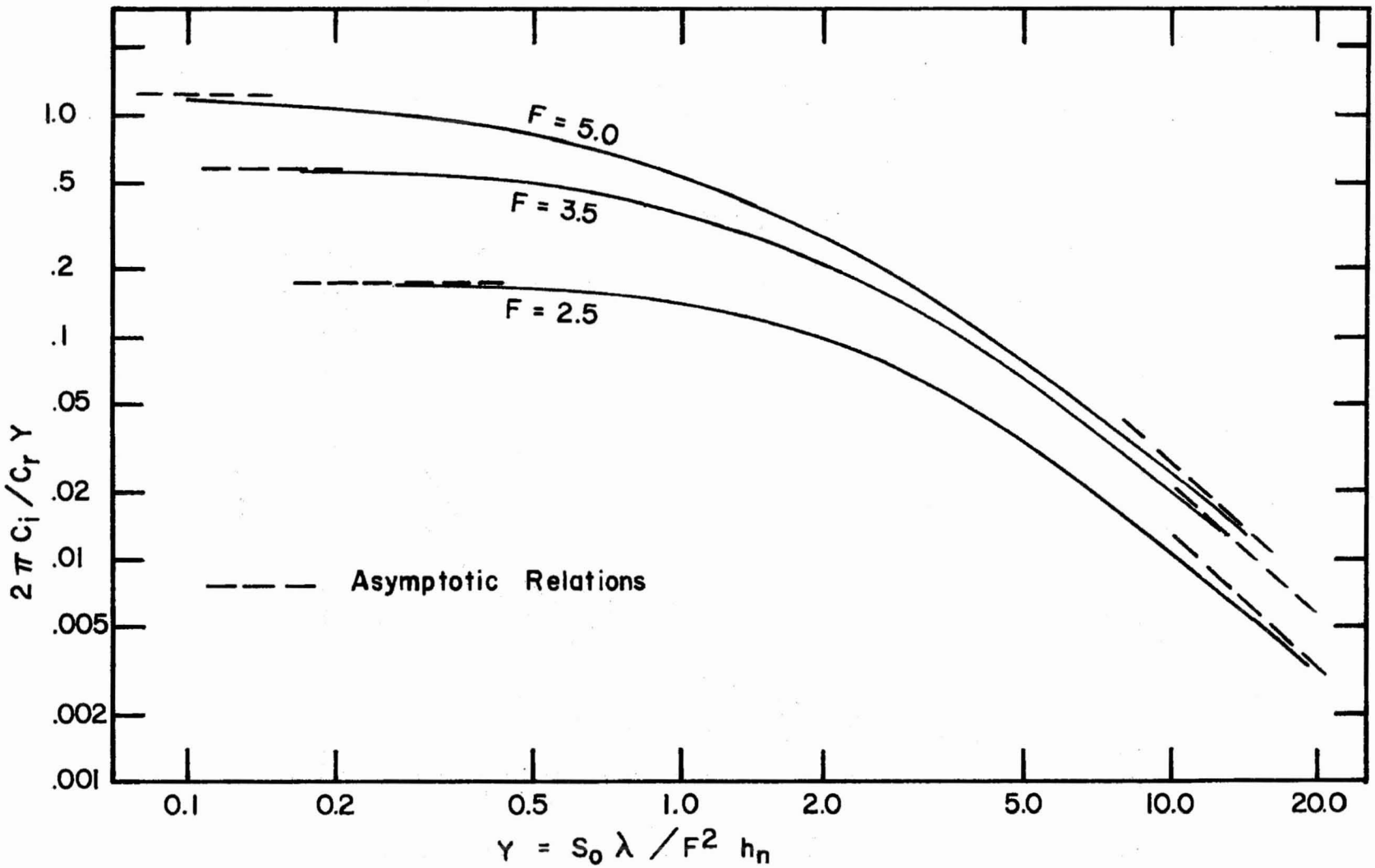

Fig. 2. Graph of dimensionless amplification factor, $2\pi C_i/C_r Y$, against $S_o\lambda/F^2h_n$ from small amplitude theory

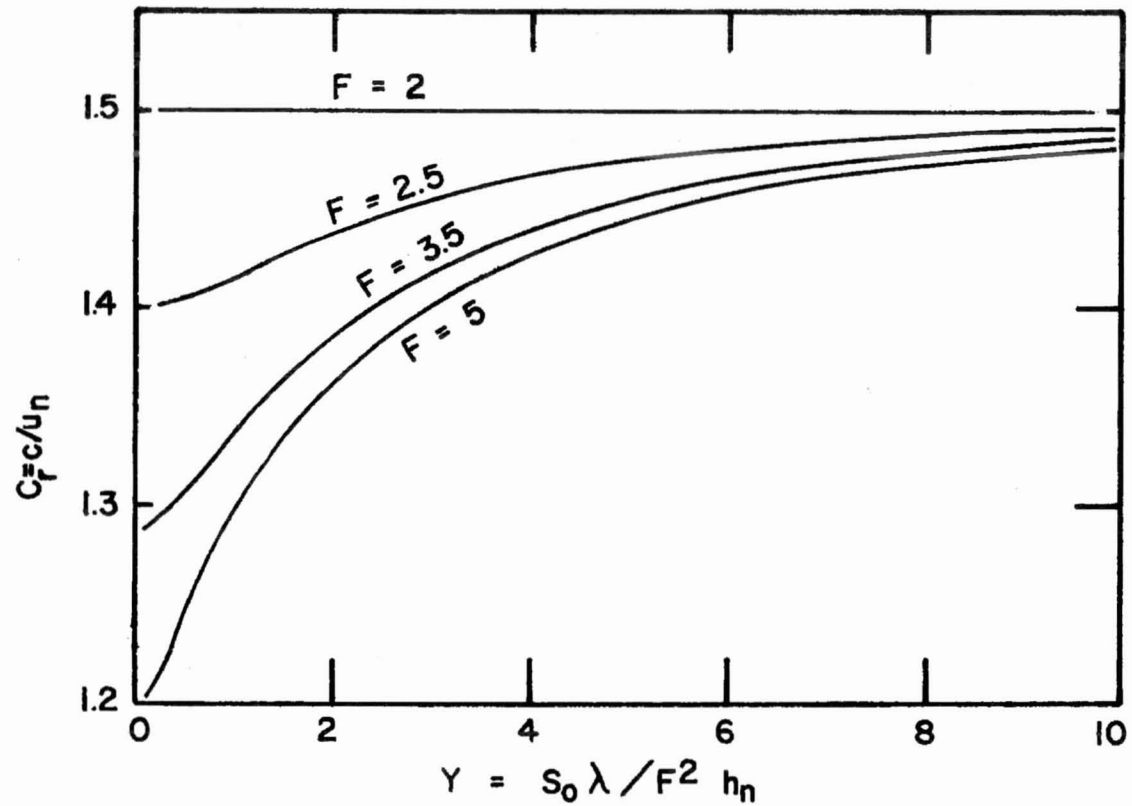

Fig. 3. Graph of dimensionless wave velocity, C_r, against $S_o\lambda/F^2h_n$ from small amplitude theory

any way. As t increases, the amplitude of each wave increases exponentially (if $F > 2$), but according to equation 3.20 the wave shape and phase velocity remain the same.

Amplitudes of natural roll waves increase as the waves travel along the channel, and ultimately shock waves are formed. Therefore it is clear that at a fixed time the amplitudes of natural roll waves increase in the downstream direction, whereas in the theory it was assumed that all waves had the same amplitude at a fixed time. It is likely that a theory in which the amplitudes of the waves increased in the x-direction (at any given time) would predict different growth rates than the periodic theory considered here.

Boundary conditions other than the initial conditions (periodic in x)used here would be required to obtain a better model for natural roll waves, although it is not obvious what these might be. In general this would lead to a more difficult problem than was considered above, because of the additional dependence on x. However the above theory is useful for obtaining at least qualitative results concerning the effect of wave length and Froude number on the growth rate.

The growth rate will be defined as the rate of increase of the maximum depth (or the amplitude) with respect to distance along the channel. From equation 3.20 the growth rate becomes,

$$\partial\eta_{max}/\partial(\ell/h_n) = \eta_{max}(2\pi C_i/C_r Y)(S_o/F^2) \qquad (3.38)$$

where η_{max} is the amplitude,

$$\eta_{max} = \eta_o \exp\left[(2\pi C_i/C_r Y)(S_o/F^2)(\ell/h_n)\right] \qquad (3.39)$$

which varies with ℓ. Equation 3.3 shows that the term S_o/F^2 is related to the friction factor which varies very little with slope or Froude number in a given channel. Therefore it suffices to examine the amplification factor to determine the effect of wave length and Froude number on the growth rate.

From figure 2 the growth rate is seen to increase as the wave length decreases and essentially to attain its maximum value at values of Y such that the shallow water theory is still valid. For example with F = 5 the maximum amplification factor is reached at about Y = .1, so that the value of λ/h_n is about 50 if the slope is .05 which is a practical situation. The occurrence of a wave length with a maximum growth rate is usually interpreted to mean that this will be the observed wave length in a situation where disturbances of all wave lengths are amplifying. In this case one would expect to observe any wave length corresponding to the small values of Y where the curves of figure 2 are almost horizontal.

Figure 2 shows that the growth rate increases as the Froude number increases. Transferring this result to natural roll waves, it is not unreasonable to expect that roll waves will appear at increasingly shorter distances from the beginning of the channel as the Froude number is increased, providing the initial disturbances are of the same size.

By considering a problem where η was prescribed as a function of time at the entrance to a channel, Lighthill and Whitham (18) found the solution valid near the wave front of the disturbance initiated at the entrance. The amplitude of their solution is precisely the same as the amplitude of the above solution for small values of Y (equations 3.33 and 3.39). Although the full significance of this is not clear, it presumably serves as a check on the present work.

III-B. LARGE AMPLITUDE PERIODIC PERMANENT ROLL WAVE THEORY

The method of solution presented here is essentially that used by Dressler (15) except that the introduction of the normal depth into the theory is new.

1. Statement and Solution of Problem

A wide rectangular channel with a friction factor that does not vary from its value at uniform flow is considered (equation 3.2). A permanent wave is one whose shape and velocity does not change with time or position. Thus for a permanent wave the t variable can be eliminated by introducing a coordinate system that moves with the wave at the velocity of the wave. Such a coordinate for a wave traveling in the + x direction is $X = x - ct$, where c is the constant wave velocity. Thus for a permanent wave, $u(x,t) = u(X)$, and $h(x,t) = h(X)$. The derivatives are transformed by,

$$\partial/\partial t = -c\, \partial/\partial X, \quad \partial/\partial x = \partial/\partial X. \tag{3.40}$$

Equations 3.1 and 3.2 reduce to two ordinary differential equations in u and h. Combining to eliminate u gives,

$$dh/dX = S_o \frac{h^3 - (ch - K)^2/gF^2}{h^3 - h_c^3} \tag{3.41}$$

where

$$K = (c - u)\, h = \text{constant} \tag{3.42}$$

and

$$h_c^3 \equiv K^2/g. \tag{3.43}$$

This definition of h_c will prove to be very convenient.

The shock condition which relates h_{max} to h_{min} is now considered (figure 4). It is assumed that the thickness of the shock is sufficiently small so that the x-component of its weight is small compared to the pressure forces, the pressure distribution is hydrostatic, and the velocity distribution is uniform ($\alpha = 1$). These assumptions will be discussed in Chapter VII, with the aid of the experimental results. Equating the pressure forces across the shock to the net momentum flux through the shock results in,

$$c = u_{min} + \sqrt{g \frac{h_{max}}{h_{min}} \frac{h_{max} + h_{min}}{2}}\,. \tag{3.44}$$

This is a familiar form for wave velocities of shallow water waves. This can also be written,

$$h_{max}/h_{min} = 1/2 \left[\sqrt{1 + 8 \frac{(c-u_{min})^2}{gh_{min}}} - 1\right]. \tag{3.45}$$

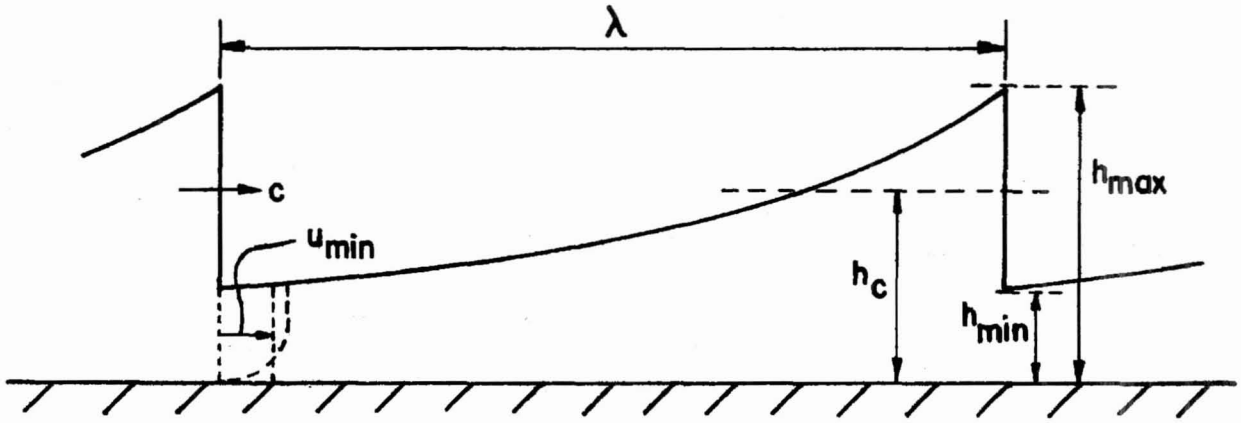

Fig. 4. Definition sketch for periodic permanent roll waves

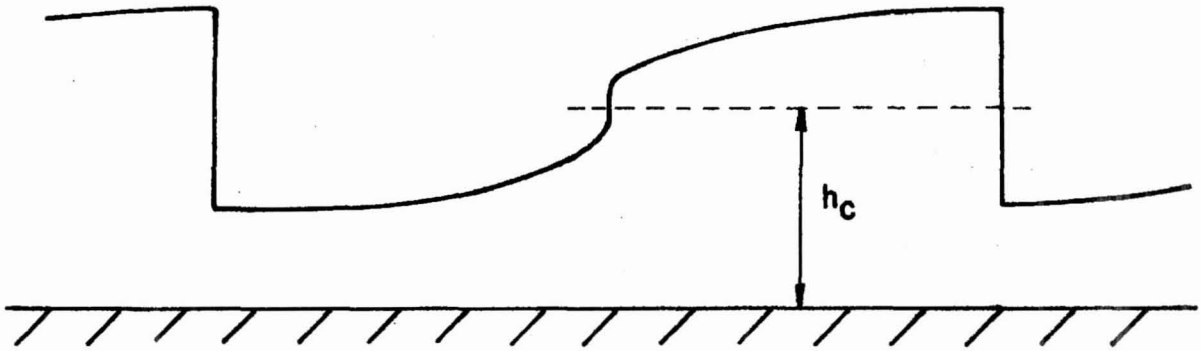

Fig. 5. Periodic permanent roll wave water-surface profile with point of inflection

Setting c equal to zero in equation 3.45 gives the expression commonly used for a hydraulic jump on a horizontal channel. Thus the shock considered here can be regarded as a moving hydraulic jump.

Using the expression for K and the definition of h_c, equation 3.45 can be written,

$$h_{max}/h_{min} = 1/2 \left[\sqrt{1 + 8\,(h_c/h_{min})^3} - 1 \right]. \qquad (3.46)$$

From equation 3.46 it is seen that when h_c/h_{min} equals unity, the value of h_{max}/h_{min} is also unity. Furthermore if h_c is less than h_{min}, h_{max} is required to be less than h_{min} which is meaningless. Therefore,

$$h_c/h_{min} \geq 1 \qquad (3.47)$$

Solving equation 3.46 for h_{max}/h_c gives,

$$h_{max}/h_c = 1/2 \left[\sqrt{(h_{min}/h_c)^2 + 8\,h_c/h_{min}} - h_{min}/h_c \right] \qquad (3.48)$$

from which it is clear that,

$$h_{max}/h_c \geq 1 \qquad (3.49)$$

Therefore h_c is in the closed interval from h_{min} to h_{max} or,

$$h_{min} \leq h_c \leq h_{max} \qquad (3.50)$$

Now if the wave train is assumed periodic, there is only one value of h_{min} and h_{max} for all waves. Equation 3.50 insures that h_c must exist at some section between successive shocks on the gradually varying water surface. However equation 3.41 requires the value of

dh/dx to approach infinity at $h = h_c$ unless the numerator vanishes at $h = h_c$. A periodic solution with dh/dx infinite at h_c would appear as in figure 5, where h_c is a point of inflection. However a point of inflection requires d^2h/dX^2 to vanish at $h = h_c$, which Dressler showed to be impossible.

The correct solution is one in which the numerator of equation 3.41 vanishes at $h = h_c$, which results in a smooth water surface, concave upwards. Setting the numerator of equation 3.41 to zero for $h = h_c$, and using equation 3.43 to eliminate K, results in an expression for c,

$$c/\sqrt{gh_c} = 1 + F, \tag{3.51}$$

Both the numerator and denominator of equation 3.41 are cubic algebraic expressions with h_c as one of the three roots. This common root can be factored out and equation 3.41 can be written as,

$$dh/dX = S_o \frac{(h^*-h_a^*)(h^*-h_b^*)}{h^{*2} + h^* + 1} \tag{3.52}$$

where an asterisk denotes division by h_c. The dimensionless quantities h_a^* and h_b^* are the other two roots, besides h_c (or $h_c^* = 1$), of the numerator. By equating the numerator of equation 3.52 to that of equation 3.41, and using equation 3.43 to eliminate K and equation 3.51 to evaluate c, there results,

$$h_{a,b}^* = (1/2F^2)\left[1 + 2F \pm \sqrt{1 + 4F}\right] \tag{3.53}$$

where the positive square root is used for h_a^*, and the negative square root for h_b^*, so that $h_a^* > h_b^*$.

Equation 3.52 can be integrated, and with $X = 0$ at $h = h_c$ there results,

$$S_o X^* = (h^* - 1) + A \ln \frac{h^* - h_a^*}{1 - h_a^*} - B \ln \frac{h^* - h_b^*}{1 - h_b^*} \tag{3.54}$$

where $$A = \frac{1 + h_a^* + h_a^{*2}}{h_a^* - h_b^*} \qquad B = \frac{1 + h_b^* + h_b^{*2}}{h_a^* - h_b^*} \tag{3.55}$$

and $X^* = X/h_c$

This relation between X^* and h^* has the general shape shown in figure 4. Evaluating equation 3.54 at h^*_{max} and h^*_{min} gives an expression involving the wave length,

$$S_o \lambda^* = (h^*_{max} - h^*_{min}) + AK_1 - BK_2 \tag{3.56}$$

where $$K_1 = \ln \frac{h^*_{max} - h_a^*}{h^*_{min} - h_a^*} \qquad K_2 = \ln \frac{h^*_{max} - h_b^*}{h^*_{min} - h_b^*} \tag{3.57}$$

and $\lambda^* = \lambda/h_c$.

In a particular problem the channel slope, S_o, and the Froude number at uniform flow, F, will be known. Then the relationship between X^* and h^* can be found from equation 3.54. However to determine h^*_{max}, equation 3.56 shows that $S_o \lambda^*$ and h^*_{min} must also be known, which requires two additional relations involving λ^*, h^*_{max}, and h^*_{min}. The shock condition, equation 3.46, provides a relation between the quantity h^*_{max}/h^*_{min} and h^*_{min}. Therefore a unique solution exists between h^* and X^* (including h^*_{max} and h^*_{min}), for a

given S_o and F, if the value of $S_o\lambda^*$ is also fixed. The above solution is essentially the form of the solution that Dressler (15) presented.

The above solution is in terms of the depth h_c which can not be found from the values of S_o and F (assumed to be given). Therefore it is desirable to have the solution in terms of some known depth. The most significant depth is the undisturbed or normal depth (h_n). Therefore an expression for $h_n^* = h_n/h_c$ will be found. With the value of h_n^* known, the solution can be expressed in terms of h_n.

From the definition of the discharge per unit width and equation 3.42,

$$q(X) \equiv uh = ch(X) - K \tag{3.58}$$

The average discharge over one wave length, and thus the average discharge over all waves, is then,

$$q_{av} = 1/\lambda \int_\lambda q(X)dX = c/\lambda \int_\lambda h(X)dX - K \tag{3.59}$$

If the average depth is defined as,

$$h_{av} = 1/\lambda \int_\lambda h(X)dX \tag{3.60}$$

then equation 3.59 is,

$$q_{av} = ch_{av} - K \tag{3.61}$$

The normal depth depends only on the average discharge and Froude number as can be seen from,

$$h_n \equiv q_{av}/u_n = q_{av}/(F\sqrt{gh_n}) \tag{3.62}$$

An expression for h_n^* is found by eliminating q_{av} between equations 3.61 and 3.62, using equation 3.51 to evaluate c, and using equation 3.43 to evaluate K. The result is,

$$h_n^{*3/2} = \left[(1 + F)\, h_{av}^* - 1\right]/F \tag{3.63}$$

The final step is to find h_{av}^*. First equation 3.60 is rewritten,

$$h_{av}^* = 1/\lambda^* \int_{h_{min}^*}^{h_{max}^*} h^*(X^*)dX^* \tag{3.64}$$

or when equation 3.52 is used to evaluate dX^*,

$$S_o \lambda^* h_{av}^* = \int_{h_{min}^*}^{h_{max}^*} h^* \frac{h^{*2} + h^* + 1}{(h^*-h_a^*)(h^*-h_b^*)} dh^* \tag{3.65}$$

This can also be written as,

$$S_o \lambda^* h_{av}^* = \int_{h_{min}^*}^{h_{max}^*} h^* d\left[h^* + A \ln(h^*-h_a^*) - B \ln (h^*-h_b^*)\right] \tag{3.66}$$

which is in a convenient form for integration by parts. Performing this integration, and using equation 3.56 to evaluate $S_o \lambda^*$, leads to,

$$h_{av}^* = \frac{1/2(h_{max}^{*2} - h_{min}^{*2}) + (A-B)(h_{max}^* - h_{min}^*) + Ah_a^* K_1 - Bh_b^* K_2}{(h_{max}^* - h_{min}^*) + AK_1 - BK_2} \tag{3.67}$$

From the above analysis it can be shown that for a given value of F and $S_o \lambda / h_n$, the wave shape and velocity are uniquely determined. Equations 3.63 and 3.67 show that,

$$h_n^* = f_1\,(F,\ h_{max}^*,\ h_{min}^*) \tag{3.68}$$

where f_1 is some function. From equation 3.56,

$$S_o\lambda/h_c = f_2\ (F,\ h^*_{max},\ h^*_{min}) \tag{3.69}$$

Dividing equation 3.69 by 3.68 gives,

$$S_o\lambda/h_n = f_3\ (F,\ h^*_{max},\ h^*_{min}) \tag{3.70}$$

The shock condition, equation 3.46, gives a relation between h^*_{max} and h^*_{min},

$$h^*_{max} = f_4\ (h^*_{min}) \tag{3.71}$$

For given values of F and $S_o\lambda/h_n$, h^*_{max} and h^*_{min} can in principle be found from the last two equations. Equation 3.68 is then used to convert these to h_{max}/h_n and h_{min}/h_n. Then the value of h^*_n from equation 3.68 is applied to equation 3.51 to get $c/\sqrt{gh_n}$. Therefore it is correct to write,

$$h_{max}/h_n = f_5\ (F,\ S_o\lambda/h_n),\quad h_{min}/h_n = f_6\ (F,\ S_o\lambda/h_n),$$

$$c/\sqrt{gh_n} = f_7\ (F,\ S_o\lambda/h_n) \tag{3.72}$$

The wave shape can be expressed as, (equation 3.54),

$$h^* = f_8\ (F,\ S_oX^*) \tag{3.73}$$

Dividing this by equation 3.68 gives,

$$h/h_n = f_9\ (F,\ h^*_{max},\ h^*_{min},\ S_oX/h_n) \tag{3.74}$$

But equations 3.70 and 3.71 show that h^*_{max} and h^*_{min} are functions of F and $S_o\lambda/h_n$. Thus equation 3.74 becomes,

$$h/h_n = f_{10}\,(F,\ S_o\lambda/h_n,\ S_oX/h_n) \tag{3.75}$$

which is equivalent to,

$$h/h_n = f_{11}\,(X/\lambda,\ F,\ S_o\lambda/h_n) \tag{3.76}$$

Therefore the wave shape (equation 3.76) and velocity (equation 3.72) are unique functions of F and $S_o\lambda/h_n$. The wave period, T, is defined by,

$$\lambda = c\,T \tag{3.77}$$

which leads to the expression,

$$S_o\lambda/h_n = (c/\sqrt{gh_n}\ )(S_oT\sqrt{g/h_n}\ ) \tag{3.78}$$

However because $c/\sqrt{gh_n}$ is a function of F and $S_o\lambda/h_n$,

$$S_o\lambda/h_n = f_{12}\,(F,\ T') \tag{3.79}$$

where

$$T' \equiv S_oT\ \ g/h_n \tag{3.80}$$

Therefore one can prescribe T' instead of $S_o\lambda/h_n$.

The form of the equations is such that the general functions in equations 3.72 and 3.76 can not be written explicitly. The solutions for $c/\sqrt{gh_n}$, h_{max}/h_n, and h_{min}/h_n are plotted in figure 6 for values of F of 2.0, 2.5, 3.5, and 5.0, and values of $S_o\lambda/h_n$ up to 60. These relations were found numerically using a digital computer and the above relations. Instead of starting with values of F and $S_o\lambda/h_n$,

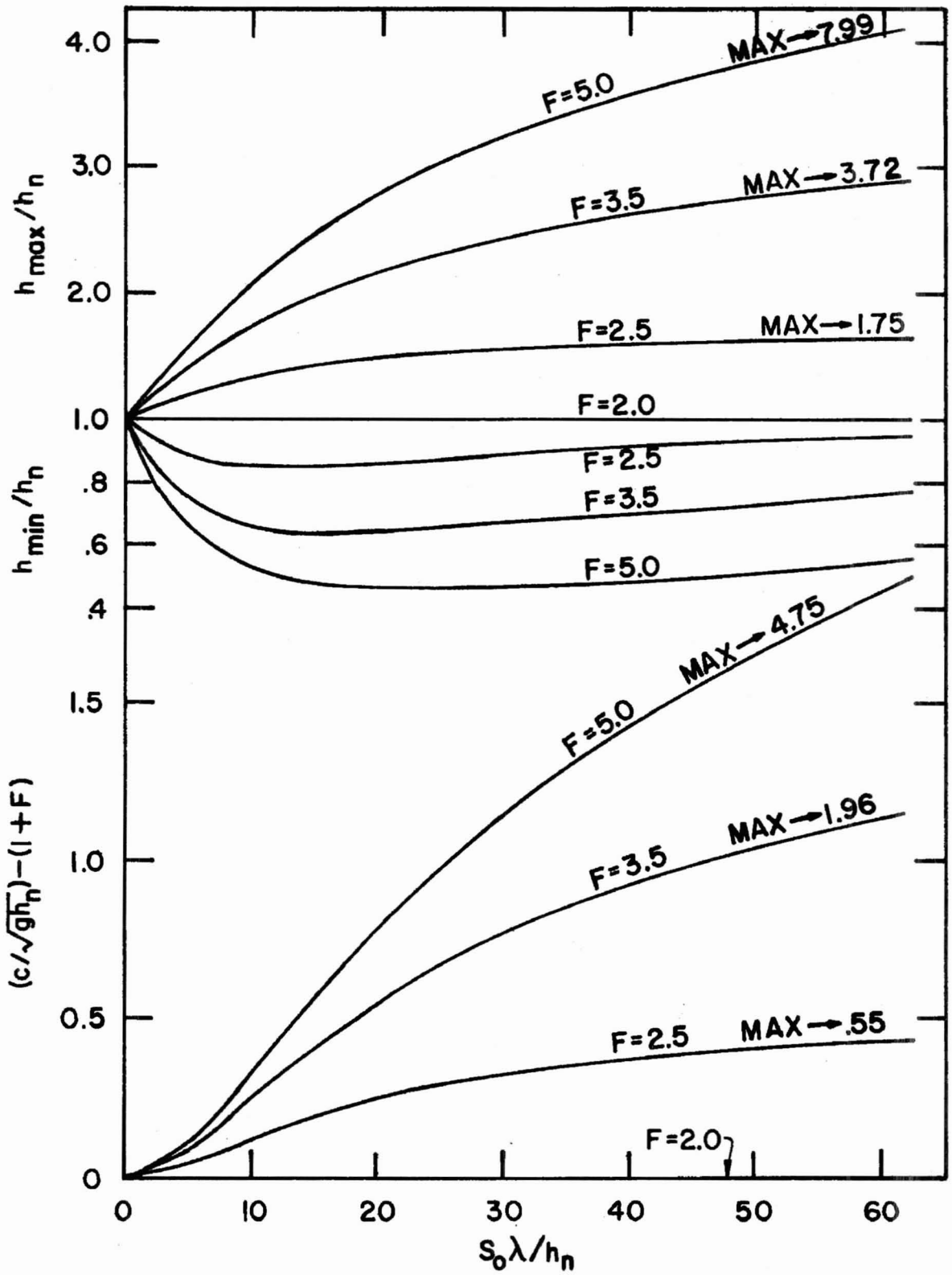

Fig. 6. Graphs of solutions for h_{max}, h_{min}, and c as functions of Froude number, F, and $S_o\lambda/h_n$ from periodic permanent roll wave theory

it was more convenient to start with values of F and h^*_{min} and find the resulting value of $S_o\lambda/h_n$. In this way no trial and error procedures were required.

The asymptotic solution for large values of $S_o\lambda/h_n$ can be obtained by first observing from equation 3.52 that because the value of dh/dX is zero at $h^* = h^*_a$, the minimum value of h^*_{min} is h^*_a. Equation 3.54 shows that S_oX^* approaches minus infinity at $h^*_{min} = h^*_a$, and equation 3.56 indicates that $S_o\lambda^*$ approaches infinity (because K_1 approaches infinity). Therefore for large values of $S_o\lambda/h_n$, h^*_{min} approaches h^*_a from above, and the water surface becomes parallel to the channel floor at h^*_{min}.

The value of h_{max}/h_{min} is a function only of F for large values of $S_o\lambda/h_n$. It can be calculated from equations 3.53 and 3.46, which for $h^*_a = h^*_{min}$ become,

$$h^*_{min} = (1/2F^2)\left[1 + 2F + \sqrt{1 + 4F}\right] \tag{3.81}$$

$$h_{max}/h_{min} = 1/2\left[\sqrt{1 + (2/h^*_{min})^3} - 1\right] \tag{3.82}$$

Because K_1 approaches infinity, equation 3.67 shows that h^*_{av} becomes equal to h^*_a or h^*_{min}. Therefore equation 3.63 can be written as,

$$h^{*3/2}_n = \left[(1 + F)\, h^*_{min} - 1\right]/F \tag{3.83}$$

As $S_o\lambda/h_n$ approaches infinity the distance from $h^* = 1$ ($X^* = 0$) to $h^* = h^*_{min}$ also approaches infinity, whereas the distance from $h^* = 1$ to $h^* = h^*_{max}$ remains finite. Thus it is clear that the average discharge must equal the discharge at h_{min} because the distance over

which h_{min} occurs is infinite, and that h_n must equal h_{min}. This can be proven by working with equations 3.83 and 3.81. To get a relation between h_n^* and h_{min}^*, F would have to be eliminated between 3.83 and 3.81, but this is not a simple manipulation. However, by using an arbitrary positive value of F in equation 3.81 and substituting the resulting value of h_{min}^* into equation 3.83, the value of h_n^* is found to correspond to that of h_{min}^*. Therefore as $S_o\lambda/h_n$ approaches infinity,

$$h_a^* = h_{min}^* = h_{av}^* = h_n^* \tag{3.84}$$

The wave velocity is then only a function of F,

$$c/\sqrt{gh_n} = (1 + F)/h_{min}^* \tag{3.85}$$

where h_{min}^* is found from equation 3.81. Asymptotic values for large $S_o\lambda/h_n$ are indicated on figure 6.

2. Discussion of Solution

From figure 6 it is seen that h_{max}/h_n increases with both F and $S_o\lambda/h_n$. At a Froude number of 2, this solution degenerates to uniform flow. This indicates that there are no periodic solutions of the type considered for Froude numbers of 2 or less. For the linear problem considered in Section III-A a non-trivial solution existed for a Froude number of 2, but the wave amplitude did not change with distance. For a Froude number above 2, the wave amplitude increased exponentially with distance. Thus, the behavior of the linear and non-linear theories is quite compatible.

The wave velocity has the expected value ($c/\sqrt{gh_n} = 1 + F$) at a vanishing wave length (uniform flow). In both the linear and non-linear theory it is seen that the term $S_o\lambda/h_n$ appears. This allows a comparison between the wave velocities at a fixed value of F and Y. For vanishing values of Y the values of $c/\sqrt{gh_n}$ are the same ($c/\sqrt{gh_n} = 1 + F$), and for $Y > 0$ the non-linear wave velocity is larger. This can be seen by comparing values given by figures 3 and 6 for fixed values of F and Y. This is because the wave amplitude of the non-linear theory is not restricted to be small, and the velocity of a shallow water wave increases with the amplitude.

As the wave length approaches infinity the wave shape and velocity approach a finite solution which gives rather substantial values of h_{max}/h_n. This corresponds to one wave of infinite length in a channel of infinite length. For this limiting case h_{min} approaches h_n.

Schonfeld (19) has claimed to have found that only the solution with $h_{max}/h_n = 2.07$ is a stable one. However, in his work relations were derived by assuming that there was a discontinuity in the water surface at $h = h_n$ (in addition to the one at the shock). The above solution has no discontinuities of this type, and therefore Schonfeld's result is doubtful. A stability analysis of the periodic permanent solution may lead to some interesting results. This remains to be done.

CHAPTER IV

LABORATORY EXPERIMENTS - APPARATUS AND PROCEDURE

IV-A INTRODUCTION AND OBJECTIVE

The two objectives of the laboratory experiments were:

1) To obtain information on roll wave trains that develop naturally from a uniform flow; and

2) To obtain information on periodic permanent roll waves to compare with theory. A long steep channel was constructed for this study in the W. M. Keck Laboratory of Hydraulics and Water Resources.

In this chapter the steep channel and the apparatus used for the measurements are described. The experimental procedure, including a description of the quantities measured and the range of variables used is also included. In the next section is a short description of some preliminary work performed in a 130-ft channel.

IV-B PRELIMINARY EXPERIMENTS

A 130-ft tiltable laboratory channel 3.61 ft wide with a maximum slope of 2% (i.e. $\sin \theta = .02$ where θ = angle of inclination from horizontal) was utilized for some initial observations. It was found that, because of insufficient length, roll waves were not formed in this channel, even at the maximum Froude number of 2.65. Therefore periodic disturbances were introduced at the inlet using a motorized reciprocating sluice gate. The plan of these experiments was first to make small disturbances and observe their growth in the 130-ft

length of the channel. The next step of the plan was to increase the size of the disturbances produced to correspond to that observed at the outlet of the channel in the first experiment and to observe their growth. By repeating this procedure it was thought that one could, in effect, study the growth of waves in a very long channel. This objective was only partially realized. The difficulty was that it was not possible to produce waves at the sluice gate that had the exact size and shape of those observed at the channel outlet. This made it impossible to reliably piece together the different segments of the growing wave and thus to predict from the experiments the wave growth as a function of distance along the channel.

In these experiments there was one run in which the artificially produced disturbances were large enough so that periodic permanent waves were established near the downstream end of the flume. Because the Froude number was less than any in the steep channel, the data on wave shape and velocity for this run will be included in the next chapter. The method of obtaining data in this 130-ft channel was quite similar to that used in the steep channel which is described below. The periodic wave profile was obtained from a pressure record similar to that in figure 14. In the 130-ft channel the maximum and minimum depths were measured with a point gage. These point gage measurements were obtained at five locations across the 3.61-ft wide channel, and at five meter intervals along the flume. The periodic waves were considered to be permanent when the maximum and minimum depth did not change over significant length. The 130-ft channel is described briefly in Appendix I and in more detail by Vanoni (20) and Fischer (21).

IV-C APPARATUS

1. Steep Channel

The bulk of the experiments was carried out in an extruded aluminum rectangular channel 4-5/8 in. wide and 1-13/16 in. high. This shape is available commercially in lengths up to 16 ft. For a channel length of 128 ft and slopes of .08429 and .05011, eight of these 16-ft lengths were joined (see figure 7). The length was later changed to 80 ft with a slope of .1192 by removing three of the 16-ft lengths. The lengths of channel were joined by plates bolted to both lengths as shown in figure 8. The ends of the two lengths were separated by about 1/8-in. and body putty was used to fill the void. Finally the joint was sanded to give a very smooth finish.

The channel was supported at 5-1/2-ft intervals by brackets bolted to 2 x 4-in. timbers which were fixed to the concrete wall of the laboratory. J-bolts were used to clamp the channel to the brackets. Two adjusting bolts at the brackets were used to level the channel transversely. For measurement of static pressure on the channel floor, 1/32-in. diameter holes were drilled through the floor at the approximate center line. These holes started at station 6 (6 ft downstream of station 0.0 shown on figure 11) and were put at 6-ft intervals over the total length. A fitting was affixed to the underside of the channel floor, to which a pressure transducer could be attached. The details of the bracket and pressure hole can be seen in figure 9. Figure 10 shows the principal dimensions at a station with a supporting bracket.

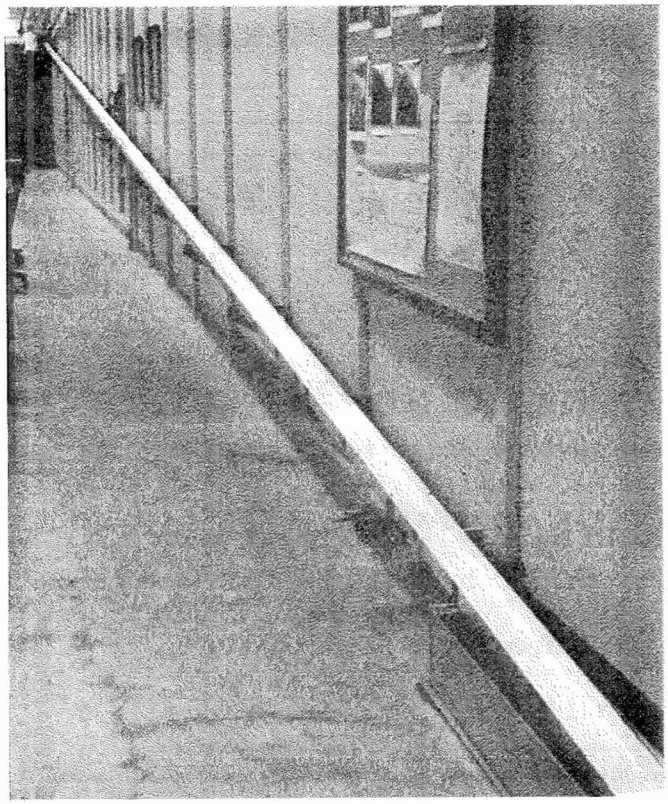

Negative No. 7835

Fig. 7. General view of channel, S_o = .08429, ℓ = 128 ft, no flow

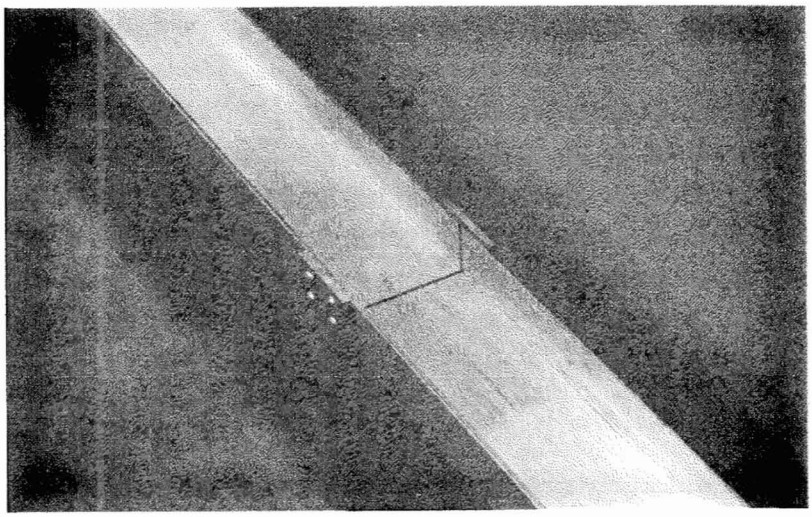

Negative No. 7836

Fig. 8. View of typical joint for channel

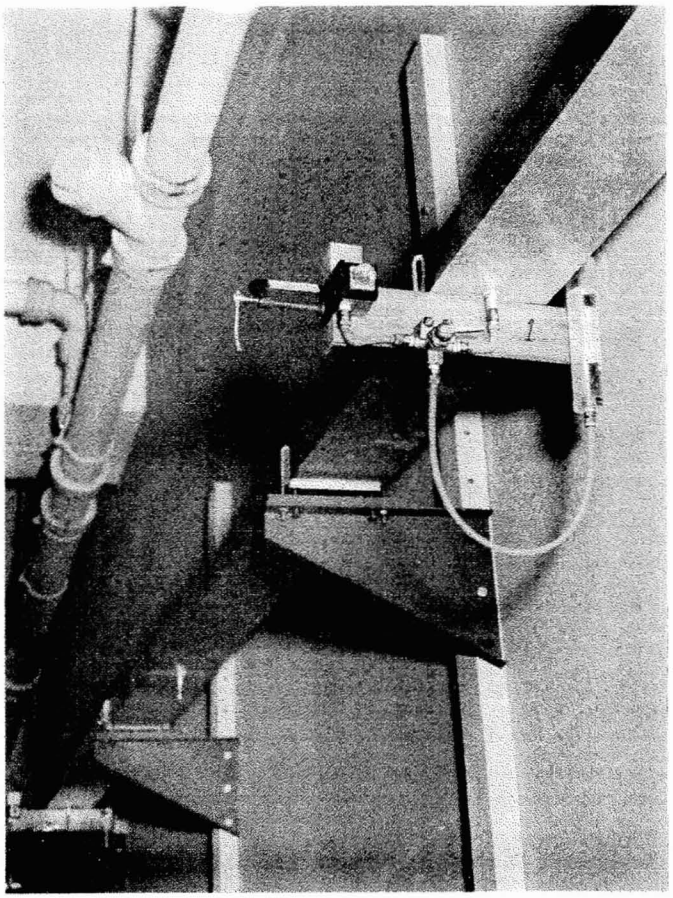

Negative No. 7837

Fig. 9. View of channel showing support bracket and pressure measuring station

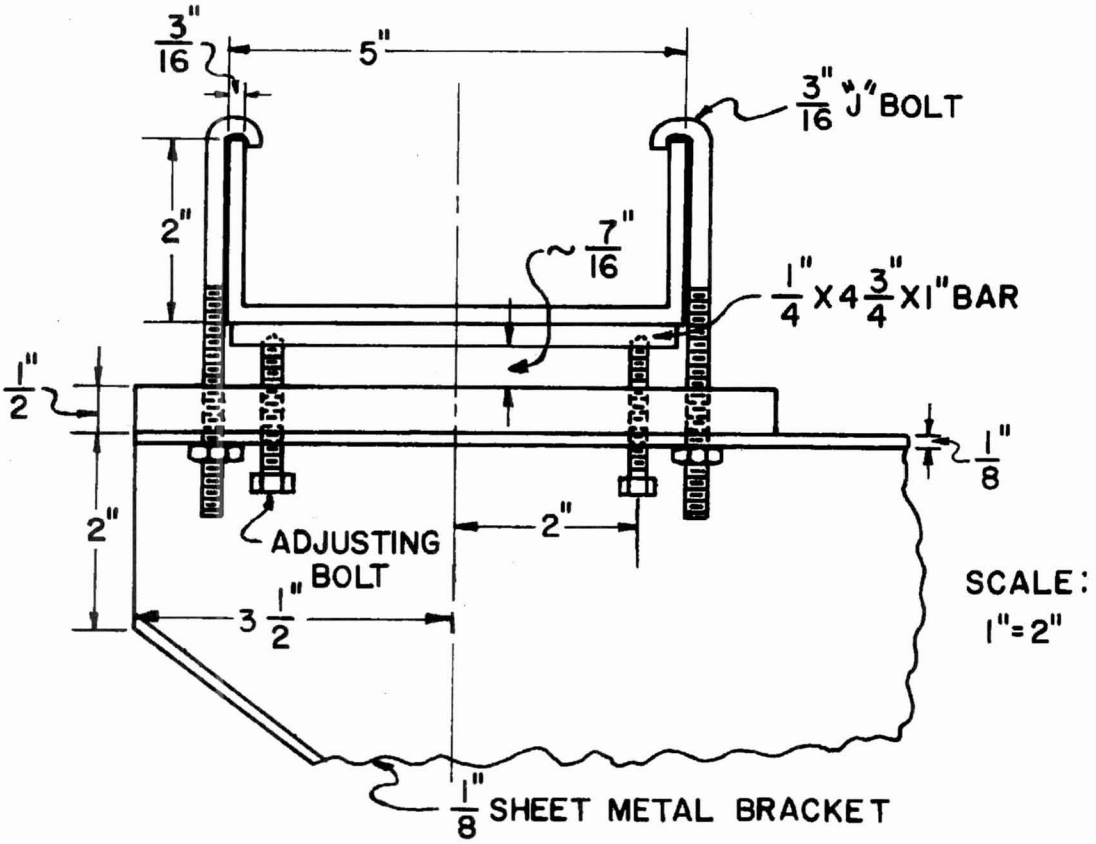

Fig. 10. Drawing of cross section of channel at a station with a supporting bracket

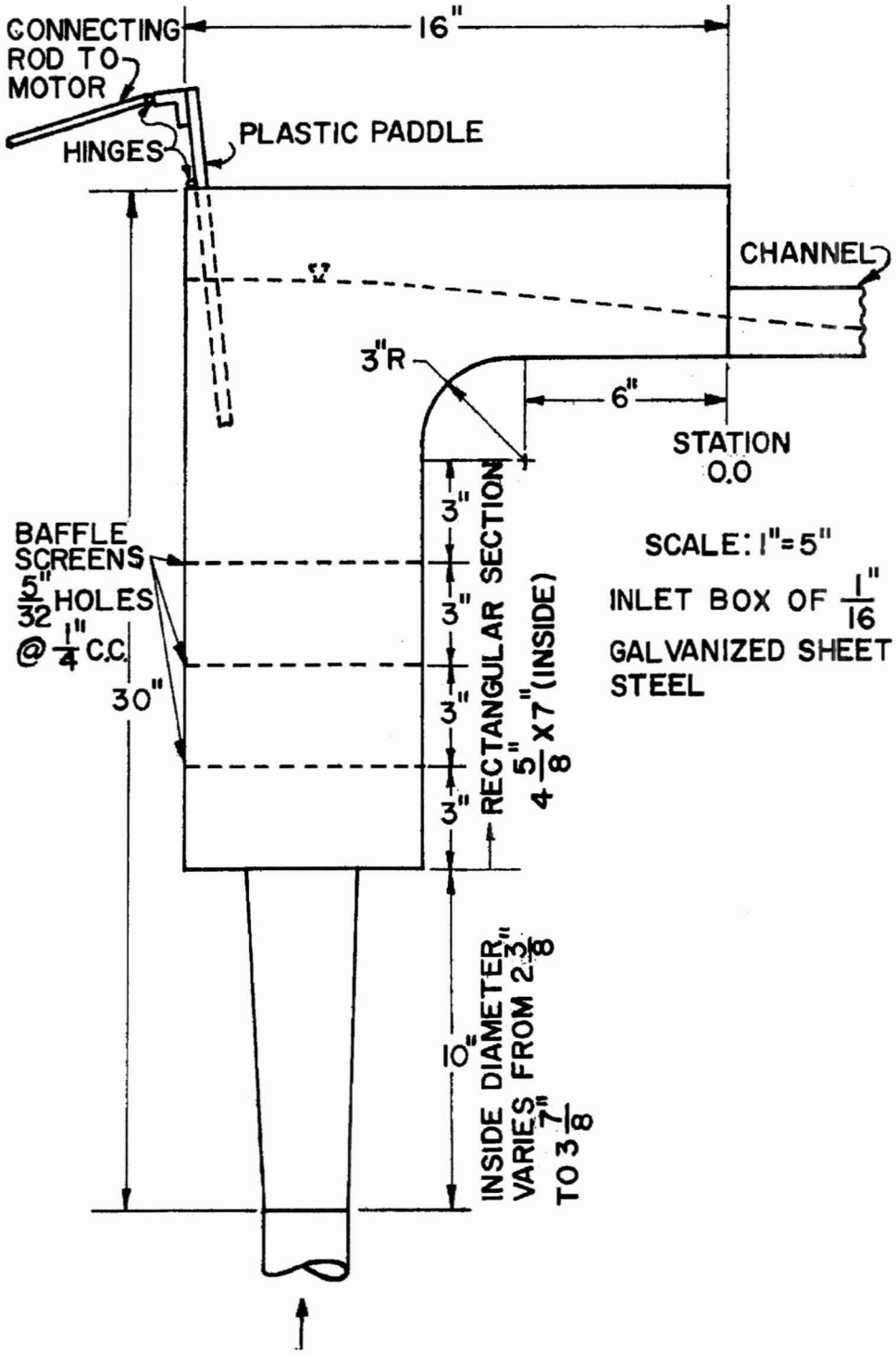

Fig. 11. Drawing of inlet box for channel

The galvanized sheet steel inlet box had the same inside width as the channel to avoid disturbances that would result from a contraction or expansion. A drawing of the box is shown in figure 11 . Observations on the flow in the inlet are discussed in Chapters V and VI. A plastic paddle hinged on the upstream wall of the inlet box and driven by a variable speed fractional horsepower motor was used to create periodic permanent waves. Figure 12 shows the inlet in operation.

Flow was supplied by a constant head tank located near the downstream end of the channel. One reach of the supply line to the inlet box was a 3-in. diameter pipe in which a 1-1/8-in. flange type orifice plate was installed for measurement of flow rates. After installation this orifice plate was calibrated volumetrically using a mercury or water manometer to record the pressure drop across the orifice plate.

The slope of the channel was changed twice after the original setting. To obtain a given slope all the brackets were first placed at approximately the desired elevation, and then the adjusting bolts at each bracket were used to obtain the final elevation. A surveyor's transit and a rod that could be attached to the channel was used in obtaining the final elevation. The rod was graduated in .01-ft intervals and was read to .001 ft with a vernier scale. The length of the channel was measured with a steel tape with graduations of 1/16 in. Thus the accuracy of the slope was controlled by the accuracy of the measurements of the vertical distances. With the vertical distances accurate to .001 ft, the channel slopes for the 120 ft channel (.05011 and .08429) were accurate to .00001 (.001/120), and for the 80 ft channel the slope (.1192) was accurate to .00002. Once one side of the channel at a

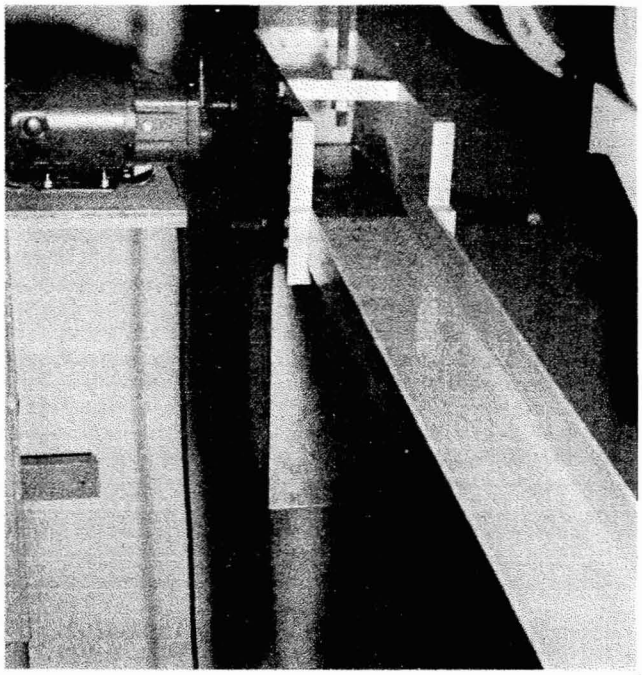

Negative No. 7838

Fig. 12. View of inlet box and channel near inlet with flow

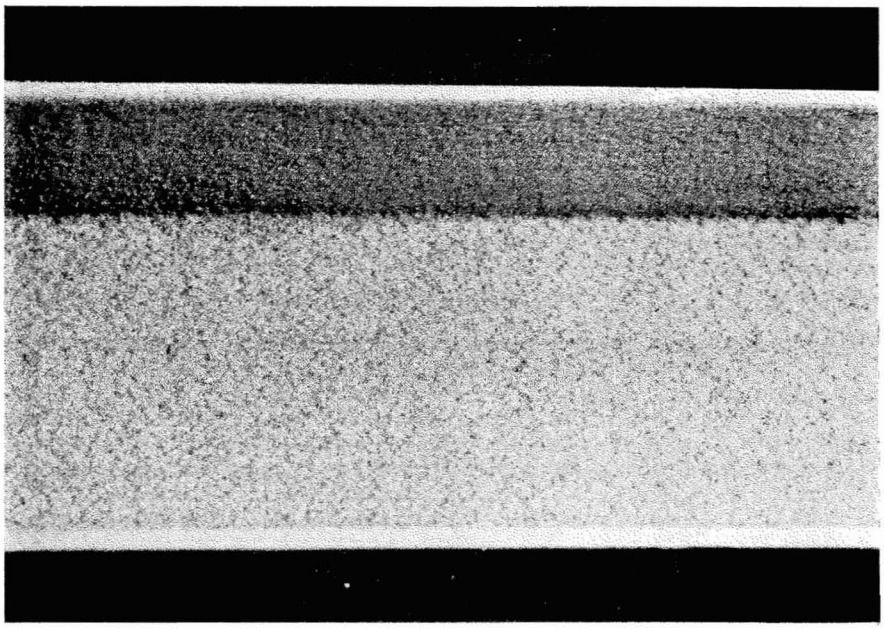

Negative No. 7839

Fig. 13. Closeup view of rough channel

particular bracket was at the correct elevation, a hand level was placed on the channel and the lateral adjustment was made. Longitudinal alignment was accomplished by placing the channel a fixed lateral distance from a 0.010 in. wire that was strung the length of the channel.

Measurements (e.g. maximum depths, periods, etc.) were taken only at the pressure hole stations. Invert readings at five locations across the channel were taken with a point gage at each of the pressure hole stations. It was found that the channel bottom was an average of about .010 in. lower at the center than it was near the side-walls for stations not near one of the supporting brackets. At pressure hole stations near one of the supporting brackets the channel bottom was flat because of the clamping action of the J-bolts. At each station a weighted average of the five invert readings was used to convert water-surface readings to depths.

Two surface finishes were used for the channel. For the smooth boundary an epoxy enamel was sprayed on the aluminum channel. A rough surface was obtained by applying a uniform sand to the bottom and walls of the channel immediately after they had been brush painted with an enamel. The application of the sand consisted of covering the bottom with sand and throwing it against the side-walls until no more sand would stick. Three days later the water was turned on and the excess sand was washed off, leaving a uniform roughness about one grain diameter thick. Figure 13 shows this rough channel. The geometric mean size of the sand grains, D_g, and geometric standard deviation, σ_g, were .595 mm and 1.11 respectively. Table 1 contains the results of the sieve analysis of the sand.

Table 1

Sieve Analysis of Sand in Rough Channel

Mesh per in (Tyler)	Sieve Opening mm	% Finer by Weight
16	.991	100.00
20	.833	99.90
24	.701	95.10
28	.589	42.70
32	.495	3.88
35	.417	.98
42	.351	.33
48	.295	.25
60	.246	.22
65	.208	.17
100	.147	.09
150	.104	.06
200	.074	.03

Geometric mean size = 0.595 mm

Geometric standard deviation = 1.11

2. Measuring and Recording Equipment

a. Pressure Transducer

Much of the data taken consisted of records of the floor pressure as a function of time at the stations with pressure holes. These pressure records were converted to depth records, except for the portion of the wave near the maximum depth, by the use of a calibration. The method by which this calibration was obtained is explained below in this section. These pressures were measured with a model P7D pressure transducer manufactured by the Pace Engineering Company. In this transducer deflections of a 0.004 in. stainless steel diaphragm were measured by changes in magnetic reluctance of two magnetic cores, and the resulting voltage changes were recorded by a Sanborn series 150 recording oscillograph system. The transducer is shown at the left end of the angle iron in figure 9. It was connected to the pressure hole with a short piece of 3/16-in. plastic tubing, via a three-way valve used for bleeding and calibration purposes. The transducer and valve were mounted on a piece of angle iron so that the whole assembly could be placed at any pressure hole station. Figure 14 shows a typical pressure record of shock-type roll waves.

b. Wire Gage and Point Gage

A particularly simple device was used to obtain the frequency distributions of maximum depths, to calibrate the pressure transducer, and to measure normal depths. The instrument will be referred to as a wire gage. The wire gage, shown in figure 15, consisted of a stainless steel micrometer head (reading to 0.001 in.) mounted vertically in a base of aluminum stock which rested on top of the channel walls.

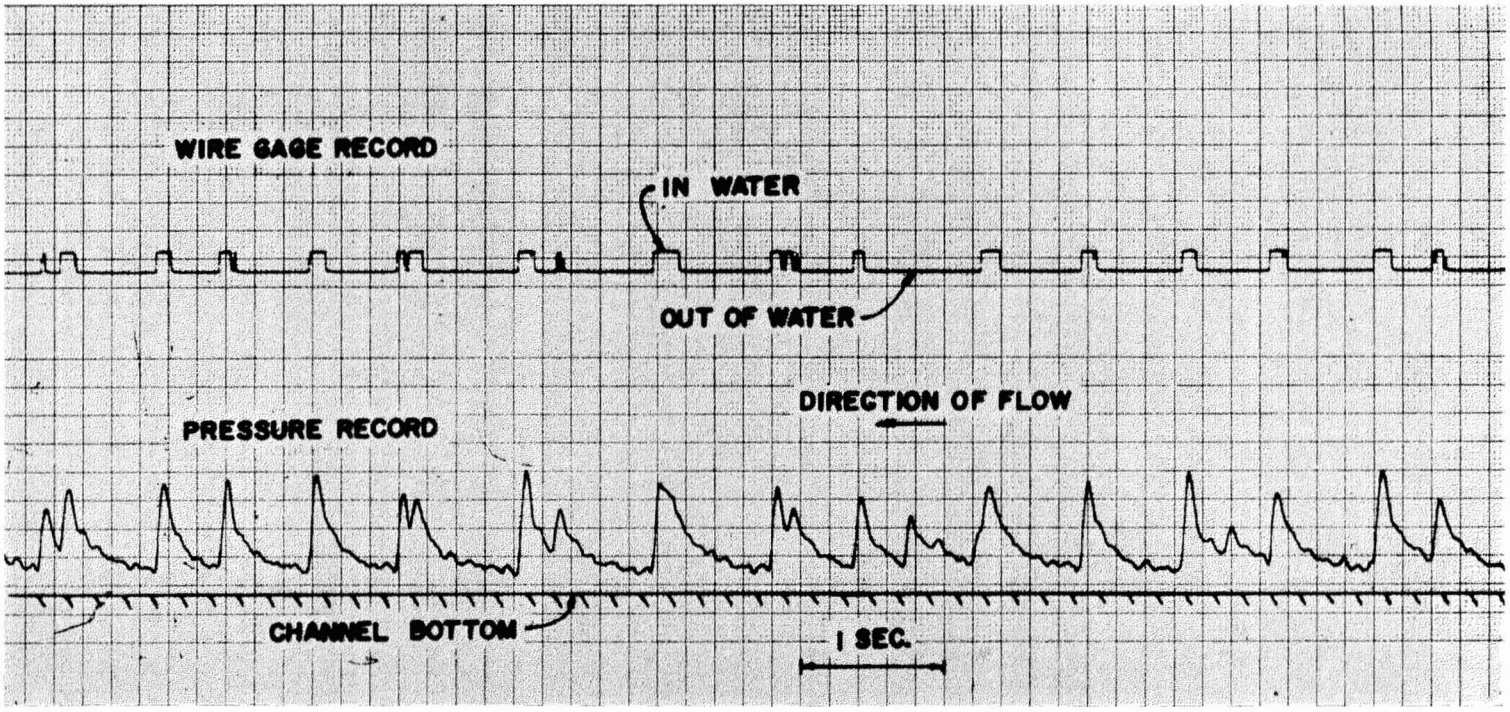

Fig. 14. Typical pressure and wire gage record for shock-type roll waves, $S_o = .1192$, $h_n = .210$ in., station 36, smooth inlet

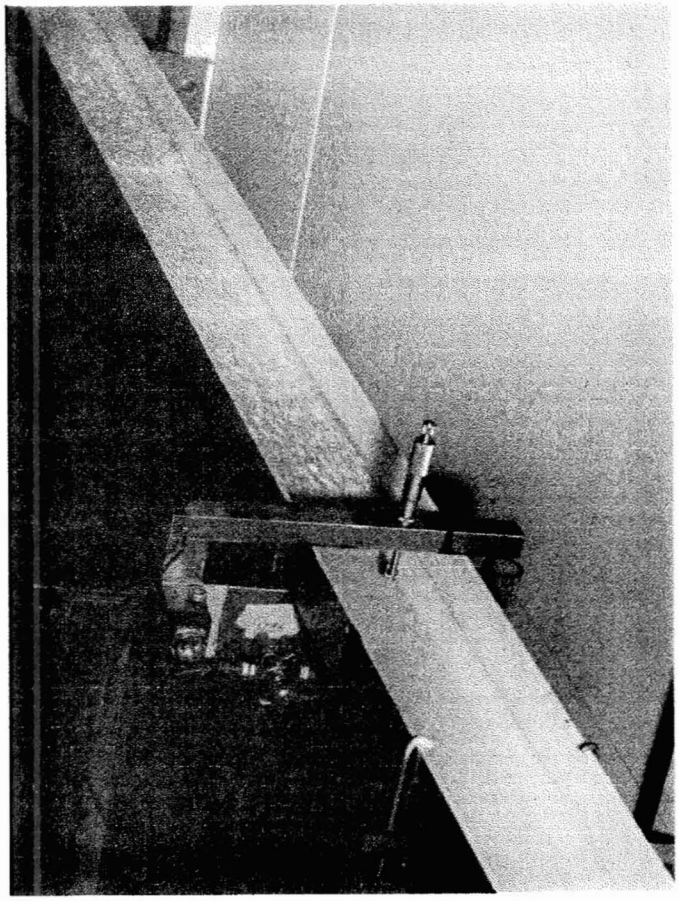

Negative No. 7840

Fig. 15. View of wire gage and pressure transducer with waves approaching

On the lower end of the micrometer head was attached a short piece of 0.020 in. diameter stainless steel wire. The aluminum base was wired to the Sanborn recording system.

The oscillograph record from a wire gage is shown in figure 14. As can be seen, the wire gage reading changed from its reading in air only when the wire was in contact with the water. In figure 14 the wire gage was directly over the pressure hole and high enough so that it was in contact only with the wave peaks. The elevation of the wire was changed by rotating the micrometer. It was found that the wire was small enough (.020 in. diameter) so that no water was observed to hang below the lower end of it which would be undesirable.

The change in the wire gage reading on the oscillograph chart when the wire was in contact with the flowing water indicates that the wire tip of the wire gage was at a different electric potential when immersed in the water than when in the air. The difference in the potential was on the order of 0.1 volt. Although the mechanism responsible for the existence of an electric potential was not investigated, the response characteristics of the wire gage were excellent for the measurements for which it was used.

A point gage was used to measure the elevation of the channel bottom, and occasionally to obtain estimates of the average maximum depth of small amplitude waves. This point gage was identical to the wire gage except that instead of a small wire, a stainless steel point was attached to the lower end of the micrometer head. These values of average maximum depth were obtained by setting the point at a given level and estimating what proportion of the wave crests that passed by

were hitting the point. The average maximum depth was taken as that depth corresponding to the elevation of the point at which about one-half of the wave crests hit the point. By this procedure, repeatable values of average maximum depth could be obtained for the small amplitude roll waves.

c. Recording Equipment

The Sanborn recording oscillograph system, series 150, was used for recording signals from the pressure and wire gages. A carrier preamplifier model 150-1100 AS was used with the pressure transducer, and a DC preamplifier model 150-1000 with the wire gage. Figure 16 shows the four channel Sanborn unit which was used to record two pressure traces and two wire gage records simultaneously.

d. Calibration of Pressure Transducer System

For conversion of a pressure record, such as in figure 14, to a depth record, a calibration was required. From the resulting depth record, only the minimum depths were taken. The maximum depths were obtained from the wire gage record by a procedure explained later. The maximum depths were not taken from the pressure record for two reasons. First, the frequency response of the system as described above was probably not adequate to record the very fast rise in pressures encountered near the steep wave fronts. Second, the pressures directly under the crests of the shock-waves were probably not hydrostatically distributed, so that even if the floor pressure were correctly recorded, the correct depth of flow could not be found from them.

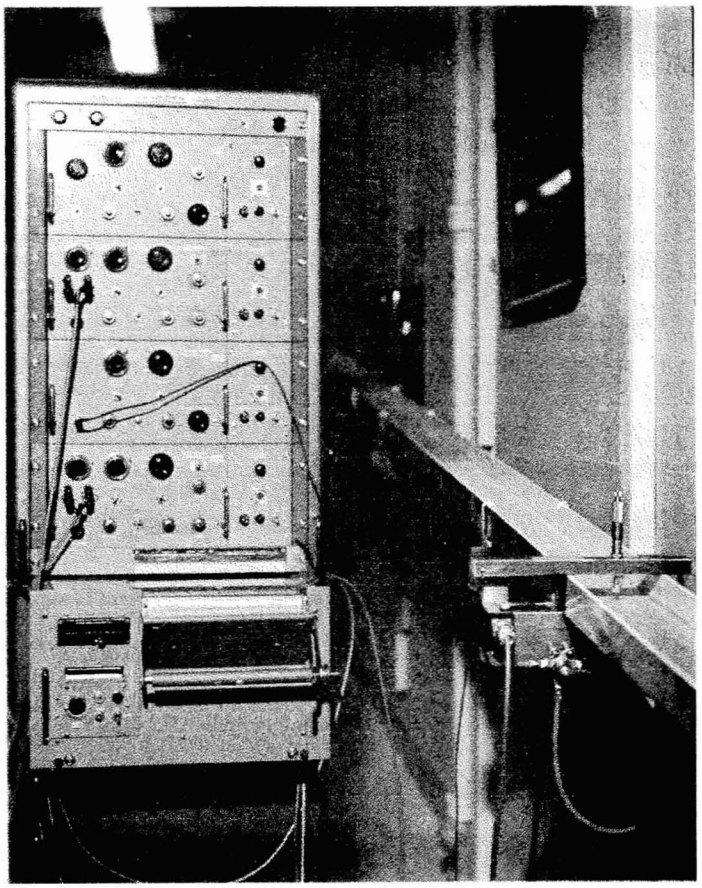

Negative No. 7841

Fig. 16. View of 4-channel oscillograph recorder with wire gage and pressure transducer

A calibration consisted of a relation between the depth of flow at the center line of the pressure station in question, and the reading on the recorder chart. An in situ calibration was obtained before each run. When a pressure transducer was moved to another station, it was calibrated again.

Both static and dynamic calibrations were obtained. A static calibration was obtained by varying the level of water in the plastic cylinder connected to the pressure transducer shown at the right side of figure 9. This changed the pressure on the transducer and thus the reading on the recorder chart. By measuring this water level in the cylinder with the point gage and noting the corresponding chart reading, a static calibration was developed. This calibration was always linear.

A dynamic calibration was obtained by using a wire gage located directly over the pressure hole. As illustrated in figure 14, when the water level dropped below the level of the wire, a change in the wire gage reading occurred. Thus at that exact time, the pressure record must have corresponded to the elevation of the wire. By changing the setting of the wire gage a complete dynamic calibration curve was constructed. This calibration was linear also. Figure 17 shows a typical calibration of the pressure measuring system.

In most cases the slopes of the static and dynamic calibrations were the same. This indicated that the pressure being recorded was in fact only the static pressure, because the velocity, and thus the velocity head, varied along the wave length. If part of this velocity head were being recorded because of some imperfections around the

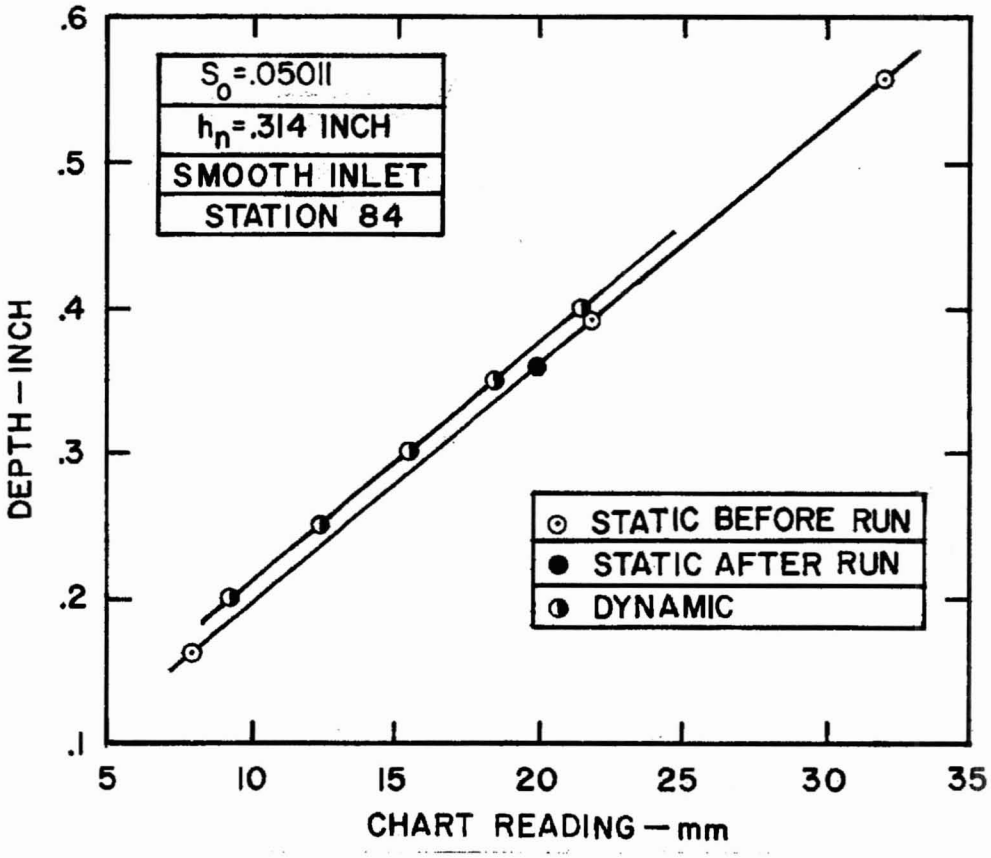

Fig. 17. Typical calibration of the pressure measuring system

pressure hole, the slopes of these two calibrations would be different. However the two calibrations were not necessarily coincident because of different reference levels from which the elevations were measured. In all cases the dynamic calibration was used to get the values of minimum depth. The static calibration was used mainly as an aid in determining the slope of the dynamic calibration, and as a check on the drift in the calibration, if any, during the run.

IV-D EXPERIMENTAL PROCEDURE

1. Design of Experiments

Data were obtained on both naturally developed and periodic roll waves for three different channel slopes. Two or three different discharges were used on each slope. For the largest slope a rough channel was also used. Normal depths were measured for all slopes and discharges. Table 2 summarizes these channel conditions and states what type of measurements were made.

The measurements desired on natural waves for a fixed slope and discharge could not all be taken in one continuous run. Therefore it was necessary to be able to duplicate a particular discharge quite accurately. It was found that a manometer reading could be set within 1/2 percent of a given value, and thus the discharge was accurate to 1/4 percent. During a run the discharge was adjusted if necessary to stay within this limit. The discharges in table 2 correspond to the desired manometer readings.

Table 2

Types of Measurements Obtained
for Each Slope and Discharge

S_o	Q-cfs	Channel Surface	Type of Measurements Obtained		
			Normal Depth	Periodic Waves	Natural Waves
.05011	.01700	Smooth	x		x
.05011	.03433	Smooth	x	x	x
.05011	.05142	Smooth	x		x
.08429	.02304	Smooth	x	x	x
.08429	.04601	Smooth	x	x	x
.08429	.06843	Smooth	x		x
.1192	.02831	Smooth	x	x	x
.1192	.08222	Smooth	x		x
.1192	.007523	Rough	x		
.1192	.01717	Rough	x	x	x
.1192	.04798	Rough	x	x	x

2. Normal Depth

Normal depths were measured in the reach of uniform flow upstream of the region in which developing roll waves were first detected. The depth of flow was measured at five locations across the channel at each station, and at a minimum of four stations that were 2 to 4 ft apart.

The water-surface level was very unsteady, which is characteristic of high velocity flows. This made it very difficult to measure the normal depth with a point gage. However the response characteristics of the wire gage were particularly well suited for measuring the normal depth. Figure 18 shows a typical oscillograph wire gage record when it was set close to the normal depth.

In figure 14 it was seen that the wire gage oscillograph record showed one reading when the lower end of the wire was in contact with the flowing water, and another reading when the wire was out of the water. When the wire was set near the normal depth in a uniform flow, the reading on the oscillograph chart fluctuated rapidly between the "in water" reading and the "out of water" reading, as seen in figure 18. It was found that by varying the elevation of the wire, the recorder stylus made a darker impression either on the "in water" or the "out of water" side of the record. In figure 18 the .280-in. record shows a darker impression on the "in water" side, whereas when the wire was raised .010 in. to .290 in., the "out of water" side of the record shows a darker impression. It was assumed that the normal depth corresponded to the case in which the recorder stylus made equivalent impressions on the "in water" and "out of water" sides of the record.

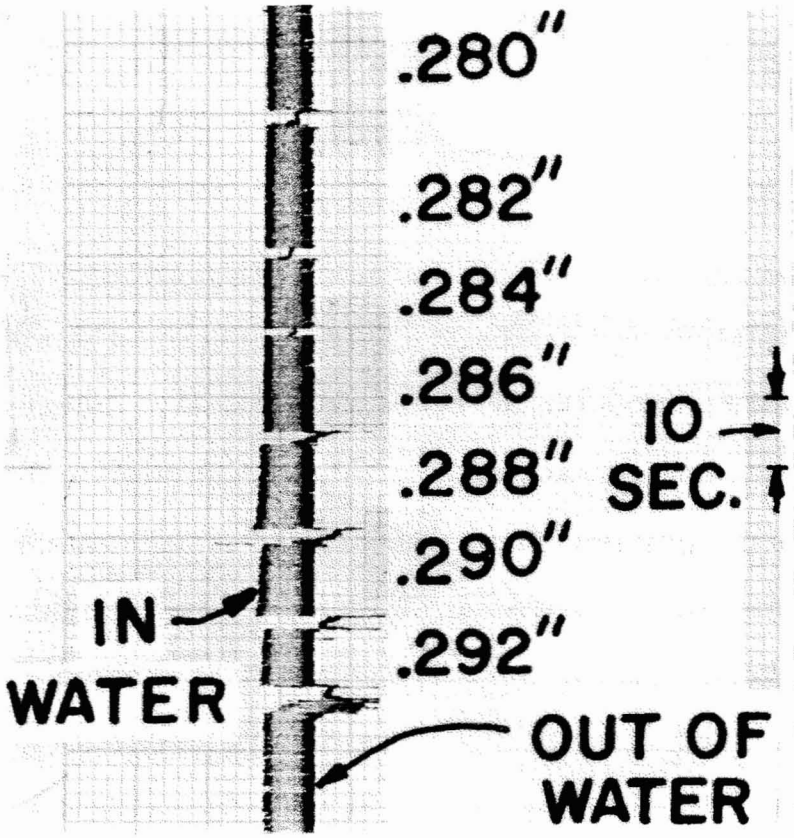

Fig. 18. Typical wire gage record used to measure normal depths

Thus for the case shown in figure 18, the normal depth was taken to correspond to the .286 in. wire gage reading with an accuracy of about .002 in. In some cases with higher velocities this accuracy was about .004 in.

3. Wave Properties Measured

a. Naturally Developed Roll Waves

Four properties were measured:

(1.) Minimum depths (h_{min}) were obtained at stations along the channel by using the pressure records (e.g. figure 14) and dynamic calibrations. At each station values of minimum depth were obtained for about 200 waves from which the average value and the standard deviation were calculated. In some cases a frequency distribution was constructed from these 200 values. This sample of about 200 measurements was found to be large enough to obtain consistent results. A minimum depth measurement that was greater than the average depth (i.e. average depth over many waves as estimated by eye from the pressure record) was not considered in these calculations. This eliminated those minimum depths between two waves that were about to combine. As an example the minimum depth between the wave crests 5 and 6 at station 72 on figure 47c would not be used in the calculations.

(2.) Periods (T) at stations along the channel were obtained from the pressure records. The period is simply the time period between successive wave crests. Thus the period of a wave is its length on the recorder chart divided by the chart speed. When two

waves were about to combine, they were considered to be two waves as long as the peak of each wave was clearly delineated on the pressure record. For obtaining standard deviations and frequency distributions about 200 values of period were used. The average period of the shock waves at a station was usually calculated from about 1500-2000 waves to obtain consistent results.

(3.) Wave velocities (c) were obtained at stations along the channel. This required using pressure records from two stations taken concurrently. These stations were usually 6 ft apart but sometimes up to 18 ft apart. A particular wave was identified in each record and then its travel time between the two stations determined. For each pair of stations the average value, standard deviation, and frequency distribution of wave velocity was based on about 200 observations. If two waves combined between the pair of stations being used, their velocities were not computed because the wave velocity changes appreciably during this overtaking process. The average wave velocity was assumed to apply to a station midway between the pair of stations.

(4.) Maximum depths (h_{max}) were obtained on the center line of the channel at stations along the channel. For the small amplitude waves, a pressure record similar to figure 41 was used to obtain the maximum depths. For reasons explained in Section IV-C, the maximum depths of the large amplitude shock-type waves were not obtained from the pressure record, but from simultaneous wire gage and pressure records. The method was first to construct a frequency distribution of the maximum depths at a given station, and then to

derive the average value and standard deviation from it. The frequency distribution was determined by placing the wire at a known level and obtaining a record of at least 200 waves. The wire gage level was then changed and again 200 waves were recorded. For each level of the wire, the percent of the waves that hit the wire could be found using the pressure record to count 200 waves and the wire gage record to count the number of hits. The wire was varied from a level where all the waves hit up to a level where none of the waves hit. The wire was moved through at least ten intervals of .025 in. at most, and less when the standard deviation of the maximum depths was small.

The standard deviation of the wave heights was found by plotting the cumulative frequency distribution (value of h_{max} vs. percent greater than or equal to) on arithmetic probability graph paper. This paper is designed so that a Gaussian distribution plots as a straight line. Figure 37 shows some typical results. In all cases the plotted values could be well represented by a straight line. Thus the standard deviation was found graphically as the difference between the 50 percent value and the 84.1 percent value. These values come from the well known properties of a Gaussian distribution.

The average value of the maximum depths was calculated by multiplying the percent of waves between two successive wire levels by the average wire level (wire level at lower end point plus 1/2 of interval), and summing all these products. This method gives a good estimate of the true average for any frequency distribution as long as the intervals are sufficiently small. Because the frequency distribution

is Gaussian in this case, the average value, computed as above, agreed with the mean value on the probability graph within about .002 in.

A digital computer was used to compute the statistical quantities for the four wave properties.

b. Periodic Permanent Roll Waves

Periods, wave velocities, and maximum depths were measured in the same way as explained above for natural waves. However for periodic waves there was only one value for each of these quantities at a given station because all waves were the same. In addition, after the waves have reached a permanent form the wave properties do not change with station.

Wave shape, including minimum depth, was determined for most of the periodic wave runs. The wire gage and bottom pressure records were used to determine the profile of the waves including the steep fronts. The sensitivity of measurement of the time interval was increased by increasing the recorder paper speed. The distance from the toe of the wave front to the point where the wire of the wire gage intersected the water surface was obtained as the product of the time interval and the wave velocity.

4. General Procedure for Natural and Periodic Roll Wave Runs

For runs with natural roll waves pressure records and wire gage records were taken at two stations concurrently. These stations were generally 6 ft apart but sometimes they were up to 18 ft apart. After obtaining static and dynamic calibrations, a record of about 200 waves

was taken at chart speeds of 25 or 50 mm/sec. Then maximum depths were measured at both stations with the wire gages at a chart speed of about 5 mm/sec for several wire elevations. Sometimes the instruments were left at a particular pair of stations and data were taken at two or three discharges before they were moved to another pair of stations. More consistent results were obtained when measurements at all stations were taken before changing the discharge. In this way the data for one discharge could be obtained in about one week.

For runs with periodic waves the paddle in the inlet box (figure 11) was oscillated at the desired period. The amplitude of the paddle motion could be varied by adjusting the stroke of the connecting arm from the motor. By suitable adjustment of the paddle amplitude a periodic permanent wave could be produced. However it took a certain length of channel before the periodic waves assumed a permanent form. This length of channel decreased for the larger paddle amplitudes. By measuring the maximum depth over a considerable reach of the channel, the region of permanent waves was found. The maximum depths reported for the periodic permanent waves are averages of measurements at four stations which generally covered about 30 to 40 ft of channel. The velocity and profile of the periodic permanent waves were also measured. In some cases, particularly for short wave periods and thus short wave lengths, a periodic permanent wave train would show signs of becoming nonperiodic near the downstream end of the channel.

CHAPTER V

PRESENTATION OF EXPERIMENTAL RESULTS

V-A INLET CONDITION

1. Smooth and Rough Inlet

a. Observations of Flow Near Inlet

The inlet condition was found to have a significant influence on the distance from the inlet where roll waves could first be seen or measured. If the channel bottom near the inlet was left smooth, just as the rest of the channel, the natural roll waves developed further upstream than they did when a small length of the channel bottom near the inlet was artificially roughened.

By using continuous dye injection in the inlet box where the velocities were low, the behavior of the flow in the channel near the inlet could be observed. Observations of this kind were made for all runs at slopes of .05011 and .1192. The general flow characteristics were similar for all runs. For a smooth channel bottom, immediately downstream of the reservoir the water surface was glassy smooth and a dye stream just below the water surface remained intact. However after a sufficient distance the dye stream began to mix with the water until it was completely mixed. This point where mixing began was not fixed for a given run, but oscillated up and down the channel in an intermittent manner. The smooth water surface became roughened at about the same station as the mixing began, and this station of surface roughening oscillated also. A dye stream near the channel bottom had

a similar appearance and did not mix with the water until it was near the station where the surface dye mixed.

The channel bottom near the inlet was made rough by placing a 6-in. length of fine mesh screen on the bottom of the inlet box, so that the downstream end of the screen was about 0.30 ft upstream of station 0.0. The widths of the screen and the channel were the same. For this condition the behavior of the dye near the water surface was similar to that in the smooth channel case, except that the mixing occurred further upstream and the initial mixing point for a given discharge was stationary. However the dye stream near the channel bottom was completely mixed at the downstream end of the screen. Dye streams at intermediate elevations began to mix at stations between the end of the screen and the station where the surface dye began to mix.

These observations can be adequately explained in terms of boundary layers. For a smooth inlet a laminar boundary layer was developed initially which eventually became turbulent in an intermittent fashion. For a rough inlet a turbulent boundary layer was initiated by the screen, and this boundary layer eventually reached the water surface. Because no transition from laminar to turbulent flow was required, no unsteadiness was introduced. More will be said about this boundary layer notion in Section VI-C.

The general flow pattern described above for a smooth channel bottom was most clearly displayed at the lowest discharges corresponding to a normal depth (h_n) of about .2 in. For this value of h_n the dye stream stayed intact further downstream and the disturbances

associated with the transition from laminar to turbulent flow were sufficiently strong to create shock-type roll waves almost immediately. However at normal depths of .3 and .4 in. the surface disturbances near the zone of dye mixing were not as pronounced, although at times these disturbances could be seen to eventually develop into roll waves.

Figure 19 shows water-surface profiles for a typical condition near a smooth inlet at a normal depth of .2 in. Three surface profiles are plotted; the depth during periods when the surface was smooth, the average depth during periods when the surface was rough, and the maximum depth during periods when the surface was rough. These depths were measured using a wire gage and point gage at the channel center line. From the trend of the maximum depth values, it is seen that appreciable disturbances were developed, even at station 5.0 ft. It is interesting to observe that the depth of the smooth water surface fell below the normal depth. For a rough inlet at the same slope and h_n as shown on figure 19, comparable disturbances did not become appreciable until about station 30.

For normal depths of .3 and .4 in., and a smooth inlet, the depth did not jump discontinuously from a low depth (smooth water surface) to a higher depth (rough water surface) as shown in figure 19. Instead there was a more gradual transition from a smooth to a rough water surface, although the point of roughening was oscillating somewhat. For normal depths of .3 and .4 in. with a rough inlet, there was also a gradual depth transition from a smooth water surface to a rough water surface. However this surface roughness, and the associated intersection of the turbulent boundary layer with the water surface,

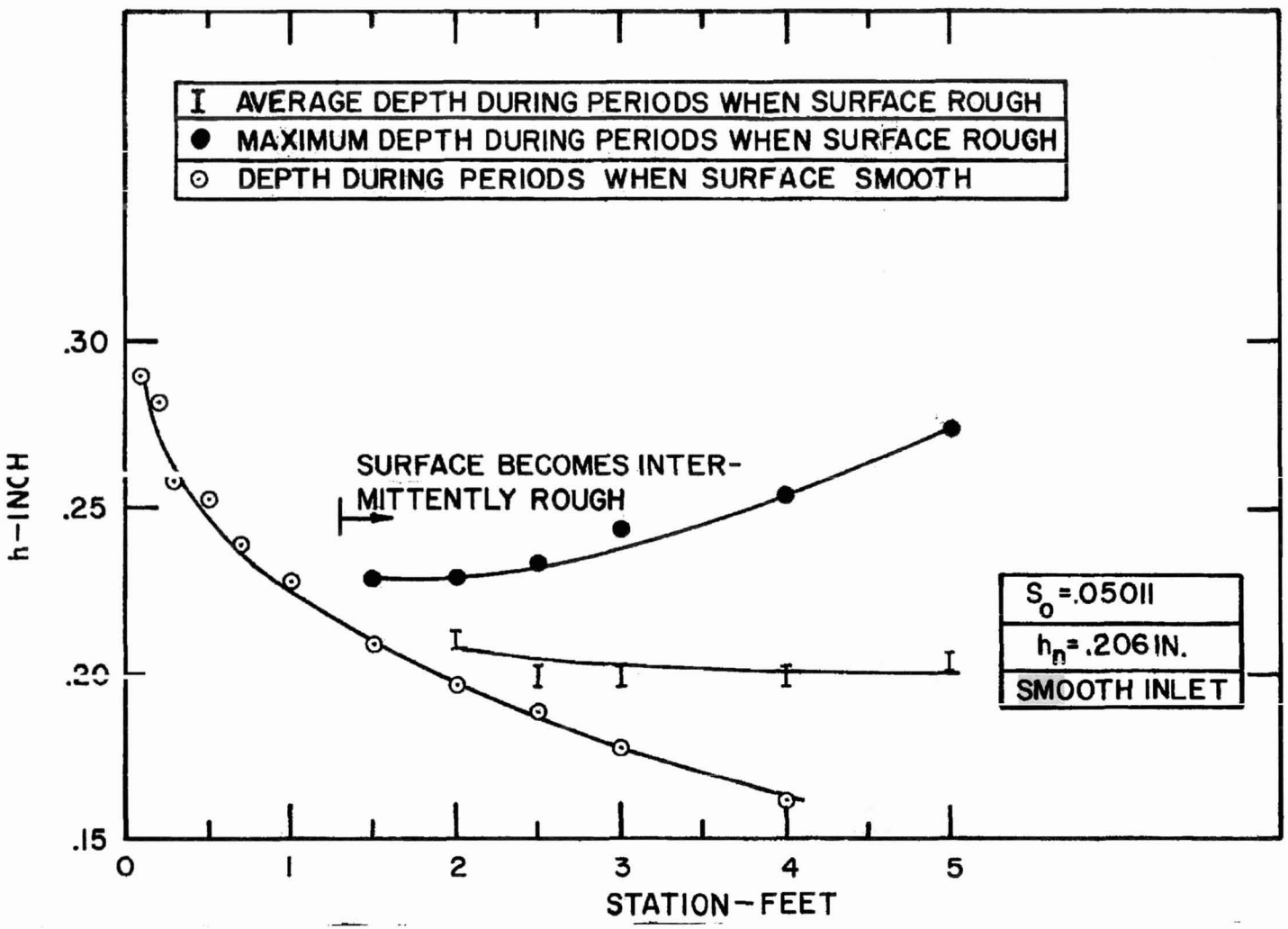

Fig. 19. Graph of typical water-surface profiles near a smooth inlet for a normal depth of .2 in.

occurred farther upstream and in a more nearly steady manner than the flow with a smooth inlet. This observation is consistent with the fact that a turbulent boundary layer develops faster than a laminar one. For the rough channel the conditions at the inlet were similar to those in a smooth channel with a rough inlet because the sand grains caused the initiation of a turbulent boundary layer as the screen did in the smooth channel.

b. Adjustment to Rough-Inlet Condition

From the experiments it was found that with a smooth inlet, a given value of average maximum depth ($\bar{h}_{max}$) occurred at a smaller value of ℓ (ℓ = distance from station 0.0) than with a rough inlet. This fact is consistent with the observations on the flow conditions near the inlet presented above. It was found that with a smooth inlet there were surface disturbances which resulted from the intermittent manner in which the water surface became rough. Presumably this intermittency resulted from the laminar boundary layer becoming turbulent. With a rough inlet the location of water-surface roughening was stationary in time, at least much more so than with a smooth inlet, and surface disturbances resulting from this surface roughening were not observed. Therefore for a smooth inlet excess disturbances (other than those present for a rough inlet) were provided to initiate the development of roll waves.

One purpose of this study is to describe some geometric properties of natural roll waves as a function of distance from the beginning of the channel (i.e. ℓ). From the above discussion it is clear that even for a fixed discharge, slope, etc., the value of a given property, say

$\overline{h}_{max}$, at a given value of ℓ depends on the inlet condition. For the data to be presented, this dependence on the inlet condition was eliminated by adjusting the smooth-inlet results to a rough inlet. For each smooth-inlet run this was done by adding a correction length to the values of ℓ so that the adjusted development relations (e.g. $\overline{h}_{max}$ vs. ℓ) were the same as those that would have been obtained with a rough inlet. For runs in which a rough inlet was used, and for the runs in the rough channel, no correction was necessary.

To obtain a correction length for a smooth-inlet run, some data are also required for the same hydraulic conditions with a rough inlet. For each run two correction lengths were determined; one from the $\overline{h}_{max}$ vs. ℓ relations for a smooth and rough inlet, and one from the T_{av} vs. ℓ relations for a smooth and rough inlet. T_{av} is the average wave period. For each of these relations the procedure was to slide the two graphical relations (smooth inlet and rough inlet) along the ℓ axis until the data points for both the smooth and rough inlet relations showed a unique relation. The amount of displacement along the ℓ axis was the correction length. For each run the two correction lengths using the $\overline{h}_{max}$ and T_{av} relations were practically the same.

In the runs with normal depths of .3 and .4 in., the data points for the smooth and rough inlet could be made to define a unique relation between $\overline{h}_{max}$ and ℓ or T_{av} and ℓ, over the range of $\overline{h}_{max}$ or T_{av} that was represented by the data. In other words the effect of the smooth inlet was to translate the development relations upstream without any change of their shape with respect to the relations for a rough inlet.

However for the runs with a normal depth of .2 in., the initial part of the smooth-inlet development relation had a different shape than the corresponding rough-inlet relation. This smooth-inlet effect on the shape of the development curve is shown in figure 20 for the $\overline{h}_{max}$ development relation. As was mentioned in the last section, in the smooth-inlet runs with a normal depth of .2 in., shock waves were established quite close to the inlet as a result of the intermittent behavior associated with the water surface becoming rough. With a rough inlet, shock waves were formed from small amplitude waves which developed from a uniform flow. These two different methods by which shock waves were formed help explain the differences in the development relations as shown for $\overline{h}_{max}$ in figure 20. The development relations to be presented in this chapter apply to roll waves that develop from a uniform flow. Therefore, for the smooth-inlet runs at a normal depth of .2 in., the data points that showed the smooth-inlet effect on the shape of the development relations (e.g. the seven smooth inlet points for $\overline{h}_{max}/h_n$ less than about 1.6 in figure 20) were not included on the development relations applicable to rough inlets.

The correction length for each run in which a smooth inlet was used is shown in table 3. It is seen that the correction length decreased as the normal depth increased, and decreased as the channel slope was increased.

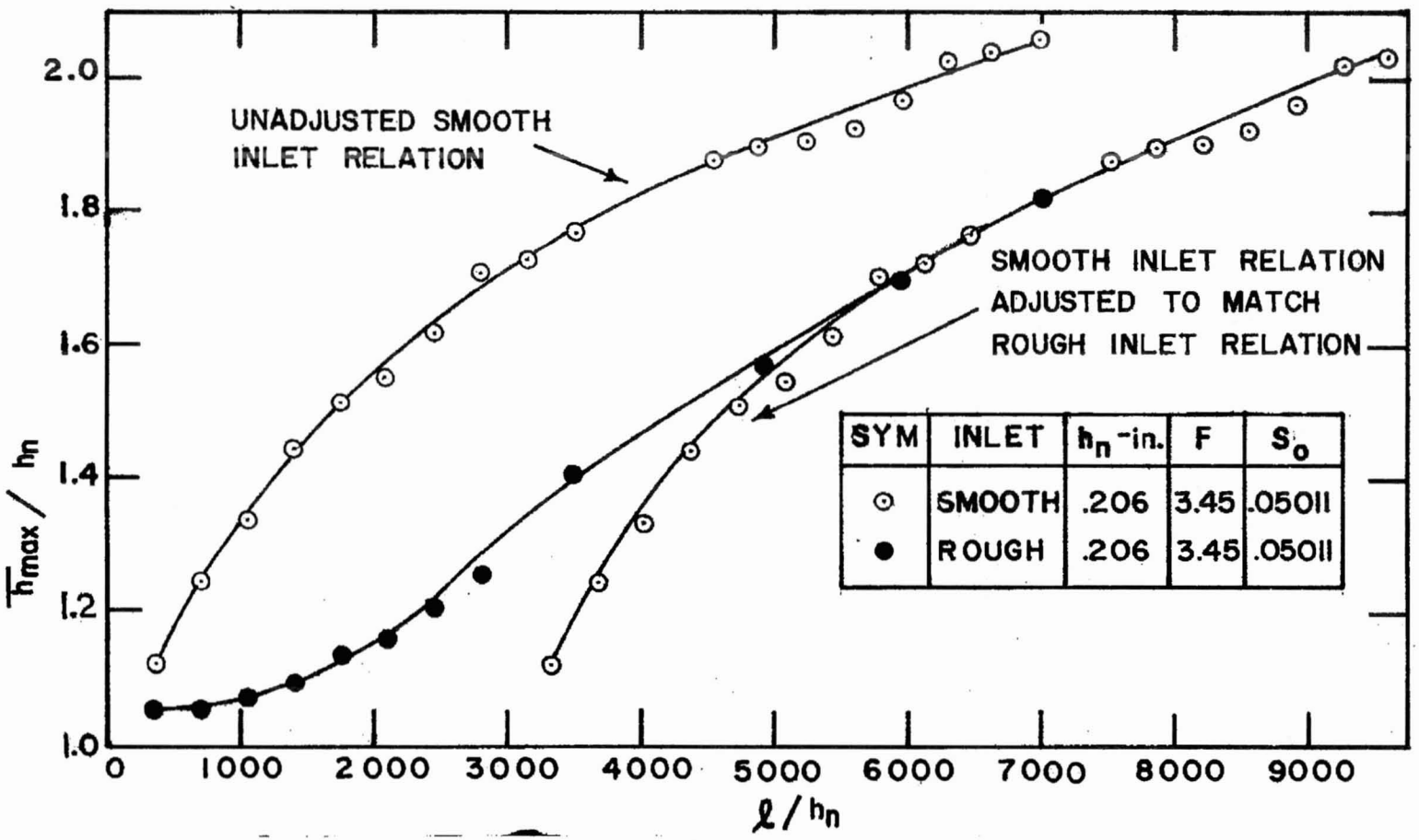

Fig. 20. Typical smooth-inlet and rough-inlet development curves for average maximum depth, $\bar{h}_{max}$, at normal depth of .2 in.

Table 3

Correction Lengths Added to Smooth-Inlet Development Relations

S_o \ h_n	.2 inch	.3 inch	.4 inch
.05011	51 ft	25	16
.08429	30	12.5	0
.1192	24	-	-

2. Drawdown Curves Near Inlet

From the water level in the inlet box the depth of flow decreased to the normal depth in a short distance. These drawdown curves were measured for most runs and several are shown in figure 21. Some depths were measured with a wire gage using the same technique to obtain the average depth as was used to obtain the normal depths. Other depths were measured with a point gage and were subject to the larger errors of this method. In both cases only center-line depths were measured. The main purpose of these measurements was to determine the conditions near the inlet.

For normal depths of .3 and .4 in. it was found that the drawdown curves were the same for a smooth or rough inlet. However for a normal depth of .2 in., the smooth-inlet condition was very unsteady as shown in figure 19. Thus the drawdown curves for a normal depth of .2 in. in figure 21 are for a rough inlet. Station 0.1 ft was the starting point of the drawdown measurements, whereas the reservoir

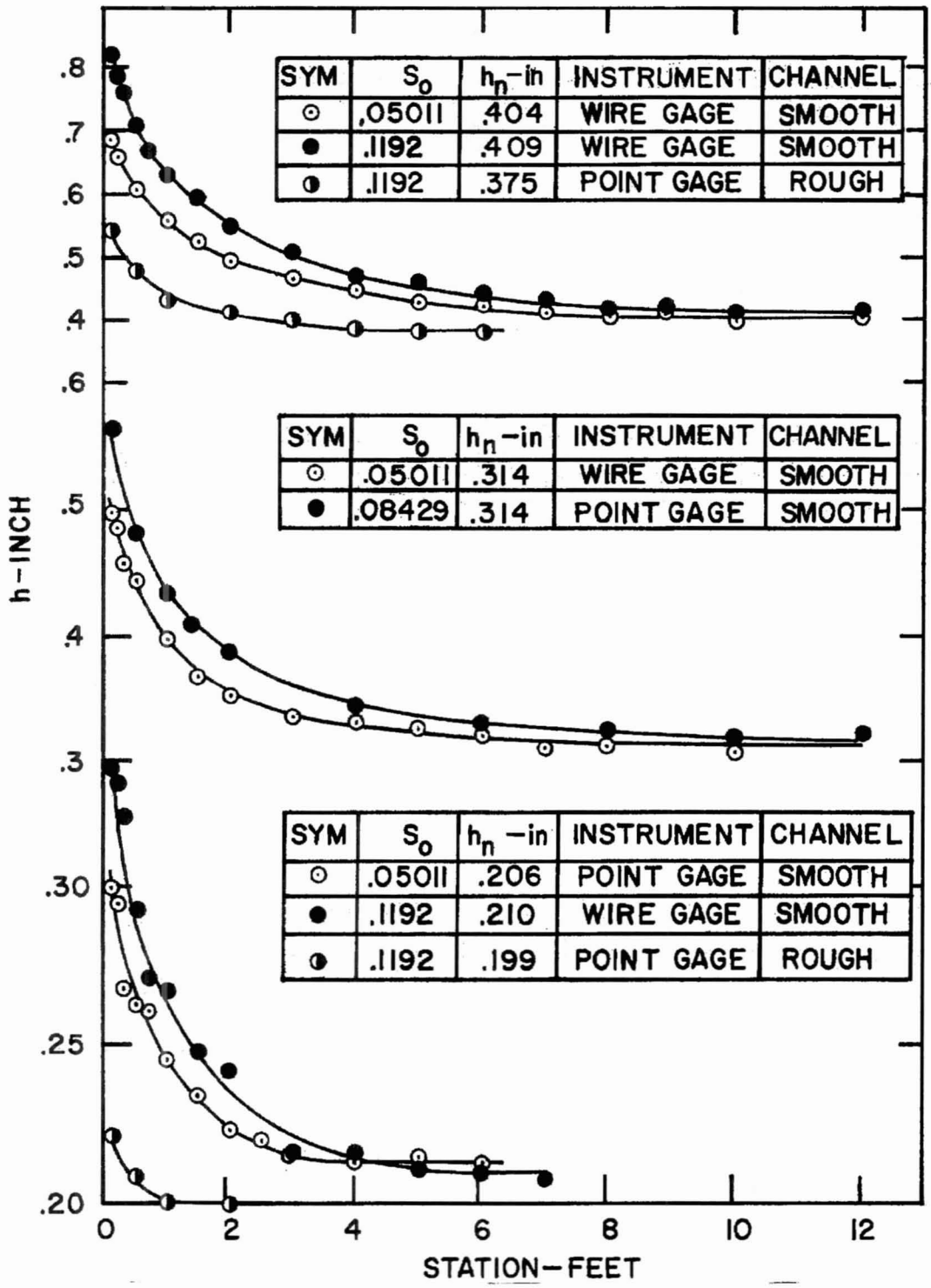

Fig. 21. Graphs of water-surface profiles near inlet of channel

is about 9 in. upstream of this station. Measurements upstream of station 0.1 ft could not be obtained conveniently because the higher walls interfered with the supporting mechanism for the depth gages.

V-B HYDRAULIC CHARACTERISTICS OF LABORATORY CHANNEL

From the measured normal depths the friction factors, Froude numbers, and Reynolds numbers were calculated. These are presented in table 4. The relation of Darcy-Weisbach friction factor, f, against Reynolds number, R, for the smooth channel is shown in figure 23, on which is plotted the relation obtained experimentally by Tracy and Lester (22) for a smooth, wide, rectangular channel. The experimental points obtained in the present study follow this relation quite well, with an average deviation of only 2.2 percent. The Froude numbers for the data in figure 23 vary from 3.45 to 5.98, which provides more evidence that the friction factor in unstable flow is not a function of the Froude number as proposed by Rouse (17).

For a rough boundary the friction factor can be expressed in the form,

$$\sqrt{1/f} = 2.03 \log_{10}(r/k) + \text{constant} \qquad (5.1)$$

which can be derived from the theoretical works of Prandtl and von Karman as Keulegan has shown (23). Here k is the size of the roughness elements which in this case was the geometric mean size (.595 mm) of the very well sorted sand. Figure 22 shows that two of the data points follow the above relation where the constant is 2.17.

Table 4

Hydraulic Characteristics of Laboratory Channel

Slope S_o	Channel Surface	Width b in	Water Temp °C	Discharge Q cfs	Normal Depth h_n in	Normal Velocity u_n fps	Froude No. F	Friction Factor f	Reynolds No. R $4ru_n/\nu$
.05011	Smooth	4.625	23.7	.01700	.206	2.57	3.45	.0308	1.63×10^4
.05011	Smooth	4.625	23.1	.03433	.314	3.40	3.71	.0257	3.11
.05011	Smooth	4.625	22.7	.05142	.404	3.96	3.81	.0235	4.47
.08429	Smooth	4.625	24.4	.02304	.208	3.45	4.63	.0289	2.24
.08429	Smooth	4.625	24.8	.04601	.314	4.56	4.96	.0241	4.33
.08429	Smooth	4.625	25.0	.06843	.404	5.27	5.06	.0224	6.26
.1192	Smooth	4.625	21.9	.02831	.210	4.20	5.60	.0279	2.60
.1192	Smooth	4.625	22.3	.08222	.409	6.26	5.98	.0227	7.07
.1192	Rough	4.55	23.2	.007523	.116	2.05	3.68	.0669	.750
.1192	Rough	4.55	22.6	.01717	.199	2.73	3.74	.0626	1.63
.1192	Rough	4.55	23.7	.04798	.375	4.05	4.04	.0501	4.37

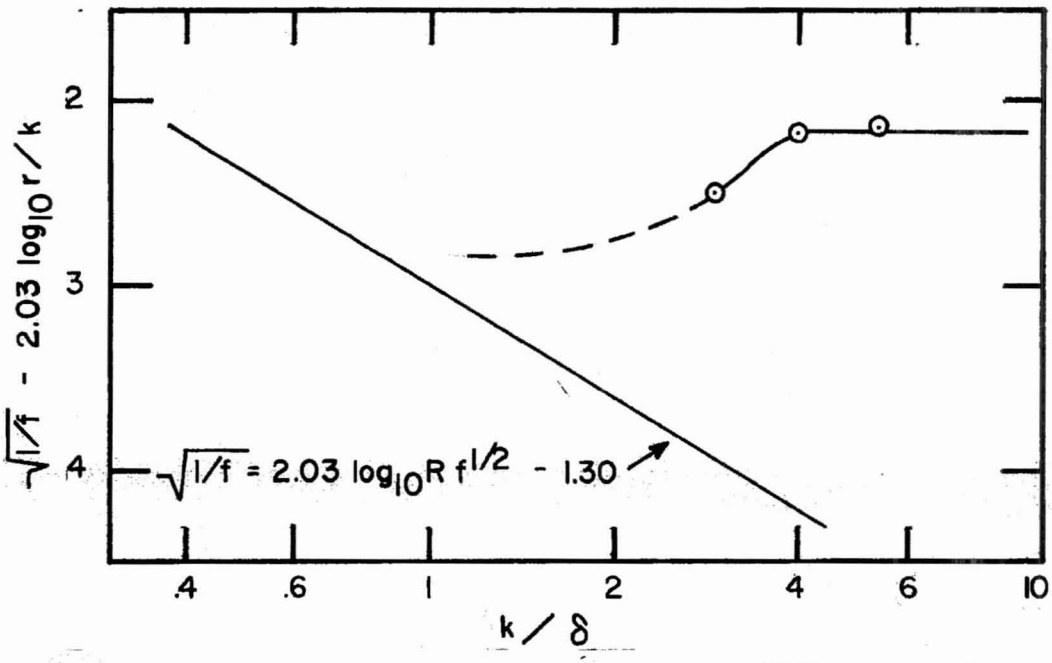

Fig. 22. Graph of the rough channel relation $\sqrt{1/f} - 2.03 \log_{10}(r/k)$ as a function of k/δ, using measured friction factors, f, in rough channel

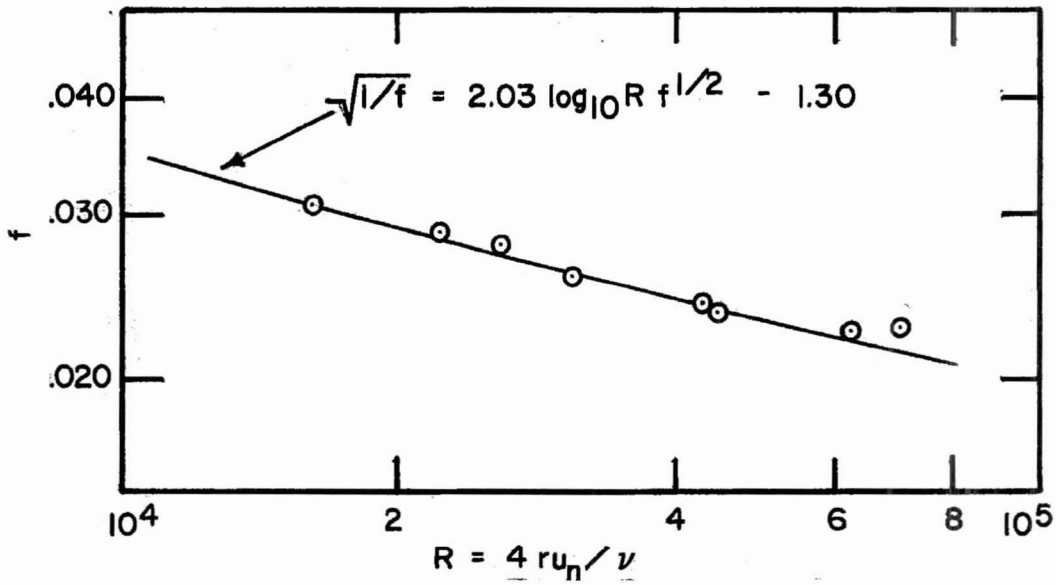

Fig. 23. Graph of friction factors, f, measured in smooth channel as a function of Reynolds number, R

In figure 22 δ is the thickness of the laminar sublayer and taken to be $11.6\ \nu/\sqrt{\tau_o/\rho}$. From Nikuradse's experiments on rough pipes with a uniform sand roughness, the equation for the velocity distribution is (23),

$$u_p/u_* = 8.5 + 5.75 \log (y/k) \tag{5.2}$$

where u_p is the velocity at a distance y from the rough wall, and u_* is the shear velocity. By applying this expression to a wide rectangular channel, the constant in equation 5.1 is found to be 2.12, which agrees quite well with the experimental value of 2.17.

One data point in figure 22 is not consistent with the other two. This is apparantly because the flow was in the transition region between a rough boundary and a smooth boundary. This transition was found in Nikuradse's data, (see for example Rouse (24) pg. 206) where the deviation from the rough-wall relation began at a k/δ value of about four. Thus the point of departure from the rough wall relation for a channel is consistent with the rough-pipe results. Nikuradse's data showed that as the value of k/δ was further decreased the data points approached the smooth-boundary relation. The dashed line in figure 22 indicates the general trend expected if more data were available.

V-C NATURAL ROLL WAVES

1. General Description

Roll waves developed from uniform flow in the laboratory channel. The waves were first clearly visible in a reach of channel downstream of the uniform flow where the waves acquired a steep front (shock wave) which extended across the channel. This point where the waves formed shocks was not fixed for a given run, but varied with each successive wave which indicated that these natural waves were not periodic. In fact, the most striking feature of these natural roll waves was the non-periodicity at all stages of their development.

It was found that there was a station downstream of which no more roll waves were formed, and the waves that had formed propagated in a nonperiodic manner. In fact the velocities of the shock waves were such that some waves would overtake and combine with the wave immediately downstream. In some cases this process was repeated two or three times by the same wave before reaching the end of the channel.

The general appearance of a typical roll wave train in the laboratory channel is shown in figure 24. The nonperiodic nature of the shock waves is evident in this photograph. Figure 25 shows a closeup view of one complete wave. The depth variation along the wave can be seen by noting the distance from the water surface to the top of the side wall. By comparison with figure 1, the similarity of the laboratory and field roll waves is seen. One noticeable difference is the absence of "white water" near the shock front of the laboratory waves. This is caused by entrained air which occurs at high wave velocities unattainable in the laboratory.

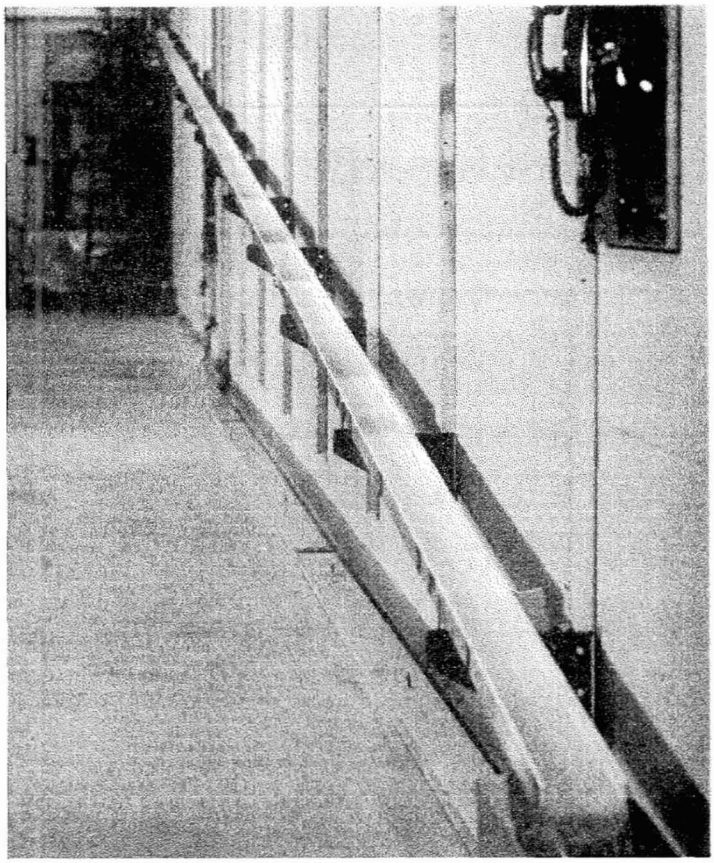

Negative No. 7842

Fig. 24. General view of channel with natural roll waves, $S_o = .1192$, $h_n = .210$ in.

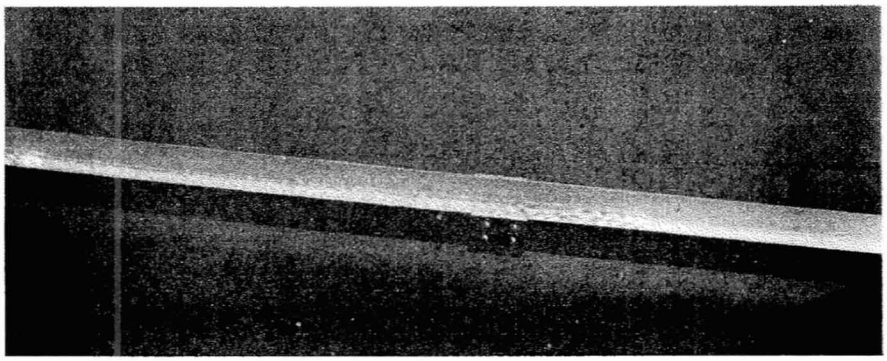

Negative No. 7843

Fig. 25. Side view of roll wave, $S_o = .08429$, $h_n = .208$ in., station 94-98

2. Tabulated Basic Data

Because of the nonperiodic nature of natural roll waves, it is necessary to measure the frequency distribution of the wave property desired. This was done for the four properties maximum depth h_{max}, minimum depth h_{min}, period T, and wave velocity c. The method of obtaining these measurements was explained in Section IV-D. The results in terms of average values and standard deviations for all runs are contained in table 5. In some cases $\overline{h}_{max}$ values were estimated by eye with a point gage. Point gage measurements were usually only used to aid in finding the correction lengths for the smooth-inlet data. For small amplitude waves (prior to forming shock waves) the $\overline{h}_{max}$ values obtained from pressure records are more accurate than estimates with the point gage. In table 5 the values which were used on the graphs are indicated. Note that for the rough channel (table 5i) only a minimum amount of data were obtained. Thus the data on the graphs are for smooth channels unless they are noted to be rough.

3. Dimensionless Development Relations

One main purpose of this study is to describe certain geometric properties of natural roll waves. To make this description applicable to any channel, these properties must be expressed in meaningful dimensionless terms. To describe the development of the four properties considered in this study, the relations $\overline{h}_{max}/h_n$ vs. ℓ/h_n, $\overline{h}_{min}/h_n$ vs. ℓ/h_n, $S_o T_{av}\sqrt{g/h_n}$ vs. ℓ/h_n, and $c_{av}/\sqrt{gh_n}$ vs. ℓ/h_n were used. These dimensionless expressions for the period and wave velocity came from the periodic permanent wave theory in Chapter III.

Table 5a Basic Data for Natural Roll Waves

$S_o = .05011$ $h_n = .206$ inch

Station ft	Rough Inlet			Smooth Inlet (Correction to match rough inlet = 51 ft)								
	$\bar{h}_{max}$ inch	$\sigma_{h_{max}}$ inch	T^b_{av} sec	$(h_{max})_{max}$ inch	$\bar{h}_{max}$ inch	$\sigma_{h_{max}}$ inch	T^c_{av} sec	σ_T sec	$\bar{h}_{min}$ inch	$\sigma_{h_{min}}$ inch	c_{av} fps	σ_c fps
6	.217[a]			.254-8	.231	.015	.457				3.53[e]	
12	.217[a]			.314-1	.256	.021	.558		.172[d]	.021[d]		
18	.221[a]			.349-1	.275	.035	.676				3.63	.15
24	.225[a]			.390-1	.297	.033	.776	.362	.157	.021		
30	.234[a]			.406-2	.311	.040	.816				3.70	.16
36	.239[a]			.405-4	.319	.043	.891	.441	.148	.019		
42	.248[a]			.455-2	.333	.046	1.030					
48	.259[a]			.469-2	.351	.049	1.119					
54				.471-1	.355	.042	1.214				3.90	.17
60	.290[f]	.023	.731	.469-3	.364	.045	1.290	.611	.144	.017		
66												
72												
78				.508-2	.387	.042	1.487				3.99	.16
84	.324[f]	.030	.964	.524-1	.391	.044	1.549	.704	.135	.015		
90				.482-6	.392	.044	1.653				4.02	.16
96				.508-2	.396	.044	1.695	.719	.133	.018		
102	.350[f]	.040	1.178	.537-1	.404	.048	1.777				4.10	.17
108				.537-1	.417	.046	1.848	.851	.140	.015		
114				.529-3	.419	.045	1.900				4.12	.18
120	.375[f]	.039	1.391	.529-1	.424	.045	1.973	.928	.134	.013		

Notes:
a. Point gage measurement
b. Based on 500 to 700 peaks
c. Based on 1200 to 2000 peaks
d. Based on 50 values
e. Based on 30 values
f. Based on 100 peaks per elevation

Unless noted otherwise, average values and standard deviations were computed from about 200 values.

Smooth inlet data for stations 6 to 42 show the effect of a smooth inlet and were not used on graphs on which wave properties were plotted as a function of ℓ/h_n.

The integers following the $(h_{max})_{max}$ values indicate the number of peaks out of 200 peaks that were higher than the value of $(h_{max})_{max}$ indicated.

Table 5b Basic Data for Natural Roll Waves

$S_o = .05011$ $h_n = .314$ inch

Station ft	Rough Inlet			Smooth Inlet (Correction to match rough inlet = 25 ft)								
	$\bar{h}_{max}$ inch	$\sigma_{h_{max}}$ inch	T_{ac} sec	$(h_{max})_{max}$ inch	$\bar{h}_{max}$ inch	$\sigma_{h_{max}}$ inch	T_{av} sec	σ_T sec	$\bar{h}_{min}$ inch	$\sigma_{h_{min}}$ inch	c_{av} fps	σ_c fps
6												
12	.328[a]				.324[d]							
18					.334[d]							
24	.320[a]				.337[d]							
30					.349[d]		.744				4.63[g]	
36	.331[a]				.358[d]		.744					
42					.372[d]		.729				4.73[g]	
48	.338[a]						.737					
54				.481-2	.401	.034	.733[e]		.248[f]	.020[f]	4.74[g]	
60	.359[a]			.499-3	.414	.040	.758[e]					
66				.539-1	.434	.042	.815[e]				4.81	.15
72				.557-1	.446	.044	.860[e]	.370	.232	.027		
78				.528-4	.446	.041	.897[e]				4.82	.15
84	.418[b]	.036	.767[c]	.564-2	.454	.042	.931[e]	.377	.221	.027		
90				.632-1	.478	.055	1.044[e]				4.89	.18
96				.608-3	.492	.056	1.084[e]	.491	.218	.032		
102	.443[b]	.036	.874[c]	.587-2	.481	.046	1.098[e]				4.90	.17
108				.612-4	.498	.053	1.156[e]	.502	.214	.028		
114				.659-2	.514	.060	1.248[e]				4.95	.18
120	.474[b]	.051	1.008[c]	.659-2	.518	.0595	1.304[e]	.538	.204	.027		

Notes:
a. Point gage measurement
b. Based on 100 peaks per elevation
c. Based on 600 peaks
d. Measured from pressure record (50 values)
e. Based on 1600 to 3000 peaks
f. Based on 50 values
g. Based on 25 values

Unless noted otherwise, average values and standard deviations were computed from about 200 values.

Rough inlet data on $\bar{h}_{max}$ for stations 12 to 60 were not used on the graphs because the smooth inlet data for this initial growth are more accurate.

The integers following the $(h_{max})_{max}$ values indicate the number of peaks out of 200 peaks that were higher than the value of $(h_{max})_{max}$ indicated.

Table 5c Basic Data for Natural Roll Waves

S_o = .05011 h_n = .404 inch

Station ft	Rough Inlet			Smooth Inlet (Correction to match rough inlet = 16 ft)								
	$\bar{h}_{max}$ inch	$\sigma_{h_{max}}$ inch	T_{av} sec	$(h_{max})_{max}$ inch	$\bar{h}_{max}$ inch	$\sigma_{h_{max}}$ inch	T_{av} sec	σ_T sec	$\bar{h}_{min}$ inch	$\sigma_{h_{min}}$ inch	c_{av} fps	σ_c fps
6												
12					.416[d]							
18					.421[d]							
24					.418[d]							
30	.413[a]				.421[d]							
36					.422[d]							
42	.410[a]				.434[d]		.808					
48							.808					
54	.416[a]				.440[d]		.805					
60					.453[d]		.805					
66	.429[a]				.459[d]		.822					
72					.480[d]		.822					
78	.441[a]			.568-2	.487	.034	.846					
84				.564-8	.495	.038	.854	.286				
90	.463[a]			.627-1	.511	.044	.877				5.56	.17
96				.608-11	.528	.052	.890	.325				
102	.509[b]	.036	.848[c]	.637-3	.528	.050	.903				5.55	.18
108				.687-1	.542	.054	.922	.402	.296	.030		
114				.684-2	.560	.055	.986				5.55	.19
120	.546[b]	.046	.916[c]	.684-4	.570	.058	1.021	.454	.293	.033		

Notes: a. Point gage measurement
b. Based on 100 peaks per elevation
c. Based on 500 peaks
d. Measured from pressure record (50 values)

Unless noted otherwise, average values and standard deviations were computed from about 200 values.

Rough inlet data on $\bar{h}_{max}$ for stations 30 to 90 were not used on the graphs because the smooth inlet data for this initial growth are more accurate.

The integers following the $(h_{max})_{max}$ values indicate the number of peaks out of 200 peaks that were higher than the value of $(h_{max})_{max}$ indicated.

Table 5d Basic Data for Natural Roll Waves

S_o = .08429 h_n = .208 inch

Station ft	Rough Inlet		Smooth Inlet (Correction to match rough inlet = 30 ft)								
	$\bar{h}^a_{max}$ inch	T^b_{av} sec	$(h_{max})_{max}$ inch	$\bar{h}_{max}$ inch	$\sigma_{h_{max}}$ inch	T^d_{av} sec	σ_T sec	$\bar{h}_{min}$ inch	$\sigma_{h_{min}}$ inch	c_{av} fps	σ_c fps
6				.229[c]							
12				.253[c]							
18			.333-9	.286	.030	.457					
24			.384-2	.314	.035	.501					
30	.251		.435-4	.344	.042	.577				4.95[e]	
36	.282		.484-4	.369	.048	.631	.280				
42	.314	.49	.534-2	.401	.056	.743				5.09[e]	
48	.320	.51	.559-4	.415	.057	.808	.362				
54	.351		.560-2	.426	.056	.851				5.18	.24
60	.378	.61	.608-1	.439	.061	.905	.402	.119	.020		
66	.386									5.23	.22
72	.383	.72	.606-2	.452	.060	.996	.400	.124	.018		
78	.405		.607-1	.467	.058	1.063				5.29	.24
84	.433	.84	.631-3	.478	.056	1.128	.479	.111	.014		
90	.441									5.41	.25
96	.432	.95	.632-2	.501	.062	1.269	.562	.097	.021		
102	.472		.685-1	.511	.069	1.304				5.45	.25
108	.474	1.15	.711-1	.517	.067	1.344	.600	.120	.019		
114	.458	1.13								5.53	.24
120	.485	1.21	.684-3	.531	.068	1.396	.630	.118	.019		

Notes:
a. Point gage measurement
b. Measured with stop watch
c. Measured from pressure record (50 values)
d. Based on 600 to 2200 peaks
e. Based on 50 values

Unless noted otherwise, average values and standard deviations were computed from about 200 values.

Rough inlet data were used only to find the correction length (30 ft); they were not used on the graphs.

Smooth inlet data for stations 6 to 30 show the effect of a smooth inlet and were not used on graphs on which wave properties were plotted as a function of ℓ/h_n.

The integers following the $(h_{max})_{max}$ values indicate the number of peaks out of 200 peaks that were higher than the value of $(h_{max})_{max}$ indicated.

Table 5e Basic Data for Natural Roll Waves

S_o = .08429 h_n = .314 inch

Station ft	Rough Inlet		Smooth Inlet (Correction to match rough inlet = 12.5 ft)								
	$\bar{h}^a_{max}$ inch	T^b_{av} sec	$(h_{max})_{max}$ inch	$\bar{h}_{max}$ inch	$\sigma_{h_{max}}$ inch	T_{av} sec	σ_T sec	$\bar{h}_{min}$ inch	$\sigma_{h_{min}}$ inch	c_{av} fps	σ_c fps
6				.329[c]							
12				.327[c]							
18				.325[c]							
24				.335[c]							
30				.343[c]							
36				.371[c]							
42			.459-5	.406	.026	.520	.197	.255	.018	6.08	.16
48	.364		.509-5	.426	.038	.520					
54	.390		.535-2	.432	.045	.505	.211	.236	.024	6.17	.20
60	.405		.583-1	.452	.052	.537					
66	.450	.56				.613				6.26	.21
72	.465	.55	.656-2	.501	.066	.649	.266	.203	.028		
78	.472	.60	.732-1	.539	.071	.695					
84	.504	.65	.756-1	.558	.073	.755					
90	.488	.66								6.39	.25
96	.521	.71	.757-2	.584	.080	.829[d]	.323	.175	.033		
102	.544		.810-2	.600	.077	.909[d]					
108	.569	.78	.811-1	.612	.080	.943[d]					
114	.600	.83								6.58	.26
120	.600	.93	.859-1	.646	.083	1.027[d]	.411	.154	.040		

Notes: a. Point gage measurement
b. Measured with stop watch
c. Measured from pressure record (50 values)
d. Based on 2000 peaks

Unless noted otherwise, average values and standard deviations were computed from about 200 values.

Rough inlet data were used only to find the correction length (12.5 ft); they were not used on the graphs.

The integers following the $(h_{max})_{max}$ values indicate the number of peaks out of 200 peaks that were higher than the value of $(h_{max})_{max}$ indicated.

Table 5f Basic Data for Natural Roll Waves

$S_o = .08429$ $h_n = .404$ inch

Station ft	Smooth Inlet (No correction to match rough inlet)								
	$(h_{max})_{max}$ inch	$\bar{h}_{max}$ inch	$\sigma_{h_{max}}$ inch	T_{av} sec	σ_T sec	$\bar{h}_{min}$ inch	$\sigma_{h_{min}}$ inch	c_{av} fps	σ_c fps
18		.427[a]							
24									
30									
36		.436[a]							
42		.440[a]							
48									
54		.461[a]							
60		.476[a]							
66				.554					
72	.631-1	.514	.044	.565					
78	.707-1	.554	.050	.566					
84	.706-2	.578	.053	.582	.215				
90				.626					
96	.732-1	.590	.065	.643	.236				
102	.785-5	.621	.080	.686					
108	.861-2	.646	.086	.735	.285				
114				.808				7.27	.24
120	.859-3	.670	.088	.865	.320	.251	.050		

Notes: a. Measured from pressure record (50 values)

Unless noted otherwise, average values and standard deviations were computed from about 200 values.

Correction length (zero) was found from rough inlet data (using point gage and stop watch) and smooth inlet data (using point gage and stop watch) which are not shown in table.

The integers following the $(h_{max})_{max}$ values indicate the number of peaks out of 200 peaks that were higher than the value of $(h_{max})_{max}$ indicated.

Table 5g Basic Data for Natural Roll Waves

$S_o = 0.1192$ $h_n = .210$ inch

Station ft	Rough Inlet									Smooth Inlet (Correction to match rough inlet = 24 ft)								
	$(h_{max})_{max}$ inch	$\bar{h}_{max}$ inch	$\sigma_{h_{max}}$ inch	T_{av} sec	σ_T sec	h_{min} inch	$\sigma_{h_{min}}$ inch	c_{av} fps	σ_c fps	$(h_{max})_{max}$ inch	$\bar{h}_{max}$ inch	$\sigma_{h_{max}}$ inch	T^f_{av} sec	σ_T sec	$\bar{h}_{min}$ inch	$\sigma_{h_{min}}$ inch	c_{av} fps	σ_c fps
6		.218[a]																
12		.223[a]																
18		.227[a]						5.51[d]										
24		.244[a]		.315														
30		.264[a]		.305	.097	.154[c]	.027[c]	5.67[d]										
36	.385-1	.311	.032	.330	.107					.585-1	.410	.061	.526	.229	.111	.026		
42	.445-1	.339	.038	.364[b]	.126	.122	.023										5.98[e]	.23[e]
48								5.79[e]	.19[e]	.634-1	.451	.069	.635	.272	.105	.023		
54	.521-1	.385	.051	.459[b]	.191	.117	.019											
60										.660-2	.493	.071	.742	.314				
66	.622-1	.437	.057	.572[b]	.233	.115	.023										6.33[c]	.27[c]
72								6.07[e]	.23[e]									
78	.627-3	.472	.066	.685[b]	.270	.118	.018			.732-2	.538	.076	.889	.422	.099[c]	.024[c]		

Notes:
a. Measured from pressure record (50 values)
b. Based on 2000 to 2200 peaks
c. Based on 50 values
d. Based on 20 values
e. Based on 100 values
f. Based on 1800 to 2400 peaks

Unless noted otherwise, average values and standard deviations were computed from about 200 values.

The integers following the $(h_{max})_{max}$ values indicate the number of peaks out of 200 peaks that were higher than the value of $(h_{max})_{max}$ indicated.

Table 5h Basic Data for Natural Roll Waves

$S_o = 0.1192$			$h_n = .409$ inch			
	Rough Inlet					
Station ft	$(h_{max})_{max}$ inch	$\bar{h}_{max}$ inch	$\sigma_{h_{max}}$ inch	T_{av} sec	σ_T sec	c_{av} fps
18		.420[a]				
24		.527[a]				
30		.437[a]				
36		.445[a]				
42		.450[a]				
48		.454[a]				
54		.468[a]		.387		
60		.477[a]		.387	.140	
66		.504[a]		.370	.147	
72						8.49[b]
78	.727-1	.551	.068	.413	.176	

Notes: a. Measured from pressure record (50 values)
b. Based on 20 values

Unless noted otherwise, average values and standard deviations were computed from about 200 values.

The integers following the $(h_{max})_{max}$ values indicate the number of peaks out of 200 peaks that were higher than the value of $(h_{max})_{max}$ indicated.

Table 5i Basic Data for Natural Roll Waves

$S_o = 0.1192$ Rough Channel					
	$h_n = .199$ inch				$h_n = .375$ inch
Station ft	$(h_{max})_{max}$ inch	$\bar{h}_{max}$ inch	$\sigma_{h_{max}}$ inch	T^b_{av} sec	$\bar{h}^a_{max}$ inch
2		.213[a]			
5		.220[a]			
6		.222[a]			.417
8		.231[a]			
10		.235[a]			
12		.243[a]			.426
18		.252[a]			.417
24		.263[a]			.437
30	.307-2	.264	.018		.443
36	.310-3	.271	.018		.451
42	.334-2	.278	.024	.488	.461
48	.342-4	.290	.024	.546	.483
54	.370-2	.302	.020	.607	
60	.330-10	.296	.019	.642	
66					
72	.370-1	.304	.017	.724	
78	.373-1	.310	.019	.760	

Notes: a. Point gage measurement
b. Based on 600 to 800 peaks

Unless noted otherwise, average values were computed from about 200 values.

The integers following the $(h_{max})_{max}$ values indicate the number of peaks out of 200 peaks that were higher than the value of $(h_{max})_{max}$ indicated.

To express distance along the channel and water depths in terms of the normal depth is suggested by the small amplitude theory (equation 3.20). Both of these theories indicate that the Froude number is an important parameter. Therefore the generality of these dimensionless terms for describing the development of natural roll waves can be tested by changing h_n with F held fixed. For each channel slope in the experiments, the value of h_n was changed by a factor of two while the value of F changed slightly. Therefore if the experimental results give unique relations for each slope, it is reasonable to assume that these unique relations would apply at any h_n for the same F and S_o. The effect of changing S_o with F held fixed will be considered in Chapters VI and VII.

The results for $\bar{h}_{max}/h_n$ vs. ℓ/h_n are shown in figures 26-29. On each figure the slope is fixed, and F is approximately constant. Because each graph tends to show a unique relation (except possibly figure 28) for a two-fold change in normal depth, the use of h_n to describe the development of $\bar{h}_{max}$ is justified. It is seen that the general shape of the relations is the same in that the initial part of the curve is concave upwards followed by a concave downward part. In no case did $\bar{h}_{max}$ reach a limiting value.

The dimensionless development relations for the average period in the smooth channel are shown in figures 30-32. In the rough channel only a few periods were measured and are not shown. The period is seen to change very little for small ℓ and then it increases almost linearly to the end of the channel. This quasi-linear increase in period is a result of wave overtaking.

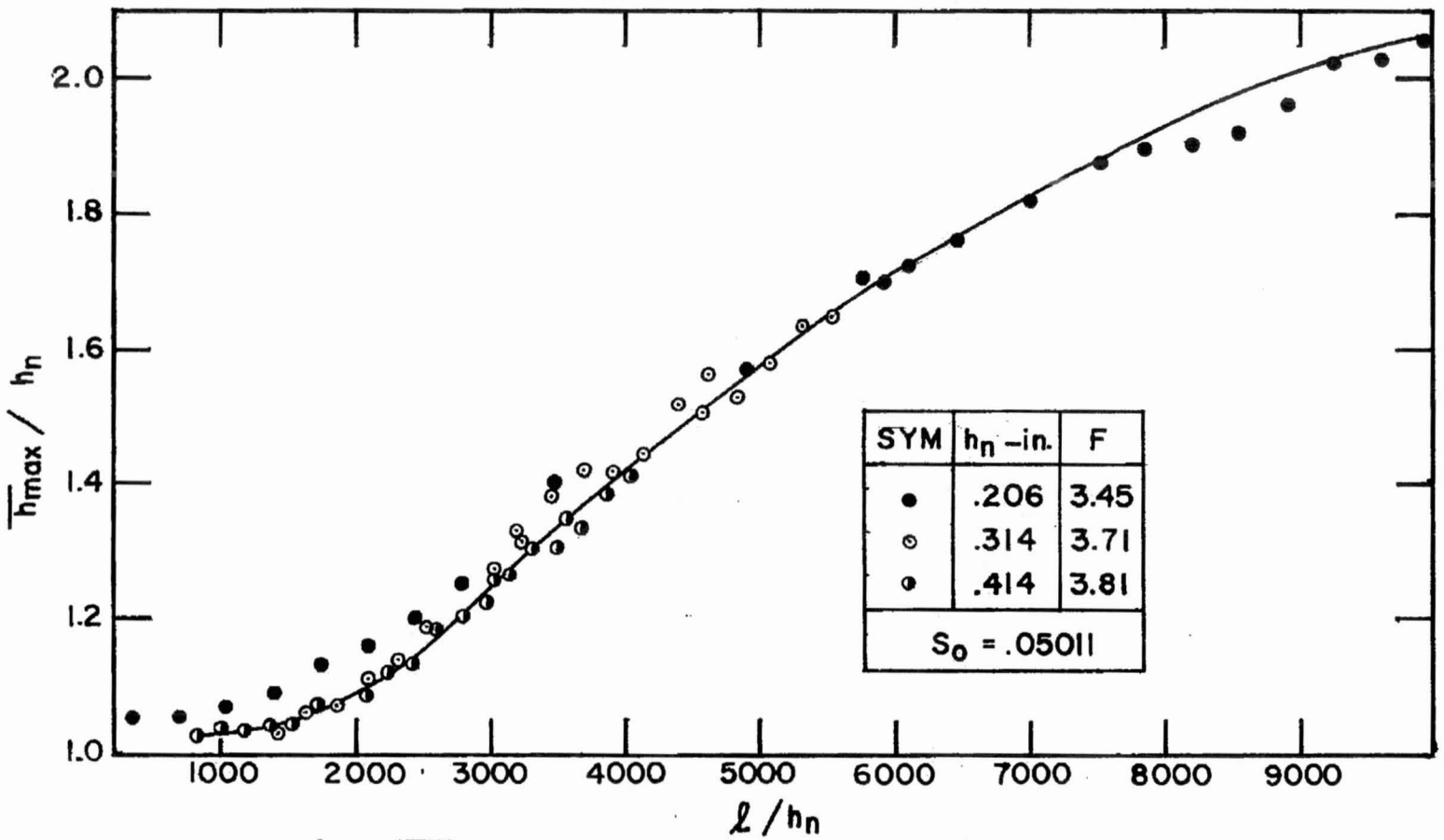

Fig. 26. Development curve for average maximum depth, $\bar{h}_{max}$, in channel with slope of .05011

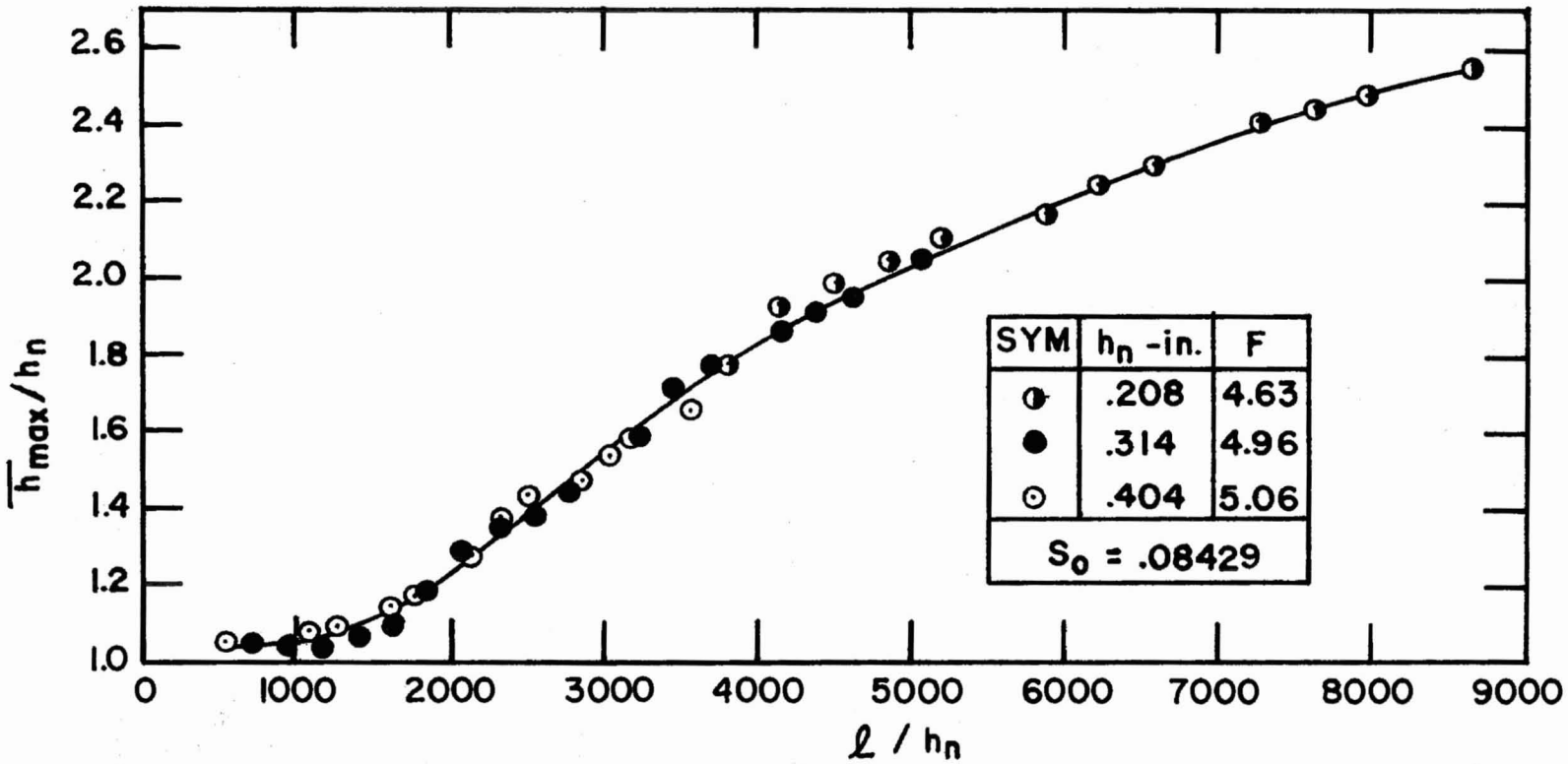

Fig. 27. Development curve for average maximum depth, $\bar{h}_{max}$, in channel with slope of .08429

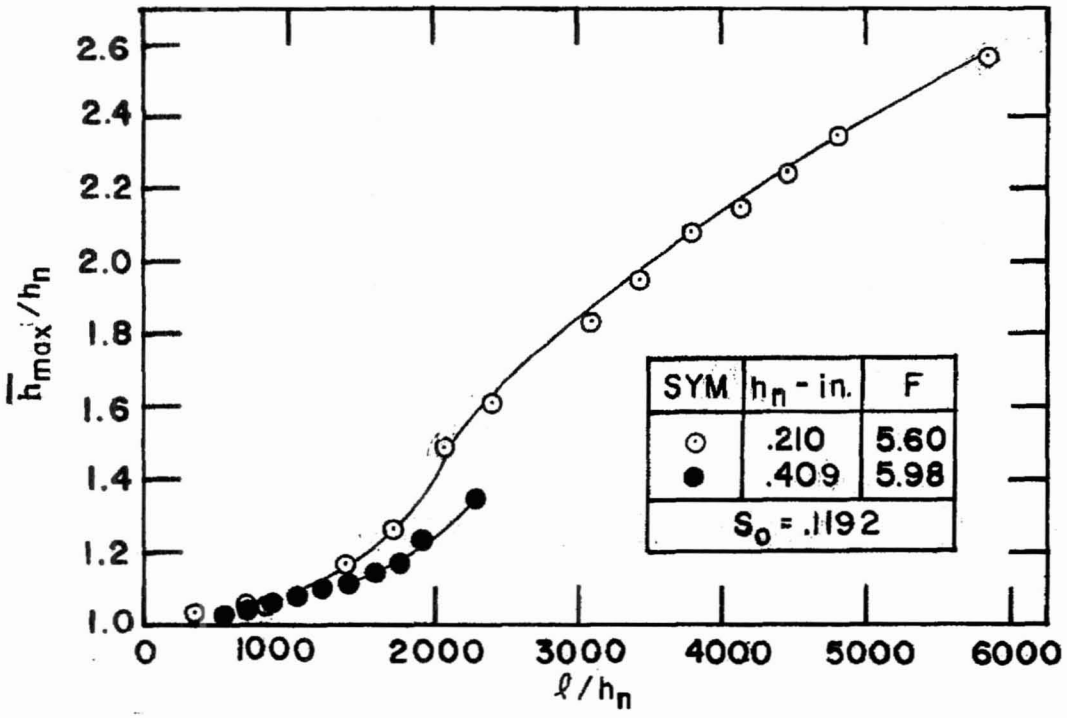

Fig. 28. Development curve for average maximum depth, $\bar{h}_{max}$, in channel with slope of .1192

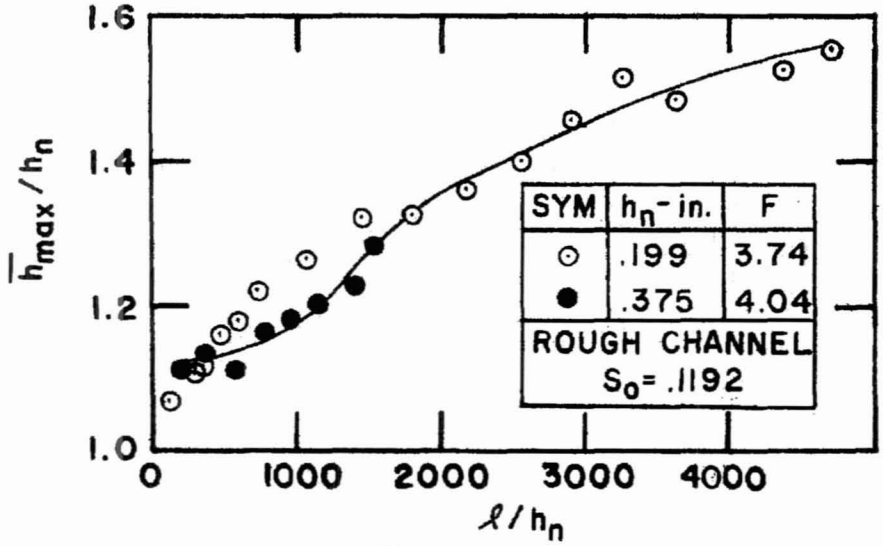

Fig. 29. Development curve for average maximum depth, $\bar{h}_{max}$, in rough channel with slope of .1192

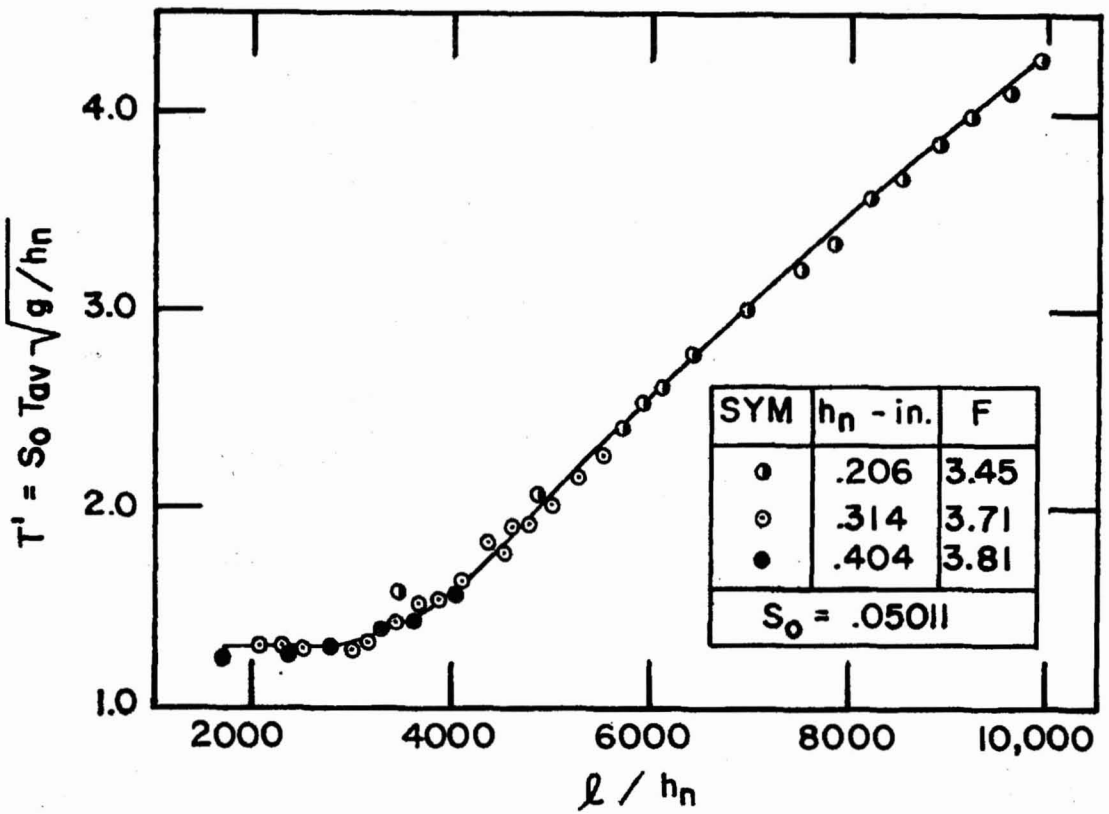

Fig. 30. Development curve for average wave period, T_{av}, in channel with slope of .05011

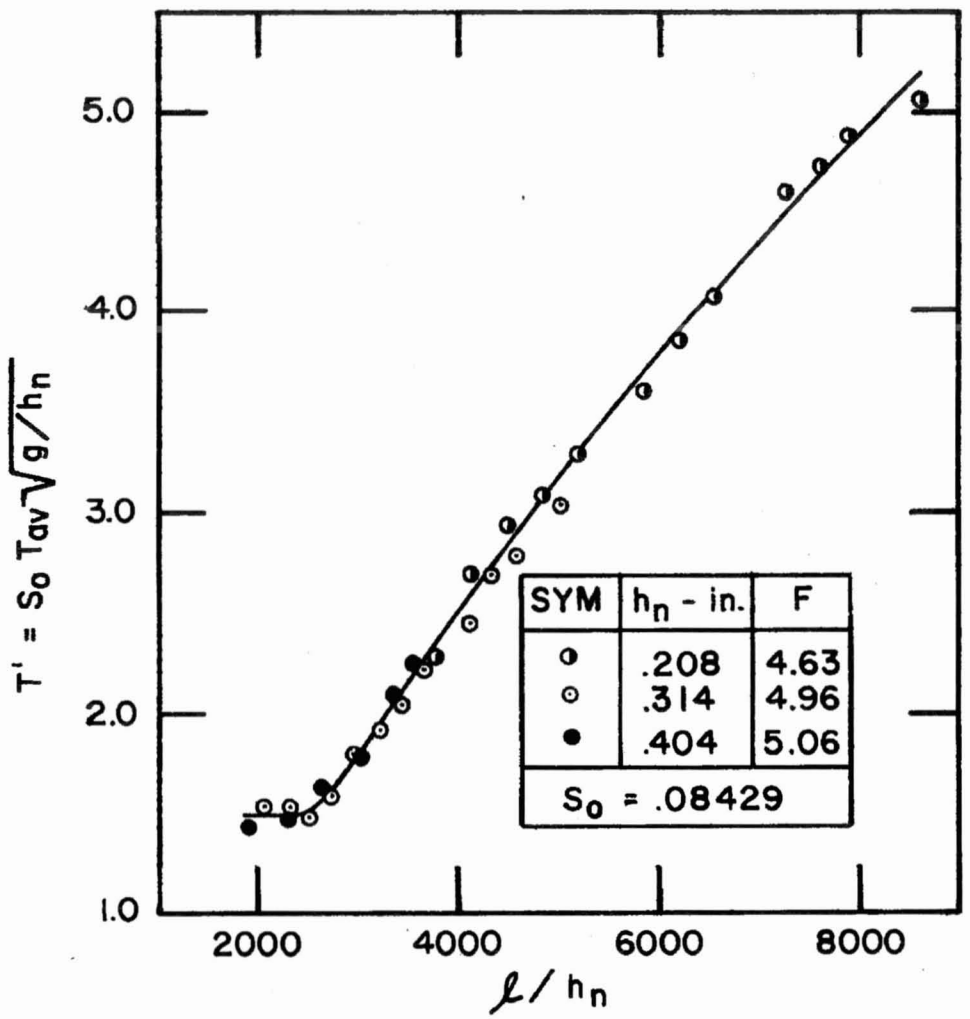

Fig. 31. Development curve for average period, T_{av}, in channel with slope of .08429

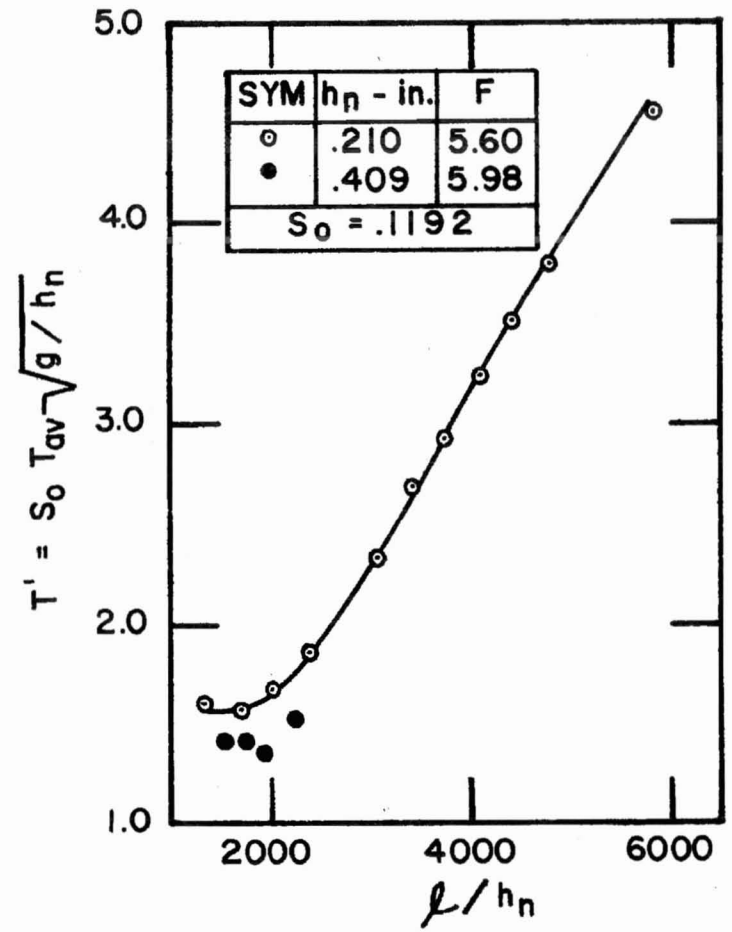

Fig. 32. Development curve for average period, T_{av}, in channel with slope of .1192

In figures 33 and 34 the development relations for $\bar{h}_{min}$ and c_{av}, respectively, are shown. The value of $\bar{h}_{min}$ reached a minimum value in the longer channel (S_o = .05011 and .08429, figure 33a and b). The wave velocity is seen to have increased linearly although there is a definite Froude number dependence even for the small variations of F on each slope. The dependence of $c_{av}/\sqrt{gh_n}$ on F is predictable from the periodic permanent theory. For example, figure 6 shows that $c/\sqrt{gh_n} = 1 + F$ for the limiting case of vanishing wave length.

In figure 35 the development curves for the standard deviation of h_{max} are shown. In contrast to $\bar{h}_{max}$, $\sigma_{h_{max}}$ attained practically a constant value near the end of the channel. On the other hand the standard deviation of the period, shown in figure 36, increased almost linearly as the average period also did.

4. Frequency Distributions and Wave Shape

Typical frequency distributions of the four measured properties h_{max}, T, h_{min} and c are shown in figures 37-40 for various stations in one run. These are plotted on arithmetic-probability paper which is designed such that a frequency distribution with a normal (Gaussian) distribution plots as a straight line. The properties h_{max} and c are well represented by a normal distribution, while the period approximately follows a normal distribution. The minimum depth shows a definite departure from the Gaussian law at the low values.

Figure 41 is a typical pressure record in a region where the waves were small. The variety of wave shapes and lengths is seen. In figure 14 the shape of shock waves is seen.

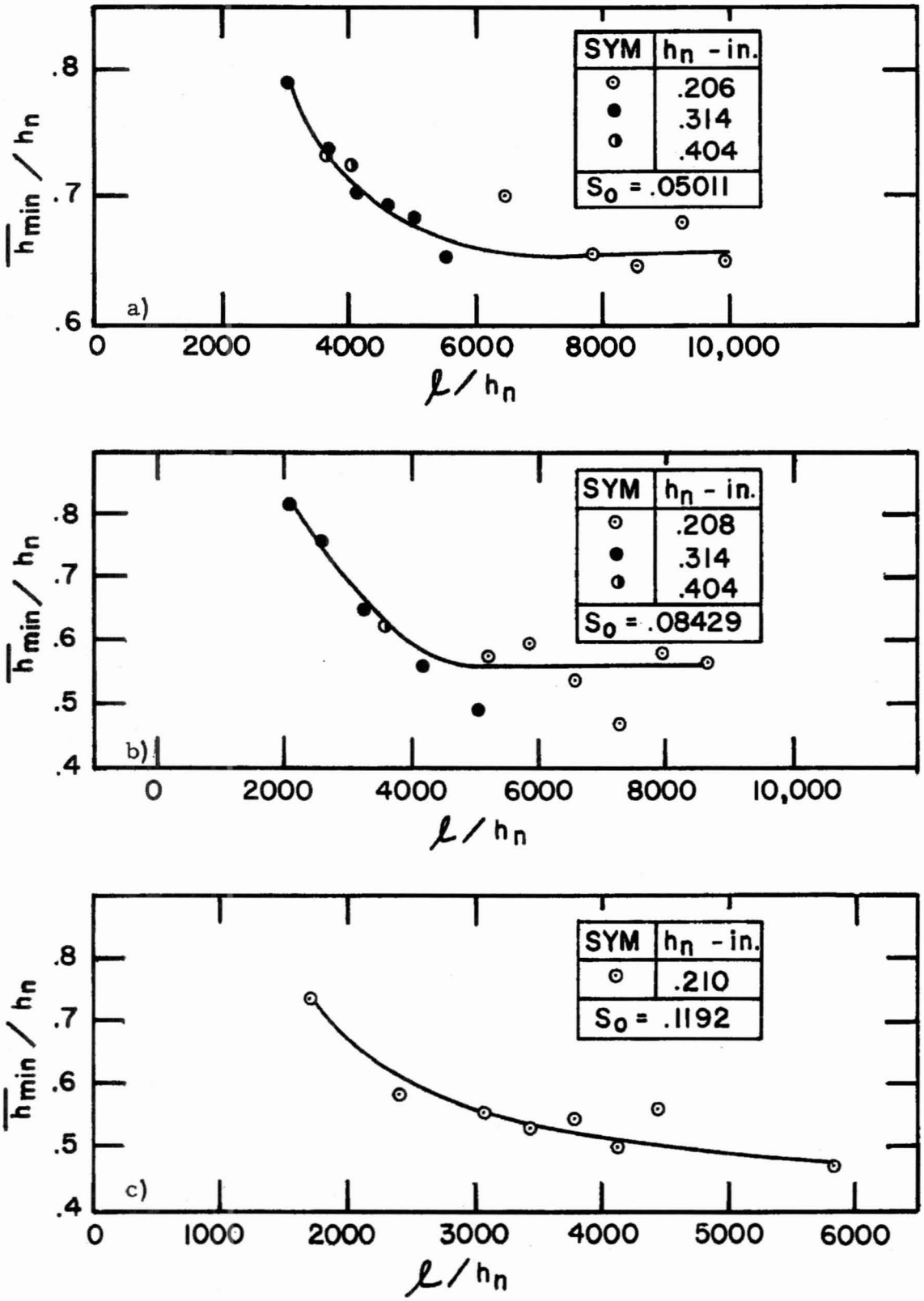

Fig. 33. Development curves for average minimum depth, $\bar{h}_{min}$, for channel slopes of .05011, .08429, .1192

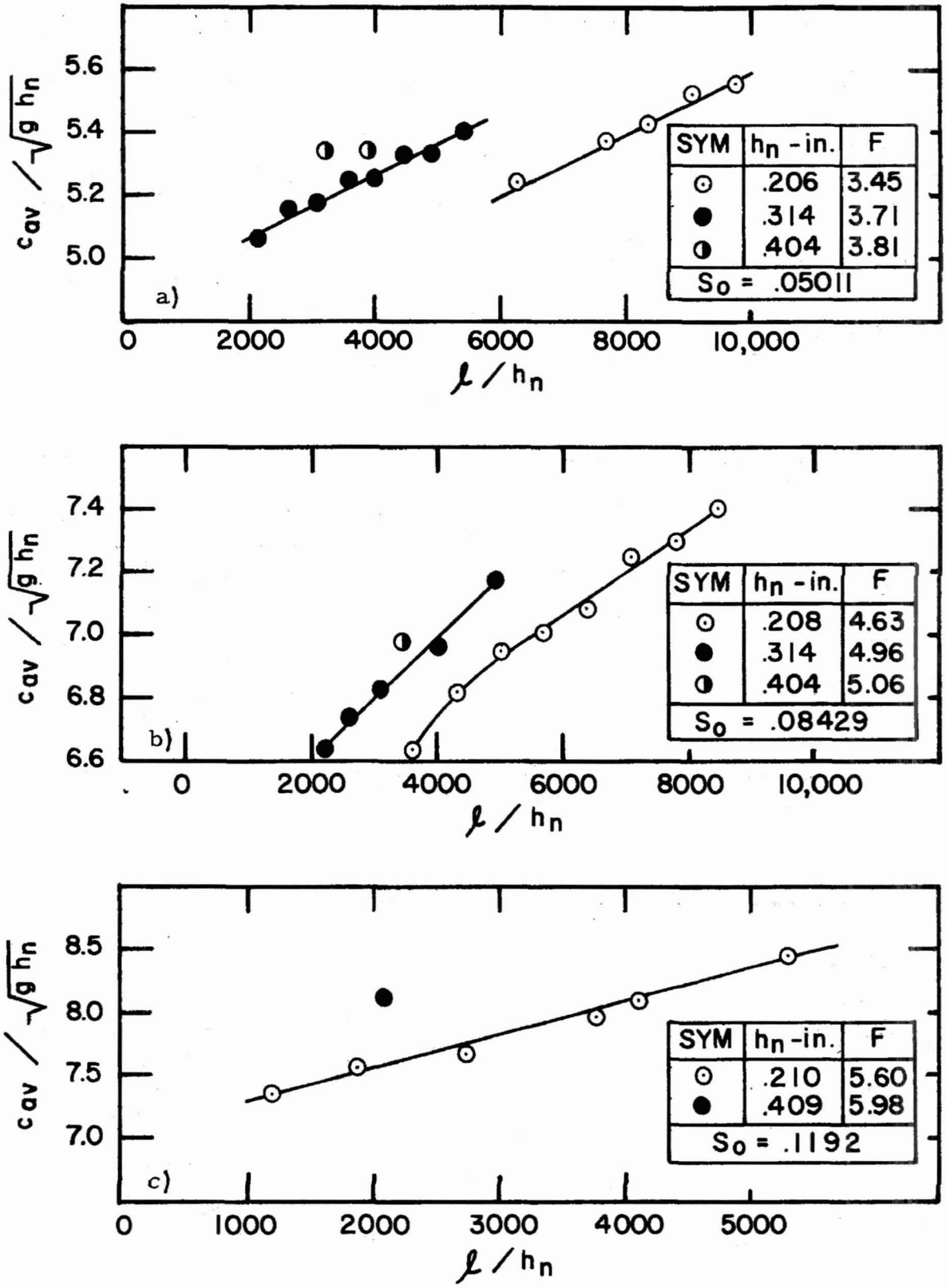

Fig. 34. Development curves for average wave velocity, c_{av}, for channel slopes of .05011, .08429, .1129

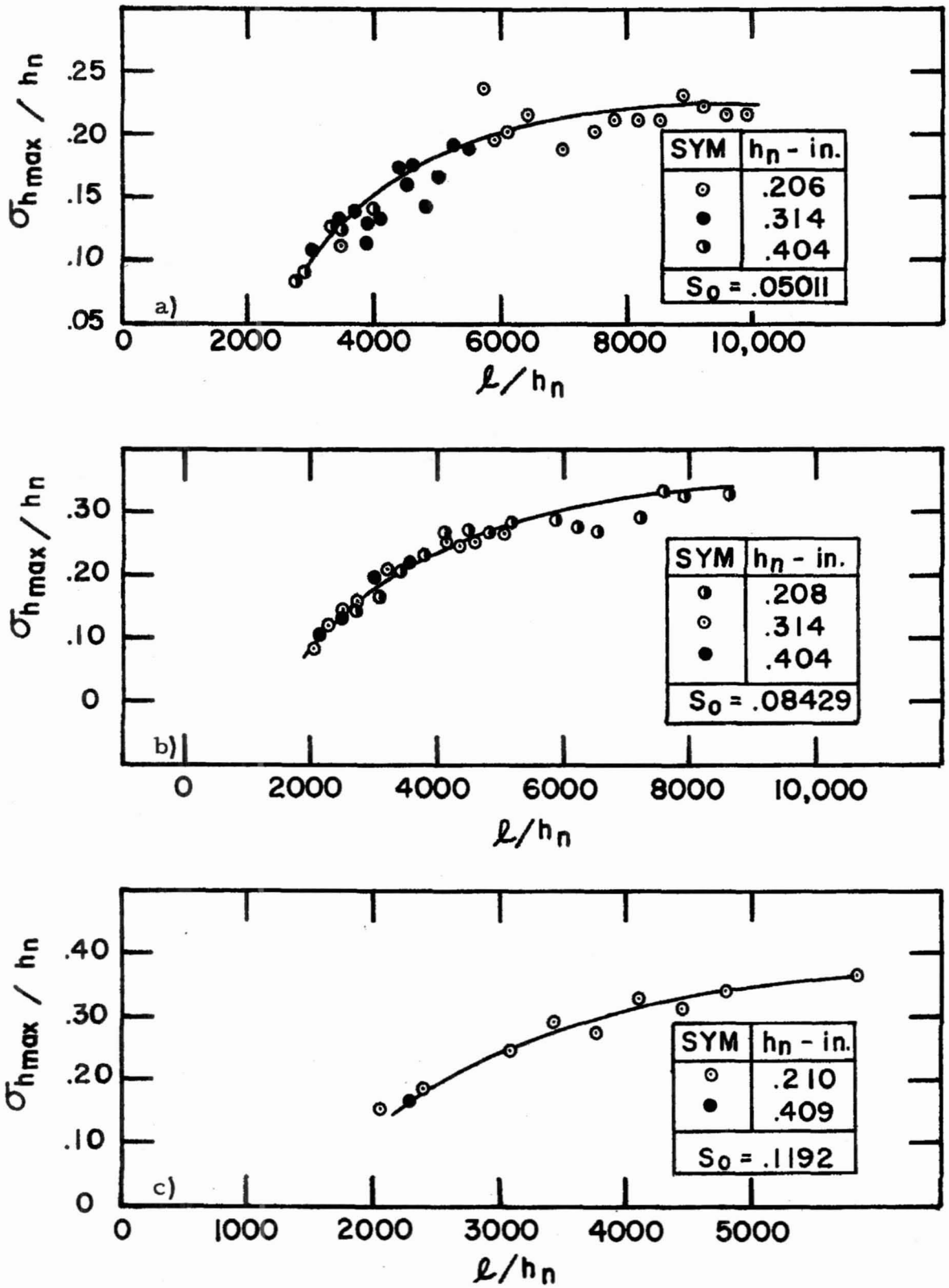

Fig. 35. Development curves for the standard deviation of the maximum depth, $\sigma_{h_{max}}$, for channel slopes of .05011, .08429, .1192

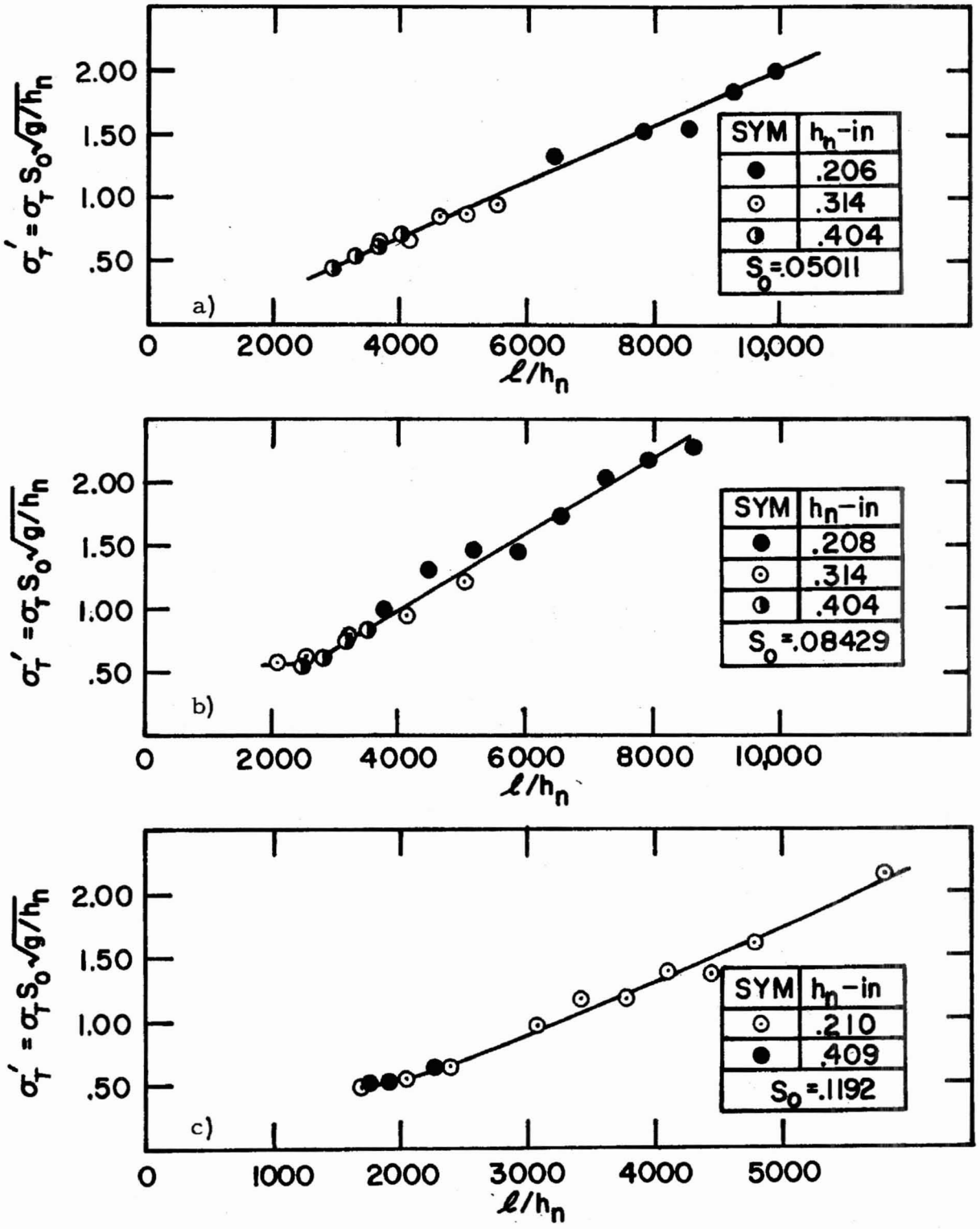

Fig. 36. Development curves for the standard deviation of the wave period, σ_T, for channel slopes of .05011, .08429, .1192

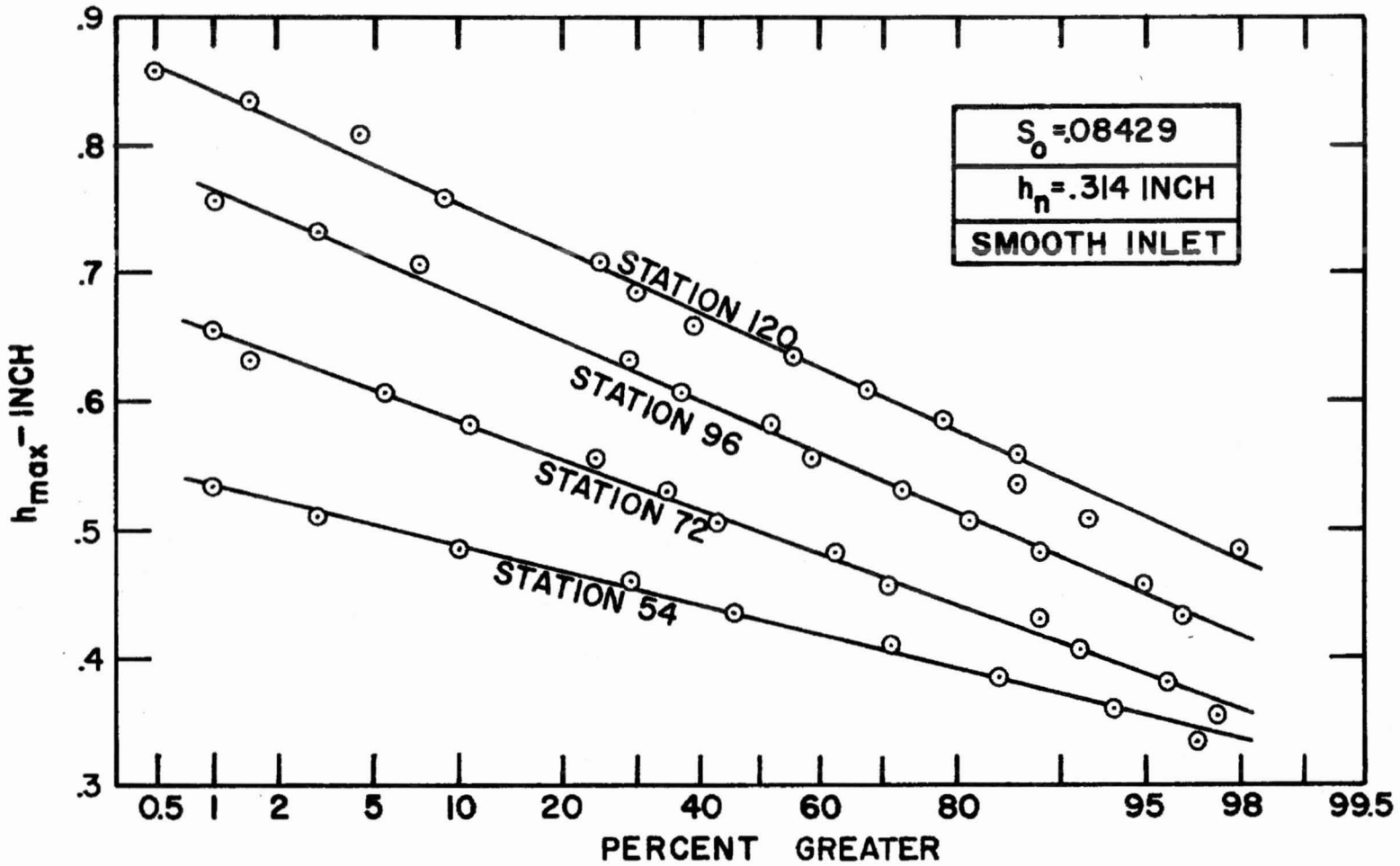

Fig. 37. Typical cumulative frequency distributions of maximum depth, h_{max}

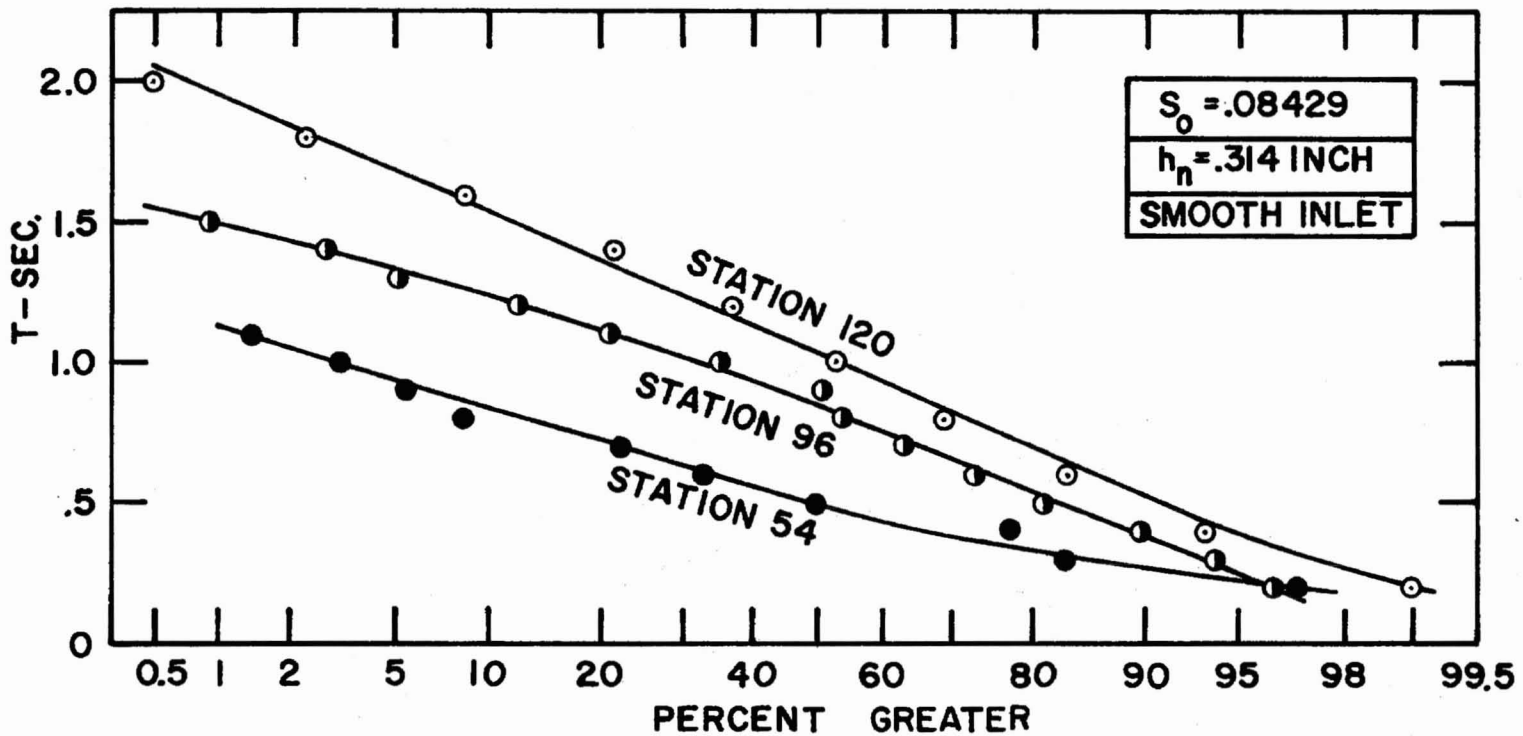

Fig. 38. Typical cumulative frequency distribution of wave period, T

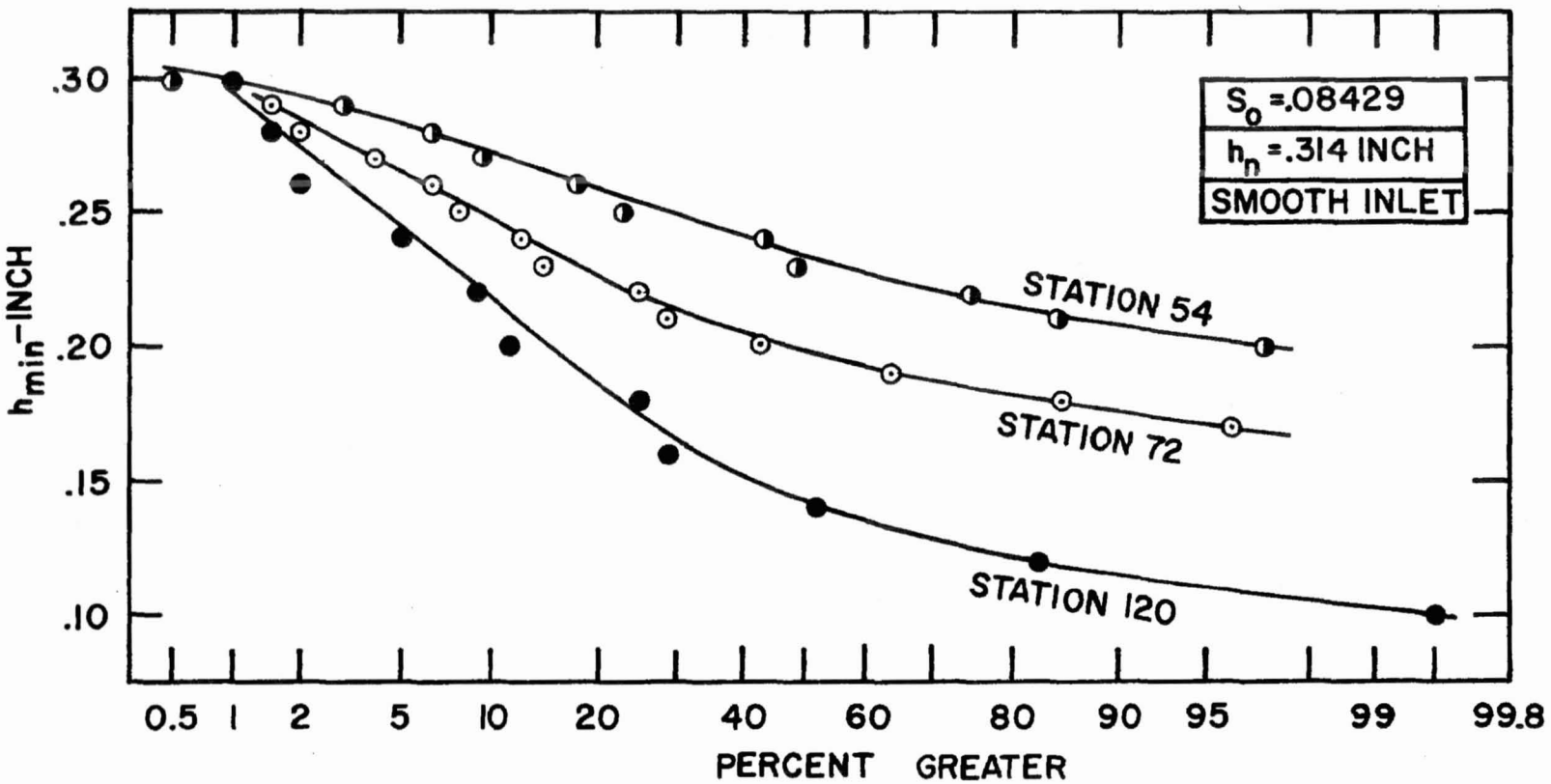

Fig. 39. Typical cumulative frequency distribution of minimum depth, h_{min}

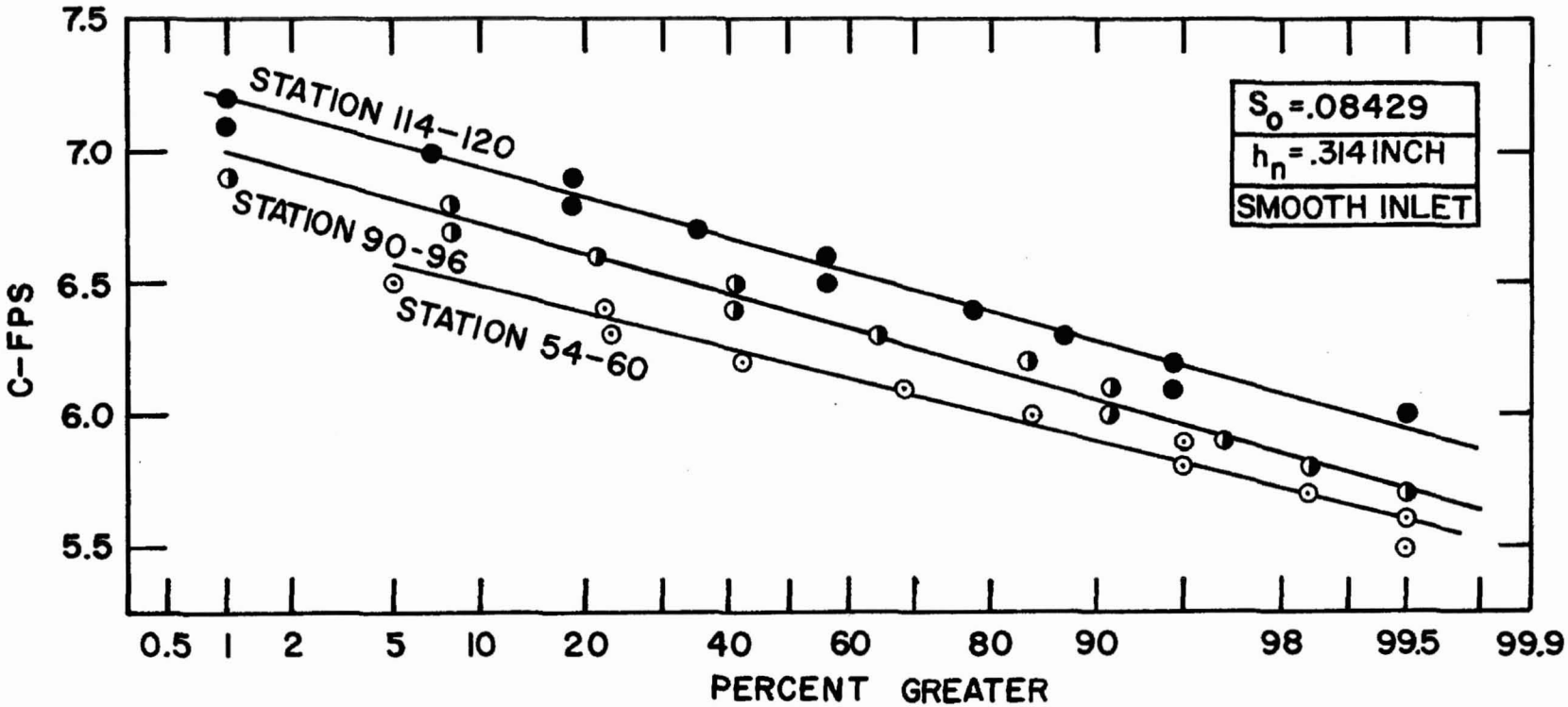

Fig. 40. Typical cumulative frequency distributions of wave velocity, c

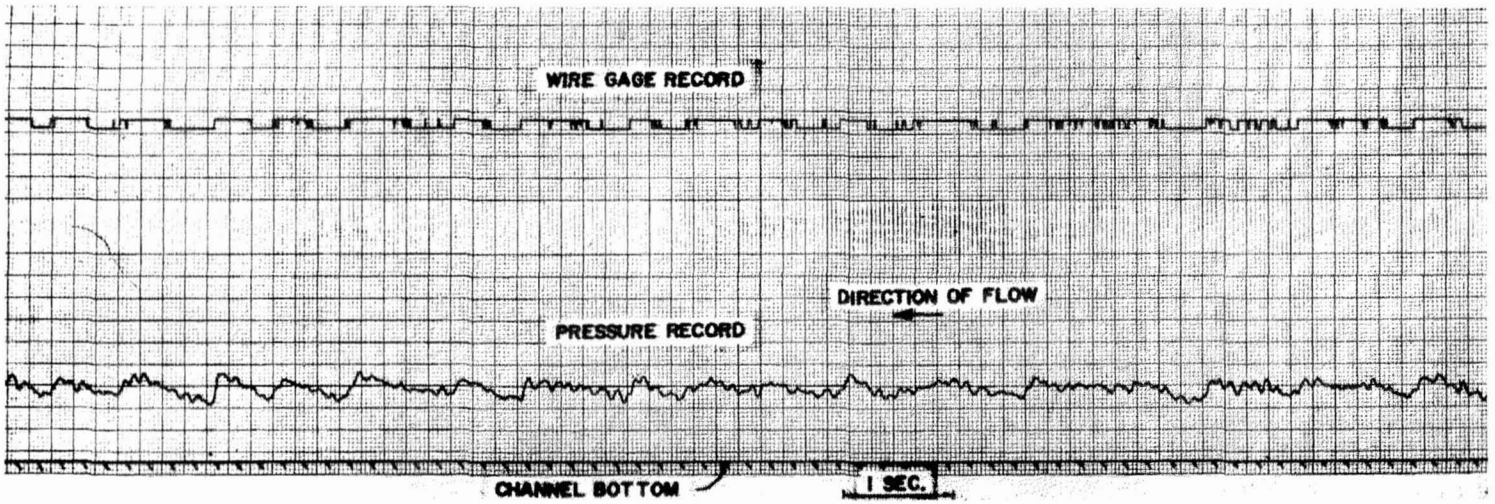

Fig. 41. Typical pressure and wire gage record for small amplitude roll waves, $S_o = .05011$, $h_n = .314$ in., station 36, smooth inlet

V-D PERIODIC PERMANENT ROLL WAVES

1. 130 ft Channel

As mentioned in Section IV-B there was one periodic permanent wave run in the 130-ft channel. The conditions for this run were: $T = 3.00$ sec, $S_o = .01942$, $h_n = .780$ in., and $c = 5.70$ fps. The measured wave profile and velocity are shown in figure 43 along with the theoretical solution for the profile for $F = 2.65$ and a dimensionless period (T') of 1.30. The wave profile agrees very closely with the theoretical solution, and the measured velocity is slightly higher than given by the theory. Figure 42 shows a definition sketch for wave profiles. The length of the shock front ($\lambda - (x_1)_{max}$) was not measured in the run in the 130-ft channel, and was assumed to be negligible as shown in figure 43.

2. Steep Channel

Wave shapes and velocities for periodic permanent waves in the steep channel were measured by methods explained in Chapter IV. Table 6 contains the F and T' values for each run, and the results for h_{max}, h_{min}, and c in dimensionless form. Because these three properties are of prime interest, they are plotted in figure 44 along with the theoretical relations. In plotting the experimental points on figure 44, the same symbol was used for all data obtained for a given slope. However for all slopes, except .05011, there was one run at a higher normal depth, and thus a higher F, than the other runs at the same slope. In most cases data for this one run are not consistent with that of other runs, which can be attributed to the slightly higher value of F.

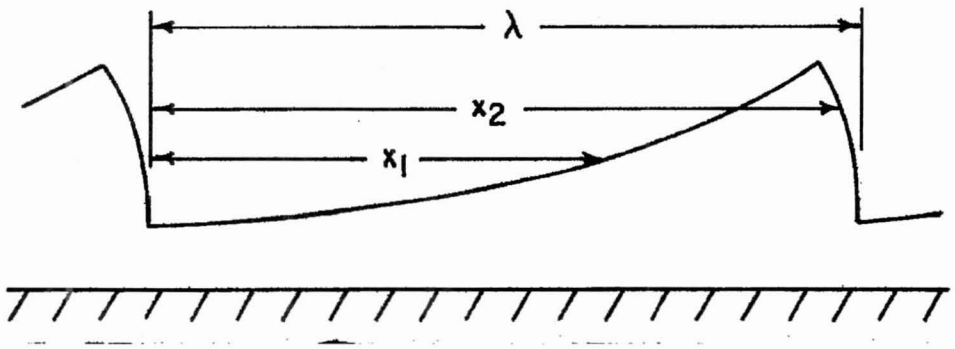

Fig. 42. Definition sketch for coordinates of water-surface profiles for periodic permanent roll waves

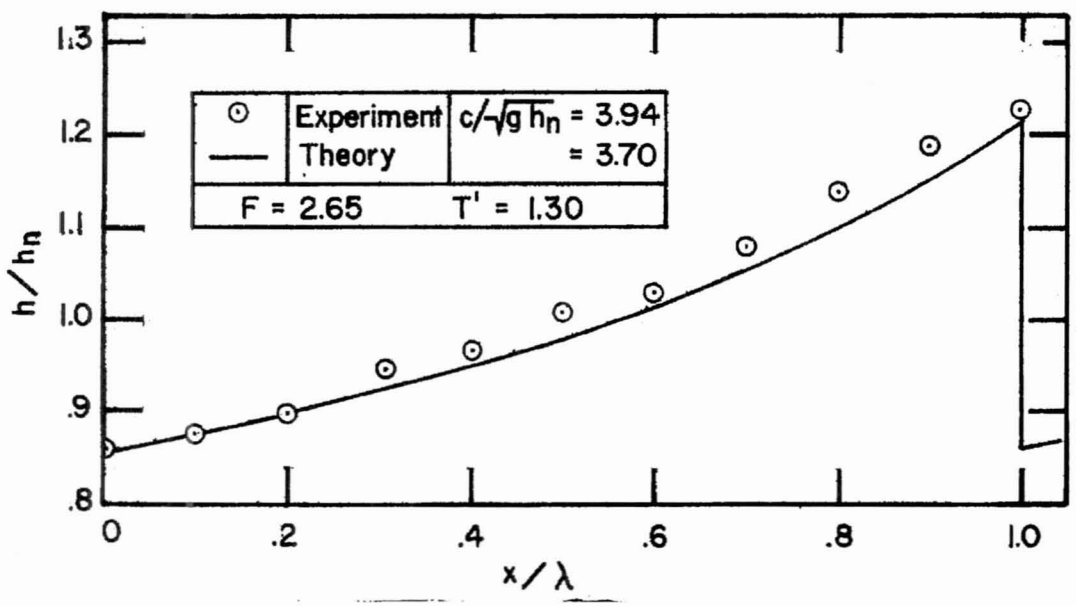

Fig. 43. Graph of measured and theoretical water-surface profile for periodic permanent roll waves in 130-ft channel, F=2.65, T'=1.30, S_o=.0194

Table 6

Basic Data for Periodic Permanent Roll Waves

S_o	Channel	h_n inch	F	T'	$c/\sqrt{gh_n}$	h_{max}/h_{min}	h_{max}/h_n	h_{min}/h_n
.05011	Smooth	.314	3.71	1.08	5.18	1.72	1.30	.76
.05011	Smooth	.314	3.71	1.64	5.27	2.15	1.46	.68
.05011	Smooth	.314	3.71	2.14	5.36	2.60	1.63	.63
.08429	Smooth	.208	4.63	1.63	6.46	2.35	1.54	.66
.08429	Smooth	.314	4.96	2.50	7.01	-	1.91	-
.08429	Smooth	.208	4.63	2.89	6.79	3.58	2.00	.56
.08429	Smooth	.208	4.63	4.07	7.15	4.37	2.35	.54
.08429	Smooth	.208	4.63	4.53	7.24	4.66	2.49	.53
.1192	Smooth	.210	5.60	2.25	7.74	3.42	2.78	.52
.1192	Smooth	.210	5.60	3.55	8.24	4.96	2.31	.47
.1192	Smooth	.308*	5.90*	4.25	8.82	5.49	2.65	.44
.1192	Smooth	.210	5.60	5.19	8.76	6.38	2.82	.45
.1192	Rough	.199	3.74	1.98	5.43	1.91	1.34	.70
.1192	Rough	.199	3.74	3.73	5.73	2.30	1.54	.67
.1192	Rough	.375	4.04	4.19	6.14	2.05	1.55	.75
.1192	Rough	.199	3.74	5.64	5.95	2.72	1.68	.62

*Normal depth and Froude Number interpolated from measured values at this slope.

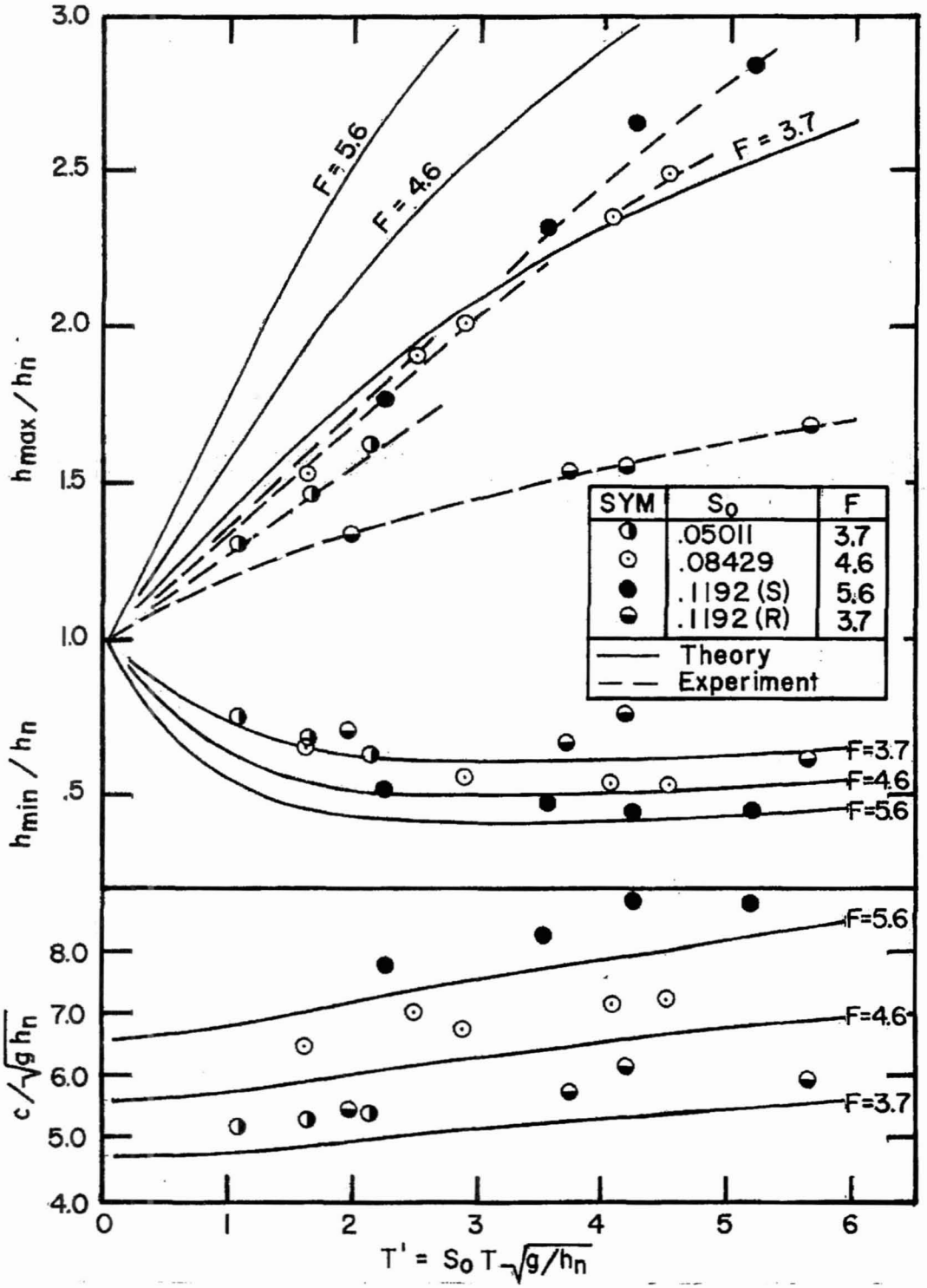

Fig. 44. Graph of experimental values and theoretical solutions for h_{max}, h_{min}, and c as functions of dimensionless wave period T' and Froude number F, for periodic permanent roll waves

This slight discrepancy should be considered when examining figure 44. The values of F used for the theoretical relations correspond to the F for the majority of the data points at a given slope as can be seen from table 6. Note that the rough channel (S_o = .1192, h_n = .199 in.) and the smooth channel (S_o = .05011, h_n = .314 in.) had an F of about 3.7. It is seen that for all three properties there is a consistent experimental relation for each F which is similar to the theoretical relation. For h_{min} and c the experimental points are slightly above the theoretical curve. For h_{max} the measurements are considerably lower than the theoretical values and for a smooth channel this discrepancy increases as the Froude number increases. The rough channel relation is even lower than the smooth channel relation for the same F.

In table 7 all of the data obtained on wave shape are presented. On figure 45 a few of these data are plotted which serve to show the significant trends. Of particular interest is the length of the shock front which was assumed to be negligible in the periodic permanent wave theory.

V-E OBSERVATIONS ON INDIVIDUAL WAVES

All of the data on natural roll waves presented above have been obtained by measuring properties at one station, then repeating the measurements at other stations at a later time. These measurements were combined to give the behavior of a particular property as a function of distance along the channel. To get some information on how the properties of an individual wave changed with distance along the flume, pressure records taken at four stations simultaneously were examined.

Table 7

Observed Wave Shape for Periodic Permanent Roll Waves

S_o = .05011 T' = 1.64			S_o = .05011 T' = 2.14			S_o = .08429 T' = 1.63		
h/h_n	x_1/λ	x_2/λ	h/h_n	x_1/λ	x_2/λ	h/h_n	x_1/λ	x_2/λ
.752	.203	1.00	.640	.048	1.00	.664	.065	1.00
.832	.349	1.00	.687	.154	1.00	.711	.149	1.00
.911	.483	1.00	.752	.298	1.00	.760	.256	1.00
.990	.571	1.00	.832	.436	1.00	.880	.425	.982
1.070	.648	1.00	.990	.599	1.00	1.000	.554	.982
1.150	.720	1.00	1.150	.715	1.00	1.120	.652	.982
1.229	.786	.992	1.308	.798	.987	1.240	.732	.973
1.308	.821	.983	1.387	.825	.980	1.361	.806	.964
1.387	.879	.949	1.467	.873	.975	1.481	.871	.911
1.467	.925	.932	1.549	.914	.957			
			1.629	.930	.934			

S_o = .08429 T' = 2.89			S_o = .08429 T' = 4.07			S_o = .08429 T' = 4.53		
h/h_n	x_1/λ	x_2/λ	h/h_n	x_1/λ	x_2/λ	h/h_n	x_1/λ	x_2/λ
.644	.264	1.00	.644	.348	1.00	.582	.211	1.00
.764	.464	1.00	.764	.526	1.00	.630	.336	1.00
1.005	.633	1.00	1.005	.689	1.00	.750	.554	1.00
1.245	.743	.995	1.245	.771	.996	.870	.650	1.00
1.486	.823	.990	1.486	.816	.989	.990	.708	1.00
1.726	.864	.970	1.726	.865	.984	1.231	.779	1.00
1.846	.900	.955	1.966	.899	.978	1.471	.828	.994
			2.207	.928	.957	1.712	.864	.987
			2.327	.947	.954	1.952	.895	.982
						2.192	.927	.972
						2.313	.946	.966
						2.433	.952	.953

Table 7 (continued)

Observed Wave Shape for Periodic Permanent Roll Waves

S_o = .1192 T' = 2.25			S_o = .1192 T' = 3.55			S_o = .1192 T' = 4.25		
h/h_n	x_1/λ	x_2/λ	h/h_n	x_1/λ	x_2/λ	h/h_n	x_1/λ	x_2/λ
.520	.017	1.00	.481	.059	1.00	.523	.125	1.00
.566	.095	1.00	.529	.152	1.00	.603	.260	1.00
.615	.210	1.00	.576	.302	1.00	.685	.334	1.00
.758	.416	1.00	.648	.412	1.00	.847	.580	1.00
.877	.522	1.00	.767	.533	1.00	1.010	.688	1.00
.995	.606	1.00	.886	.600	1.00	1.332	.772	.988
1.113	.684	1.00	1.005	.683	1.00	1.658	.824	.980
1.352	.774	.986	1.124	.723	1.00	1.982	.880	.976
1.470	.830	.982	1.243	.764	1.00	2.305	.924	.956
1.588	.867	.968	1.481	.815	1.00	2.635	.934	.936
1.710	.901	.931	1.719	.847	.985			
1.827	.915	.920	1.838	.869	.979			
			1.957	.887	.968			
			2.076	.911	.957			
			2.195	.922	.945			
			2.314	.933	.939			

S_o = .1192 T' = 5.19			S_o=.1192 Rough Channel T'=1.98			S_o=.1192 Rough Channel T'=3.73		
h/h_n	x_1/λ	x_2/λ	h/h_n	x_1/λ	x_2/λ	h/h_n	x_1/λ	x_2/λ
.433	.009	1.00	.713	.024	1.00	.677	.027	1.00
.481	.062	1.00	.814	.225	1.00	.728	.117	1.00
.529	.198	1.00	.864	.405	1.00	.778	.210	1.00
.648	.357	1.00	.990	.599	.996	.828	.321	.994
.767	.598	1.00	1.040	.718	.991	.878	.444	.989
.885	.662	1.00	1.120	.794	.989	.978	.617	.983
1.124	.751	.988	1.170	.868	.981	1.080	.717	.983
1.361	.800	.988	1.222	.893	.963	1.181	.818	.989
1.719	.856	.988	1.272	.933	.958	1.283	.854	.980
1.905	--	.984	1.322	.952	.953	1.383	.912	.973
2.195	.903	.976				1.433	.944	.978
2.435	.919	.969				1.483	.953	.976
2.550	.935	.965				1.533	.959	.965
2.665	.948	.961				1.584	.955	.956
2.735	.950	.953						
2.910	.956	.957						

Table 7 (continued)

Observed Wave Shape for Periodic Permanent Roll Waves

S_o=.1192 Rough Channel T'=4.19			S_o=.1192 Rough Channel T'=5.64		
h/h_n	x_1/λ	x_2/λ	h/h_n	x_1/λ	x_2/λ
.787	.149	1.00	.657	.077	1.00
.853	.289	1.00	.707	.122	1.00
.920	.466	1.00	.758	.261	1.00
.987	.605	1.00	.808	.326	.994
1.120	.755	1.00	.858	.459	.992
1.253	.843	.993	.908	.590	.992
1.320	.894	.990	1.008	.733	.988
1.388	.933	.984	1.109	.806	.989
1.455	.942	.968	1.209	.843	.985
1.520	.958	.964	1.310	.888	.982
			1.410	.907	.983
			1.510	.942	.980
			1.610	.959	.960

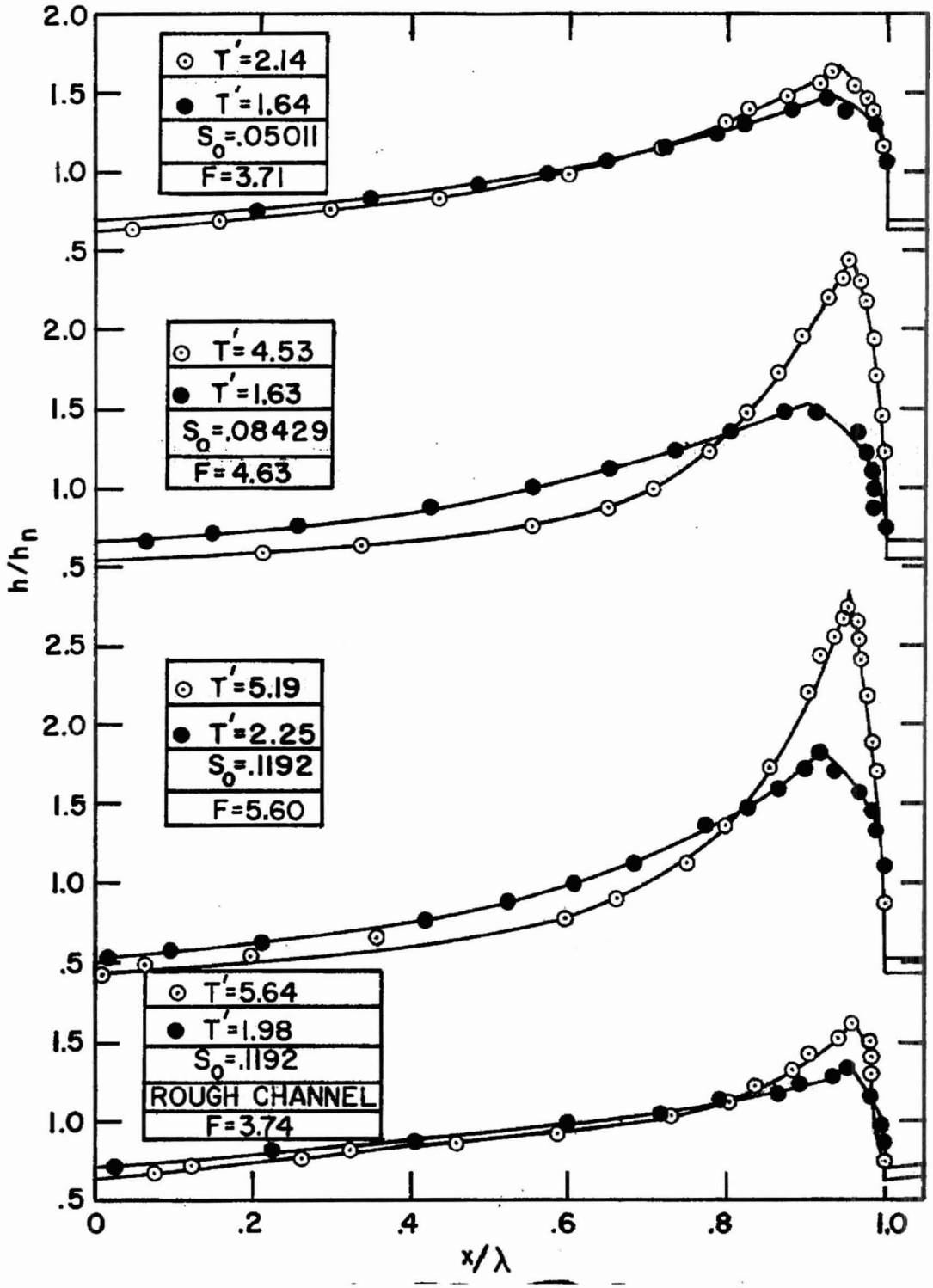

Fig. 45. Graphs of measured water-surface profiles for periodic permanent roll waves

In figure 46 pressure records for stations 42, 54, 66, and 78 are shown. At station 42 twelve waves are numbered and these same waves are identified at each station. From a dynamic calibration and this pressure record, the values of h_{max}/h_n for these twelve waves were found and are listed in table 8. The important role of the overtaking process is clear from this table and figure 46.

In order to examine the behavior of the wave velocities when waves overtake each other, the simultaneous pressure records for stations 60, 66, 72, and 78 presented in figure 47 were examined. From these records one can see three cases in which one wave overtook another. The calibration for this pressure record was not obtained and is indeed not required to measure wave velocities. In table 9 the measured velocities for the peaks delineated in figure 47 are tabulated.

V-F ADDITIONAL DATA - LABORATORY AND FIELD

1. Ghambarian Laboratory Data

Ghambarian's (13) experiments were discussed briefly in Section II-C. He presented his results for $\bar{h}_{max}$ on a graph of $\bar{h}_{max}/h_{cr}$ vs. $S_o\ell/h_{cr}$ where h_{cr} is the critical depth which for a rectangular channel is

$$h_{cr} = (q^2/g)^{1/3} \tag{5.3}$$

where q is the discharge per unit width. Ghambarian found that the value of $\bar{h}_{max}/h_{cr}$ attained a constant value after a sufficient distance. Because the value of S_o is not indicated on his graph ($\bar{h}_{max}/h_{cr}$ vs. $S_o\ell/h_{cr}$), this distance cannot be determined. From his graph it was

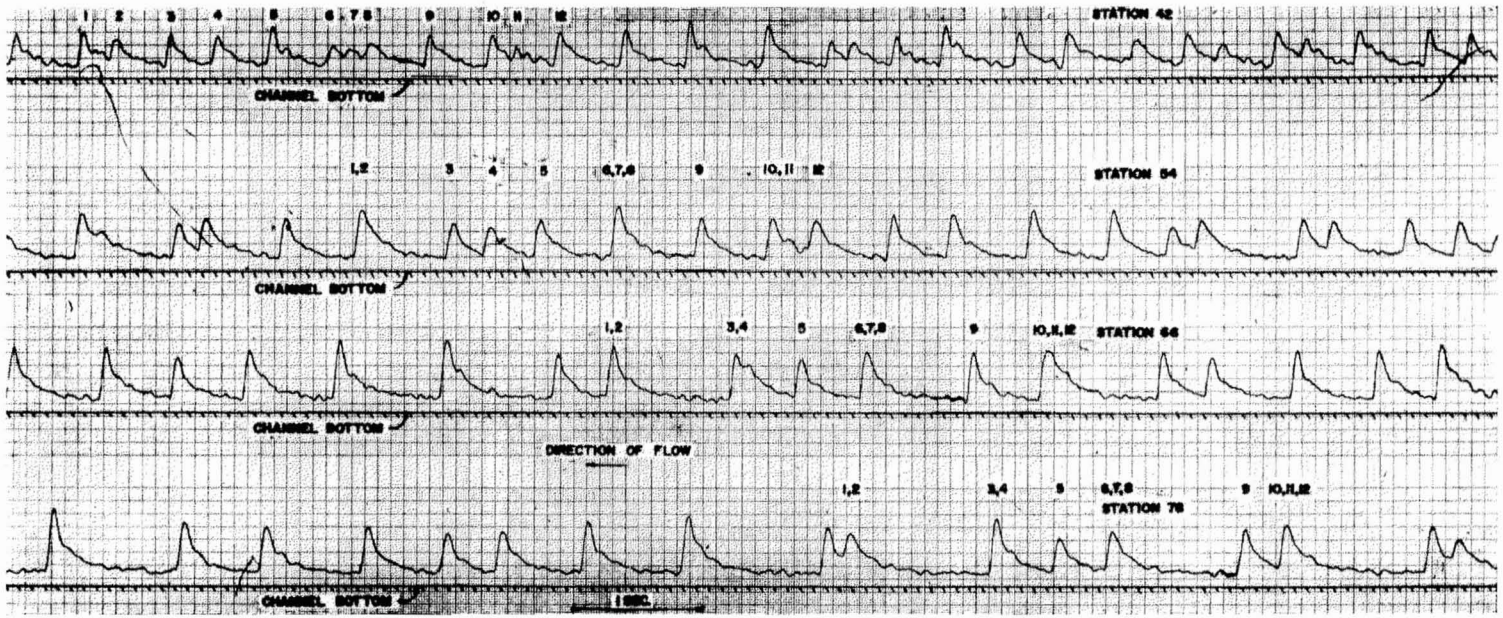

Fig. 46. Pressure records for a train of 12 shock-type roll waves at stations 42, 54, 66, 78, for h_n = .210 in., S_o = .1192, rough inlet

Table 8

Values of h_{max}/h_n For Twelve Consecutive Natural Waves

Peak No.	Station 42	Station 54	Station 66	Station 78
1	1.98	2.26	2.52	2.18
2	1.63			
3	1.85	1.77	2.16	2.77
4	1.79	1.64		
5	2.18	1.91	1.99	1.97
6	1.36			
7	1.25	2.40	2.28	2.23
8	1.47			
9	1.85	2.01	2.25	2.34
10	1.82	1.96		
11	1.30		2.37	2.50
12	1.96	1.87		

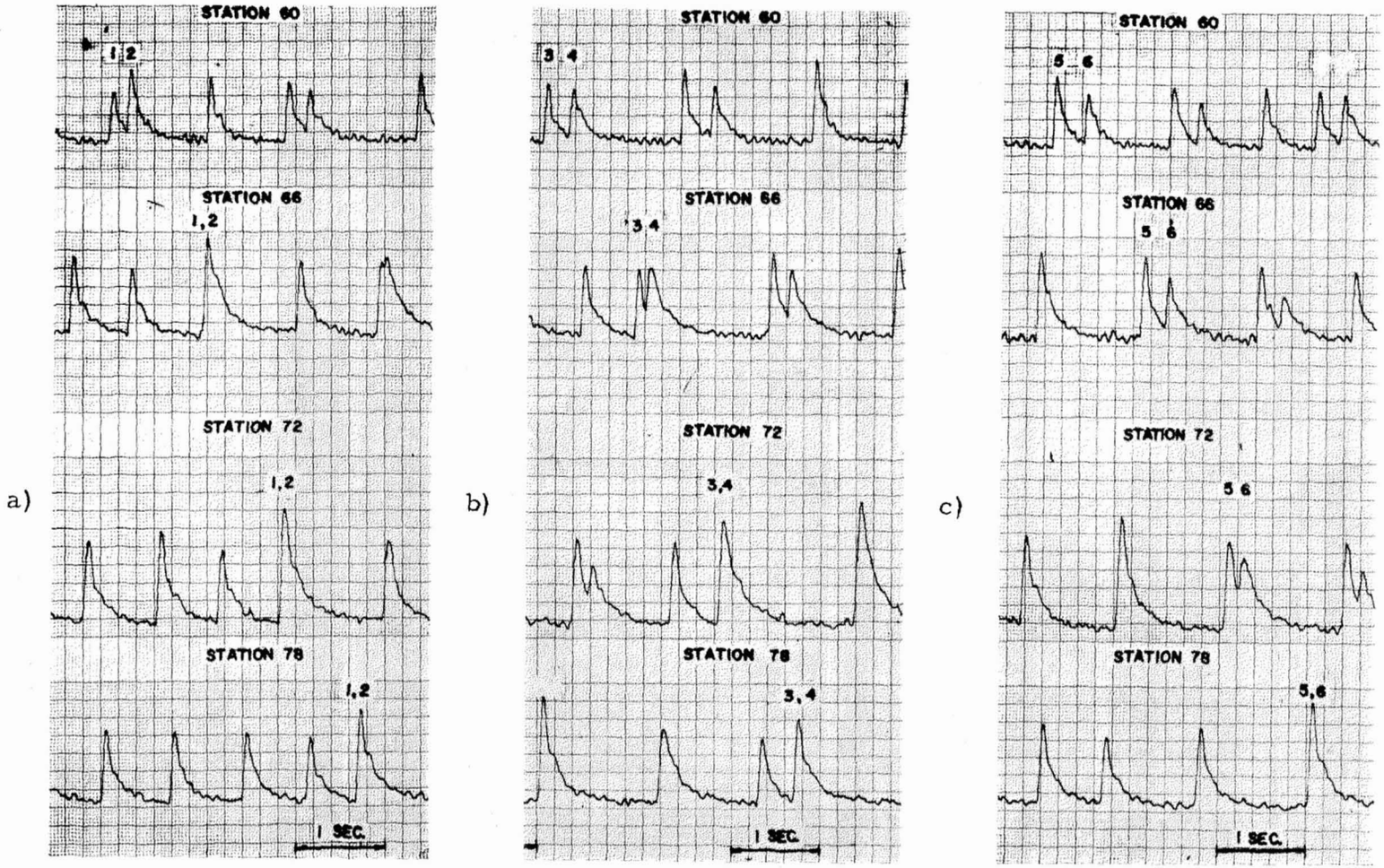

Fig. 47. Pressure records for shock-type roll waves at stations 60, 66, 72, 78, for h_n=.210 in., S_o=.1129, smooth inlet, showing 3 overtakes: waves 1 and 2 in fig. 47a; waves 3 and 4 in fig. 47b; and waves 5 and 6 in fig. 47c

Table 9

Wave Velocities During Overtaking

Stations	Fig. 47a		Fig. 47b		Fig. 47c	
	leading wave -1	following wave -2	leading wave-3	following wave-4	leading wave-5	following wave-6
60-66	5.90 fps	7.30	5.90	6.89	6.01	6.59
66-72	6.77(combined)		6.26	7.15	6.15	6.86
72-78	6.81(combined)		7.04(combined)		6.17	7.50

possible to read off three of these maximum values of $\bar{h}_{max}/h_{cr}$. To convert these to values of $\bar{h}_{max}/h_n$ the relation,

$$h_{cr}/h_n = F^{2/3} \tag{5.4}$$

was used. This follows from the definition of h_{cr} and continuity ($q = u_n h_n$). These three values are shown in table 10. The maximum F of 11.58 can probably be assumed to correspond to the maximum channel slope of .86 (channel length of 10 meters), but the slopes for the other two values are not known.

Table 10

Maximum Average Wave Depths After Ghambarian

F^2	Maximum value of $\bar{h}_{max}/h_{cr}$	F	h_{cr}/h_n	Maximum value of $\bar{h}_{max}/h_n$
14.6	.75	3.82	2.44	1.83
50.1	.74	7.08	3.69	2.73
134.0	.65	11.58	5.12	3.33

All the data points were read from a graph of $\bar{h}_{max}/h_{cr}$ vs. ℓ/h_{cr} in the paper by Ghambarian and Mayilian (14) where the results for $S_o = 0.10$ were presented. These values of $\bar{h}_{max}/h_{cr}$ and ℓ/h_{cr} were converted to values of $\bar{h}_{max}/h_n$ and ℓ/h_n by using equation 5.4. For this slope the channel was 60 meters long and the channel roughness was reported in terms Manning "n" values. For a n of .011 the F was 3.96, and for a n of .015 the F was 3.30. These values of F are about the same as for the smooth channel used in this investigation for a

slope of .05011. Thus it can be deduced that the channel Ghambarian used for the runs at a slope of 0.10 was rough.

The values of $\bar{h}_{max}/h_n$ are shown in figure 48 along with the experimental relations obtained in this study for values of F comparable to those used by Ghambarian. Although some of the points tend to show the same trend as the present study, there is considerable scatter. Some of the data points fall below the normal depth which is physically impossible for a reservoir type of inlet as used by Ghambarian (and in the present study).

Ghambarian reported that he measured the frequency distributions of maximum depth, period, wave velocity, and wave length, and that they obeyed the normal distribution law.

2. Field Data

On April 16, 1965 measurements on roll waves were obtained by the Los Angeles County Flood Control District (LACFCD) in the Santa Anita Wash flood-control channel. The water entered the channel over a 160-ft wide spillway shown in figure 49. The discharge was determined from measured velocities on the spillway crest during the test. At about 5000 ft downstream of the spillway, observations on maximum depths were obtained by using gages painted on the side of the channel (see figure 1) to visually estimate values of h_{max}. Wave periods were also determined by measuring the time for waves to travel a known distance with stop watches. The data for h_{max} and T were obtained for groups of about five consecutive roll waves. Therefore the values of $\bar{h}_{max}$ and T_{av} in table 11 are averages for five waves.

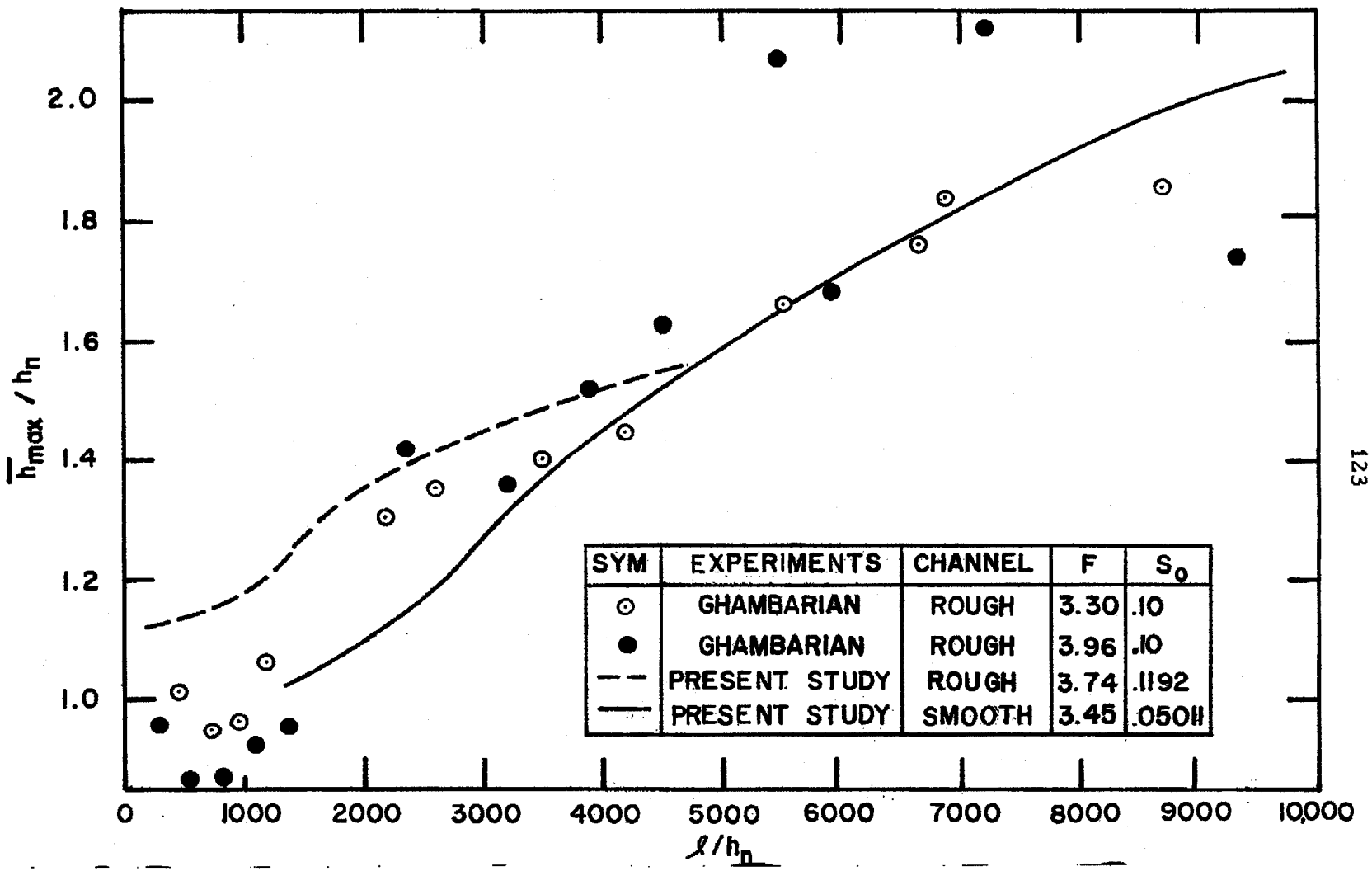

Fig. 48. Graph of Ghambarian's results for average maximum depth $\bar{h}_{max}$ as a function of distance from beginning of channel ℓ, for channel slope = .10

Negative No. 7805

Fig. 49. View of inlet to Santa Anita Wash, Arcadia, California, discharge about 210 cfs

Table 11

Summary of Santa Anita Data

Discharge cfs	$\bar{h}_{max}$ ft	T_{av} sec	At measuring station			Weighted values	
			$\bar{h}_{max}/h_n$	$T'(= S_o T_{av} \sqrt{g/h_n})$	F	F	ℓ/h_n
90	.72	14.5	2.36	3.74	3.40	3.93	18,700
94	.80	16.3	2.56	4.16	3.42	3.95	18,300
96	.76	12.1	2.40	3.07	3.42	3.95	18,000
170	.94	15.6	2.11	3.34	3.63	4.18	12,800
186	.83	8.2	1.76	1.71	3.67	4.22	12,200
193	.94	13.8	1.96	2.84	3.69	4.24	11,900
234	.99	9.8	1.84	1.90	3.76	4.33	10,600
262	1.04	10.5	1.80	1.98	3.80	4.37	9,900
268	1.09	9.3	1.87	1.75	3.81	4.38	9,800
272	1.00	8.5	1.70	1.57	3.81	4.39	9,700

h_{max} values are measured to within about .05 ft.

In table 12 the channel slopes and widths from the downstream end of the spillway to the measuring station are listed. The channel has one bend, station 1588 ft to 2007 ft, which is visible in figure 1. The data from this study are contained in a LACFCD file report which was kindly made available.

The normal depths for each discharge were calculated using a Manning roughness coefficient (n) of .010. This value was derived from float velocities and water depths obtained from motion pictures taken during the test. These surface velocities were corrected to mean velocities by assuming a logarithmic velocity distribution. Roughness coefficients were determined in this manner only when the water depth was practically constant, so that the flow was essentially uniform. The average n value of .010 was based on 41 sets of observations.

The slope of the channel, and thus the normal depth and Froude number for a given discharge, varied from the spillway to the measuring station. Each value of ℓ/h_n listed in table 11 was obtained by summing the values of ℓ/h_n computed for each reach of constant slope between the inlet and the measuring station. However because the h_{max} values were observed only at the measuring station, the value of h_n in $\bar{h}_{max}/h_n$ was calculated using $S_o = .0251$. The dimensionless period was calculated using the values of S_o and h_n at the measuring station also. Table 11 includes a Froude number for each discharge that was computed as a weighted average of the values of F for each reach of constant slope. The weighting factors were taken as proportional to the length of the reaches of constant slope.

Table 12

Slopes and Widths for Santa Anita Channel

Station ft	Length ft	Width ft	Slope S_o
0-508	508	139.7 to 72	.0242
508-838	330	72 to 28	.0415
838-1588	750	28	.0415
1588-2074	486	28	.0354
2074-4169	2095	28	.0332
4169-5044	875	28	.0251

In figure 50 the data for the Santa Anita Channel are shown as a graph of $\bar{h}_{max}/h_n$ against ℓ/h_n along with the laboratory results for a comparable F. Although the points do not fall on the laboratory curve, the growth rate is roughly the same. For periodic permanent waves, it was shown that h_{max}/h_n is a function of T' for a given F. It will be shown in the next chapter that this same concept can be carried over to natural waves if h_{max} is replaced by $\bar{h}_{max}$ and T by T_{av}. Thus in figure 51 the field data are plotted on a graph of $\bar{h}_{max}/h_n$ vs. T' along with the theoretical and laboratory relations for comparable values of F. Although this plot indicates the same trend as the laboratory results and theory, the field data give slightly higher values of $\bar{h}_{max}/h_n$.

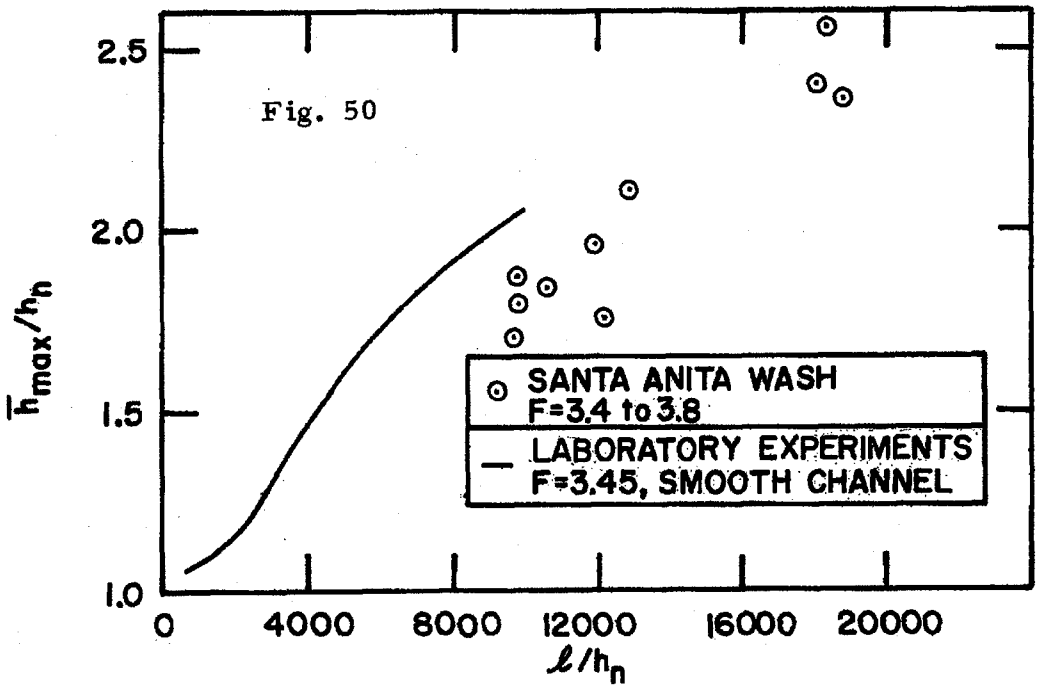

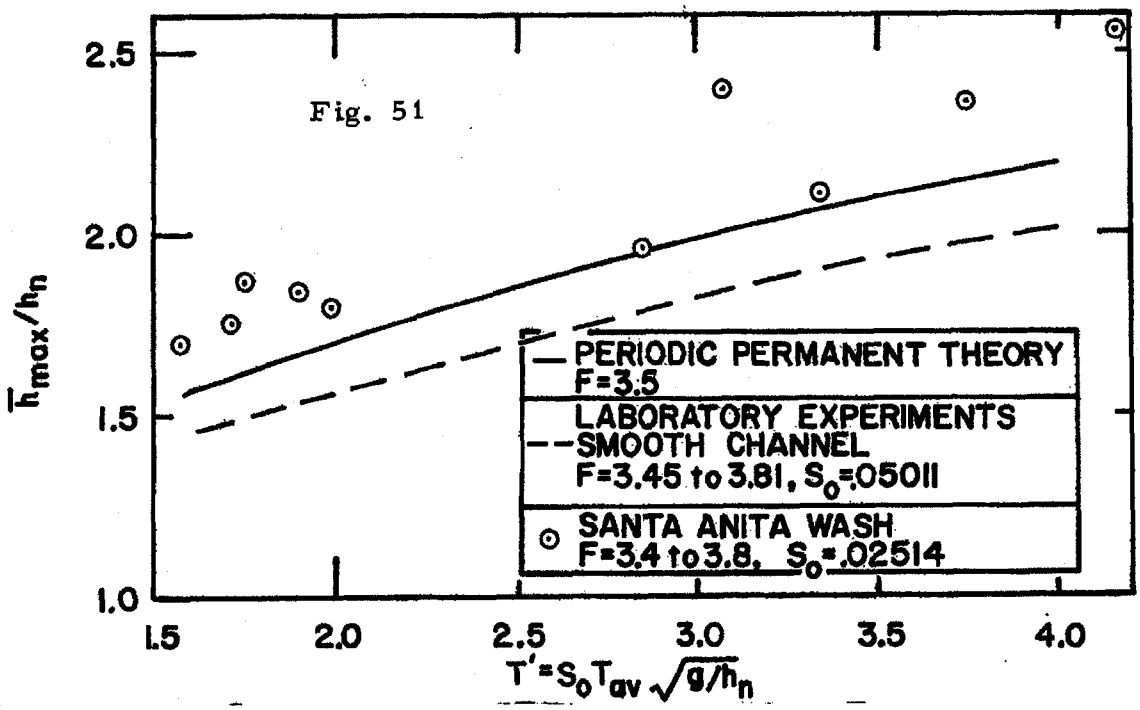

Fig. 50. Graph of average maximum depth $\bar{h}_{max}$ as a function of distance from beginning of channel ℓ, for Santa Anita Wash

Fig. 51. Graph of average maximum depth $\bar{h}_{max}$ as a function of dimensionless wave period T', for Santa Anita Wash

CHAPTER VI

DISCUSSION OF RESULTS

VI-A DEVELOPMENT OF NATURAL ROLL WAVES IN TERMS OF DISTANCE ALONG CHANNEL

1. Average Maximum Depth and Average Period

The development curves for $\bar{h}_{max}$ shown in figures 26-29, indicate that a unique relation exists between $\bar{h}_{max}/h_n$ and ℓ/h_n for each Froude number. The effect of the Froude number on these development curves is seen in figure 52 where all the $\bar{h}_{max}$ development curves for the smooth channel are shown. For values of $\bar{h}_{max}/h_n$ above about 1.2, the growth rate (slope of the curve) at a fixed average maximum depth increased as the Froude number increased. Also a given value of $\bar{h}_{max}/h_n$ occurred at a smaller value of ℓ/h_n as F increased. In other words, as the Froude number increased roll waves developed closer to the inlet and grew at a faster rate in terms of distance along the channel.

The curvature of the $\bar{h}_{max}$ development curve is initially concave upwards and finally concave downwards. On the concave upward portion, the roll waves have small amplitudes and have not yet acquired the steep wave front. Recorder traces of waves of this type can be seen in figure 41. Eventually all the waves will "break" and it was determined from pressure records that in the smooth channel this occurred at values of h_{max}/h_n of about 1.18 at the .05011 slope, 1.30 at the .08429 slope, and 1.34 at the .1192 slope. These values are

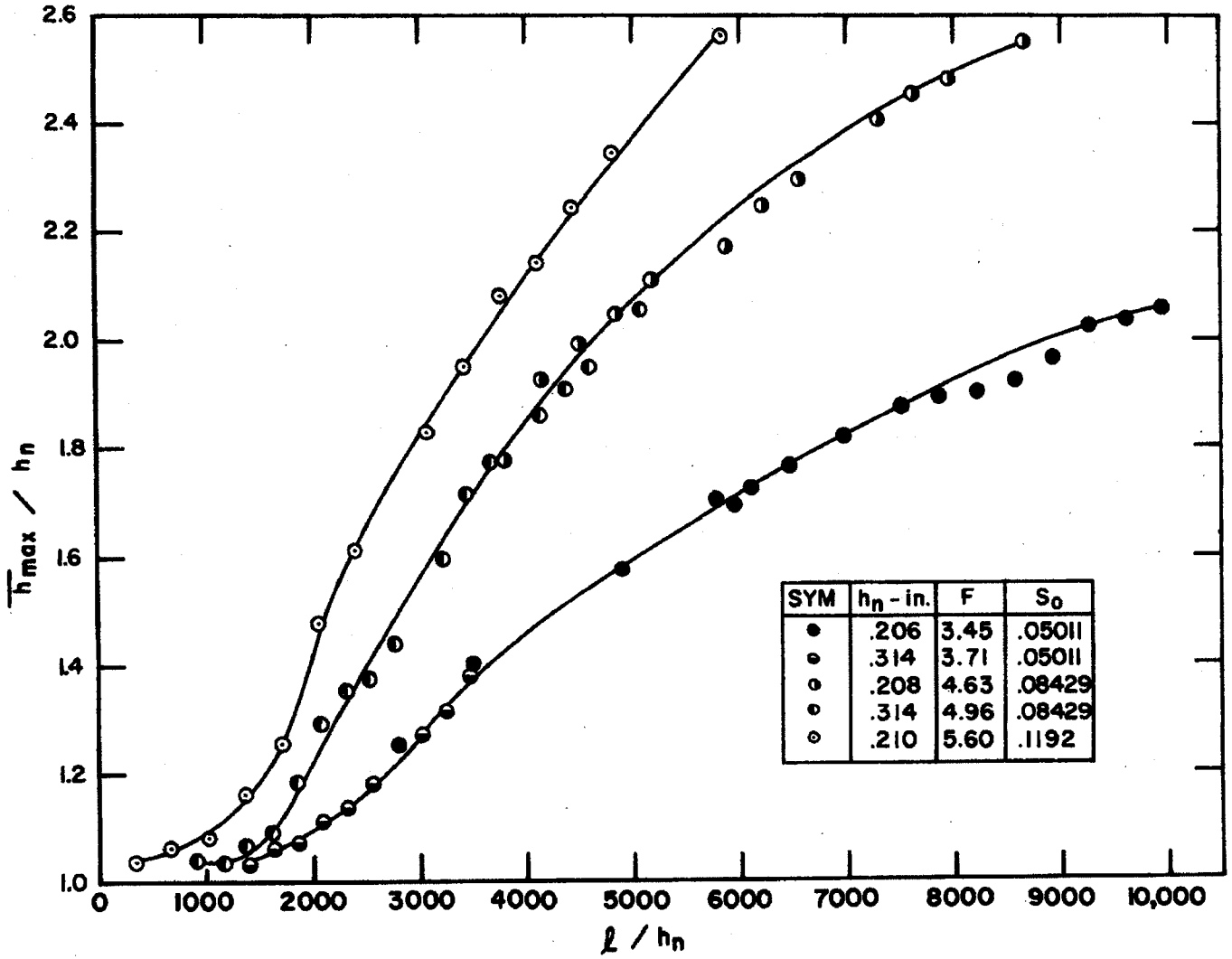

Fig. 52. Development curves for average maximum depth $\overline{h}_{max}$ for channel slopes of .05011, .08429, and .1192

in the vicinity of the points of inflection of the development curves in figure 52. Thus the part of the curve that is concave upward pertains to small amplitude waves with a continuous water surface, and the part that is concave downward pertains to waves with a discontinuous water surface (shock waves).

The development curves for the average periods (figures 30-32) show a constant period portion followed by a transition to a practically linear period increase with length. The point on these curves where the period starts to increase from the initial value is where the wave overtaking begins. By examining the $\overline{h}_{max}$ development curves, it is seen that this overtaking begins after shock waves have formed and an appreciable amount of growth has taken place. For example at a slope of .05011 overtaking begins at about $\ell/h_n = 3000$ which corresponds to $\overline{h}_{max}/h_n = 1.25$, whereas shock waves formed at $\overline{h}_{max}/h_n = 1.18$ approximately. This growth without overtaking will be called natural growth, and the phase of the development in which the average period does not change will be referred to as the initial development phase.

Downstream of the initial development phase the observed average period was practically a linear function of distance. To understand why this should be, one would have to investigate the details of the movement of trains of shock waves that have a normal distribution of periods and velocities. To complicate the problem further, the velocities change appreciably during and immediately after an overtake. An investigation of this type has not been made. One consequence of the observed linear function for the average period, is that the average

frequency of overtakes (number per unit time), $\overline{\omega}_o$ in a reach of channel $\Delta \ell$ can be expressed as;

$$\overline{\omega}_o = a\ \Delta\ell / \left[(T_{av})_u \times (T_{av})_d \right], \tag{6.1}$$

where a is the slope of the T_{av} vs. ℓ relation ($T_{av} = a\ell + b$), and subscripts u and d refer respectively, to the upstream and downstream end of the reach $\Delta\ell$ in question. This relation follows directly from the continuity of wave peaks where the overtaking process acts as a sink for wave peaks. If ℓ is now measured from the point of the linear increase (i.e. $b \equiv 0$), and $\Delta\ell$ is small compared to ℓ, equation 6.1 can be written,

$$\overline{\omega}_o = \Delta\ell / a\,\ell^2 \tag{6.2}$$

or the frequency of overtaking varies inversely as the square of the distance from the point where overtaking begins.

It has been shown that most of the experimentally determined development curves for $\overline{h}_{max}$ and T' described a unique relation for each value of F and S_o. It is reasonable to expect that these relations will be valid for any wide rectangular channel with equivalent inlet conditions and the same value of F and S_o as was used in this study. However for channels with the same value of F but on a different slope, the relations found in the laboratory may not apply. The effect of channel slope on the $\overline{h}_{max}/h_n$ vs. ℓ/h_n relation is seen by comparing the results for the smooth channel at a .05011 slope (figure 26), and the rough channel at a .1192 slope (figure 29) since these two sets of data are for the same range of Froude numbers. One obvious

difference between these two relations is that in the rough channel roll waves developed to a given value of $\bar{h}_{max}/h_n$ at a smaller value of ℓ/h_n than in the smooth channel. Another difference is that for a given $\bar{h}_{max}/h_n$, the growth rate of the shock waves ($\bar{h}_{max}/h_n > 1.4$ approximately) was larger in the smooth channel than in the rough channel. The effect of channel slope on the development of small amplitude waves (from which shock waves are formed) will be considered in Part 3 of this section. The effect of channel slope on the growth rate of shock waves will be considered further in Chapter VII.

2. Small Amplitude Roll Waves and the Linear Theory

The linear theory in Chapter III considered the motion of a small amplitude sinusoidal perturbation on an otherwise undisturbed uniform flow of depth h_n. The growth rate of the perturbation was shown to be,

$$\partial \eta_{max}/\partial (\ell/h_n) = \eta_{max} (2\pi C_i/C_r Y)(S_o/F^2) \qquad (3.38)$$

where the amplification factor $(2\pi C_i/C_r Y)$ is a function of F and Y (figure 2), and η_{max} is the amplitude which increases exponentially with distance (equation 3.39). If this theory is valid as a simplified model for the motion of small amplitude natural roll waves, it is expected that the observed average wave lengths would correspond to values of Y indicating a maximum amplification factor (F fixed) on figure 2. Furthermore it is expected that the observed growth rates would increase with the Froude number, and thus, if the initial disturbances are of the same size, roll waves are expected to occur at increasingly smaller distances from the beginning of the channel as

the Froude number is increased. This interpretation of the theory was given in Section III-A, and follows directly from equation 3.38 and figure 2.

Figure 53 shows portions of all the development curves for $\overline{h}_{max}$ for which a pressure record was used to obtain the values of $\overline{h}_{max}$ of the small amplitude waves. The term small amplitude will be used for waves that have not developed into shock waves. Therefore small amplitude waves correspond to the parts of the development curves for $\overline{h}_{max}$ that are concave upward (see Part 1 of this section). Since overtaking did not start until after shock waves were formed, small amplitude waves are only part of the initial development phase. Values of Y were calculated for each of the six runs shown on figure 53 using the average wave length for the values of λ. This average wave length was computed as the product of the average period, which did not vary during the initial development phase and the wave velocity. These computed values of Y are shown in table 13. The observed average wave lengths were in the range of maximum growth rate as can be seen from figure 2. Furthermore, as F was increased the observed Y decreased which follows the trend indicated on figure 2. However this qualitative agreement is not a good criterion for judging the applicability of the small amplitude theory to natural roll waves because of the relatively wide range of values of Y near the maximum growth rate as seen on figure 2.

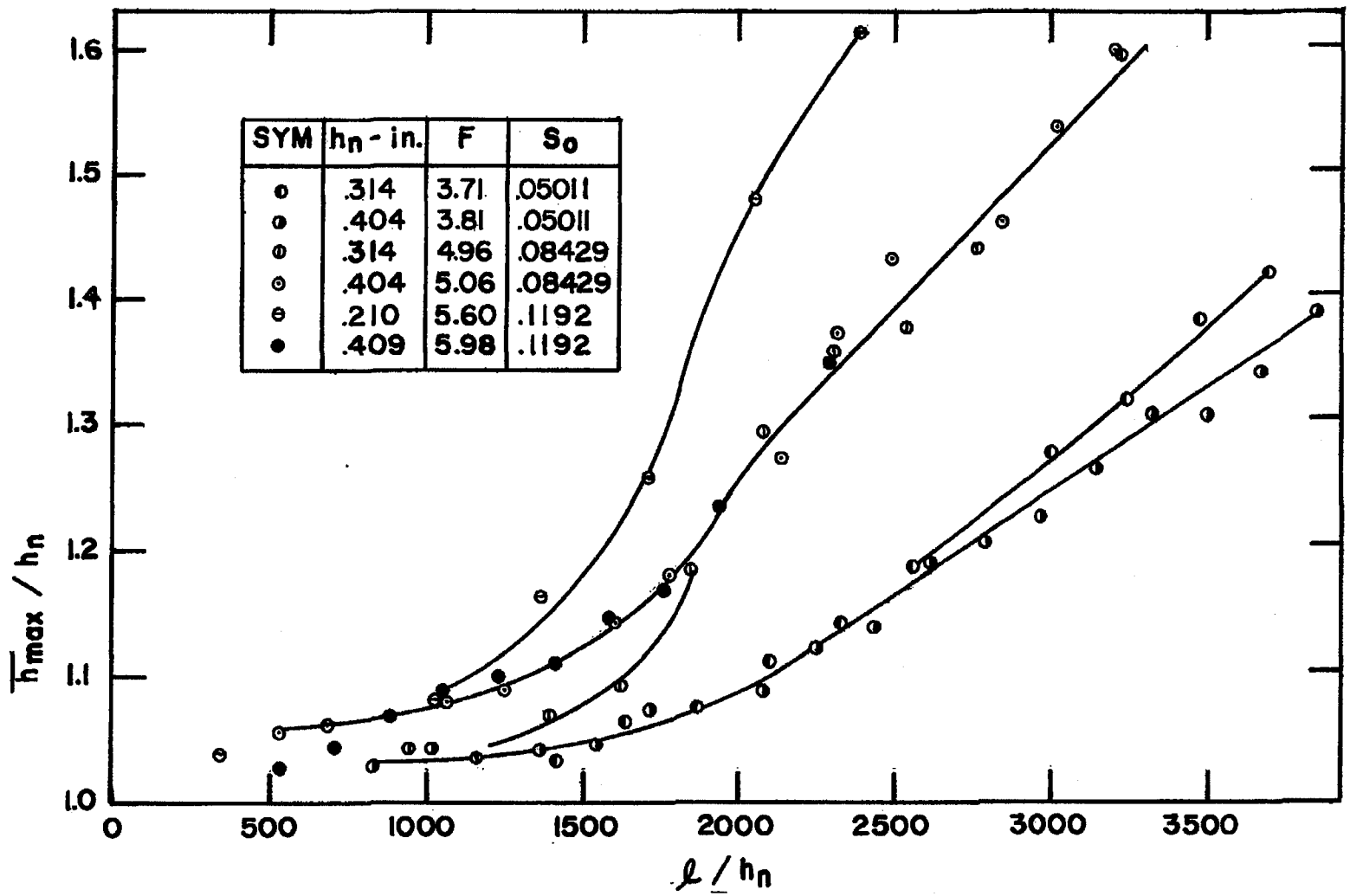

Fig. 53. Development curves for small values of average maximum depth $\overline{h}_{max}$ for channel slopes of .05011, .08429, and .1192

Table 13

Observed Dimensionless Wave Lengths of
Small Amplitude Natural Roll Waves

S_o	F	$Y = \frac{S_o \lambda}{F^2 h_n}$
.05011	3.71	.475
.05011	3.81	.460
.08429	4.96	.405
.08429	5.06	.377
.1192	5.60	.370
.1192	5.98	.316

The small amplitude theory predicts that the amplification factor should increase as the Froude number is increased. In fact, for the range of values of F and Y in table 13, the amplification factor should have varied by a factor of about 2.5. This factor can be estimated from figure 2. The observed amplification factors for each run were found by plotting $\log_{10}(\bar{h}_{max}/h_n)$ vs. ℓ/h_n, fitting a straight line to the plotted data points, and calculating the amplification factors from the slope of the straight line and the known values of S_o and F. The data points indicated exponential growth for values of $\bar{h}_{max}/h_n$ between about 1.05 and 1.20. Except for the run with F = 4.96, the amplification factors were all about the same (ratio of maximum to minimum value was about 1.2), and did not show any dependence on the Froude number. In addition, the measured amplification factors were all less

than the predicted values from the theory. This of course means that the growth rates, for a given value of $\overline{h}_{max}/h_n$, were about the same for all the runs except one. However it was found that roll waves did occur at increasingly smaller distances from the inlet as the Froude number was increased (e.g. with $\overline{h}_{max}/h_n = 1.1$ in figure 53). Coupling this fact with the observed trend of the growth rates (for $\overline{h}_{max}/h_n \geq 1.05$) leads to the conclusion that roll waves did not begin to develop at the beginning of the channel, but began to develop at increasingly smaller distances from the beginning of the channel as the Froude number was increased. It must be noted that values of $\overline{h}_{max}/h_n$ below about 1.05 may not be very indicative of the actual magnitudes of the roll waves, if there were any, because of the distrubances on the flow which exist even for a uniform flow. Thus to delineate a point at which roll waves began to develop is difficult, but for purposes of discussion the location corresponding to $\overline{h}_{max}/h_n = 1.1$ can be taken as the one where roll waves of "significant size" appeared.

As noted above the small amplitude theory does not predict the observed trends in the growth rates. However the theory did predict that waves of a given size would occur at increasingly shorter distances from the beginning of the channel as the Froude number was increased providing the initial distrubances were of the same size. Thus by considering only the location of roll waves of significant size, the theory predicts the observed trend as F was varied.

3. Effect of Channel Slope on Small Amplitude Natural Roll Waves

In Section VI-A.1. it was concluded that the functional relationships between $\bar{h}_{max}/h_n$ and ℓ/h_n determined from the experiments in the laboratory channel should be valid for any wide rectangular channel with the same values of F and S_o that were obtained in the laboratory. The effect of changing S_o with F held fixed will be considered now.

The small amplitude linear theory predicts that the growth rate increases as S_o increases with F fixed. This is seen from equation 3.38. The linear theory also predicts that the growth rate increases as the Froude number increases (see Section VI-A.2.), but this was not observed for the natural roll waves. Therefore on the basis of the linear theory alone, it is not justified to assume that there will be an effect of channel slope on the growth rates of small amplitude natural roll waves.

Unfortunately the experimental evidence concerning the slope effect is inconclusive. For the smooth channel at S_o = .05011, and the rough channel at S_o = .1192, the values of F (for h_n of about .3 in. and .4 in.) ranged from about 3.7 to 4.0, so that differences in the $\bar{h}_{max}/h_n$ vs. ℓ/h_n relations cannot be due to a Froude number effect. In figures 26 and 29 the development curves for $\bar{h}_{max}/h_n$ are shown, and on figure 48 both of the curves are shown. In the rough channel the values of $\bar{h}_{max}/h_n$ were never less than about 1.1, even very close to the inlet, which can be seen in figure 29. However for the smooth channel the minimum values of $\bar{h}_{max}/h_n$ were less than 1.05 (figure 26).

Therefore it can be said that the initial disturbances were larger in the rough channel than in the smooth channel, with the result that roll waves appeared at smaller values of ℓ/h_n in the rough channel than in the smooth channel (figure 48). For a rough comparison of the growth rates of the small amplitude waves figure 48 can be used. It appears that the growth rates were not greatly affected by the channel slope, however the range in $\bar{h}_{max}/h_n$ for small amplitude waves (i.e. 1.1 to 1.2 approximately) in the rough channel was not large enough to reach any definite conclusions. It is important to note that for $\bar{h}_{max}/h_n > 1.2$ the growth rates are clearly less on the larger slope. This slope effect on shock waves will be considered in Chapter VII. In summary, roll waves developed at smaller values of ℓ/h_n in the rough channel than in the smooth one, but this was primarily because the initial disturbances were larger than in the smooth channel. The effect of channel slope on the growth rates of small amplitude waves could not be ascertained from the experimental results because of the differences in the initial disturbances.

Near the inlet of the rough channel the value of $\bar{h}_{max}/h_n$ was about 1.1, whereas in the smooth channel, for all slopes, the initial values of $\bar{h}_{max}/h_n$ were less than 1.05 at the locations where growth began. This can be seen in figures 26 to 29. Table 4 shows that the discharge in the rough channel at F = 4.04 was about the same as in the smooth channel at F = 3.81. It is reasonable to assume that the flow pattern in the inlet box was about the same for about the same discharge. The primary difference between the rough and smooth channel at F = 3.7

to 4.0, besides the slope, was the texture of the channel bottom and sides. In the smooth channel a 6-in. length of screen was placed on the bottom (see Section V-A) so that the downstream end was .30 ft upstream of station 0.0. The purpose of this screen was to eliminate the laminar boundary layer. In the rough channel the sand grains were fixed to the bottom and sides of the channel over the total length of the channel, and also to the sides and bottom of the inlet for the portion extending 8 inches upstream of station 0.0 (see figure 11).

It is reasonable to suspect that the larger initial disturbances in the rough channel were due to the influence of the sand grains on the structure of the turbulent flow near the inlet. These sand grains were more than four times larger than the thickness of the laminar sublayer (figure 22), so that eddies generated by the sand grains had an influence on the flow as evidenced by the increased friction factors in the rough channel. It seems reasonable that the influence of these eddies could have extended to the water surface, resulting in disturbances to the water surface. These disturbances would have resulted in larger values of $\bar{h}_{max}/h_n$ than generated in the smooth channel.

For the experiments in the rough channel with h_n = .375 in., the value of h_n/k was only about 16, where k is the geometric mean size of the sand (.595 mm). As the value of h_n/k is increased, it is reasonable to believe that the influence of the eddies (generated by the sand grains) on the water surface will be less. Therefore in a rough channel with h_n/k much larger than 16, but otherwise equivalent to the laboratory rough channel (i.e. F of about 4.0, S_o of about .12), roll

waves would probably not develop as close to the inlet (in terms of ℓ/h_n) as they did in the rough channel in the laboratory.

4. Frequency Distributions

The development curves for the standard deviation of h_{max} and T, shown in figures 35 and 36, indicate that a unique relation exists between $\sigma_{h_{max}}$ and ℓ/h_n and between σ_T and ℓ/h_n for each Froude number. Although $\overline{h}_{max}$ increased over the entire length of the channel, its standard deviation tended to reach a constant value at about $\ell = 8,000\ h_n$. The standard deviation of the period increased linearly to the end of the channel.

The frequency distributions for h_{max} were found to be approximated by a normal distribution (figure 37). However, these distributions were measured only after shock waves had formed and only average values, $\overline{h}_{max}$, were obtained for the small amplitude waves before shock waves appeared. To measure h_{max} for shock waves, 200 wave crests were observed at each setting of the wire gage and the number of crests that struck the wire was recorded. This was continued until the wire was high enough so that no crests (out of 200) struck the wire. Thus the maximum recorded value of h_{max} would appear at 0.5 percent on the cumulative frequency scale if only one crest out of 200 struck the wire. This maximum value can also be expressed as,

$$(h_{max})_{max} = \overline{h}_{max} + 2.58\ \sigma_{h_{max}} \tag{6.3}$$

by using the properties of a normal distribution. It is clear that if a larger number of crests had been used at each wire gage setting, the maximum recorded h_{max} may have been higher, but it is not correct to assume that these higher values (with frequencies less than 0.5 percent) would also follow the normal distribution. For this reason one is not justified in merely extending the relations in figure 37, for example, to obtain values of h_{max} with lower frequencies than 0.5 percent. For all practical purposes, the value from equation 6.3 represents the maximum value of h_{max} at a given station.

The frequency distributions for T (figure 38) show some deviation from the normal law at the small values of T. In figure 38 the minimum T was the same at all three stations. This merely means that the minimum value of T corresponded to the smallest distance between two peaks that could be recognized on the pressure record. If the crests had been closer together, they could not have been distinguished as two separate crests. The largest value of h_{min} in figure 39 is about the same for all three stations. This is because h_{min} was defined to be less than the average depth (as estimated by eye from the pressure record, see Section IV-D) which is about equal to the normal depth. Thus the maximum values of h_{min} for all three stations shown in figure 39 were slightly less than the normal depth. The curves in figure 39 show that at each station the small values of h_{min} deviate from the normal distribution indicated by the large values. At the low values of h_{min} a relatively large percentage of the values were in a given interval as compared to the high values. As a result the frequency distribution for h_{min} was skewed towards the small values and the mean was less than the median.

VI-B DEVELOPMENT OF NATURAL ROLL WAVES IN TERMS OF WAVE PERIOD

In figure 44 the results of experiments on the periodic permanent roll waves were presented. It was shown that there was a consistent relation between the dimensionless measured properties (h_{max}, h_{min}, and c) and the dimensionless period for a given Froude number and channel slope. Comparison of the experimental and theoretical results shows the measured wave velocity and minimum depth to be slightly higher, and the maximum measured depth to be considerably lower than given by the theory. The deviation of the maximum depth from the theory increases with the Froude number. In the 130-ft channel the theory and experiments were in very close agreement (figure 43). In the next chapter a modification to the periodic permanent theory will be made which will greatly reduce the discrepancy for the maximum depth.

Thus far, natural roll waves and periodic permanent roll waves have been treated independently. However, it was found that the average maximum depth of a developing natural roll wave train can be described in the same manner as a periodic permanent roll wave train. This is shown in figures 54-57 where $\overline{h}_{max}$ for both natural and periodic waves is plotted as a function of T'. In this manner of presentation no correction for inlet condition is required, as it was for the development curves expressed as functions of ℓ/h_n. The natural-wave data for h_n = .2 in. that indicated a smooth-inlet effect (see Section V-A) are included. The line drawn through the data points is based primarily on the periodic permanent wave data, especially at the low values of T'.

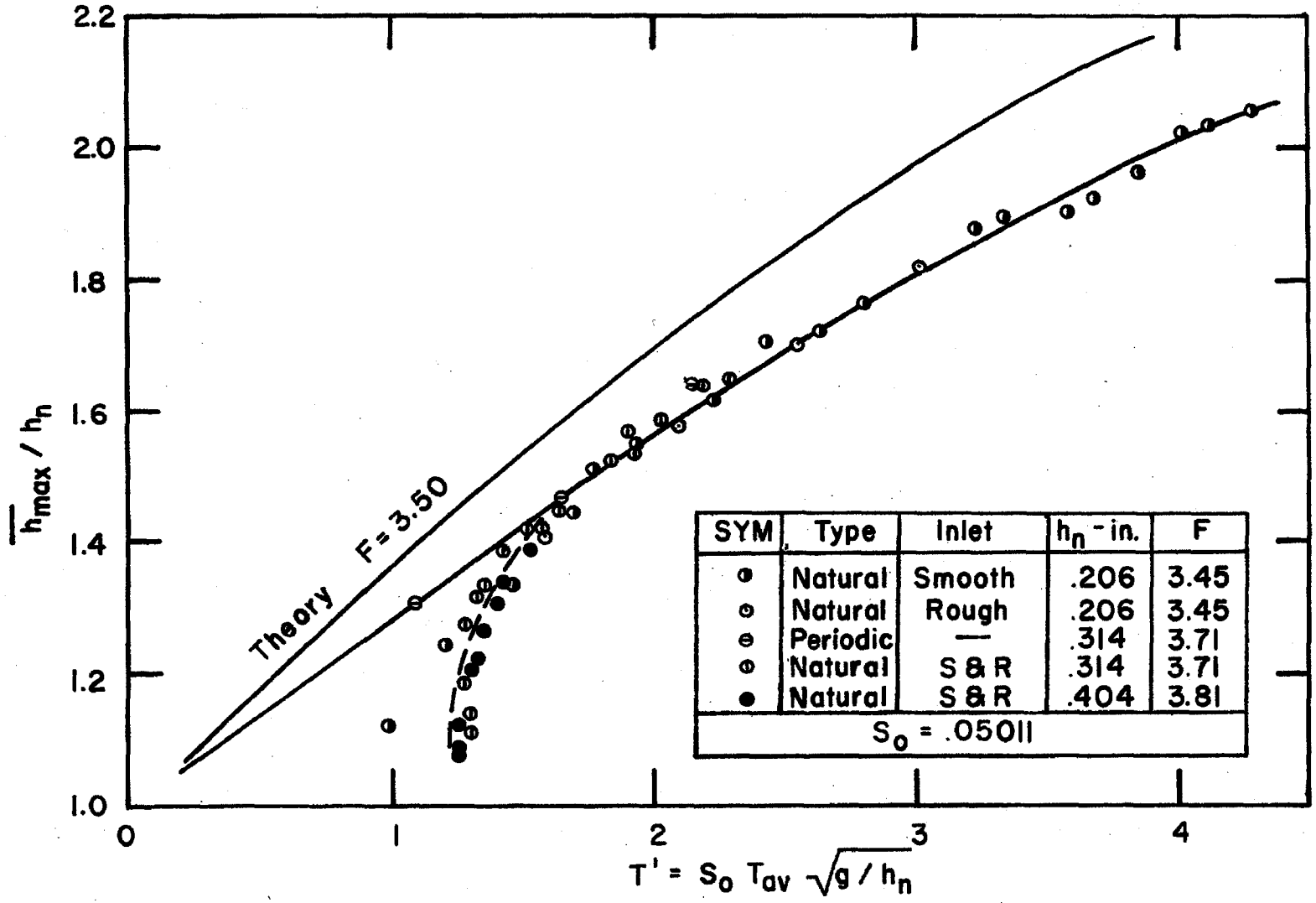

Fig. 54. Graph of relations between average maximum depth $\overline{h}_{max}$ and dimensionless wave period T' for: periodic permanent wave theory with Froude number of 3.5, periodic permanent wave experiments in channel with slope of .05011, and natural wave experiments in channel with slope of .05011

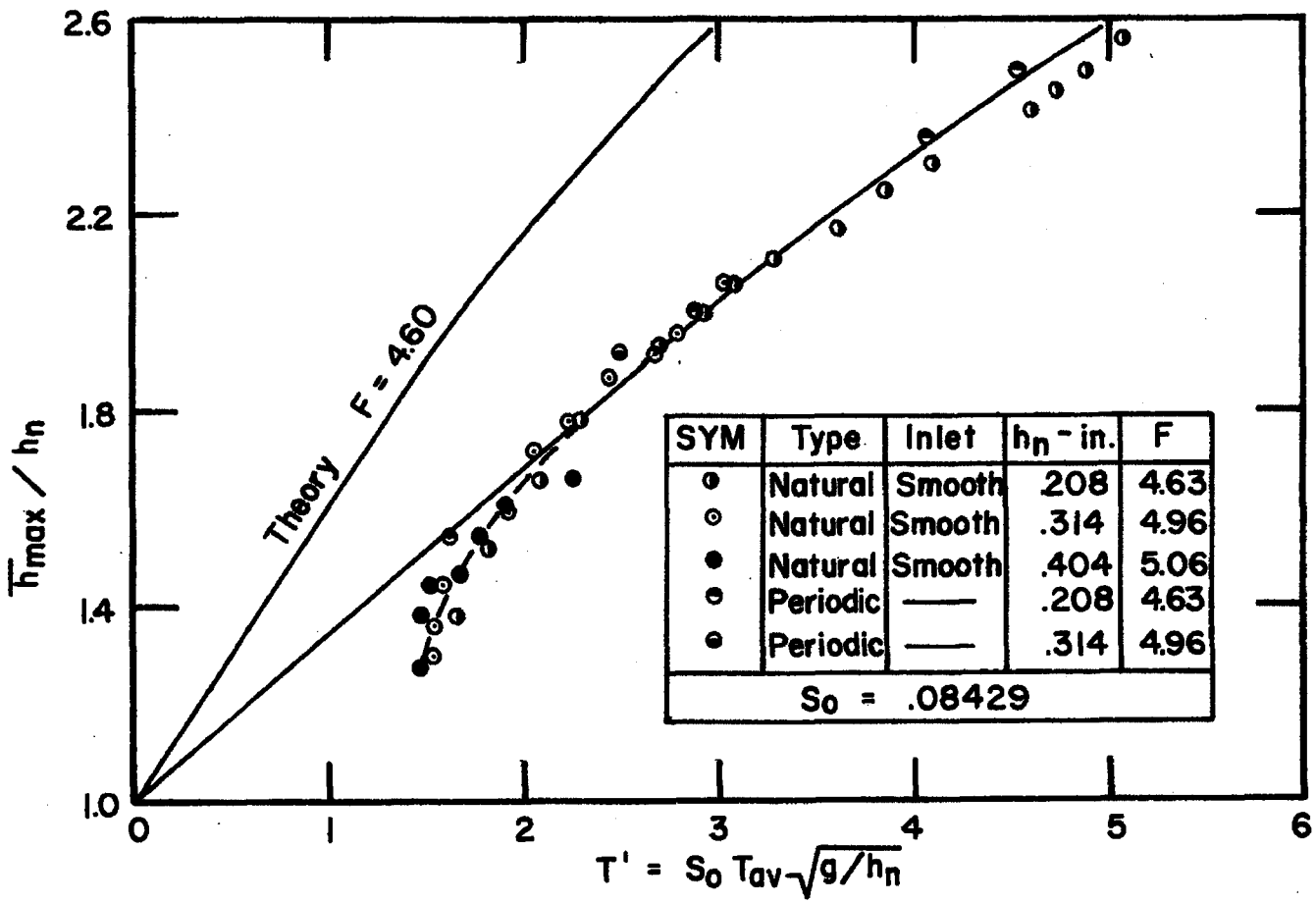

Fig. 55. Graph of relations between average maximum depth $\overline{h}_{max}$ and dimensionless wave period T' for: periodic permanent wave theory with Froude number of 4.6, periodic permanent wave experiments in channel with slope of .08429, and natural wave experiments in channel with slope of .08429

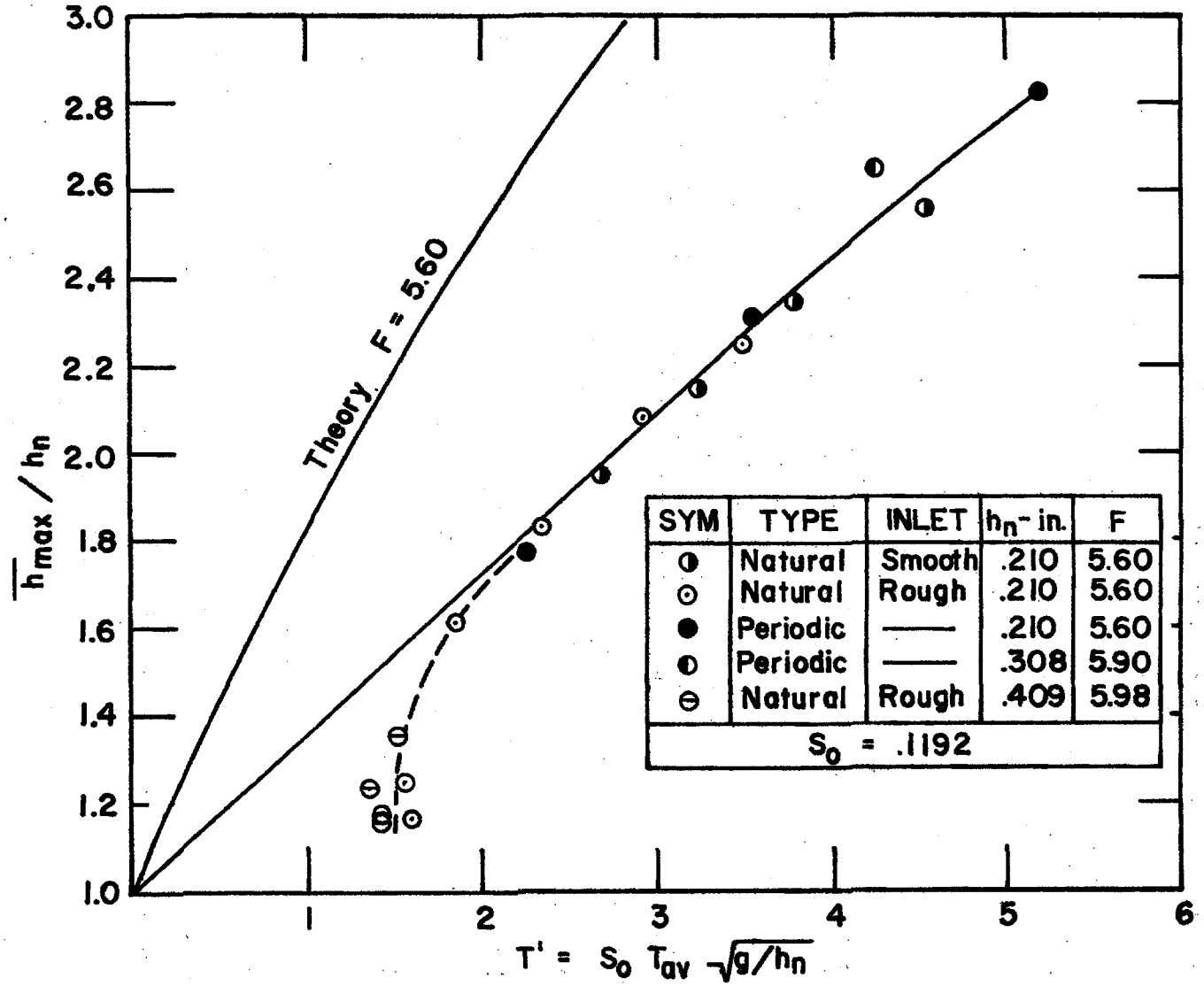

Fig. 56. Graph of relations between average maximum depth $\overline{h}_{max}$ and dimensionless wave period T' for: periodic permanent wave theory with Froude number of 5.6, periodic permanent wave experiments in channel with slope of .1192, and natural wave experiments in channel with slope of .1192

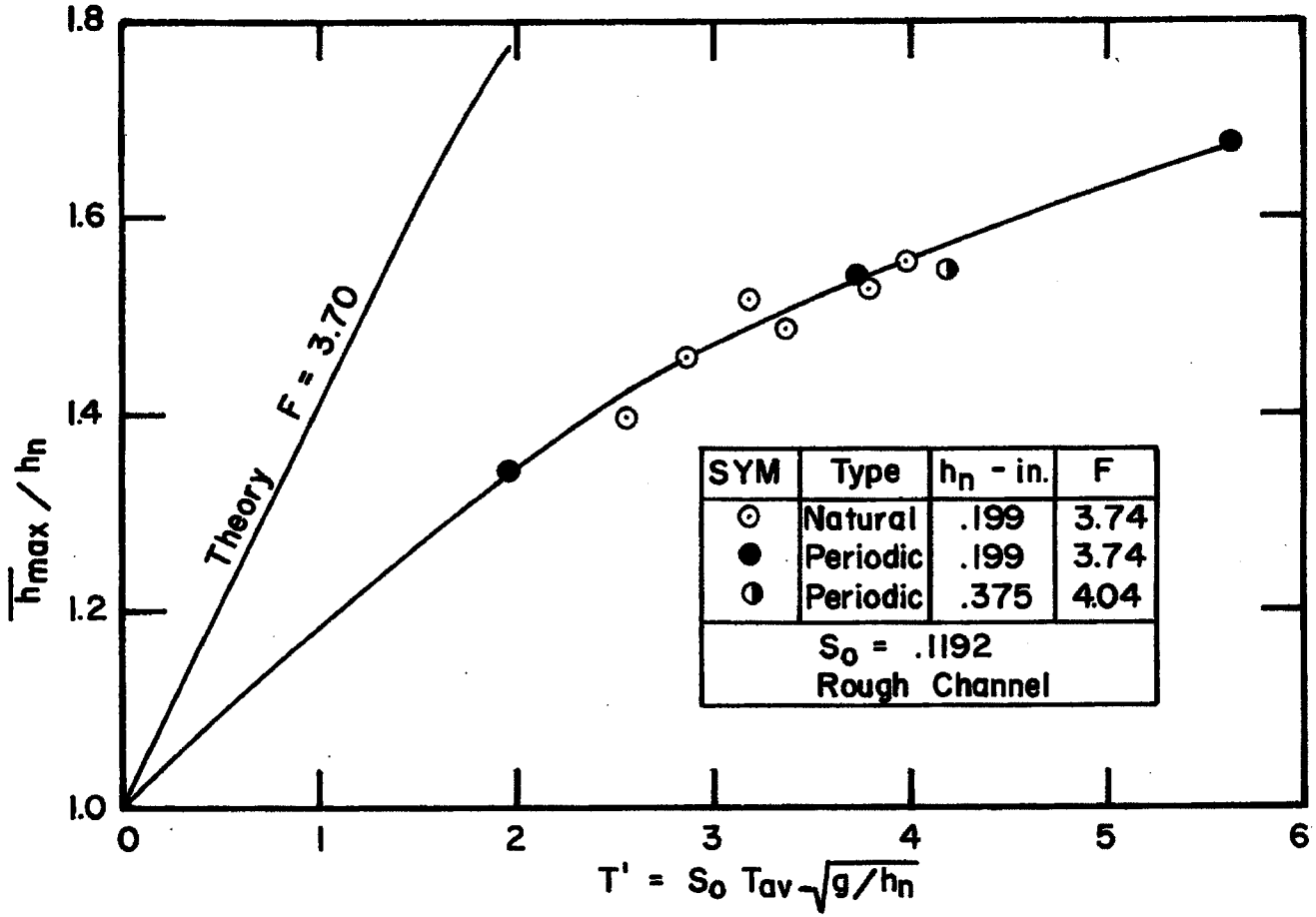

Fig. 57. Graph of relations between average maximum depth $\overline{h}_{max}$ and dimensionless wave period T' for: periodic permanent wave theory with Froude number of 3.7, periodic permanent wave experiments in rough channel with slope of .1192, and natural wave experiments in rough channel with slope of .1192

The data for the natural waves indicate that for small T' and $\overline{h}_{max}$ the depth $\overline{h}_{max}$ increases without a change in T'. This indicates that growth occurs without overtaking. As already noted above this kind of growth has been termed natural growth, and the development without overtaking has been termed the initial development phase. During this initial development phase the small amplitude waves form shock waves. Following this initial development phase, the natural-wave data show a gradual transition to the curve defined by the periodic-wave data. In this transition phase the shock waves were overtaking and the period was increasing. In the final development phase the periodic and natural waves follow the same relation. The values of $\overline{h}_{max}/h_n$ at the end of the transition phase were about 1.4 for $S_o = .05011$, 1.7 for $S_o = .08429$, and 1.8 for $S_o = .1192$. Figure 57 shows that data for natural waves in the rough channel were not obtained in the transition phase, but the minimum value of $\overline{h}_{max}/h_n$ that was in the final development phase was about 1.4.

In the final development phase the average maximum depth is a well-defined function of the period. For periodic waves the period and maximum depth were fixed for a given run, and the maximum depth could only be increased by increasing the period. For natural waves the average maximum depth increased along the channel for a given run, and this increase was found to be related to the average period by the same relation found for periodic waves. This implies that the dominant mechanism by which natural waves grow in this final phase is overtaking, which is the process by which the average period increases along the channel. In the transition phase, the average maximum depth is a

relatively "weak" function of the average period, in that a large change in average maximum depth can occur with only a small change in average period. Thus it can be expected that both natural growth and growth by overtaking are important in this transition phase.

VI-C EFFECT OF INLET ON DEVELOPMENT OF NATURAL ROLL WAVES

In Section V-A the effect of the inlet condition on the development of natural roll waves was considered. With a smooth inlet the water surface a short distance from the inlet was observed to alternate between glassy smooth and roughened in an intermittent fashion. This unsteadiness was observed to contribute directly to the development of roll waves, especially at the lowest normal depth of .2 in. However, if the floor near the inlet was made rough, the transition from the smooth water surface to the roughened water surface was steady, and occurred farther upstream. The observations of the water-surface texture were correlated with observations of dye streams introduced in the flow. These showed that water-surface roughening corresponded to mixing of the dye stream near the water surface. Furthermore, for a rough inlet this point of dye mixing moved upstream as the dye stream was moved towards the channel floor. For a smooth inlet the station at which the dye mixed with the flow did not change appreciably as the location of the dye stream above the floor was varied. These observations were also correlated with measurements of the h_{max} vs. ℓ relation. This showed that with a smooth inlet roll waves developed further upstream than with a rough inlet. Thus the unsteadiness in

the region of surface roughening with a smooth inlet provided a sufficient amount of disturbance to hasten roll wave development.

The observations and measurements can all be explained in terms of boundary layer development. In a smooth inlet a laminar boundary layer started to develop on the channel floor. The thickness of this layer increased with distance until the Reynolds number was high enough for transition to turbulent flow to occur. The resulting turbulent boundary layer then quickly expanded to intersect the water surface and caused the observed surface roughening. However, this transition from laminar to turbulent flow was not a steady one, but rather of an intermittent nature similar to that observed in pipes (25). It is unlikely that the laminar boundary layer grew to the full water depth before becoming turbulent, because then the Reynolds number would remain constant and the flow would remain laminar.

For the sake of a better defined and repeatable boundary condition at the channel entrance, all the results for natural waves were corrected to a rough inlet in the manner described in Section V-A. The important consideration here is that this correction was made for each run entirely independently of the other runs, and yet all the runs for a fixed Froude number collapsed to essentially the same dimensionless development curves for $\overline{h}_{max}$, T_{av}, $\overline{h}_{min}$, $\sigma_{h_{max}}$, and σ_T.

By observing the motion of dye injected into the inlet box, it appeared that some disturbances initiated in the inlet did lead to roll waves. This was more often observed at the higher discharges when the unsteady component of motion in the inlet box was much easier to detect than at the low discharge.

At the low discharges it was possible to inject dye near the top of the last baffle (figure 11) and observe a continuous dye stream to at least the beginning of the channel, which indicates that the flow was not turbulent in the inlet box. However this dye stream slowly moved from side to side indicating that the flow was unsteady. At the higher discharges it was very difficult to get a continuous dye stream established in the inlet box because the direction of flow was changing much more rapidly than at the lower discharges. However the dye stream did not spontaneously mix with the flow, but rather it was broken up into segments, as a result of the changing flow direction, and carried into the channel with the dye still visible. Occasionally at the higher discharges a vortex tube could be observed curling out of the inlet box into the channel.

From the above observations it can be concluded that disturbances were being generated both in the inlet box, and in the channel near the inlet. In particular the flow in the inlet box was more unsteady at the higher discharges than the lower discharges, and with a smooth inlet the transition from laminar to turbulent flow in the channel was unsteady. For low discharges with a rough inlet, disturbances may have originated in the developing turbulent boundary layer. In spite of the apparently different sources of disturbances at different discharges, the fact remains that most of the data for a given Froude number (and thus different discharges) collapsed to a unique dimensionless development curve after correction to a rough inlet was made.

VI-D MOTION OF INDIVIDUAL NATURAL ROLL WAVES

From figures 46 and 47 and tables 8 and 9 some interesting observations on the motion of individual waves can be derived. At station 42 (figure 46) the flow is in the transition phase of wave development and at stations 54, 66, and 78 it is in the final phase (growth by overtaking dominant).

From table 8 it can be seen that when one wave overtakes another, the resulting h_{max} is greater than that of either wave before overtaking. However, this resulting h_{max} value can decrease as the wave moves downstream as occurred in wave 6, 7, 8, between stations 54 and 78. The h_{max} of wave 1, 2 decreased between stations 66 and 78, but this may be because it was starting to overtake the next wave. Growth by overtaking was the dominant growth mechanism for the waves in figure 46, yet wave 9 grew appreciably without overtaking. This shows that natural growth takes place in the final development phase. Wave 5 did not overtake and its h_{max} was about constant between stations 54 and 78.

Because roll waves are shallow water waves, it is reasonable to expect that the waves with larger h_{max} have higher wave velocity and thus will overtake smaller, slower waves. This is the case for wave 8, and the overtake shown in figure 47a. However, waves are seen to overtake waves with larger h_{max} also. This is seen for wave 4 and the overtake in figure 47c. This seemingly contradictory situation can be explained by use of the shock condition,

$$c = u_{min} + \sqrt{g \frac{h_{max}}{h_{min}} \left[\frac{h_{max} + h_{min}}{2}\right]} \tag{3.44}$$

which was presented in Chapter III. Because u_{min} is the average velocity in a region where the water surface is practically parallel to the channel bottom, it can be approximated by the expression for normal velocity,

$$u_{min} \cong F \sqrt{gh_{min}} \quad , \tag{6.4}$$

which shows that u_{min} is about proportional to $h_{min}^{1/2}$. Now consider two waves with the same value of h_{min}, and equation 3.44 shows that the wave with the greatest value of h_{max} travels faster. On the other hand if two waves have the same h_{max}, the wave with the largest value of h_{min} may have a larger value of c if the difference in the values of h_{min} is sufficiently large. Furthermore, a wave may overtake a wave with a large value of h_{max}, if the h_{min} value of the overtaking wave is sufficiently larger than that of the overtaken wave. Wave 4, the overtake in figure 47c, and all other cases observed, showed that when a small wave overtook a large wave, the value of h_{min} of the small wave was greater than that of the large wave.

From records similar to figure 46, the changes in the values of h_{max} during the overtaking process, but before the two waves actually combined, were examined. Almost every conceivable combination of increase or decrease of the h_{max} value of the following or leading wave was found. For example: h_{max} for both waves were the same; h_{max} for the leading wave increased and that of the following wave did not change; h_{max} of the leading wave increased more than that of the following wave; and the maximum depth for the leading wave decreased

while that of the following wave was constant. In figure 46 between station 66 and 78, wave 1, 2 (following wave) decreased in height while the leading wave increased from h_{max}/h_n of 2.19 to 2.42. A correlation between the relation of the maximum depths during overtaking and the maximum depths before overtaking began could not be detected. However, as discussed above, the maximum depth of the combined wave was greater than either of the maximum depths during or before overtaking.

The wave velocities during the overtaking showed a consistent pattern which can be derived from figure 47 and table 9. From the three overtakes at different stations shown in this figure, it is seen that the following wave accelerates as it overtakes, and the velocity of the combined wave is greater than that of the leading wave during overtaking. This acceleration results primarily because the following wave is propagating in water that is continually getting deeper and thus the value of u_{min} in equation 3.44 increases. Immediately after the combination, the value of u_{min} decreases appreciably (since h_{min} of the combined wave is considerably less than that of the overtaking wave just before the combination) and the combined wave velocity is less than that of the following wave just before the combination. Experienced observers were able to visually detect this acceleration process in the laboratory channel.

VI-E GHAMBARIAN AND LACFCD DATA

1. Ghambarian Laboratory Data

Ghambarian found that the value of $\bar{h}_{max}$ reached a constant maximum value (table 10) although he does not give the corresponding values of ℓ/h_n. In the present study a constant maximum value of $\bar{h}_{max}$ was not attained, but the trend indicated that this might have occurred had the channel been somewhat longer. For an F of 3.82, the computed constant maximum value of $\bar{h}_{max}/h_n$ from table 10 is 1.83. For the smooth channel at an F of 3.45 (figure 26), the maximum value of $\bar{h}_{max}/h_n$ obtained in the present study was 2.06 and increasing. Thus at about the same value of F the $\bar{h}_{max}/h_n$ value from the present study is larger than Ghambarian's result. If Ghambarian's channel was rough the slope would have been much greater than .05011, in which case this discrepancy may be due to the slope effect to be discussed in Chapter VII.

In figure 48 the data for $\bar{h}_{max}/h_n$ with a channel slope of .10 show a rather large amount of scatter. The fact that some of the values of $\bar{h}_{max}/h_n$ (which were calculated from reported values of $\bar{h}_{max}/h_{cr}$ and computed values of h_{cr}/h_n using equation 5.4) are less than 1.0, indicates that the reported values of F were not accurate enough. In the present study it has been shown that considerable care must be taken to measure normal depths, from which the value of F is calculated. It is unfortunate that more information could not be extracted from Ghambarian's publications.

2. LACFCD Field Data

The field data from Santa Anita Wash (figures 50 and 51) show that reasonably consistent relations for the development of $\bar{h}_{max}/h_n$ in terms of ℓ/h_n and T' can be found by taking data for several discharges at only one station.

In figure 50 the laboratory curve does not extend far enough to compare with the highest values of $\bar{h}_{max}/h_n$ obtained from the Santa Anita Wash, but the lowest values are about 18 percent less than the laboratory values. Two important differences between the laboratory channel and Santa Anita Wash were the inlet condition and the variable slope. In the field (figure 49) there was a spillway followed by a transition section of variable width which was considerably different than the reservoir inlet used in the laboratory. For each discharge, the values of ℓ/h_n were computed by summing the values of ℓ/h_n for each reach of constant slope. However, the correct method of treating this variable slope (which is not known) may be considerably at variance with this procedure.

In figure 51 the field data for $\bar{h}_{max}/h_n$ are about 10 percent higher than the theory. After a change in channel slope, it takes a certain distance before the flow can adjust to the new slope. Thus there is a possibility that the slope change 875 ft upstream of the measuring station had some effect on the results. At a discharge of 272 cfs, the F on the steeper slope (S_o = .0332) was about 4.32 compared to 3.81 at the measuring station. This means that if the 875 ft was in fact not long enough for the flow to adjust to the smaller slope, the values of $\bar{h}_{max}/h_n$ at the measuring station would tend to be high.

There are two other considerations that affect the observed values of $\overline{h}_{max}$ in the field. One is that only five consecutive values of h_{max} were used to find the average values. This could account for some of the scatter in the plotted data. Finally, the method of obtaining the h_{max} values was subject to some error. This was done by two observers reading a scale painted on the channel wall with the smallest division of 0.2 ft, and values were usually read to 0.1 ft. Thus it is most optimistic to estimate that the accuracy was 0.05 ft which could lead to errors in h_{max} as high as about 7 percent. In light of this and all the other uncertainties mentioned above, the accuracy of the field results are within acceptable limits.

CHAPTER VII

MODIFIED PERIODIC PERMANENT ROLL WAVE THEORY

Observed mean maximum depths, $\overline{h}_{max}$, for the periodic permanent roll waves were seen to be in substantial disagreement with the theory. In this chapter the principal source of difficulty will be shown to be in the shock condition, which will be modified and the discrepancy between the modified theory and the data will be greatly reduced. The consequences of this modification with respect to natural roll waves will be discussed. Before considering the shock condition, some of the other assumptions used in the theory and the effects of a variable friction factor and the side-walls will be discussed.

VII-A ASSUMPTIONS IN PERIODIC PERMANENT ROLL WAVE THEORY

The momentum equation from which the theory for periodic permanent waves was derived in Section III-B is,

$$u_t + \alpha u u_x + (1-\alpha) \frac{u}{A} A_t + g h_x = g S_o - \frac{1}{\rho} \frac{\tau_o}{r}, \qquad (2.2)$$

which was given in Section II-A. In addition the continuity condition, equation 2.1, was used, but because it is an exact equation for flow of an incompressible fluid no comments regarding its assumptions are necessary.

In deriving equation 2.2 from the Navier-Stokes equations (4) numerous assumptions concerning the order of magnitude of terms

were made. These assumptions were primarily based on the fact that the dominant motion was in the x-direction, and thus it is not surprising that equation 2.2 implies a hydrostatic pressure law. A wave theory based on a hydrostatic pressure law is generally referred to as a first-order shallow-water theory. If the vertical accelerations are not negligible, Keulegan(4) has found the additional terms that are needed in equation 2.2. The addition of these terms results in a second-order theory.

For the analysis of periodic permanent roll waves the first-order theory was used on the part of the wave profile that is concave upward. From the wave profiles in figure 45, the maximum water surface slope occurred near the shock. Yet the maximum value of dh/dX for the run at an F of 5.60 and T' of 5.19 was found to be about 0.03. With a maximum water surface slope of this magnitude it can usually be assumed that the motion was primarily in the x-direction, the pressure was hydrostatic, and thus the first-order theory is sufficient. In this case there is the additional difficulty of the influence of the shock. As the water particles pass through this shock, from the wave trough (where $h = h_{min}$) to the wave crest (where $h = h_{max}$), they are accelerated upward normal to the channel floor. This motion normal to the channel floor is usually confined to the region within the length of the shock, at least for stationary shocks in steady flows (hydraulic jumps). If this was the case for the roll wave shocks, the pressure would have been hydrostatic at h_{max} and the use of the first-order theory would be justified. Measurements relating to the detailed motion in the shock were not taken. However, since the measured

shock lengths were comparable to the lengths of hydraulic jumps (to be discussed in VII-C) where the use of a hydrostatic pressure assumption has been successful in predicting the relation between h_{max} and h_{min}, it can be conjectured that the vertical accelerations in the section of maximum depth were negligible.

In applying equation 2.2 to periodic permanent roll waves the average shear stress on the solid boundary was evaluated by,

$$\tau_o = \rho f u^2/8, \tag{7.1}$$

as discussed in Section II-A. This expression is valid for uniform, steady flow with a fully developed turbulent boundary layer. The use of this expression for unsteady, nonuniform flow (periodic roll waves) can certainly be questioned. An attempt to justify this assumption will not be made here except to mention that this same assumption is made in practically all investigations of nonuniform (gradually varied) open channel turbulent flow, both steady (e.g. backwater curves) and unsteady (e.g. flood waves). Perhaps the strongest argument for the use of equation 7.1 is that no other alternative is available.

The friction factor is evaluated from relations for uniform flow. This implies that the boundary layer is fully developed, which was probably true over most of the roll wave profile except possibly near the wave crest. In this region the effect of the rapidly expanding flow in the shock may not have died out, or in other words the velocity profile had not reached its fully developed state. Thus the shear stress, τ_o, near the wave crest may have been substantially different

than assumed. The need for detailed measurements of the velocity profile near the shock is apparent.

The value of α in equation 2.2 was assumed to be 1.0. Iwasa (8) has shown that for a fully developed logarithmic velocity distribution,

$$\alpha = 1 + .781\ f. \tag{7.2}$$

From the measured values of f at normal depth in the laboratory channel, this equation gives maximum values of α of about 1.02 for the smooth channel and 1.05 for the rough channel. However, the value of α near the wave crest may have been larger if a fully developed velocity distribution was not established.

VII-B EFFECT OF SIDE-WALLS AND VARIABLE FRICTION FACTOR

1. Problem and Method of Solution

In the periodic permanent theory it was assumed that the friction factor did not vary along the wave length and the rectangular channel was wide enough such that the side-walls had negligible influence. These simplifications resulted in a form of the differential equation that could be integrated (equation 3.52). However, when the friction factor is permitted to vary (in the same manner as it varies in uniform steady flow), and/or the hydraulic radius concept is used to account for side-wall friction, numerical integration must be used to find solutions. This was done for one set of values of F and $S_o\lambda/h_n$ (5.60 and 27.3 respectively) for the purpose of finding the qualitative effects. The friction factor was assumed to vary according to the relation found

for uniform flow in the smooth channel (figure 22), which was approximated by,

$$f = .3557/R^{.2513}. \tag{7.3}$$

This experimental relation is convenient because the approximate values of quantities such as h_c and h_n are known from the experiments on the .1192 slope ($F \sim 5.6$). Therefore, the slope was fixed at .1192, and the width of the channel was taken as 4-5/8 in., the same as the laboratory flume.

Two different conditions were considered; a variable friction factor with no side-wall effect, and a variable friction factor with a side-wall effect. The methods of finding the solutions (wave shape and velocity) for the given values of F and $S_o\lambda/h_n$ were basically the same for both conditions. Therefore, the method used when the side-wall effect was included will be outlined, and the method for the other condition follows by letting the hydraulic radius equal the depth.

The differential equation for a permanent wave profile is,

$$dh/dX = \frac{gS_o h^3 - f\dfrac{u^2 h^3}{8r}}{gh^3 - K^2} \tag{7.4}$$

which corresponds to equation 3.41. The requirement that the slope of the water surface (dh/dX) remain finite at $h = h_c$ leads to,

$$c = \sqrt{gh_c}\left(1 \pm \sqrt{\frac{8S_o}{f_c}\,\frac{r_c}{h_c}}\right). \tag{7.5}$$

This results from setting the numerator of equation 7.4 equal to zero at $h = h_c$, and using the expressions,

$$K = (c-u)h, \tag{7.6}$$

$$\text{and } h^3_c \equiv K^2/g, \tag{7.7}$$

which were given in Chapter III.

In equation 7.5 the quantity f_c denotes f at the section $h = h_c$. Equation 7.5 reduces to the expression for c in Chapter III (equation 3.51) for a wide channel ($r_c = h_c$) with an unvarying f over the wave length ($f_c = f_n$).

Before explaining the details the general procedure is given. First a value of h_c was assumed, and then the relation between h and X was obtained. Then a pair of values of h_{min} and h_{max} were obtained that gave the desired value of $S_o\lambda/h_n$. However, the resulting F was, in general, not the one desired. Thus the procedure was repeated with a different value of h_c until the desired F resulted. By increasing the value of h_c, the resulting F was increased.

With the assumed value of h_c, the value of K was calculated from equation 7.7. The value of r_c was obtained from the general formula for r,

$$r = bh/(b+2h) \tag{7.8}$$

where b was .3854 ft.

To evaluate u and f in equation 7.4 the expressions

$$u = (ch - K)/h, \tag{7.9}$$

$$R = 4ru/\nu, \tag{7.10}$$

and equation 7.3 were used. This required the value of c which was calculated from the expressions,

$$u_c = (ch_c - K)/h_c, \tag{7.11}$$

$$R_c = 4r_c u_c/\nu, \tag{7.12}$$

$$f_c = .3557/R_c^{.2513}, \tag{7.13}$$

in addition to equation 7.5. These four equations in four unknowns (f_c, c, u_c, R_c) were solved by a trial and error method.

The relation between h and X was obtained using equation 7.4. For values of h greater than h_c, the slope (i.e. dh/dX) at a particular value of h (i.e. h_i) was extended to the next larger value of h (i.e. h_{i+1}) where the interval in h(i.e. $h_{i+1} - h_i = \Delta h > 0$) was sufficiently small such that the change in the slope from h_i to h_{i+1} was a small fraction of the slope at h_i. Using the slope evaluated at h_i(i.e. $(dh/dX)_i$), the distance between h_i and h_{i+1} was calculated by

$$\Delta X_i = X_{i+1} - X_i = \Delta h / \left[(dh/dX)_i\right],$$

and the area between h_i and h_{i+1} was calculated by

$$\Delta A_i = A_{i+1} - A_i = (h_i + \Delta h/2)\Delta h.$$

For values of h less than h_c, the slope at h_i was extended to the next smaller value of h (i.e. h_{i-1} where $h_{i-1} < h_i$) so that the distance between h_{i-1} and h_i was given by

$$\Delta X_i = X_i - X_{i-1} = \Delta h / \left[(dh/dX)_i \right],$$

and the area between h_{i-1} and h_i was given by

$$\Delta A_i = A_i - A_{i-1} = (h_i - \Delta h/2)\Delta h.$$

In this way the distances and the areas between all the successive values of h were calculated. Note that the slope can not be evaluated at $h = h_c$ from equation 7.4 because both the numerator and denominator are then zero. However, the slopes at $h_c + \Delta h$ and $h_c - \Delta h$ were practically the same, and this value was used at h_c.

The next step was to assume a value of h_{min} and to calculate the corresponding value of h_{max} from equation 3.46. The value of h_i closest to this value of h_{max} was found and the wave length was found by summing all ΔX_i between h_{max} and h_{min}. Similarly the average depth was calculated by summing all ΔA_i and dividing by the wave length. The average discharge was obtained from;

$$q_{av} = c\, h_{av} - K, \tag{7.14}$$

The next step was to calculate u_n and h_n from,

$$r_n = bh_n/(b+2h_n) \tag{7.15}$$

$$u_n = q_{av}/h_n \tag{7.16}$$

$$f_n = .3557/R_n^{.2513} \tag{7.17}$$

$$R_n = 4r_n u_n/\nu \tag{7.18}$$

$$f_n = 8gr_n S_o/u_n^2 \tag{7.19}$$

where the unknowns were r_n, h_n, u_n, f_n, and R_n. With this value of h_n, the value of $S_o\lambda/h_n$ was calculated. If this was not equal to 27.3, another value of h_{min} was assumed, the calculation was repeated and the corresponding value of $S_o\lambda/h_n$ found. After the value of $S_o\lambda/h_n$ was reasonably close to 27.3, the F was computed from,

$$F = u_n/\sqrt{gh_n} \tag{7.20}$$

and if it did not agree closely with 5.60, another value of h_c was assumed and the entire procedure repeated. As a check on the accuracy of the numerical integration procedure, a case with a constant f and wide channel was done by the above method. The difference between these results and the exact results (by the method in Chapter III) was negligible.

2. Discussion of Results

The results of the wave-profile calculations are shown in figure 58. Qualitatively it is seen that a variable f increased h_{max}, and the effect of the side-walls decreased h_{max}. Both of these trends can be deduced by examining equation 7.4. As the depth along the wave profile increases the Reynolds number increases, and thus for a smooth channel the value of f decreases. Similarly as the depth decreases,

f increases. Thus for a given h sufficiently large (i.e. so that $f < f_n$), the slope of the water surface is greater than the slope computed with $f = f_n$. Also for a given h sufficiently small (i.e. so that $f > f_n$), dh/dX is less than that computed with $f = f_n$. Therefore, for a given normal depth (or approximately a given average depth) the trend shown in figure 58 (e.g. larger h_{max}/h_n with variable f theory as compared to constant f theory) is consistent with the relations between the slopes as stated above. The same trend shown in figure 58 for a smooth channel can also be expected for a rough channel. This is because f depends on the depth in the same way as for a smooth channel; as the depth increases, and thus the relative roughness decreases, the f decreases.

The effect of the side-walls can also be predicted from equation 7.4 by observing that the value of r is always less than the value of h. Furthermore, this difference is greater as the value of h increases. Thus for a given h the water-surface slope is less in a narrow channel than in a wide channel, particularly at the higher depths. Therefore, the relation between the wave profiles in a wide channel and a finite-width channel must be as shown in figure 58 for the variable f theories, and similar results can be expected for a constant f theory. In figure 6 it was shown that as F decreased the value of h_{max} decreased and the value of h_{min} increased. This is the same effect that the side-walls have. F is simply the quantity $\sqrt{8S_o/f_n}$ for a wide channel, so that a decrease in F can be considered as an increase in the frictional resistance. Similarly the effect of the side-walls can be considered as adding more frictional resistance.

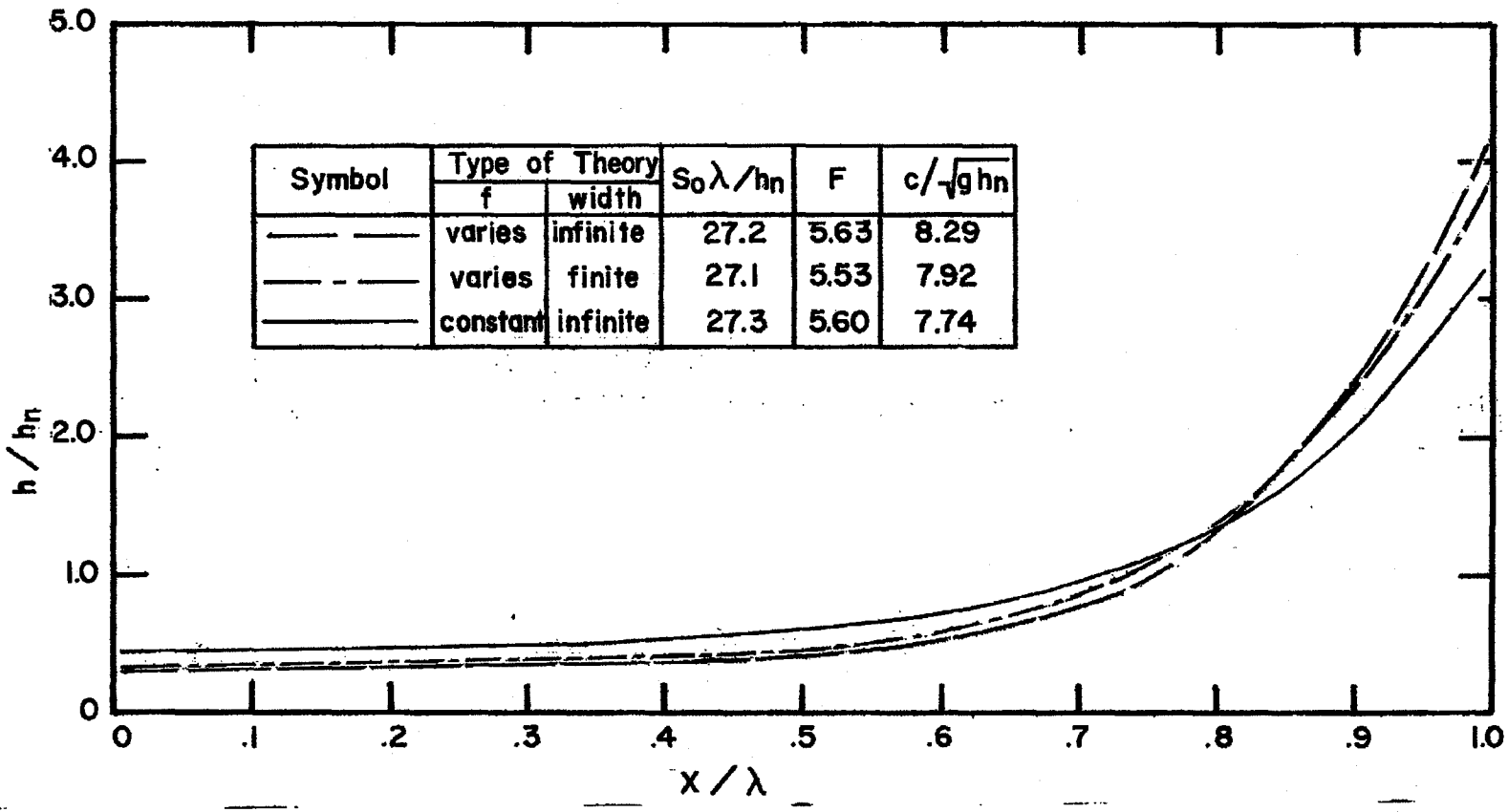

Symbol	Type of Theory f	Type of Theory width	$S_o\lambda/h_n$	F	$c/\sqrt{g h_n}$
——— ———	varies	infinite	27.2	5.63	8.29
——— - - ———	varies	finite	27.1	5.53	7.92
———	constant	infinite	27.3	5.60	7.74

Fig. 58. Graph of theoretical periodic permanent water-surface profiles including effects of variable friction factor f and side-walls, Froude number = 5.6, dimensionless wave length $S_o\lambda/h_n = 27.3$

In figure 58 it is seen that the value of h_{max} was increased appreciably when the friction factor was assumed to vary, and that the value of h_{max} was decreased by a relatively smaller amount when the side-wall effect was considered. However, the magnitude of these two changes will depend not only on the values of F and $S_o\lambda/h_n$, but also on the relative width of the channel (relative width = b/h_n), and the relation between the friction factor and the Reynolds number (smooth channel) or relative roughness (rough channel). For a relatively narrow channel the side-wall effect is obviously greater. In a smooth channel at large values of R the value of f is a weak function of R. This is seen from the equation shown on figure 23. Therefore at large Reynolds numbers the effect of a variable friction factor on the predicted values of h_{max} may be negligible. From the above it is clear that a complete description of the magnitude of the two effects considered in this section depends on many parameters. In this section only the qualitative effects were discussed.

VII-C MODIFIED SHOCK CONDITION

1. General Shock Condition

In the derivation of the shock condition (equation 3.46) it was assumed (as did Dressler (15)) that the shock thickness in the longitudinal direction was small. The results of some measured wave profiles (figure 45) show that this was not the case. The effect of this finite shock length, as well as some other factors which were not included in equation 3.46, on the shock condition will now be considered.

Figure 59 shows a sketch of a shock front drawn approximately to scale. It should be noted that the part of the shock front drawn vertical on figure 59 corresponds to the sharply rising portion of the shock easily observed in figures 1 and 24. The velocity distributions at the wave crest and trough have been drawn to be typical of a fully developed turbulent boundary layer. The shock wave can be analyzed as a case of steady flow by imposing a constant velocity of -c on the system. The momentum theorem can then be applied to a control volume consisting of the fluid between the wave crest and trough. For this steady flow the momentum theorem states that the net difference in flux of momentum through the surfaces of the control volume is equal to the sum of all the external forces acting on the control volume. At the wave crest or trough the momentum flux in the x-direction for the steady flow is,

$$\rho \int_0^h (u_p - c)^2 \, dy = \rho(c^2 h - 2cuh + \alpha u^2 h) \tag{7.21}$$

where u is the average velocity,

$$u = \frac{1}{h} \int_0^h u_p \, dy, \tag{7.22}$$

and α is defined as,

$$\alpha = \frac{1}{u^2 h} \int_0^h u_p^2 \, dy. \tag{7.23}$$

The continuity equation for this steady flow is,

$$(u-c)h = \text{constant} = -K \tag{7.24}$$

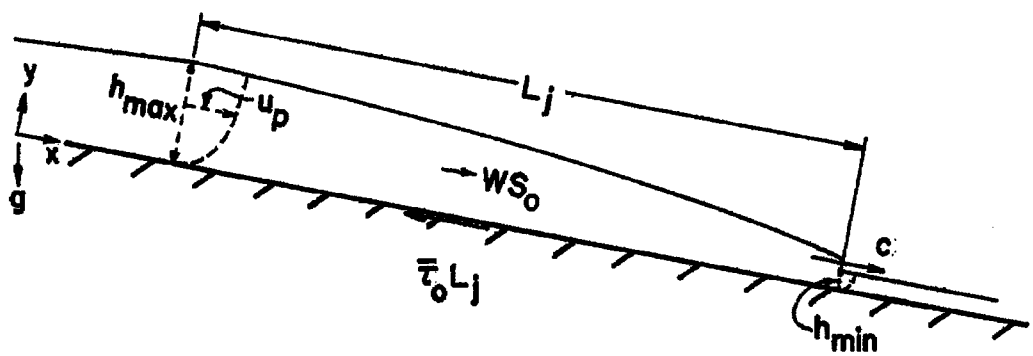

Fig. 59. Drawing of typical shape of shock front, based on periodic permanent wave run with F = 5.60, S_o = .1192, T' = 4.25

so that the momentum flux can be written,

$$\rho(cK - cuh + \alpha u^2 h), \tag{7.25}$$

and the net difference in momentum flux through the surfaces of the control volume becomes,

$$\Big[\rho uh(\alpha u - c)\Big]_{h = h_{min}} - \Big[\rho uh(\alpha u - c)\Big]_{h = h_{max}} \tag{7.26}$$

The external forces in the x-direction acting on the control volume are the pressure forces at the crest and trough, the x-component of the weight of the water in the control volume, and the shear force at the solid boundary. Using a hydrostatic pressure distribution the momentum theorem applied along the x-axis takes the form,

$$1/2\ g \cos\theta\ (h^2_{max} - h^2_{min}) + \frac{WS_o - \overline{\tau}_o L_j}{\rho} = u_{min} h_{min} (\alpha_{min} u_{min} - c)$$
$$- u_{max} h_{max} (\alpha_{max} u_{max} - c) \tag{7.27}$$

where W is the weight of water in the control volume per unit width, $\overline{\tau}_o$ is the shear stress at the solid boundaries averaged over the length of the shock, L_j. The value of $\cos\theta$ will be taken as 1.0 which is within one percent of its true value up to a slope ($\sin\theta$) of 0.14.

The effect of a nonuniform velocity distribution can be seen by substituting equation 7.24 on the right side of equation 7.27 to obtain,

$$g/2\ (h^2_{max}-h^2_{min}) + \frac{WS_o-\bar{\tau}_o L_j}{\rho} = K(u_{max}-u_{min}) + (\alpha_{min}-1)u^2_{min}h_{min}$$

$$-(\alpha_{max}-1)u^2_{max}h_{max} \qquad (7.28)$$

For a uniform velocity distribution (i.e. $u_y = 0$) the value of α is unity, and its value is greater than unity for any other distribution. Thus the effect of a nonuniform velocity profile at the trough is to increase the right side of equation 7.28 which can be shown to result in an increase in h_r (i.e. $h_r = h_{max}/h_{min}$). Similarly a nonuniform velocity distribution at the crest would reduce the value of h_r. If $\alpha_{max} \geq \alpha_{min}$, the right side of equation 7.28 would be decreased from its value with $\alpha_{max} = \alpha_{min} = 1$, which can be shown to result in a decrease in h_r.

In this discussion of the shock condition, the results of measurements pertaining to the hydraulic jump will be referred to. The hydraulic jump is a stationary shock wave where the fluid passes through the shock from the low depth (high velocity) to the high depth (low velocity). The wave velocity of the moving shock wave is greater than the fluid velocity so that the fluid in front of the shock passes through the shock from the low depth (low velocity) to the high depth (high velocity). Thus the hydraulic jump and the moving shock are basically the same phenomenon. By setting the wave velocity equal to zero, and changing the sign of the shear stress because the flow direction with respect to the solid boundary changes, equation 7.28 for a horizontal channel becomes,

$$g/2\,(h^2_{max}-h^2_{min})+\bar{\tau}_o L_j/\rho=q(u_{min}-u_{max})+(\alpha_{min}-1)qu_{min}-(\alpha_{max}-1)qu_{max} \tag{7.29}$$

For this case the average velocity at the minimum depth (u_{min}) is greater than u_{max} as required by continuity. Therefore the right side of equation 7.29 is more sensitive to changes in α_{min} than to changes in α_{max}. Furthermore it can be shown that for $\alpha_{min} \geq \alpha_{max}$ the value of h_r is larger than for the condition $\alpha_{max} = \alpha_{min} = 1$. It is reasonable to expect that in most cases the value of α_{max} is greater than α_{min}, particularly when the hydraulic jump is located a short distance from a sluice gate so that α_{min} would be practically unity. Therefore it is difficult to make any general remark concerning the effect of nonuniform velocity distribution on the value of h_r for a hydraulic jump. From the last two equations it can be shown that the effect of the shear stress would be to increase the value of h_r for a moving shock wave, and to decrease the value of h_r for a hydraulic jump.

Measurements of pressure and velocity distributions at the wave crest and trough, and shear stresses on the solid boundary for hydraulic jumps will not be discussed here, and indeed are relatively scarce. Perhaps it is sufficient to note that equation 7.29, with $\alpha = 1.0$, and $\bar{\tau}_o$ neglected, has been substantially verified by many investigators (27). Thus it is tempting to assume that the combined effects of nonhydrostatic pressure distribution, nonuniform velocity distribution, and shear stress for a moving shock (equation 7.28) are

minor. However, it was stated above that the shock condition for a hydraulic jump is more sensitive to changes in α_{min} than changes in α_{max}, whereas for the moving shock wave, the shock condition is more sensitive to α_{max}. Therefore if α_{max} for a moving shock wave is much different than α_{min} for a hydraulic jump, the relative effect of a nonuniform velocity distribution for a moving shock wave will be different than it is for a hydraulic jump.

For hydraulic jumps on sloping channels the weight term has been found to be important. Bakhmeteff and Matzke (28) found from their experiments that neglecting the weight term led to substantial discrepancies for values of h_r. However after evaluating the weight term by using their measured jump profiles, but still neglecting the solid boundary shear force and assuming $\alpha = 1$, they found good agreement between theoretical and measured values of h_r. From this experience with hydraulic jumps, it is reasonable to expect that the weight term for a moving shock will be important. Equation 7.28 shows that inclusion of the weight will decrease the value of h_r, and this effect will increase with the slope. Figure 44 shows that this is the trend required to decrease the discrepancy between the predicted and measured values of h_{max}/h_n.

2. Theory Based on Modified Shock Condition

The shock condition with the weight term will now be put in a convenient form for use in the theory. The theory with this modified shock condition will be referred to as the modified theory. Neglecting the effects of nonuniform velocity distribution and shear stress,

equation 7.28 can be written as,

$$1/2(h_r^2-1) + WS_o/(\gamma h_{min}^2) = (1-1/h_r)(c-u_{min})^2/(gh_{min}) \qquad (7.30)$$

after using equation 7.24. The last term has the form of a Froude number. This will be designated as,

$$F^*_{min} = (c-u_{min})/\sqrt{gh_{min}} \quad . \qquad (7.31)$$

The value of W must be evaluated from measurements of the shape of the shock front. Once again it is convenient to refer to the hydraulic jump where it has been found that the length of the jump can be expressed as a function of the Froude number at the minimum depth ($F_{min} = u_{min}/\sqrt{gh_{min}}$). The length of the jump is usually expressed in terms of the value of h_{max}. Therefore the weight term in equation 7.30 is expressed as,

$$S_o W/(\gamma h_{min}^2) = S_o h_r^2 (h_e/h_{max})(L_j/h_{max}) \qquad (7.32)$$

where h_e is the average depth over the length L_j, so that,

$$W = h_e L_j \gamma . \qquad (7.33)$$

Now equation 7.30 can be written,

$$h_r^3 (G+1/2) - h_r (F^{*2}_{min} + 1/2) + F^{*2}_{min} = 0 \qquad (7.34)$$

where,

$$G = S_o(h_e/h_{max})(L_j/h_{max}) \qquad (7.35)$$

The wave shapes of the periodic permanent roll waves included some information on the geometry of the shock front. The method of obtaining this shock data was given in IV-D-3-b, and the results are in table 7. When these data were taken the importance of the shock front was not realized, and consequently the oscillograph chart speeds were slower than would be desirable. This required measuring distances on the oscillograph charts of the order of 0.5 mm to define the shock geometry. Therefore the shock geometry to be presented should be considered preliminary in nature.

The lengths of hydraulic jumps are usually expressed as a function of the value of F_{min}. This suggests that for a moving shock wave the geometry could be expressed as a function of F^*_{min}. In this study velocities were not measured so that the value of F^*_{min} for each periodic permanent roll wave run is not known. From equation 7.34 it can be shown that h_r increases as F^*_{min} increases. Thus it is expected that h_e/h_{max} and L_j/h_{max} can also be expressed as a function of h_r. This expectation was at least partially realized as figure 60 shows. These data points represent all the periodic permanent roll wave runs listed in table 7 except two for which a shock profile was not well defined by the measurements.

Having the relations in figure 60 it would be desirable to use them in equation 7.34 and compute the values of h_r for each periodic permanent wave run and compare these with the observed values of h_r. However this requires the values of F^*_{min} for each run which are not obtainable. Therefore an indirect check on the modified shock condition was made by using equation 7.34 and the relation for $h_e L_j/h^2_{max}$

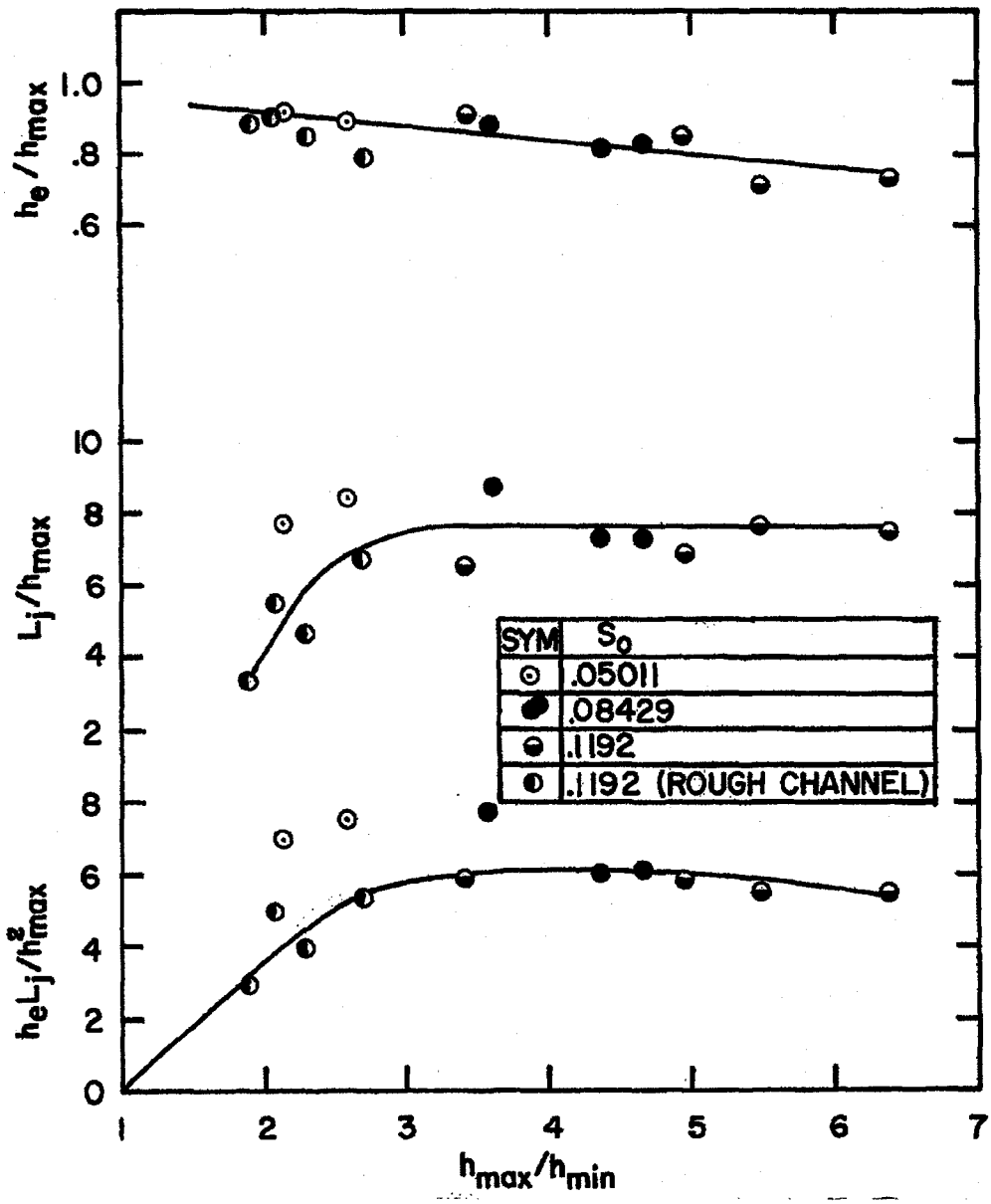

Fig. 60. Graph of measured geometric properties for shock front: average depth of shock front h_e, length of shock front L_j and volume of shock front per unit width h_eL_j, all expressed as a function of ratio between depth at crest and depth at trough h_{max}/h_{min}

from figure 60 in the periodic permanent roll wave theory. From this modified theory there results a relation between the values of h_r and T' for each value of F and slope. It is to be noted that the slope as well as F must be specified (equation 7.35). This relation between h_r and T' will be compared with the measured values. In addition the quantities h_{max}/h_n, h_{min}/h_n, and $c/\sqrt{gh_n}$, computed from the modified theory, will be compared to the measured values. Before presenting these results, the procedure for incorporating the modified shock condition into the theory will be briefly explained.

Equations 3.42 and 3.43 can be combined to give,

$$F^*_{min} = (h_c/h_{min})^{3/2} . \tag{7.36}$$

Thus the value of h_r is a function of h_{min}/h_c and G. When the value of G is set equal to zero, equation 7.34 becomes

$$(h_r - 1)\left[h_r^2/2 + h_r/2 - (h_c/h_{min})^3\right] = 0 \tag{7.37}$$

and the nontrivial solution for h_r is given by equation 3.46. However for a nonzero value of G, the shock condition remains a cubic equation and was solved by a numerical procedure. The method used to find the solutions for h_r, h_{max}/h_n, etc., was basically the same as for the original theory. With a given value of F and S_o a value of h^*_{min} was chosen ($h^*_a \leq h^*_{min} \leq 1$). Then in order to find h_r from equation 7.34 a value of G was assumed and h_r was then computed. If this value of h_r did not correspond to the assumed value of G (figure 60), another value of G was assumed and the process repeated until the values of

G and h_r corresponded. Once the shock condition was satisfied, the rest of the solution was found in the same manner as before.

The modified theory was used to obtain solutions for h_r, h_{max}/h_n, h_{min}/h_n, and $c/\sqrt{gh_n}$ as functions of T' for the values of F and S_o used for the periodic permanent roll wave experiments. These solutions, along with those predicted from the original (or unmodified) theory, are shown in figures 61-64. The results of the periodic wave experiments (table 6) are also shown on these figures. For the values of h_{max}/h_n, the experimental relations from figures 54 to 57 are plotted. The range in the values of T' for the periodic experiments for S_o = .05011 was relatively small. Therefore the results for two natural-wave runs (h_n = .206 in., F = 3.45, station 120, smooth inlet; h_n = .314, F = 3.71, station 120, smooth inlet) at S_o = .05011 were also shown on figure 61.

3. Discussion of Modified Theory

Figures 61 to 64 show that, in general, the modified theory offers better agreement with the measurements than the original theory except for the values of h_{min}/h_n. The amount of improvement provided by the modified theory increases with the slope. The modification (addition of S_oW term) to the original theory decreases the values of h_{max}/h_{min} and h_{max}/h_n, and increases the values of h_{min}/h_n and $c/\sqrt{gh_n}$. The average discrepancies (over the range of T' used in the experiments) between the modifed theoretical relations and the experimental relations for h_{max}/h_n are: 4.5 percent, S_o =.05011; 3.0 percent, S_o = .08429; 9.5 percent, S_o = .1192; and 8.5 percent, S_o = .1192,

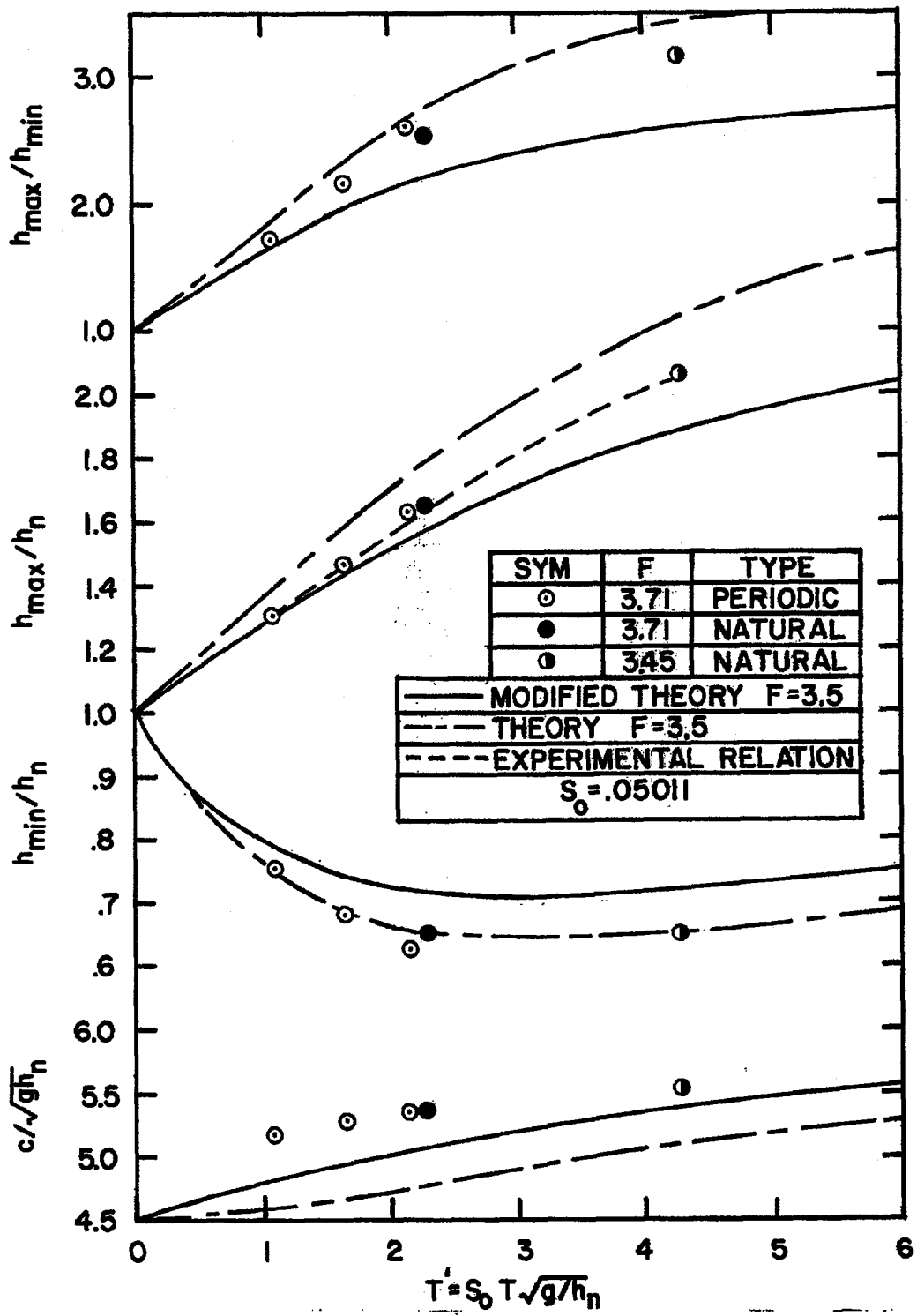

Fig. 61. Graph of experimental values and theoretical solutions (from modified and unmodified theory) for h_{max}, h_{min}, and c as functions of dimensionless wave period T' for periodic permanent waves: Froude number = 3.5, channel slope = .05011

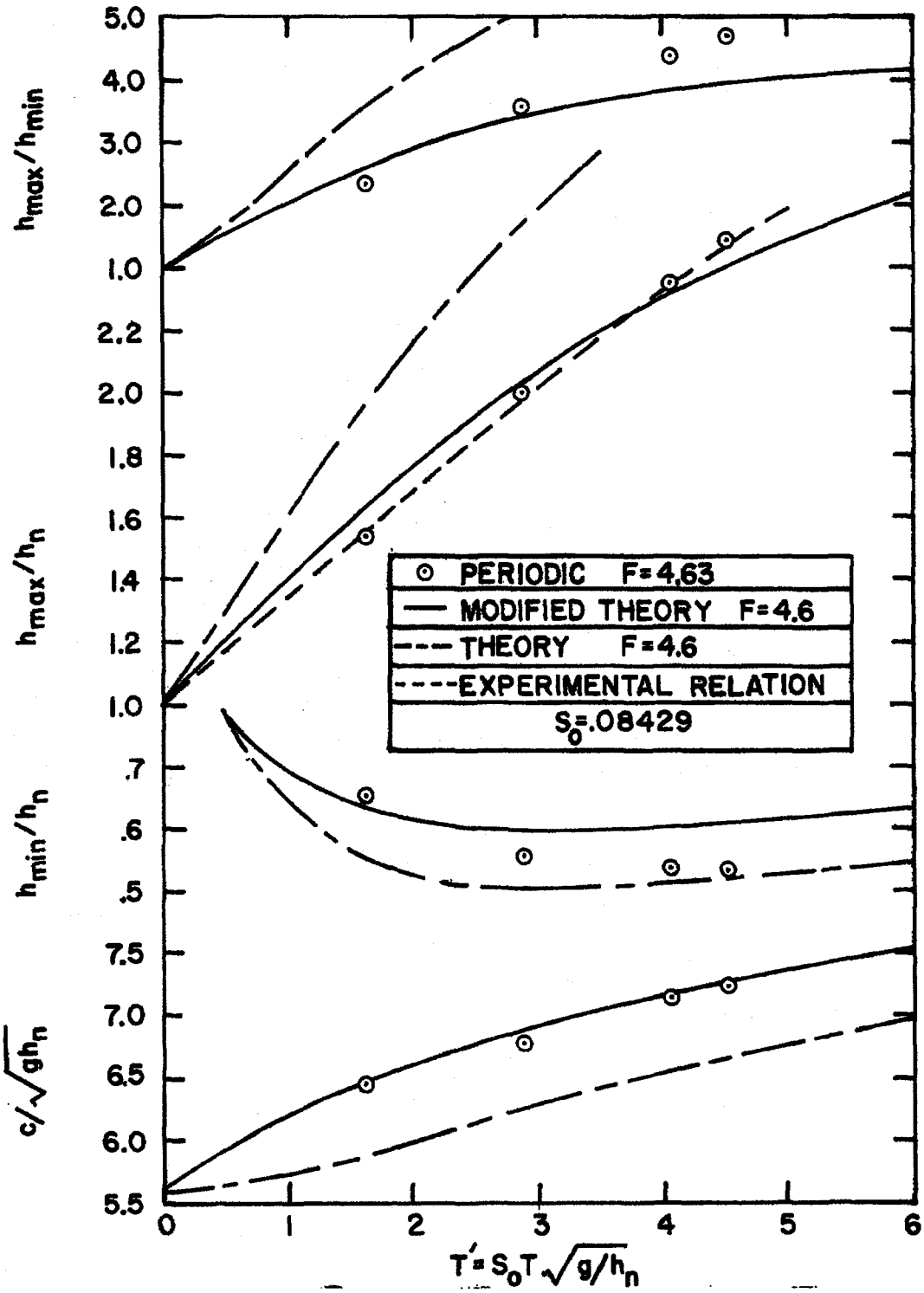

Fig. 62. Graph of experimental values and theoretical solutions (from modified and unmodified theory) for h_{max}, h_{min}, and c as functions of dimensionless wave period T' for periodic permanent waves: Froude number = 4.6, channel slope = .08429

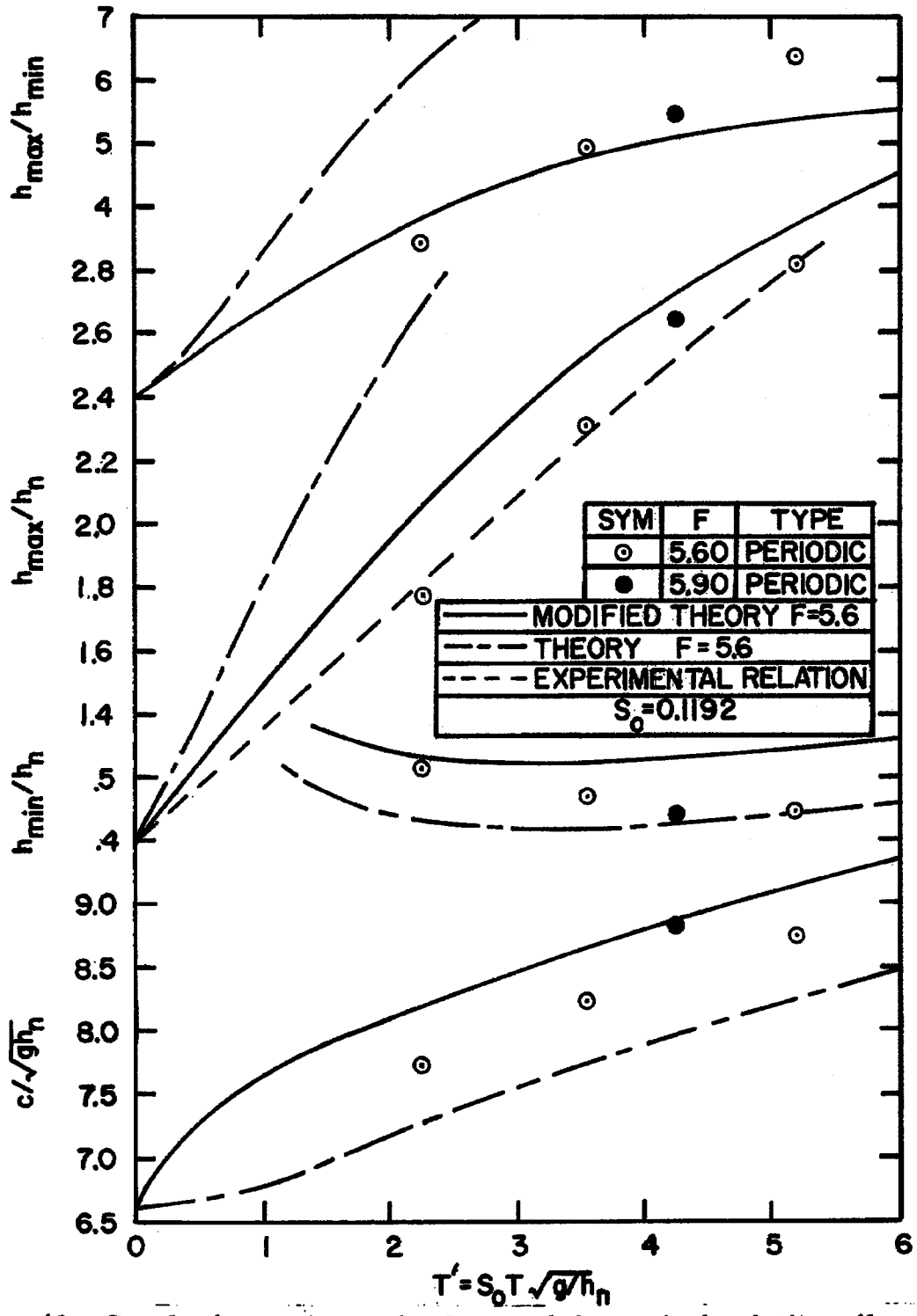

Fig. 63. Graph of experimental values and theoretical solutions (from modified and unmodified theory) for h_{max}, h_{min}, and c as functions of dimensionless wave period T' for periodic permanent waves: Froude number = 5.6, channel slope = .1192

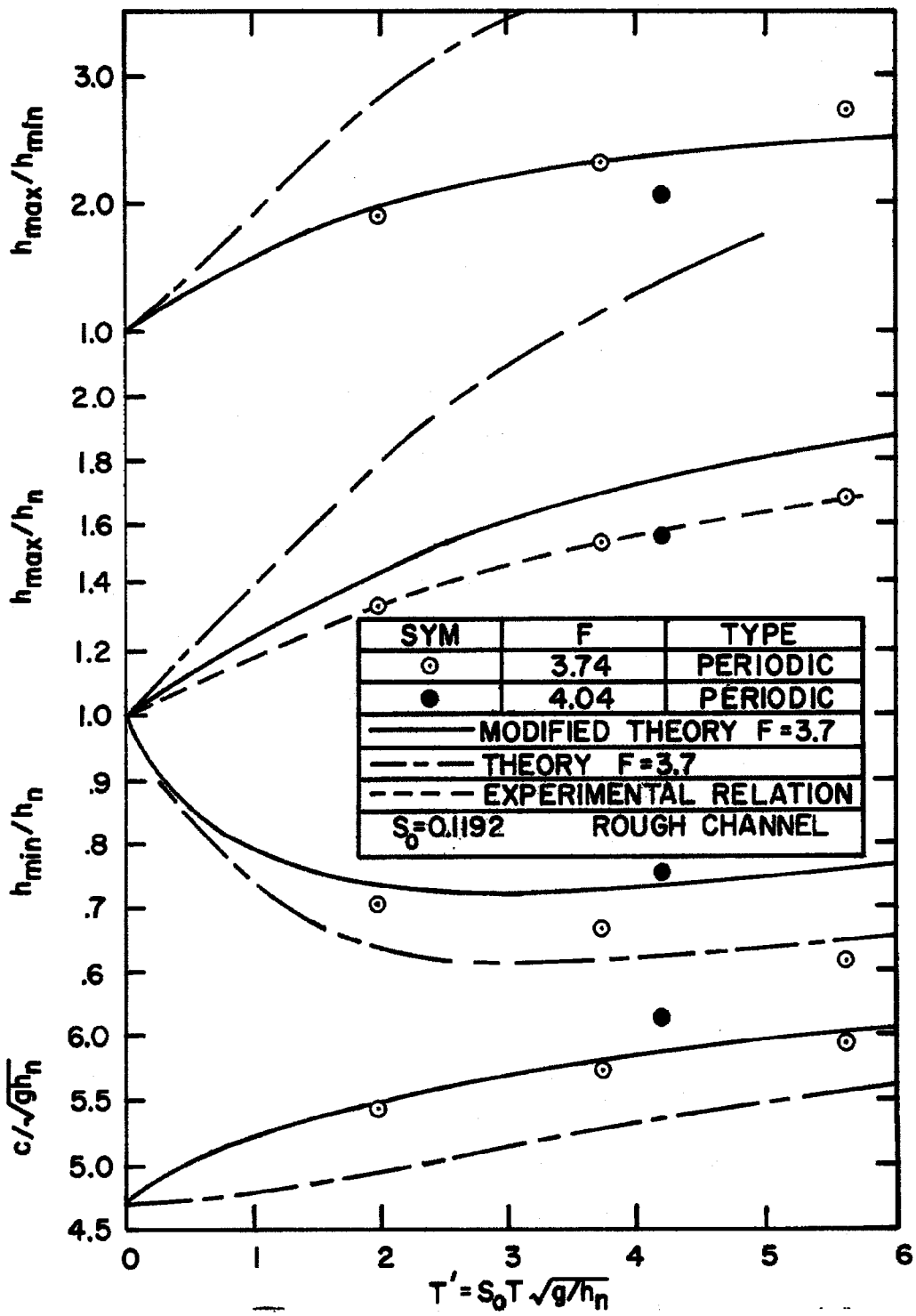

Fig. 64. Graph of experimental values and theoretical solutions (from modified and unmodified theory) for h_{max}, h_{min}, and c as functions of dimensionless wave period T' for periodic permament waves: Froude number = 3.7, rough channel, channel slope = .1192

rough channel. The corresponding maximum discrepancies are 9.0, 4.5, 13.5, and 9.5 percent.

At $S_o = .05011$, the modified relation predicts values of h_{max}/h_n less than the measured values. At $S_o = .08429$ the predicted and measured values of h_{max}/h_n are in close agreement. For both the smooth and rough channel at $S_o = .1192$, the predicted values of h_{max}/h_n are greater than the measured values. Thus the discrepancies in the values of h_{max}/h_n show a dependence on the channel slope. One possible explanation for this may be that the geometry (i.e. L_j/h_{max} and h_e/h_{max}) of the shock wave should depend on the channel slope, although the somewhat preliminary data in figure 60 did not show this. However for hydraulic jumps the length of the jump has been found to depend on the slope. This is shown in figure 65 which was taken from Chow's book (29). The relations in figure 65 are for hydraulic jumps in which the minimum depth was upstream of the maximum depth. Therefore the moving shock waves (figure 59) must be considered to be on a negative slope with respect to the slopes shown in figure 65. Therefore if subsequent measurements of the lengths of moving shock waves did in fact reveal a slope effect, and it followed the trend in figure 65, one would expect the values of L_j/h_{max} to increase as the slope increased. This would tend to compensate for the effect of channel slope on the discrepancies in h_{max}/h_n shown on figures 61-64. The maximum value of L_j/h_{max} in figure 60 of about 7.5 is larger than the maximum value of L_j/h_{max} shown in figure 65. This indicates that the lengths of moving shock waves and hydraulic jumps are compatible.

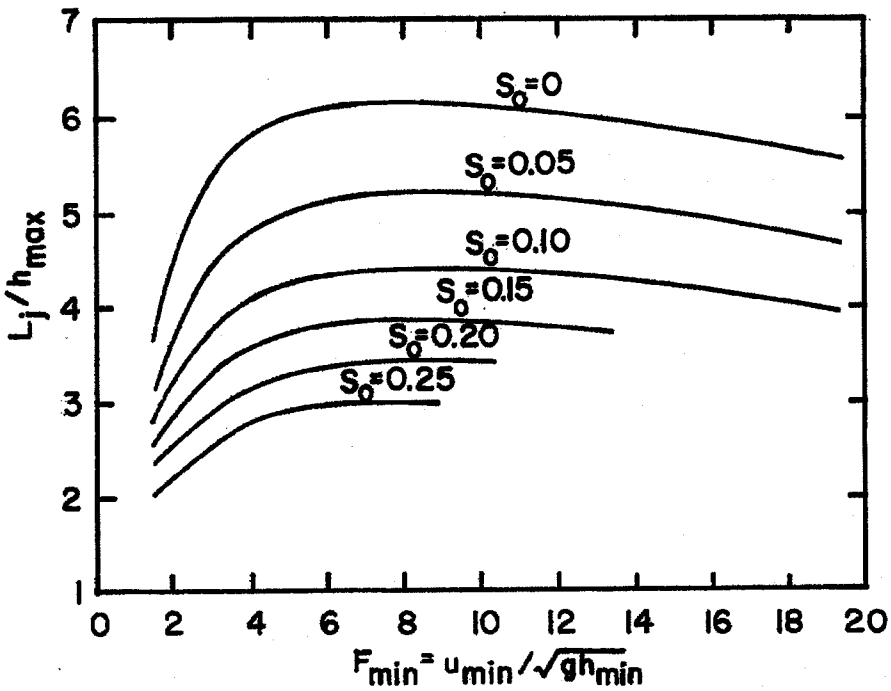

Fig. 65. Graph of the length of hydraulic jumps L_j in sloping channels as a function of the Froude number at the minimum depth F_{min} (from Chow(29))

VII-D RE-EVALUATION OF LABORATORY RESULTS WITH CONSIDERATION TO EFFECT OF CHANNEL SLOPE

1. Periodic Permanent Waves

The laboratory experiments with periodic roll waves showed that even with the values of F and T' fixed, the value of h_{max}/h_n depended on the channel slope. This can be seen by comparing the values of h_{max}/h_n for $S_o = .05011$ (figure 61) to those in the rough channel with $S_o = .1192$ (figure 64). It is seen that, for a fixed value of F and T', as the slope increases the value of h_{max}/h_n decreases.

This slope effect for periodic permanent waves was predicted by the theoretical analysis only after the shock condition was modified to include the x-component of the weight of the shock. This force due to the shock weight was previously (Dressler (15)) assumed to be negligible compared to the pressure forces. The modified theory greatly reduced the discrepancies in h_{max}/h_n between the original theory and the experimental results.

The h_{max}/h_n vs. T' experimental relations (figures 44, 61-64) should apply to periodic permanent roll waves in all wide rectangular channels with slopes comparable to those used in this study. In other words both the slope and the Froude number must correspond to the values of S_o and F listed on figures 61-64. If the slope is less than that used to obtain a h_{max}/h_n vs. T' relation, the magnitude of h_{max}/h_n will be greater than predicted from the experiments. For example in a channel with a Froude number of about 3.5 and a value of T' of 4.0, figure 61 shows that h_{max}/h_n would be about 2.0 for a slope of about .050. If the slope were significantly less than .050, then h_{max}/h_n would be larger. As an upper limit for h_{max}/h_n, the

unmodified theory can be used, which in this case predicts a value of h_{max}/h_n of 2.2.

Although the use of the unmodified theory to predict an upper limit for h_{max}/h_n is somewhat speculative, the water-surface profile for the periodic wave run in the 130-ft channel (figure 43), in which the slope effect was probably of minor importance, agreed quite well with the theory. It is reasonable to assume that the unmodified theory should predict an upper limit for h_{max}/h_n with about the same accuracy as the modified theory predicted h_{max}/h_n in the experiments, at least over the range of F and T' used in the experiments.

For the case in which the channel slope is less than that used in the experiments, the range between the value of h_{max}/h_n from the unmodified theory (upper limit) and the value from the experiments may be quite large. In the example considered above the range of h_{max}/h_n was only from 2.0 to 2.2. However, for a case with $F = 4.6$, $T' = 3.5$, and $S_o = .06$, the range of h_{max}/h_n would be from 2.2 to 2.75 (figure 62). To get the value of h_{max}/h_n corresponding to $S_o = .06$, the modified theory would have to be used in the manner described in Section VII-C, using the shock geometry relations from figure 60. For cases in which the channel slope is greater than that used in the experiments, the value of h_{max}/h_n will be less than predicted from the experimental relations. If the slope is considerably greater, the modified theory could be used to find out how much lower the value of h_{max}/h_n would be than the experimental value.

2. Natural Roll Waves

The influence of this slope effect on the experimental results for natural roll waves will now be considered. In Section VI-B it was shown that the h_{max}/h_n vs. T' experimental relations for periodic waves were also valid for natural roll waves in the final development phase, if $\bar{h}_{max}$ was used for h_{max} and T_{av} was used to calculate T'. Therefore the $\bar{h}_{max}/h_n$ vs. T' experimental relations for natural waves will be influenced by channel slope in the same way as the h_{max}/h_n vs. T' relations for periodic waves. The field measurements in Santa Anita Wash (figure 51) serve as an example of the effect of the slope on the h_{max}/h_n vs. T' relation. The field values of $\bar{h}_{max}/h_n$ were greater than predicted from the laboratory relation, and the field slope was .025 as compared to .050 in the laboratory. The magnitude of the slope effect on the values of $\bar{h}_{max}/h_n$ can be evaluated in the same way as described above for periodic waves. However the slope effect (if any) on the standard deviation of h_{max}/h_n can not be evaluated from existing knowledge.

Because of the slope effect on the $\bar{h}_{max}/h_n$ vs. T' relation for natural waves, there should also be a slope effect on the growth rates of natural waves in the final development phase. Stated symbolically, it is expected that for a fixed value of F and $\bar{h}_{max}/h_n$ (for $\bar{h}_{max}/h_n$ sufficiently large), the value of $\partial\bar{h}_{max}/\partial\ell$ will also depend on the slope such that as the slope is increased the value of $\partial\bar{h}_{max}/\partial\ell$ will be decreased. This dependance of $\partial\bar{h}_{max}/\partial\ell$ on the slope was found in the laboratory experiments. Figure 26 shows the $\bar{h}_{max}/h_n$ vs. ℓ/h_n

relation for $S_o = .05011$, and the relation for $S_o = .1192$ (rough channel) is shown on figure 29. For the large values of $\bar{h}_{max}/h_n$ the Froude numbers were about 3.5 and 3.7 respectively. Figures 54 and 57 show that for $\bar{h}_{max}/h_n$ greater than about 1.4 the natural waves were in the final development phase. Figures 26 and 29 show that for a given value of $\bar{h}_{max}/h_n$ above 1.4, the value of $\partial\bar{h}_{max}/\partial\ell$ was greater for the smaller slope. This is more readily seen from figure 48 on which both development curves are shown.

The growth rate $(\partial\bar{h}_{max}/\partial\ell)$ can be expressed as the product of the slope of the $\bar{h}_{max}/h_n$ vs. T' relation $(\partial(\bar{h}_{max}/h_n)/\partial T')$ and the slope of the T' vs. ℓ/h_n relation $(\partial T'/\partial(\ell/h_n))$. Therefore if the slope effect on both of these relations could be evaluated, the magnitudes of $\partial\bar{h}_{max}/\partial\ell$ for slopes other than those used in the laboratory could be determined. Unfortunately the slope effect can only be evaluated for a $\bar{h}_{max}$ vs. T' relation. However the experimental evidence showed that the slope effect on both $\partial\bar{h}_{max}/\partial\ell$ and $\partial(\bar{h}_{max}/h_n)/\partial T'$ was qualitatively the same (i.e. an increased slope resulted in lower values of $\partial\bar{h}_{max}/\partial\ell$ and $\partial(\bar{h}_{max}/h_n)/\partial T'$). Therefore the slope influence on a T' vs. ℓ/h_n relation must be less important than on a $\bar{h}_{max}/h_n$ vs. T' relation. Thus for purposes of obtaining somewhat rough estimates of the magnitude of $\partial\bar{h}_{max}/\partial\ell$ for channel slopes other than those used in the experiments, the slope effect on a T' vs. ℓ/h_n relation may be considered negligible.

Thus far in this section the influence of channel slope on the values of h_{max}/h_n or $\bar{h}_{max}/h_n$ for large amplitude shock-type roll waves has been considered. The theoretical analysis was able to predict (at least qualitatively) all the observed slope effects only after the shock condition was modified to include the x-component of the shock weight. For small amplitude waves with continuous water surfaces (before the waves break) no shock condition is required. However, as explained in Section VI-A, there still may be an effect of channel slope on growth rates of small amplitude natural roll waves. This is because the periodic small amplitude theory predicts a slope effect (equation 3.38).

The prediction of a slope effect on growth rates of small amplitude waves based on equation 3.38 should probably not be considered as sufficient evidence that there actually will be such an effect. This is because this same theory was unsuccessful in predicting the effect of Froude number on the growth rates of small amplitude waves. The theory predicted the growth rates to increase as F was increased. The experimental results showed that the growth rates were about the same for all values of F, however the value of ℓ/h_n at which the growth began decreased as F was increased.

The experiments in which F was fixed and the slope was changed (i.e. $F \approx 3.5$, $S_o = .05011$, and $S_o = .1192$ (rough channel)) were inconclusive on the effect of channel slope on growth rates of small amplitude natural roll waves. The results showed that a given value of $\bar{h}_{max}/h_n$ occurred at smaller values of ℓ/h_n for $S_o = .1192$ as

compared to $S_o = .05011$. However the initial disturbances (minimum values of $\bar{h}_{max}/h_n$) were significantly larger at $S_o = .1192$ than at $S_o = .05011$. These larger initial disturbances were attributed to the differences in the channel surfaces (i.e. hydraulically rough at $S_o = .1192$, and hydraulically smooth at $S_o = .05011$) rather than the differences in the channel slopes.

CHAPTER VIII

PREDICTION OF MAXIMUM DEPTHS IN LARGE CHANNELS

When designing open channels to convey a certain discharge it is important to know if roll waves will occur or not. If they will occur it is important to know the height of the waves (h_{max}) at all stations along the channel. Estimates of these values of h_{max} can be made by utilizing the experimental results of the present study. In an existing channel in which roll waves appear at low discharges, there is the question of whether roll waves will also appear at much larger discharges. This question, along with the problem of predicting values of h_{max} for a proposed channel will be discussed in this chapter.

The laboratory measurements were taken in a wide rectangular channel on a constant slope. Therefore a channel with these properties will be treated first. In many practical cases the channel slope changes at various intervals so that a channel may consist of a series of short reaches at constant slopes. A few methods of treating a wide rectangular channel of this type will be proposed, and the methods compared by use of a numerical example. In the final section a method of predicting values of h_{max} for rectangular channels that are not wide will be suggested. First the effect of the channel slope on the predicted values of h_{max} will be discussed.

VIII-A CHANNEL SLOPE EFFECT

For a Froude number equal to one of those in the laboratory channel, well constructed concrete channels will usually have a smaller slope. This was the case for Santa Anita Wash (figure 51). In these cases the values of h_{max} predicted from the laboratory results should really be increased because of the slope effect on the growth rates of shock waves (Section VII-D). However it was shown that the channel slope only began to influence the growth rates of $\bar{h}_{max}$ after they had developed into shock waves. There is no experimental evidence to indicate a slope effect on the growth rates of small amplitude roll waves, and for practical purposes it is probably sufficient to neglect any such effect. Furthermore because of lack of data concerning the influence of slope on the T' vs. ℓ/h_n relation, and the necessity of a lengthy analysis to adjust the $\bar{h}_{max}/h_n$ vs. T' relation to apply to a slope other than that used in the experiments, the corrections to the predicted values of h_{max} would only be approximate with some unknown degree of accuracy. Therefore in most cases the slope correction need not be calculated, however it should be realized that if the channel slope is significantly less than the laboratory channel slope (at the same Froude number), the growth rate of the shock waves ($\partial\bar{h}_{max}/\partial\ell$) will be greater than it was in the laboratory.

VIII-B PREDICTION OF MAXIMUM DEPTHS IN WIDE RECTANGULAR CHANNELS WITH A CONSTANT SLOPE

Figures 52 and 53 contain the information needed to predict values of $\bar{h}_{max}$ for channels with inlet conditions equivalent to that used in the laboratory. This would include any channel in which the flow was introduced with a negligible amount of disturbances due to flow contraction or expansion. The experimental evidence clearly indicated that with larger initial disturbances the roll waves developed closer to the inlet. Therefore any particular inlet condition should be compared to the inlet condition in the laboratory with respect to disturbances that might exist. Large inlets will almost certainly have sufficient irregularity to insure that a turbulent boundary layer, as opposed to a laminar boundary layer, will be developed from the beginning of the channel. With a turbulent boundary layer the inlet would be a rough inlet which is the type of inlet to which figures 52 and 53 apply.

With inlet conditions equivalent to those of the laboratory channel, it is a simple matter to find $\bar{h}_{max}$ at any distance from the inlet once the values of F and h_n are known. For purposes of designing channels the maximum value of h_{max} is also required and can be found from the relation given in Section VI-A,

$$(h_{max})_{max} = \bar{h}_{max} + 2.58\,\sigma_{h_{max}} \tag{6.3}$$

Figure 35 gives values of $\sigma_{h_{max}}/h_n$ as a function of ℓ/h_n. From figures 35 and 52 it is seen that for small values of $\bar{h}_{max}/h_n$ the standard deviations were not measured. The relations for $\sigma_{h_{max}}/h_n$ in figure 35 can be extrapolated to smaller values of ℓ/h_n (and thus smaller values of $\bar{h}_{max}/h_n$), but for values of $\bar{h}_{max}/h_n$ on the part

of the development curve that is concave upward it is sufficient to assume that the standard deviations of h_{max} were zero.

Consider a channel with $S_o = .03$, $F = 3.7$, and $\ell/h_n = 6000$. The data points on figure 53 for an F of 3.71 and 3.81 indicate a definite increase in $\bar{h}_{max}/h_n$ at a value of ℓ/h_n of 1500 and a value of $\bar{h}_{max}/h_n$ of 1.05. Therefore small amplitude waves start to grow at about $\ell/h_n = 1500$. At $\ell/h_n = 2400$ the waves would reach a value of $\bar{h}_{max}/h_n = 1.15$ and form shock waves. Figure 35 shows that $\sigma_{h_{max}}/h_n$ would still be quite small. At the end of the channel, $\ell/h_n = 6000$, the value of $\bar{h}_{max}/h_n$ would be 1.70 (figure 52) and $\sigma_{h_{max}}/h_n$ would be .20, so that $(h_{max})_{max}/h_n$ becomes equal to 2.22.

Because the slope of .03 is smaller than the .05011 used in the laboratory, the growth rate of the shock waves would be somewhat greater. This increased growth would occur from $\ell/h_n = 2400$ to 6000, but the slope correction to the growth rate can only be computed for the final development phase. From figure 54 this final development phase is seen to start at $\bar{h}_{max}/h_n = 1.45$ and $T' = 1.6$. Figure 30 shows that $T' = 1.6$ corresponds to $\ell/h_n = 4000$. As explained in Section VII-D the increased growth rate at smaller slopes can be computed if the $\bar{h}_{max}/h_n$ vs. T' relation for the smaller slope is known. In this case the $\bar{h}_{max}/h_n$ vs. T' relation for $S_o = .03$ is not known, but it is suspected that it would lie between the experimental relation for $S_o = .05011$ and the theoretical relation for $F = 3.5$ shown on figure 54. Actually the theoretical relation for $F = 3.7$ should be used. Figure 30 shows that at the end of the channel the value of T' would be 2.55. On figure 54 it can be seen that between values of T' of 1.6 and 2.55, the

change in the values of $\bar{h}_{max}/h_n$ is greater for the theoretical curve than the experimental curve. For the experimental curve with $S_o = .03$ (Froude number still about 3.5), the change in the values of $\bar{h}_{max}/h_n$ between values of T' of 1.6 and 2.55 would presumably be between the two changes observed on figure 54. Therefore the maximum increase in the growth rate $(\partial\bar{h}_{max}/\partial\ell)$ occurs by using the relation from the unmodified theory. The change in the value of $\bar{h}_{max}/h_n$ between T' = 1.6 and T' = 2.55 is .29 for the theoretical relation (1.57 to 1.86), and .25 for the experimental relation (1.45 to 1.70). Thus the corrected value of $\bar{h}_{max}/h_n$ at the end of the channel is 1.74 (1.45 + .29), and $(h_{max})_{max}/h_n$ becomes 2.26.

In the above example the increase in the growth rate was very small, but for larger Froude numbers and greater differences between the channel slope in the field and those used in the laboratory the correction to the value of $\bar{h}_{max}/h_n$ will be more significant. In this example the slope correction was easy to estimate because the growth rates predicted from the unmodified theory were only slightly larger than those predicted from the experimental relation. In figure 56 the values of $\partial(\bar{h}_{max}/h_n)/\partial T'$ from the theoretical curve are considerably larger than those from the experimental relation. Thus for channels with slopes considerably smaller than .1192, say .07, the $\bar{h}_{max}/h_n$ vs. T' relation based on this smaller slope would be desirable. This relation could be obtained using the modified theory (as given in Chapter VIII), but it would require considerable calculation. Of course the unmodified theory could always be used to obtain the maximum value of $\bar{h}_{max}$, as was done in the numerical example above, but this

would give values of $\bar{h}_{max}$ that would be much too large in cases similar to those of figure 56 in which the slope of the curve for the unmodified theory is significantly larger than for the experimental curve.

The inlet conditions may not be equivalent to those of the laboratory inlet. In this case the maximum value of $\bar{h}_{max}$ at any station can be found by assuming that the roll waves begin to develop at the upstream end of the channel. Thus for the channel with $\ell/h_n = 6000$ and $F = 3.7$: at $\ell/h_n = 900$, $\bar{h}_{max}/h_n = 1.15$; at $\ell/h_n = 4500$, $\bar{h}_{max}/h_n = 1.70$; and at $\ell/h_n = 6000$, $\bar{h}_{max}/h_n = 1.90$.

Consider the case of an existing channel in which values of $\bar{h}_{max}$ are measured at low discharges and it is required to predict values of $\bar{h}_{max}$ for much larger discharges. This is done by finding the relation between $\bar{h}_{max}/h_n$ and ℓ/h_n which can then be used for all discharges and at any station in the channel. Of course other measured quantities such as $\sigma_{h_{max}}$ and T' could be treated in the same way. The concept of a unique relation between $\bar{h}_{max}/h_n$ (and other quantities) and ℓ/h_n, for the Froude number (nearly) constant, was verified in the laboratory (figures 26-29). It is only valid if the inlet condition is the same at all discharges.

VIII-C PREDICTION OF MAXIMUM DEPTHS IN WIDE RECTANGULAR CHANNELS WITH A CHANGING SLOPE

The effect of a slope change on a developing roll wave train was not investigated. In a wide rectangular channel the Froude number can be written as

$$F = \sqrt{8S_o/f} \tag{8.1}$$

Because $\bar{h}_{max}/h_n$ depends on F, it is clear that a slope change will influence the wave depths. This influence will not take place immediately downstream of the slope change, but over some length of channel downstream of it. As an example of what could occur, consider a roll wave train in a long steep channel with a large slope change so that the Froude number in the lower section is about 1.2. For this situation, because the Froude number is less than the critical value (Chapter II), $\bar{h}_{max}/h_n$ would actually decrease and at some distance far downstream from the change of slope a uniform flow would be attained.

The mechanics of a roll wave train propagating in a channel with reaches of different slope is quite complex, and indeed not yet understood. However it is interesting to speculate on what would happen in such a channel, based on what is known for a channel on a constant slope. To this end three methods of analysis of the problem will be shown by means of a numerical example.

Consider a wide rectangular channel with ℓ = 2400 ft, S_o = 0.10, F = 5.6, and h_n = 1.0 ft. Downstream of this channel is a reach with ℓ = 3350 ft and F = 3.5. For the same friction factor in each channel, equation 8.1 shows that the slope of the downstream channel must be .0392 (i.e. $.10 \times (3.5/5.6)^2$). For the same discharge and channel width in both reaches, the uniform flow equation

$$Q = bh_n \sqrt{8g/f} \sqrt{h_n S_o} \tag{8.2}$$

shows that the normal depth in the .0392 slope reach must be 1.37 ft (i.e. $1.0 \times (.10/.0392)^{1/3}$). Three methods will be used to find the

average maximum depth and the maximum of the maximum depths at the downstream end of the reach with the slope of .0392. These methods are easily extended to cases of more than two slopes.

In table 14 the calculations are shown for each method. The development relations for $\sigma_{h_{max}}/h_n$ (figure 35) and $\bar{h}_{max}/h_n$ (figure 52) were used in these calculations. In method I the first step is to calculate $\bar{h}_{max}$ and $\sigma_{h_{max}}$ at the downstream end of the first reach with $S_o = 0.10$. Then these values are expressed in terms of the normal depth of the second reach and used as "input" to this reach. The values of ℓ/h_n that would have been required to develop these values of $\bar{h}_{max}/h_n$ (1.17) and $\sigma_{h_{max}}/h_n$ (.13) had the value of F been 3.5 are then found. Then with these values of ℓ/h_n, the additional growth along the reach with a slope of .0392 was found. The basic assumption employed in this method was that the development relations (figure 35 and 52) do not depend on the upstream conditions, or in other words, for any given value of $\bar{h}_{max}/h_n$ or $\sigma_{h_{max}}/h_n$, regardless of how these values were obtained, the rates of growth are given by the laboratory relations.

In method II the channel was assumed to be on a single slope with the same vertical drop between the two ends as the original channel had. The values of F and h_n are then calculated keeping the total discharge and the friction factor fixed. The values of $\bar{h}_{max}$ and $\sigma_{h_{max}}$ are then calculated for this "equivalent" channel.

In method III it was assumed first that the entire channel had $S_o = .10$, then $S_o = .0392$. For each case the values of $\bar{h}_{max}$ and

Table 14

Sample Calculations Of Maximum Depth
For Channel With A Break In Slope

Upstream reach - ℓ=2400 ft, S_o=0.10, F=5.6, h_n=1.0 ft

Downstream reach - ℓ=3350 ft, S_o=.0392, F=3.5, h_n=1.37 ft

Method I

At downstream end of S_o=.10 reach:

ℓ/h_n=2400, $\bar{h}_{max}/h_n$=1.6, $\bar{h}_{max}$=1.6 ft

$\sigma_{h_{max}}/h_n$=.18, $(h_{max})_{max}$=1.6+2.58x.18=2.06 ft

At upstream end of S_o=.0392 reach:

$\bar{h}_{max}/h_n$=1.6/1.37=1.17 which corresponds to ℓ/h_n=2500

$\sigma_{h_{max}}/h_n$=.18/1.37=.13 which corresponds to ℓ/h_n=3600

At downstream end of S_o=.0392 reach:

for $\bar{h}_{max}$: ℓ/h_n=2500+2440=4940, $\bar{h}_{max}/h_n$=1.58,

$\bar{h}_{max}$=1.58x1.37=2.16 ft

for $\sigma_{h_{max}}$: ℓ/h_n=3600+2440=6040, $\sigma_{h_{max}}/h_n$=.20,

$\sigma_{h_{max}}$=.20x1.37=.27 ft

$\therefore$ $(h_{max})_{max}$ = <u>2.87 ft</u>

Method II

Average $S_o = \frac{2400}{5750} \times .10 + \frac{3350}{5750} \times .0392 = .0645$

Equivalent $h_n = (.10/.0645)^{1/3} \times 1.0 = 1.16$ ft

Equivalent $F = (.0645/.10)^{1/2} \times 5.6 = 4.5$

$\therefore$ use lab curves for S_o=.08429

ℓ/h_n=5750/1.16=4950, $\bar{h}_{max}/h_n$=2.06,

$\bar{h}_{max}$=1.16x2.06=2.39 ft, $\sigma_{h_{max}}/h_n$=.27,

$\sigma_{h_{max}}$=1.16x.27=.31 ft

$\therefore$ $(h_{max})_{max}$ = <u>3.20 ft</u>

Table 14 (continued)

Method III

$\ell = 5750$ ft, $F = 5.6$, $h_n = 1.0$ ft

$\ell/h_n = 5750$, $\bar{h}_{max}/h_n = 2.55$, $\bar{h}_{max} = 2.55$ ft

$\sigma_{h_{max}}/h_n = .36$, $(h_{max})_{max} = 3.48$ ft

$\ell = 5750$ ft, $F = 3.5$, $h_n = 1.37$ ft

$\ell/h_n = 5750/1.37 = 4200$, $\bar{h}_{max}/h_n = 1.48$,

$\bar{h}_{max} = 2.03$ ft, $\sigma_{h_{max}}/h_n = .155$, $\sigma_{h_{max}} = .21$,

$(h_{max})_{max} = 2.58$ ft

Weighted averages:

$$\bar{h}_{max} = \frac{2400}{5750} \times 2.55 + \frac{3350}{5750} \times 2.03 = 2.24 \text{ ft}$$

$$(h_{max})_{max} = \frac{2400}{5750} \times 3.48 + \frac{3350}{5750} \times 2.58 = \underline{2.95 \text{ ft}}$$

$\sigma_{h_{max}}$ were found. Then to obtain the predicted values of $\bar{h}_{max}$ and $\sigma_{h_{max}}$ at the downstream end of the channel with two slopes, a weighted average was found. The weighting factors were based on the lengths of the reaches.

For all methods the value of $(h_{max})_{max}$ was evaluated using equation 6.3. Table 14 shows that for method II the value of $(h_{max})_{max}$ was about 10 percent greater than for the other two methods. It is difficult to say which method predicts the most reliable values. Method II is obviously easier to apply, expecially for cases involving many different slopes. For method I at least the assumptions employed are clear, whereas in the other two methods the justifications are obscure.

For predicting values of h_{max} at high discharges in existing channels with changing slope from measured values of h_{max} at low discharges, the method used for Santa Anita Wash (figure 50) should be adequate. In this method the measured values of $\bar{h}_{max}$ at one particular station were divided by the concurrent value of h_n at that same station. These values of $\bar{h}_{max}/h_n$ were then plotted against a value of ℓ/h_n that was computed by adding up the individual values of ℓ/h_n for each reach of constant slope upstream of the measuring station (i.e. $\ell/h_n = \sum_i \ell_i/(h_n)_i$ where ℓ_i is the length of the ith reach and (h_n) is the normal depth for the ith reach). Strictly speaking the resulting h_{max}/h_n vs. ℓ/h_n relation is only valid at the station at which the measurements were taken because of the slope variations.

This restriction stems from the fact that the growth rate $(\partial \bar{h}_{max}/\partial \ell)$ for a particular value of $\bar{h}_{max}$ increases as the Froude number increases (figure 52). In a system in which the slope decreases in the downstream direction, the relation $\bar{h}_{max}/h_n$ vs. ℓ/h_n determined from measurements at one station will predict values of $\bar{h}_{max}/h_n$ that are too low when the relation is used at stations upstream of the measuring station, and similarly this same relation will predict values of $\bar{h}_{max}/h_n$ that are too high when used at stations downstream of the measuring station.

VIII-D INFLUENCE OF SIDE-WALLS

In Section VII-B the results of a calculation concerning the effect of the side-walls on the periodic permanent roll wave theory were presented. It was found that for a fixed value of F and T', the value of h_{max}/h_n was less when the frictional resistance of the side-walls was included in the calculation using the concept of a hydraulic radius. From this result it is reasonable to conclude that for natural roll waves in the final development phase, the value of $\bar{h}_{max}/h_n$ for a given T' and F would be less in a narrow channel as compared to a wide channel. If it is assumed that the T' vs. ℓ/h_n relation is not influenced by the side-walls, then the value of $\bar{h}_{max}/h_n$ at a given ℓ/h_n will be less for a narrow channel. Unfortunately there is no experimental evidence to either support or refute this argument.

The concept of a critical Froude number, F_{cr}, was discussed briefly in Section II-B. By definition, a flow with $F < F_{cr}$ is insensitive to small perturbations of the free surface. This is usually interpreted

to mean that roll waves will not develop in flows with $F < F_{cr}$. In the laboratory experiments the minimum value of F was about 3.5. The value of F_{cr} was not determined experimentally, and indeed would be quite difficult to obtain because of the very small growth rates for values of F near F_{cr}. However the theoretical value of F_{cr} for a wide rectangular channel is larger for a narrow channel than a wide channel. Unfortunately there is no experimental evidence to bring to bear on what the value of F_{cr} is for a rectangular channel, and what influence the side-walls have on the value of F_{cr}.

From what little analytical evidence that exists, it appears that by neglecting the effect of the side-walls, the values of $\bar{h}_{max}$ that would be predicted from the laboratory relations would be somewhat high. However the actual effect of the side-walls can not be evaluated until experimental evidence is available. In the meantime the only alternative is to neglect the possible effect of the side-walls.

CHAPTER IX

RESULTS AND CONCLUSIONS

The purpose of this study was to describe some of the properties of roll waves that develop from a uniform flow in a steep wide rectangular channel.

A. From the measurements obtained in the laboratory channel, the following results concerning natural roll waves were obtained:

1. For a given Froude number F and channel slope S_o the following quantities could be expressed as unique functions of ℓ/h_n, the ratio of the distance ℓ from the beginning of the channel to h_n, the normal depth of the uniform flow:

a) $\bar{h}_{max}/h_n$, where $\bar{h}_{max}$ is the mean value (at a fixed ℓ) of the depths at the wave crests.

b) $T' = S_o T_{av} \sqrt{g/h_n}$ = dimensionless wave period in which T_{av} is the mean wave period (i.e. time for the wave to pass a given station) and g is the acceleration of gravity.

c) $\bar{h}_{min}/h_n$, where $\bar{h}_{min}$ is the mean value of the depths at the wave troughs.

d) $\sigma_{h_{max}}/h_n$, where $\sigma_{h_{max}}$ is the standard deviation of $\bar{h}_{max}$.

e) σ'_T, the standard deviation of T'.

2. For a given value of $\bar{h}_{max}$, the growth rate $\partial \bar{h}_{max}/\partial \ell$ of the shock waves (i. e. large amplitude roll waves) increased as Froude number was increased by increasing the channel slope.

3. Small amplitude roll waves of significant magnitude, taken as $\bar{h}_{max}/h_n = 1.1$, occurred at values of ℓ/h_n that decreased as Froude number increased.

4. In any given flow, T_{av} remained unchanged in a reach that extended from the station where small amplitude waves had developed sufficiently so that individual waves could be identified, to some station downstream of where the small amplitude waves formed into shock waves. This portion of the development where T_{av} remained unchanged was termed the initial development phase. Downstream of the initial development phase, shock waves were overtaking and T_{av} increased approximately linearly with ℓ.

5. Two types of wave growth (i. e. increase in h_{max}) were identified:

a) natural growth - that growth which occurs without wave overtaking. This was the type of growth that occurred in the initial development phase.

b) growth by overtaking - that growth which occurs when a shock wave overtakes and combines with another shock wave to form a single shock wave with h_{max} greater than that of either wave before combination.

6. After a sufficient amount of growth ($\bar{h}_{max}/h_n$ > approximately 1.5) the $\bar{h}_{max}/h_n$ vs. T' relation for natural roll waves was practically identical to the experimental h_{max}/h_n vs. T' relation for periodic permanent roll waves at the same Froude number and slope. From this correspondence between natural and periodic waves it was deduced that growth by overtaking was the dominant type of growth during this portion of the development which was termed the final development phase.

7. The velocity of an individual shock wave increased as the depth at the crest h_{max} increased, and as the depth at the trough immediately in front of the shock front increased. Consequently, the h_{max} of an overtaking wave was occasionally less than that of the wave being overtaken. In addition an overtaking wave accelerated while it was propagating on the gradually increasing depth behind the wave being overtaken. The velocity of the combined wave was greater than that of the overtaken wave, and less than that of the overtaking wave just before the two waves combined.

8. The frequency distributions of h_{max}, T, and c for a given flow at a given station were approximated by the Gaussian distribution, whereas the frequency distribution for h_{min} was skewed toward the small values so that the mean value was less than the median.

B. The following results concerning periodic permanent roll waves were obtained:

1. The experimentally obtained h_{max}/h_n vs. T' relations did not agree with the theory in which the weight of the shock front was neglected. After the theory was modified to include this weight, the observed values of h_{max}/h_n were within an average of 6.5 percent of the predicted values, and the maximum discrepancy was 13.5 percent.

2. The modified theory, with the weight of the shock front included, predicts a channel slope effect, such that for a given value of F and T', the value of h_{max}/h_n increases as the slope decreases. Furthermore the modified theory predicts that the slope of the h_{max}/h_n vs. T' relation ($\partial (h_{max}/h_n)/\partial T'$), at a given value of h_{max}/h_n, increases as the channel slope decreases. These predicted channel slope effects on the h_{max}/h_n vs. T' relation were observed in the periodic wave experiments.

C. Conclusions concerning natural roll waves:

1. From results A 6 and B 2 it can be concluded that with F held fixed and for a given value of $\overline{h}_{max}/h_n$ in the final development phase, the growth rate of natural waves will decrease as the channel slope is increased, providing the effect of the channel slope on the approximately linear portion of the T' vs. ℓ/h_n relation is small compared to its effect on the $\overline{h}_{max}/h_n$ vs. T' relation. By comparing the natural roll wave results for the rough channel (S_o = .1192) with those of the smooth channel at about the same Froude number (S_o = .05011), it was found that the growth rates of the shock waves were appreciably less on the larger slope.

2. Based on the fact that, for a given Froude number and channel slope, unique relations resulted when the measured wave properties were expressed in terms of ℓ and h_n (see result A 1), it is reasonable to conclude that these same relations will be valid for any wide rectangular channel with inlet conditions equivalent to those in the laboratory, providing the Froude number and channel slope are the same as those obtained in the laboratory. If, for the same Froude number, the channel slopes are not the same, the growth rates of the shock waves in the final development phase will be different than those in the laboratory (see conclusion C 1).

LIST OF SYMBOLS

A	area of cross section of flow
b	width of rectangular channel
C	dimensionless complex velocity $= C_r + iC_i$
C_r	dimensionless wave velocity $= c/u_n$
C_i	dimensionless number pertaining to growth rate
c	wave velocity
c_{av}	average wave velocity
D_g	geometric mean size of sand grains
F	Froude number of uniform flow $= u_n/\sqrt{gh_n}$
F_{cr}	critical Froude number
f	Darcy-Weisbach friction factor
g	acceleration of gravity
h	depth of flow normal to channel floor
h_n	normal depth of uniform flow
h_c	a depth defined by $h_c^3 = K^2/g$
h_e	mean depth of shock front
h_{cr}	critical depth $= (q^2/g)^{1/3}$
h_{av}	average depth over a wave length
$h_{max}, \bar{h}_{max}$	depth at wave crest and average depth of wave crests respectively
$(h_{max})_{max}$	maximum value of h_{max}
$h_{min}, \bar{h}_{min}$	depth at wave trough and average depth of wave troughs respectively
H	dimensionless depth $= h/h_n$
K	a constant of integration with units of discharge per unit width $= (c-u)h$

LIST OF SYMBOLS (Cont'd)

k	geometric mean size of sand grains
ℓ	distance along channel from beginning of channel
L_j	length of shock front
Q	discharge
q	discharge per unit width
q_{av}	average discharge per unit width over a wave length
R	Reynolds number $= 4ru_n/\nu$
r	hydraulic radius
S_o	channel slope $= \sin\theta$
T	wave period
T_{av}	average wave period
T'	dimensionless wave period $= S_o T \sqrt{g/h_n}$ or $S_o T_{av} \sqrt{g/h_n}$
t	time
t'	dimensionless time $= u_n t/\lambda$
U	dimensionless velocity $= u/u_n$
U'	dimensionless perturbation velocity $= u/u_n - 1$
u	average velocity over cross section of flow $= Q/A$
u_p	velocity in x-direction at distance y from channel bottom
u_n	normal velocity
u_*	shear velocity $= \sqrt{\tau_o/\rho}$
u_{max}, u_{min}	velocity at wave crest and trough respectively
W	weight of shock front per unit width
x	cartesian coordinate parallel to channel bottom
X	coordinate moving in x-direction at velocity c, $X = x - ct$

LIST OF SYMBOLS (Cont'd)

Y	dimensionless parameter $= S_o \lambda / F^2 h_n$
y	cartesian coordinate perpendicular to channel bottom
α	velocity distribution coefficient
γ	specific weight of fluid
δ	thickness of laminar sublayer
η	dimensionless perturbation depth $= h/h_n - 1$
θ	angle of inclination of channel bottom
ν	kinematic viscosity of fluid
λ	wave length
ρ	mass density of fluid
σ	standard deviation
σ_g	geometric standard deviation of sand sizes
τ_o	shear stress in x-direction averaged over the channel boundaries
$_^*$	denotes division by h_c e.g. $h_n^* = h_n/h_c$
$\overline{\omega}_o$	average frequency of wave overtakes in a reach of channel $\Delta \ell$

BIBLIOGRAPHY

1. Cornish, V., "Ocean waves", Cambridge University Press, 1934, pp. 92-101.
2. Personal communication with R.L. Schreve, observed on Blue Glacier, Mount Olympus, Washington on 26 August 1965.
3. Holmes, W.H., "Traveling waves in open channels", Civil Engineering, v 6, n 7, July 1936, pp 467-468.
4. Keulegan, G.H. and Patterson, G.W., "Effect of turbulence and channel slope of translation waves", Journal of Research of the National Bureau of Standards, v 30, RP 1544, June 1943, pp. 461-512.
5. Jeffreys, H.J., "The flow of water in an inclined channel of rectangular section", Philosophical Magazine, series 6, v 49, May 1925, pp. 793-807.
6. Craya, A., "The criterion for the possibility of roll-wave formation", Gravity Waves, National Bureau of Standards Circular 521, 1952, pp. 141-151.
7. Dressler, R.F. and Pohle, F.V., "Resistance effects on hydraulic instability", Communications on Pure and Applied Mathematics, v 6, 1953, pp. 93-96.
8. Iwasa, Y., "The criterion for instability of steady uniform flows in open channels", Memoirs of the Faculty of Engineering, Kyoto University, Japan, v 16, n 6, March 1954, pp. 264-275.
9. Koloseus, H.J. and Davidian, J., "Free-surface instability correlations", Geological Survey Water-Supply Paper 1592-C, 1966, 72 pp.

BIBLIOGRAPHY (Cont'd)

10. Montouri, C., "La formazione spontanea dei treni d'onde su canali a pendenza molto forte" (Spontaneous formation of wave trains in steep channels), Relazioni su ricerche e studi promossi dall' ANIDEL, 1961, pp. 1-19. Translated to English by J.C. Van Tienhoven, U.S. Army Waterways Experiment Station, translation no. 65-12, 1965.

11. Thomas, H.A., "The propagation of waves in steep prismatic conduits", Proc. of Hydraulic Conference, Iowa City, Iowa, 1940, pp. 214-229.

12. Ishihara, T., Iwagaki, Y. and Iwasa, Y., Discussion of "Roll waves and slug flows" by P. Mayer, Trans. ASCE, v 126, part I, 1961, pp. 548-563.

13. Ghambarian, N.N., "On waves in inclined open channels", IAHR, 11th International Congress, paper no. 1.1, Leningrad, 1965, 13 pp.

14. Ghambarian, N.N. and Mayilian, N.N., "An experimental study of roll waves in superrapid flow" (in Russian), Akademiia Nauk Armianskoi SSR, Izvestiia, Seriia Tekhnicheskikh Nauk, v 12, n 2, 1959, pp. 3-8.

15. Dressler, R.F., "Mathematical solution of the problem of roll-waves in inclined open channels", Communications on Pure and Applied Mathematics, v 2, 1949, pp. 149-194.

16. Koloseus, H.J., "The effect of free-surface instability on channel resistance", Ph.D. Thesis, University of Iowa, August, 1958, 39 pp.

BIBLIOGRAPHY (Cont'd)

17. Rouse, H., "Critical analysis of open-channel resistance", Proc. ASCE, J. Hyd. Div., v 91, n HY 4, July 1965, pp. 1-25.

18. Lighthill, M.J. and Whitham, G.B., "On kinematic waves, I. Flood movement in long rivers", Proc. Royal Society of London, series A, v 229, May 1955, pp. 281-316.

19. Schonfeld, J.C., "Distortion of long waves; Equilibrium and stability", International Association of Scientific Hydrology, publication no 35, Assemblée générale de Bruxelles, v 4, 1951, pp. 140-157.

20. Vanoni, V.A., "130-foot precision tilting flume", Tech. Memo. No. 64-7, W.M. Keck Laboratory of Hydraulics and Water Resources, Calif. Inst. of Tech., Pasadena, California, January, 1964.

21. Fischer, H.B., "Longitudinal dispersion in laboratory and natural streams", Report No. KH-R-12, W.M. Keck Laboratory of Hydraulics and Water Resources, Calif. Inst. of Tech., Pasadena, California, June 1966, pp. 58-61.

22. Tracy, H.J. and Lester, C.M., "Resistance coefficients and velocity distribution smooth rectangular channel", Geol. Survey Water Supply Paper 1592-A, U.S. Dept. of the Interior, Washington, D.C., 1961, 18 pp.

23. Keulegan, G.H., "Laws of turbulent flow in open channels", Journal of Research of the National Bureau of Standards, v 21, RP 1151, Dec. 1938, pp. 707-741.

BIBLIOGRAPHY (Cont'd)

24. Rouse, H., "Elementary mechanics of fluids", John Wiley, 1946.

25. Prandtl, L. and Tietjens, O.G., "Applied hydro- and aeromechanics", Dover Publications, 1957, p. 36.

26. Rouse, H., "Engineering hydraulics", John Wiley, 1950, chapter X by B.R. Gilcrest.

27. Elevatorski, E.A., "Hydraulic energy dissipators", McGraw Hill, 1959, p. 26.

28. Bakhmeteff, B.A. and Matzke, A.E., "The hydraulic jump in sloped channels", T. ASME, paper Hyd. 60-1, v 60, n 2, Feb. 1938, pp. 111-118.

29. Chow, V.T., "Open channel hydraulics", McGraw Hill, 1959, p. 428.

APPENDIX I

Discussion by the writer of "Critical analysis of open-channel resistance" by Hunter Rouse(17).

Published in the Proceedings of the American Society of Civil Engineers, Journal of the Hydraulics Division, 92, HY2, March, 1966, pp. 403-409.

The following correction should be made: p. 406, last paragraph, 2nd sentence, should read "To aid in the determination of the water-surface levels with the point gage, a static pressure-tap installed flush with the flume floor was used."

The writer received the J.C. Stevens Award for 1966 from the American Society of Civil Engineers for this discussion.

RICHARD R. BROCK,[72] A. M. ASCE.—This discussion will be confined to the section of the paper dealing with free-surface instability leading to the development of roll waves. Following the order of presentation in the author's paper, these comments will deal with the stability criterion as derived from Eq. 26, experimental data on friction factors in smooth rectangular channels, and the author's hypothesis that, "In reality, the augmented rate of loss indicated by mean-flow considerations is not a true dissipation but a transformation from mean-flow energy to wave energy."

Stability Analysis.—The author's criterion for stability for wide rectangular channels as expressed by Eqs. 29 and 30 indicates that F_s is a function of f only. Actually, κ is also involved because the numerical factor 1.30 in Eq. 29 was evaluated from $3/2\sqrt{8}\,\kappa$, and 0.87 in Eq. 30 was evaluated from $1/\sqrt{8}\,\kappa$. For the commonly accepted value of κ of 0.40, these factors would be 1.326 and 0.884. The author's factors result when $\kappa \approx 0.407$ is used.

It should be kept in mind that this stability analysis is only valid for surface disturbances that have wave lengths that are long compared to the depth. This restriction comes from the fact that the shallow water wave equations used, are based on a hydrostatic pressure distribution.

Experimental Data in Smooth Rectangular Channels.—The author cites data by Nemec in a smooth rectangular channel which shows that an unstable flow has a higher friction factor than a stable flow at the same Reynolds number. The criterion of stability used was Eq. 29. To the writer's knowledge, the only other data that shows this effect in smooth channels is that of Powell.(5) However, published data by Tracy[73] and unpublished data by the writer obtained at the California Institute of Technology (CIT), to be presented herein, indicate that the friction factor does not depend on the Froude number even when the values are in excess of those given by Eq. 29 and instability is expected. These contradictory findings are quite perplexing and an explanation for the discrepancy is necessary for a complete acceptance of one or both findings. In this discussion, an explanation of the contradiction will not be given. Instead, for each of the experiments, a short description of the apparatus and techniques used will be given where available. Also, the results will be shown on an f-R plot for each experiment. In addition, a few comments will be made concerning experimental procedure that may help to explain why differences in findings do exist.

Before going to the four sets of experiments in question, some brief general remarks on measuring friction factors are in order. The normal method of obtaining friction factors involves measuring the discharge, depth, and flume slope, and then calculating f by Eq. 27a. In most cases, the discharge and slope are quite accurate. Assuming that discharge and slope are fixed for a rectangular channel of width b, the variation of f with d is given by

---

[72] NSF Graduate Trainee, California Inst. of Tech., Pasadena, Calif.

[73] Tracy, H. J., and Lester, C. M., "Resistance Coefficients and Velocity Distribution Smooth Rectangular Channel," Water Supply Paper 1592-A, Geol. Survey, U. S. Dept. of the Interior, Washington, D. C., 1961.

$$\frac{f'}{f} = \frac{1+2\,d/b}{1+2\,d'/b}\left(\frac{d'}{d}\right)^3 \quad \ldots\ldots\ldots\ldots\ldots\ldots \quad (77)$$

in which f and f' are the friction factors corresponding to depths d and d', respectively. This shows, for example that in a wide channel, a 5% positive error in measuring d(d'/d = 1.05) results in a 15.8% positive error in f(f'/f = 1.158).

Obviously, one method of minimizing errors in measuring the depth is to run at high depths, which is generally the case in subcritical flow. However, for supercritical flow in the laboratory, the depths are generally consideribly smaller because the slopes are larger and the discharge capacity is limited. Thus, it can generally be stated that an accurate measurement of depth is needed to assure a reliable f value, especially in supercritical flow.

The stability analysis indicates that, if the Froude number is above a certain value, small sinusoidal disturbances on the free surface will be amplified. These amplifying disturbances presumably lead to the large amplitude waves called roll waves. However, this process requires some length along the channel in which the small waves can grow. It has been the writer's experience that, for flows of appreciable depth, the usual laboratory flume is not long enough for waves to grow sufficiently so that they are visible to the eye. Only when the depth of flow is small and the slope is large can surface disturbances be observed near the downstream end of the flume. Because of this, friction factors in an unstable flow are measured in the reach where the flow is at normal depth and the surface disturbances that eventually lead to roll waves have not developed appreciably.

Nemec's data, shown in Fig. 17, were obtained in a smooth rectangular channel 2.5 ft wide, 85 ft long, having glass floor and walls. The numerical data for plotting Fig. 17 were read from Fig. 10. The experimental technique followed by Nemec is not available and it is hoped that the author will supply this in his closure. In plotting Fig. 17 all of the points for stable flows from Fig. 10 were used, but only four of the points for unstable flows were used in each group with approximately equal Reynolds numbers. In selecting these four points, the two extreme values of f were used as well as two points between these extremes.

Fig. 17 shows that the friction factor for unstable flow can be considerably larger than for stable flow. At $R = 5.2 \times 10^4$, the maximum f is 32% larger than the value on the curve based on stable flow, and at $R = 6.7 \times 10^5$, the maximum f is 16% higher. From Fig. 10, it can be seen that, for a constant Froude number, the percentage increase in f is greatest at the lower Reynolds numbers. This observation may be related to the fact that, for a constant F, the depth increases with R, and thus if a constant absolute error is made in measuring the depth, the resulting error in f would be larger at the lower values of R.

Powell's[5] results from a smooth rectangular channel at Iowa State University are shown in Fig. 18. The flume was 8 in. wide, 50 ft long, and lucite walls, and a structural steel floor protected with aluminum paint. The four flume slopes used and the resulting ranges in Froude numbers are also shown on Fig. 18. For the maximum slope, where the flow is unstable, the f values are well above the curve obtained from data for the other three slopes where the flow is stable. The equation shown was determined by the writer and is not the one Powell reported.

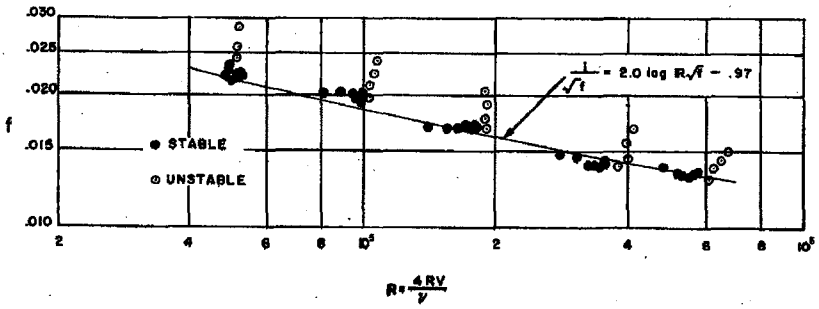

FIG. 17.—NEMEC'S DATA FOR A SMOOTH RECTANGULAR CHANNEL

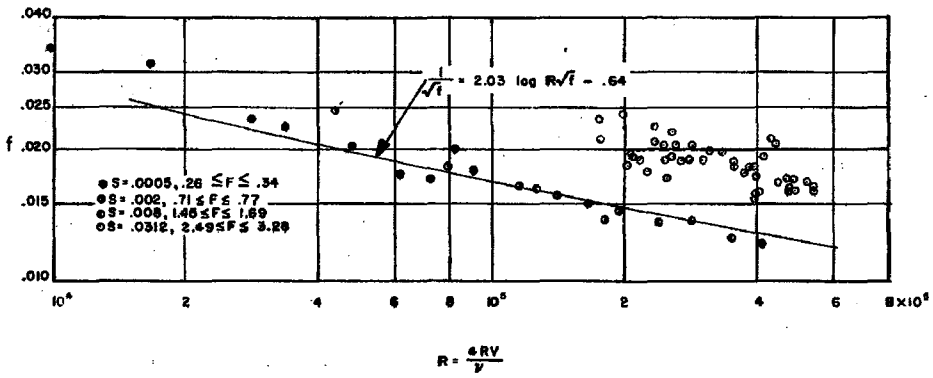

FIG. 18.—POWELL'S DATA FOR A SMOOTH RECTANGULAR CHANNEL

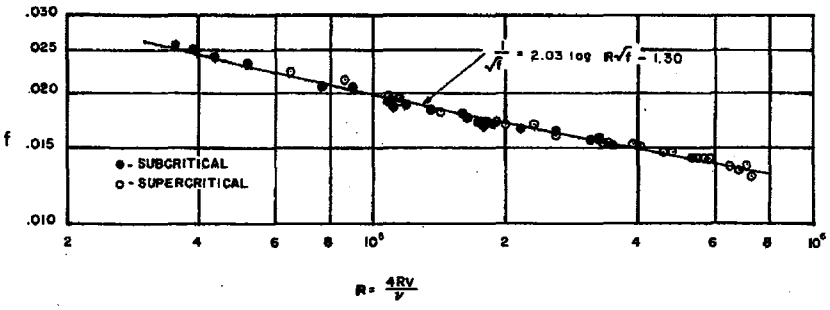

FIG. 19.—TRACY'S DATA FOR A SMOOTH RECTANGULAR CHANNEL

From Powell's report[5] it was determined that a static pressure tube was used to measure the depth at five locations over the length of the flume. This tube was connected to a well where hook gages were used to measure the water level. No mention was made of any surface disturbances that would lead to roll waves, and none would be expected in the short channel used.

In view of the importance of an accurate depth measurement in supercritical flow, it seems that only five measurements over the length of the flume are inadequate. The technique of using a static pressure tube in a high velocity flow has the objection that a slight misalinement of the tube may cause a part of the relatively large dynamic head to be recorded also. Finally, the writer questions whether Powell had uniform flow conditions, because his tabulated energy slopes were not equal to the flume slopes. Comparing Figs. 17 and 18 shows that the percentage increase in f (to 66%) for the unstable flows in Powell's experiments is considerably larger than Nemec found for the same Reynolds number.

Tracy[73] used a smooth rectangular flume at the Georgia Institute of Technology which was 3.5 ft wide, 80 ft long, had steel walls and floor covered by one seal coat and two coats of synthetic enamel, and had a motorized slope control. Tracy's results for 49 runs ranging in Froude number from 0.144 to 3.96 are shown in Fig. 19. It is seen that one relationship adequately fits all the data.

Water-surface profiles were obtained from point-gage readings taken at 1-ft intervals over the length of the flume and at five locations in the cross section. In supercritical flow, the S2 and S3 profiles vary gradually when near the normal depth, as do the M1 and M2 profiles in subcritical flow. Because these gradual variations may not be perceptible over a short distance, Tracy measured both of the profiles and then the normal depth was interpolated between them.

Tracy stated[73] that, in supercritical flow, the free surface was "characterized by highly agitated transverse waves of short length." Considering the length of his channel and the depths of flow used, the waves he referred to are not the small roll wave disturbances that are sometimes visible at the downstream end of flumes. Rather, these waves are probably of the type that are inherent with turbulent flow. To obtain a mean depth, Tracy measured the elevation of the crest and the trough of these waves and the average was used as the mean depth. It is significant that this method agreed well with measurements made with static pressure-taps installed in the flume floor.

The writer has made a few friction factor measurements in supercritical ($1.19 \leq F \leq 2.88$) flow at CIT which do not show a Froude number dependence. The basic data are presented in Table 2 and Fig. 20 shows the f-R plot. The flume is 3.61 ft wide, 130 ft long, has glass side walls and a stainless steel floor. The flume slope is varied by means of electrically-operated mechanical jacks.

Point-gage readings at five locations in the cross section and at 5-m intervals along the flume determined the water surface profiles. To aid in the determination of the water-surface levels with the point gage, a static pressure at the pressure-tap installed flush with the flume floor was used. A continuous recording of the static pressure at the pressure-tap location was provided by a strip paper recorder and a pressure transducer. From this recording, the average static pressure (depth) at the pressure-tap location was obtained. Then the point-gage was set at this average depth and the appearance of the

TABLE 2.—CIT DATA FOR A SMOOTH RECTANGULAR CHANNEL

Run	S	Q, in cubic feet per second	d, in feet	R, in feet	V, in feet per second	f	R	F	T, in degrees centigrade	ν, in square feet per second	f'/f
1	0.003984	0.904	0.111	0.105	2.25	0.0212	8.99×10^4	1.19	21.3	1.049×10^{-5}	1.044
2	0.006085	0.884	0.0938	0.0891	2.61	0.0205	8.87×10^4	1.50	21.3	1.049×10^{-5}	1.052
3	0.01942	0.878	0.0639	0.0618	3.80	0.0213	8.83×10^4	2.65	20.7	1.064×10^{-5}	1.078
4	0.009979	1.41	0.105	0.0993	3.71	0.0186	1.42×10^5	2.02	21.9	1.036×10^{-5}	1.047
5	0.004069	2.42	0.200	0.180	3.35	0.0168	2.27×10^5	1.32	20.8	1.060×10^{-5}	1.024
6	0.009979	2.42	0.146	0.135	4.59	0.0165	2.40×10^5	2.12	21.9	1.036×10^{-5}	1.033
7	0.01942	2.44	0.120	0.112	5.64	0.0176	2.39×10^5	2.88	20.8	0.060×10^{-5}	1.041

water surface at the point was observed both from above and the side. Armed with this visual picture of the water surface in contact with the point at the average depth level, the point-gage readings were taken at the locations indicated above. Occasionally during the run, the point-gage was returned to the pressure-tap location to check on the visual method of setting the point at the average depth.

Using this procedure to find the average depth, it was found that readings could be repeated within approximately 0.02 cm to 0.04 cm. To get some idea of the accuracy of the f values, Eq. 77 was used with $d' = d + 0.05$ cm and the resulting values of f'/f are shown in Table 2. The most error occurs for the lowest depth which was in Run 3. Small waves, apparently resulting from a free surface instability, were clearly visible at the lower end of the flume for Run 3 only. These waves impaired the depth measurement and the normal

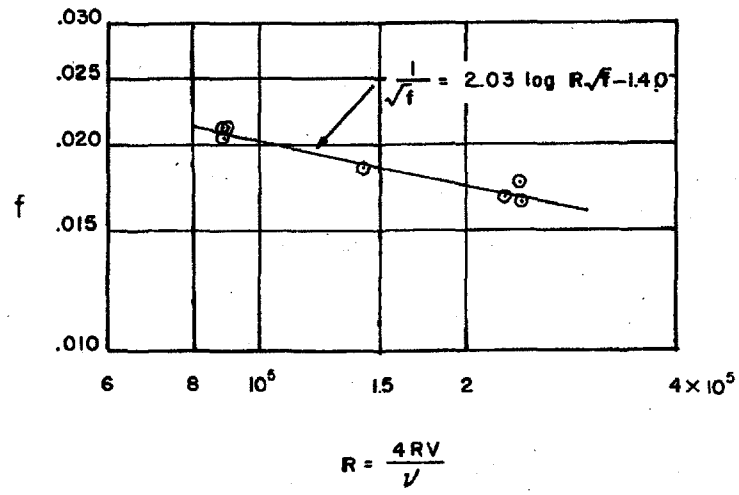

FIG. 20.—CIT DATA FOR A SMOOTH RECTANGULAR CHANNEL

depth was taken from the water surface profile upstream of the point where these waves first appeared. It is interesting to note that the relationship in Fig. 20 gives friction factors less than 3% greater than Tracy's relationship over the range of Reynolds numbers tested.

Wave Energy.—In the final paragraph of the paper, the author presents the idea that the increased friction factors in unstable flow, as found by Nemec, result from assuming that all of the computed energy loss is from boundary resistance alone. The author indicates that, in reality, a part of this computed energy loss has been transformed from "mean-flow energy to wave energy."

Considering a uniform flow in a wide rectangular channel, the rate at which energy is supplied to the flow, per unit surface area, is γSVd, and the rate of energy dissipation because of boundary resistance is $\rho V^3 f/8$ per unit surface area. If the writer interprets the author's concept correctly, in unstable flow there is also an energy dissipation rate associated with the small-amplitude progressive waves on the surface of the flow. Let the rate of this energy

dissipation per unit surface area be D_w. Conservation of energy requires that

$$\gamma S V d = \frac{\rho V^3 f}{8} + D_w \quad \text{(78)}$$

If f_i is the friction factor computed with $D_w = 0$, Eq. 78 gives

$$\frac{f_i}{f} = \frac{1}{1 - \frac{D_w}{\gamma S V d}} \quad \text{(79)}$$

which indicates that a friction factor computed by neglecting the dissipation associated with the waves is larger than the true friction factor that reflects only the dissipation caused by boundary resistance.

Eq. 79 indicates that, unless D_w is not small compared to $\gamma S V d$, the two friction factors are essentially the same. Although the exact form D_w is not known, it certainly depends on the amplitude of the surface waves in some manner, because for a stable flow (no surface waves) $D_w = 0$. Thus, for unstable flows that have small surface wave amplitudes, the writer feels that the term $D_w/\gamma S V d$, must be considerably less than unity. The experiments by Tracy and the writer tend to confirm this. Some analytical work on the form of D_w would be a significant contribution to this problem.

Summary.—The main purpose of this discussion was to bring out the fact that contradictory findings exist regarding the Froude number effect on friction factors in unstable flow. Findings from several sources were shown in a similar manner to permit direct comparison. Some of the techniques and apparatus used to obtain the data were discussed where possible. The importance of an accurate depth measurement was emphasized. The writer's interpretation of the author's explanation for increased friction factors in unstable flow was presented. This required an energy dissipation rate associated with the surface waves to be introduced. The form of this dissipation term is not known, but the writer feels that it is negligible for small amplitude waves.

Acknowledgments.—The writer wishes to thank his advisor, V. A. Vanoni, for suggesting this discussion, and for his helpful criticism during its preparation.